Development of semi-empirical exchange- correlation functionals

Thomas W. Keal

Development of Semi-Empirical Exchange-Correlation Functionals

Thomas W. Keal

Durham University

Department of Chemistry

2005

Submitted in conformity with the requirements for the degree of Doctor of Philosophy

Declaration

The material contained within this thesis has not previously been submitted for a degree at the University of Durham or any other university. The research reported within this thesis has been conducted by the author unless indicated otherwise.

Copyright Notice

Abstract

Development of Semi-Empirical Exchange-Correlation Functionals

Thomas W. Keal

Kohn-Sham density functional theory (DFT) is the most widely-used method for quantum chemical calculations. For most chemical properties it offers relatively accurate results for a relatively low computational cost. This accuracy is governed by the quality of the exchange-correlation functional used. The development and assessment of new functionals is a vital aspect of DFT research, and is the focus of this thesis.

In Chapter 1, the theory of traditional wavefunction-based quantum chemistry methods and of DFT is outlined, and the two approaches compared and contrasted. Chapter 2 considers the relatively poor performance of conventional DFT functionals for NMR shielding constants. A simple generalised gradient approximation (GGA) functional, denoted KT1, is developed, which improves this performance significantly. A more flexible functional fitted to experimental energetic data, denoted KT2, is also presented. In Chapter 3, KT1 and KT2 are assessed for other magnetic properties, such as chemical shifts, magnetisabilities, and indirect spin-spin coupling constants.

Chapter 4 details the development of a third GGA denoted KT3, which is designed to address the shortcomings of KT2 for non-magnetic properties. In Chapter 5, the more flexible functional form of KT3 is shown to give results competitive with the best GGAs for a wide range of chemical properties and for solid state calculations.

In Chapter 6, we attempt to improve performance for classical chemical reaction barriers, for which KT3 is relatively poor. This requires a more flexible form in the resulting GGA functional, denoted KT4. A hybrid functional, B97-3, is also developed with a similar emphasis on reaction barriers. Chapter 7 presents an extensive chemical assessment for KT4 and B97-3. For the systems considered, B97-3 is shown to be the most accurate semi-empirical functional developed to date. Concluding remarks are presented in Chapter 8.

Acknowledgements

I would like to express my sincere gratitude to David Tozer for his tremendous support and encouragement over the past three years. I am also grateful to Stewart Clark, Trygve Helgaker, and Pawel Salek for their invaluable assistance with their computer codes. Thanks also to Phil, Giusy, Phil, Mark, Andy, Michael, and Ola for their help and entertaining company.

Finally, a special thank you to Kim for always being there for me, despite having a thesis of her own to write.

For my family

Contents

List of Tables

List of Figures

Chapter 1

Quantum chemistry

The field of quantum chemistry applies the principles of quantum mechanics to the simulation of chemical systems, which in practice means finding approximate solutions to the electronic Schrödinger equation. This chapter compares two approaches to that problem, namely wavefunction theory and density functional theory.

1.1 The Schrödinger equation

In Schrödinger's formulation of quantum mechanics [1], a chemical system can be completely described by its wavefunction, Ψ. The wavefunction is not surprisingly a very complex quantity, depending on all the coordinates of every particle in the system. It also has no direct physical interpretation, although its square is a probability density.

To extract information about the system that can be compared with experiment, a mathematical operator must be applied to the wavefunction. For example, the total energy of the system can be found by applying the Hamiltonian operator ($\hat{H}$), which is the sum of the kinetic energy and potential energy operators. For a molecular system with N electrons and M nuclei, in the absence of an external perturbation, the Hamiltonian operator (in atomic

units) is

$$\begin{aligned}\hat{H} &= -\frac{1}{2}\sum_{i}^{N}\nabla_i^2 - \frac{1}{2}\sum_{A}^{M}\frac{1}{M_A}\nabla_A^2 \\ &\quad -\sum_{i}^{N}\sum_{A}^{M}\frac{Z_A}{r_{iA}} + \sum_{i}^{N}\sum_{j>i}^{N}\frac{1}{r_{ij}} + \sum_{A}^{M}\sum_{B>A}^{M}\frac{Z_A Z_B}{R_{AB}}\end{aligned} \tag{1.1}$$

where the first two operators describe the kinetic energies of the electrons and the nuclei, the third is the Coulomb attraction between the electrons and the nuclei, and the last two are the Coulomb electron-electron and nuclear-nuclear repulsions. M_A and Z_A are the mass and atomic number of nucleus A, and r and R represent the distances between the electrons and the nuclei.

The Schrödinger equation involves the application of the Hamiltonian to the many-particle wavefunction. Its time-independent form is

$$\hat{H}\Psi = E\Psi \tag{1.2}$$

The Schrödinger equation is an example of an eigenvalue equation, because the result of applying the Hamiltonian operator to the wavefunction gives a constant E (the eigenvalue, in this case the total energy) multiplied by the original wavefunction. The wavefunction is said to be an eigenfunction of the Hamiltonian. For any given Hamiltonian there are an infinite number of eigenfunctions, each with a corresponding eigenvalue. The eigenfunction with the lowest eigenvalue (E_0) is known as the ground state wavefunction, Ψ_0, and E_0 is the ground state energy.

The problem of solving the Schrödinger equation is the central problem of quantum chemistry. By choosing this equation to solve, we have already made some approximations. For example, the Schrödinger equation ignores the effect of special relativity (a deficiency corrected by the more complex Dirac equation [2]), as well as other less relevant physical phenomena. Unfortunately, with the exception of very simple chemical systems, more approximations have to be made. The first of these is the Born-Oppenheimer approximation [3]. This recognises that the nuclei in the system move much more slowly than the electrons because they have a much larger mass, and assumes that the

electrons can be treated as if they are moving in a field of fixed nuclei. This approximation gives the electronic Schrödinger equation

$$\hat{H}_{\text{elec}}\Psi_{\text{elec}} = E_{\text{elec}}\Psi_{\text{elec}} \tag{1.3}$$

which takes the same form as the original Schrödinger equation but with a simplified Hamiltonian where the kinetic energy of the nuclei and the nuclear-nuclear repulsion terms have been removed, giving

$$\begin{aligned}\hat{H}_{\text{elec}} &= -\frac{1}{2}\sum_{i}^{N}\nabla_i^2 - \sum_{i}^{N}\sum_{A}^{M}\frac{Z_A}{r_{iA}} + \sum_{i}^{N}\sum_{j>i}^{N}\frac{1}{r_{ij}} \\ &= \hat{T} + \hat{V}_{\text{Ne}} + \hat{V}_{\text{ee}}\end{aligned} \tag{1.4}$$

The electronic wavefunction again has no physical meaning, though its square is a probability density. The solution to the electronic Schrödinger equation gives the electronic energy, to which the constant nuclear repulsion energy must be added to give the total energy

$$E_{\text{tot}} = E_{\text{elec}} + \sum_{A}^{M}\sum_{B>A}^{M}\frac{Z_A Z_B}{R_{AB}} \tag{1.5}$$

The total energy depends parametrically on the nuclear coordinates. By solving the electronic Schrödinger equation at various nuclear coordinates, a potential energy surface can be constructed. All calculations in this thesis are performed under the Born-Oppenheimer approximation, so all the wavefunctions we consider are electronic wavefunctions and from this point on we drop the 'elec' subscript for clarity.

Before the electronic Schrödinger equation can be solved, there remains the problem of the mathematical form of the wavefunction. It is here that the two competing approaches, wavefunction theory and density functional theory, diverge.

1.2 Wavefunction theory

Until the recent flourishing of density functional theory (DFT) for chemical applications, the dominant methods of quantum chemistry were those known collectively as wavefunction theory. These are all based ultimately on the Hartree-Fock approximation, which we describe below. Many of the concepts in this section reappear in density functional theory, but in a different context.

1.2.1 The variational principle

In the discussion of the Schrödinger equation above, it was assumed that the exact wavefunction was known. But if we only know an approximate wavefunction, $\tilde{\Psi}$, it will no longer be an eigenfunction of the Hamiltonian and there will be no eigenvalues associated with it. Instead, the expectation value of the Hamiltonian must be calculated

$$\tilde{E} = \int \tilde{\Psi}^* \hat{H} \tilde{\Psi} \mathrm{d}\tau \tag{1.6}$$

or in Dirac bra-ket notation

$$\tilde{E} = \langle \tilde{\Psi} | \hat{H} | \tilde{\Psi} \rangle \tag{1.7}$$

where $\tilde{\Psi}$ is an approximate (or trial) normalised wavefunction. The expectation value is an example of a function of a function, or a 'functional'. The link between this quantity and the exact ground state energy E_0 is provided by the variational principle [4], which states that

$$\tilde{E} \geq E_0 \quad \text{for any} \quad \tilde{\Psi} \tag{1.8}$$

Therefore we can be confident that the trial wavefunction that gives the lowest expectation value of the energy is the best approximation to the true wavefunction. If the true wavefunction was used as the trial wavefunction, then the expectation value would be equal to the exact ground state energy, E_0.

1.2.2 The antisymmetry principle

The variational principle shows how to evaluate the quality of an approximate wavefunction, but it does not give any clue to its mathematical form. The first clue is provided by electron spin. The wavefunction must depend on the coordinates of the electrons, which consist of three spatial coordinates $\mathbf{r}$ and one spin coordinate s (spin up or spin down). However, there is no reference to electron spin in the Hamiltonian of Eq. 1.4, and it is not inherently present in the Schrödinger equation at all (electron spin arises naturally only in the Dirac equation). However, the spin-dependence of the wavefunction can be deduced from the antisymmetry (or Pauli) principle of quantum mechanics [5], which states that an electronic wavefunction must be antisymmetric with respect to the interchange of the spatial and spin coordinates of any two electrons. That is

$$\Psi(\mathbf{x}_1, \ldots, \mathbf{x}_i, \ldots, \mathbf{x}_j, \ldots, \mathbf{x}_N) = -\Psi(\mathbf{x}_1, \ldots, \mathbf{x}_j, \ldots, \mathbf{x}_i, \ldots, \mathbf{x}_N) \tag{1.9}$$

where $\mathbf{x}$ denotes the four electron coordinates collectively. Any approximate wavefunction must satisfy the antisymmetry principle.

1.2.3 The orbital approximation

The orbital approximation assumes that the form of the many-electron wavefunction Ψ can be simplified by writing it in terms of one-electron wavefunctions called orbitals. To incorporate the effect of spin, the one-electron wavefunctions are written as spin orbitals $\chi(\mathbf{x})$, which are defined as

$$\chi(\mathbf{x}) = \begin{cases} \psi(\mathbf{r})\alpha(s) \\ \quad \text{or} \\ \psi(\mathbf{r})\beta(s) \end{cases} \tag{1.10}$$

where $\psi(\mathbf{r})$ is a spatial orbital and $\alpha(s)$ and $\beta(s)$ correspond to the up and down spin functions.

The simplest method of devising a many-electron wavefunction of this form is to consider what would happen if the electron-electron interactions were re-

moved from the Hamiltonian (giving a non-interacting system). The Hamiltonian can then be written as

$$\begin{aligned} \hat{H} &= -\frac{1}{2}\sum_{i}^{N}\nabla_i^2 - \sum_{i}^{N}\sum_{A}^{M}\frac{Z_A}{r_{iA}} \\ &= \sum_{i}^{N}\hat{h}(\mathbf{x}_i) \end{aligned} \tag{1.11}$$

where $\hat{h}(\mathbf{x}_i)$ is the core one-electron Hamiltonian for electron i. The simplest exact eigenfunction for a Hamiltonian which is a sum of one-electron operators is a product of one-electron spin orbitals, known as a Hartree product [6]

$$\Psi^{\mathrm{H}}(\mathbf{x}_1, \mathbf{x}_2, \ldots, \mathbf{x}_N) = \chi_1(\mathbf{x}_1)\chi_2(\mathbf{x}_2)\cdots\chi_N(\mathbf{x}_N)\,. \tag{1.12}$$

where the spin orbitals are eigenfunctions of $\hat{h}$. However, the Hartree product is not a useful approximation to the wavefunction because it does not satisfy the antisymmetry principle.

1.2.4 Hartree-Fock theory

Hartree-Fock theory [7] reconciles the orbital approximation and the antisymmetry principle by writing the wavefunction as a Slater determinant [8]

$$\Psi^{\mathrm{HF}}(\mathbf{x}_1, \mathbf{x}_2, \ldots, \mathbf{x}_N) = \frac{1}{\sqrt{N!}}\begin{vmatrix} \chi_1(\mathbf{x}_1) & \chi_2(\mathbf{x}_1) & \cdots & \chi_N(\mathbf{x}_1) \\ \chi_1(\mathbf{x}_2) & \chi_2(\mathbf{x}_2) & \cdots & \chi_N(\mathbf{x}_2) \\ \vdots & \vdots & & \vdots \\ \chi_1(\mathbf{x}_N) & \chi_2(\mathbf{x}_N) & \cdots & \chi_N(\mathbf{x}_N) \end{vmatrix} \tag{1.13}$$

In this case the interchange of coordinates of two electrons is equivalent to swapping two rows of the determinant, which by definition changes the sign of the wavefunction and therefore complies with the antisymmetry principle.

The expectation value of the Hamiltonian obtained using this wavefunction

is known as the Hartree-Fock energy, E^{HF}, and is given by

$$E^{\mathrm{HF}} = \sum_{i}^{N}(i|\hat{h}|i) + \frac{1}{2}\sum_{i}^{N}\sum_{j}^{N}[(ii|jj) - (ij|ji)] \tag{1.14}$$

where

$$(i|\hat{h}|i) = \int \chi_i^*(\mathbf{x}_1)\hat{h}(\mathbf{x}_1)\chi_i(\mathbf{x}_1)\mathrm{d}\mathbf{x}_1 \tag{1.15}$$

is a one-electron integral whose sum over the orbitals is the sum of the kinetic energy and the electron-nuclear interaction energy (and is the expectation value of the Hamiltonian defined in Eq. 1.11). The two-electron term consists of Coulomb integrals of the form

$$(ii|jj) = \iint \chi_i^*(\mathbf{x}_1)\chi_i(\mathbf{x}_1)\frac{1}{r_{12}}\chi_j^*(\mathbf{x}_2)\chi_j(\mathbf{x}_2)\mathrm{d}\mathbf{x}_1\mathrm{d}\mathbf{x}_2 \tag{1.16}$$

and exchange integrals

$$(ij|ji) = \iint \chi_i^*(\mathbf{x}_1)\chi_j(\mathbf{x}_1)\frac{1}{r_{12}}\chi_j^*(\mathbf{x}_2)\chi_i(\mathbf{x}_2)\mathrm{d}\mathbf{x}_1\mathrm{d}\mathbf{x}_2 \tag{1.17}$$

The Coulomb integrals correspond to the classical Coulomb interaction between the electrons, whereas the exchange integrals are a purely quantum-mechanical effect arising from the requirement that the wavefunction must be antisymmetric with respect to exchange of two electrons (if we had used a Hartree product as the wavefunction, the exchange term would not arise).

By the variational principle, we minimise E^{HF} with respect to the spin orbitals, under the constraint that they remain orthonormal. This results in the Hartree-Fock equations

$$\hat{F}\chi_i = \sum_{j}^{N}\varepsilon_{ij}\chi_j \tag{1.18}$$

Diagonalisation of the Lagrange multiplier matrix ε_{ij} gives the more usual canonical form

$$\hat{F}\chi_i = \varepsilon_i\chi_i \tag{1.19}$$

These are eigenvalue equations of the one-electron Fock operator, $\hat{F}$, which

can be written as

$$\hat{F} = \hat{h} + \hat{J} - \hat{K} \tag{1.20}$$

This is the sum of the core one-electron Hamiltonian and the two-electron Coulomb and exchange operators, which describe the average field experienced by electron i due to the other electrons in the system. The Coulomb operator is

$$\hat{J} = \sum_{j}^{N} \int \chi_j^*(\mathbf{x}_2) \frac{1}{r_{12}} \chi_j(\mathbf{x}_2) \mathrm{d}\mathbf{x}_2 \tag{1.21}$$

and the exchange operator (which, unlike the Coulomb operator, can only be defined by its effect on an orbital) is

$$\hat{K}\chi_i(\mathbf{x}_1) = \left[\sum_{j}^{N} \int \chi_j^*(\mathbf{x}_2) \frac{1}{r_{12}} \chi_i(\mathbf{x}_2) \mathrm{d}\mathbf{x}_2 \right] \chi_j(\mathbf{x}_1) \tag{1.22}$$

Following the Aufbau principle, the lowest N solutions of the Hartree-Fock equations are the occupied orbitals, each of which has a corresponding eigenvalue (the orbital energy). The Hartree-Fock ground state wavefunction Ψ_0^{HF} consists of a Slater determinant of these occupied orbitals as defined in Eq. 1.13, with the Hartree-Fock energy given by Eq. 1.14. In terms of computational cost, Hartree-Fock theory formally scales with system size N as N^4.

1.2.5 Electron correlation

The use of a Slater determinant as the wavefunction in Hartree-Fock theory is an approximation, and so by the variational principle the Hartree-Fock energy is higher than the exact energy by an amount known as the correlation energy [9], defined as

$$E_{\mathrm{C}}^{\mathrm{HF}} = E_0 - E^{\mathrm{HF}} \tag{1.23}$$

The correlation energy is traditionally divided into two contributions. Dynamic correlation is caused by instantaneous electron-electron interactions that the average Hartree-Fock treatment cannot model. The true wavefunction exhibits a cusp that represents the reduced probability of finding electrons close to each other. In Hartree-Fock theory this cusp is not modelled and the elec-

trons get too close together, raising the energy of the system.

Non-dynamic or left-right correlation occurs when a single Slater determinant is not sufficient to describe the system correctly. An example of this is the H_2 molecule under dissociation. The single determinant wavefunction for H_2 gives equal probability to one electron on each nucleus (i.e. $H \cdots H$) and both electrons on a single nucleus ($H^+ \cdots H^-$). This is acceptable at equilibrium geometries, but fails when the nuclei are far apart as the ionic contribution should be zero.

Methods that include correlation are called post-Hartree-Fock methods and work by expressing the wavefunction in terms of more than one Slater determinant. The N occupied orbitals are not the only orbitals that can be obtained by solving the Hartree-Fock equations. The Fock operator has an infinite number of eigenfunctions (orbitals). The lowest energy N solutions correspond to the N occupied orbitals from which the wavefunction is formed, whereas the solutions with higher energies are called virtual orbitals.

It is possible to construct Slater determinants from a combination of occupied and virtual orbitals. A determinant where one electron has been promoted from an occupied orbital χ_i to a virtual orbital χ_a is a singly excited determinant, Ψ_i^a. Similarly, a doubly excited determinant, Ψ_{ij}^{ab} involves the promotion of two electrons, and so on. These determinants are known as configuration state functions (CSFs). In principle, it is possible to write the many-electron wavefunction of any system exactly as a linear combination of CSFs

$$\Psi^{\mathrm{CI}} = c_0\Psi_0^{\mathrm{HF}} + \sum_{ia} c_i^a\Psi_i^a + \sum_{\substack{i<j\\a<b}} c_{ij}^{ab}\Psi_{ij}^{ab} + \sum_{\substack{i<j<k\\a<b<c}} c_{ijk}^{abc}\Psi_{ijk}^{abc} + \ldots \tag{1.24}$$

Configuration interaction (CI) expresses the wavefunction in this form, determining optimal expansion coefficients using the variational principle. In practice, only a limited number of virtual orbitals are available (see Section 1.4.2) and the number of possible CSFs is finite (but usually still very large). If all available CSFs are used to construct the wavefunction then the method is called full CI. Full CI is only feasible for very small systems, and so truncated CI methods which use only a subset of the CSFs are used as an alternative. Singly-excited determinants are denoted S, doubly-excited deter-

minants D, triply-excited determinants T, and so on. For example, the CISD method uses only singly- and doubly-excited determinants.

Truncated CI methods are problematic because they are not size-consistent, which means that the energy of a molecule at infinite dissociation will not be equal to the sum of the constituent fragments of the molecule. The quadratic CI (QCI) [10] and coupled cluster (CC) [11] methods are size-consistent alternatives. QCI forces size-consistency by introducing new terms which are quadratic in the configuration coefficients, whereas coupled cluster methods achieve the same result by expressing the wavefunction in terms of an exponential excitation operator. They are also named according to their truncation level, with examples including QCISD and CCSD. Higher level excitations are increasingly complex and are often calculated by perturbation methods, giving, for example, CCSD(T) (where the triple excitations are treated by perturbation theory). Brueckner theory [12] is a similar variant, and again comes in forms such as BD and BD(T).

The methods above use fixed spin orbitals derived from the solution of the Hartree-Fock equations. The multiconfiguration self-consistent field (MCSCF) method goes one step further by optimising the form of the spin orbitals at the same time as optimising the parameters in Eq. 1.24. This procedure increases the accuracy when only a limited number of CSFs are used. A popular variant is the complete active-space self-consistent field method (CASSCF) [13]. It is also possible to do configuration interaction using an MCSCF wavefunction, a method known as multireference configuration interaction (MRCI) [14].

In general, these methods have a very high computational cost. Full CI grows exponentially with system size and so it is only feasible for extremely small systems. Truncated methods are less costly but still very expensive compared to Hartree-Fock. For example, methods such as CCSD and BD scale with system size as N^6, whereas the higher level CCSD(T) scales as N^7, and the still more accurate CCSDT scales as N^8.

An alternative approach is to apply many-body perturbation theory to the Hartree-Fock Hamiltonian, which is known as Møller-Plesset perturbation theory [15]. The Hartree-Fock Hamiltonian, $\hat{H}^{\mathrm{HF}}$, is defined as the sum of the

one-electron Fock operators

$$\hat{H}^{\mathrm{HF}} = \sum_{i}^{N} \hat{F}(\mathbf{x}_i) \tag{1.25}$$

That is, the two electron terms of the form $1/r_{ij}$ in the true Hamiltonian have been replaced by the Coulomb and exchange terms in the Fock operator. This can be thought of as the exact Hamiltonian of a fictional non-interacting system. The Hartree-Fock ground state wavefunction is not an eigenfunction of the true Hamiltonian (as it is an approximation to the exact wavefunction) but it is an eigenfunction of the Hartree-Fock Hamiltonian, so

$$\hat{H}^{\mathrm{HF}}\Psi^{\mathrm{HF}} = E^0\Psi^{\mathrm{HF}} \tag{1.26}$$

where the eigenvalue of this equation (E^0) is the sum of the orbital energies

$$\begin{aligned} E^0 &= \sum_{i}^{N} \varepsilon_i \\ &= \langle \Psi^{\mathrm{HF}} | \hat{H}^{\mathrm{HF}} | \Psi^{\mathrm{HF}} \rangle \end{aligned} \tag{1.27}$$

Note this is not the same as the Hartree-Fock energy E^{HF}, which is the expectation value of the true Hamiltonian. The difference between the true Hamiltonian and the Hartree-Fock Hamiltonian can be considered to be a perturbation, $\hat{H}^1$:

$$\begin{aligned} \hat{H}^1 &= \hat{H} - \hat{H}^{\mathrm{HF}} \\ &= \hat{H} - \sum_{i}^{N} \hat{F}(\mathbf{x}_i) \end{aligned} \tag{1.28}$$

If the Hamiltonian is perturbed, the wavefunction and energy will also be perturbed, giving expansions of the form

$$\Psi = \Psi^{\mathrm{HF}} + \lambda\Psi^1 + \lambda^2\Psi^2 + \ldots \tag{1.29}$$

$$E = E^0 + \lambda E^1 + \lambda^2 E^2 + \ldots \tag{1.30}$$

where λ is an ordering parameter. By substituting these expansions into the

Schrödinger equation and collecting terms of the same order, the first order correction to the energy can be written as

$$E^1 = \langle \Psi^{\mathrm{HF}} | \hat{H}^1 | \Psi^{\mathrm{HF}} \rangle \tag{1.31}$$

The Hartree-Fock energy is

$$\begin{aligned} E^{\mathrm{HF}} &= \langle \Psi^{\mathrm{HF}} | \hat{H} | \Psi^{\mathrm{HF}} \rangle \\ &= \langle \Psi^{\mathrm{HF}} | \hat{H}^{\mathrm{HF}} + \hat{H}^1 | \Psi^{\mathrm{HF}} \rangle \\ &= \langle \Psi^{\mathrm{HF}} | \hat{H}^{\mathrm{HF}} | \Psi^{\mathrm{HF}} \rangle + \langle \Psi^{\mathrm{HF}} | \hat{H}^1 | \Psi^{\mathrm{HF}} \rangle \\ &= E^0 + E^1 \end{aligned} \tag{1.32}$$

Therefore the Hartree-Fock energy already includes the first perturbation correction to the 'unperturbed energy' E^0. The first correction to the Hartree-Fock energy therefore occurs at the second-order perturbation correction, E^2

$$E^2 = -\frac{1}{4} \sum_{ijab} \frac{[(ai|bj) - (aj|bi)]^2}{\varepsilon_a + \varepsilon_b - \varepsilon_i - \varepsilon_j} \tag{1.33}$$

MP2 theory involves the calculation of this correction, as well as similar corrections to the wavefunction. It formally scales as N^5. Higher-order corrections can be calculated, giving MP3, MP4, etc., which scale as N^6, N^7, and so on. MP theory is size-consistent at all levels, but it is not variational, so the corrections can result in energies below the exact energy.

1.3 Density functional theory

Density functional theory (DFT) presents a radically different approach to handling the electronic Schrödinger equation. Instead of calculating the electronic energy by determining an approximate wavefunction, the energy is written in terms of the electron density, $\rho(\mathbf{r}_1)$, defined as

$$\rho(\mathbf{r}_1) = N \int \dots \int |\Psi(\mathbf{x}_1, \mathbf{x}_2 \dots \mathbf{x}_N)|^2 \mathrm{d}s_1 \mathrm{d}\mathbf{x}_2 \dots \mathrm{d}\mathbf{x}_N \tag{1.34}$$

The electron density has only 3 dimensions, those of space, and is therefore far more easily visualised than the wavefunction. The electron density integrates to the total number of electrons, and has cusps at the locations of the nuclei, the slopes of which are related to their charge. As observed by Bright-Wilson [16], the density therefore appears to contain all the information required to write the Hamiltonian of Eq. 1.4 and hence the electronic wavefunction. The task remains to write the electronic energy in terms of the density.

1.3.1 Early models

The earliest density functional theories were written in 1927 by Thomas [17] and Fermi [18]. They formulated the kinetic energy of an atom as a functional of the electron density based on the uniform electron gas (UEG) approximation. The UEG is an imaginary infinite system in which the electron density has a constant value everywhere in space, with a similarly uniform positive charge background to make the system neutral. Although this system is unrealistic as an approximation to the highly inhomogeneous densities of atoms and molecules, it does provide an analytical expression for the kinetic energy. The Thomas-Fermi (TF) theory treats the nuclear-electron and electron-electron interactions classically, giving the atomic energy

$$E^{\mathrm{TF}}[\rho] = \frac{3}{10}(3\pi^2)^{2/3}\int \rho^{5/3}(\mathbf{r})\mathrm{d}\mathbf{r} - Z\int \frac{\rho(\mathbf{r})}{r}\mathrm{d}\mathbf{r} + \frac{1}{2}\iint \frac{\rho(\mathbf{r}_1)\rho(\mathbf{r}_2)}{r_{12}}\mathrm{d}\mathbf{r}_1\mathrm{d}\mathbf{r}_2 \quad (1.35)$$

The first term is the kinetic energy functional, the second the nuclear-electron interaction (where Z is the nuclear charge) and the third is the classical Coulomb interaction.

Although crude, this model was the first to describe the energy of an atom solely in terms of functionals of the electron density. However, it is not useful for chemical calculations because it neglects quantum effects such as exchange and correlation and the kinetic energy model gives large errors for real systems. It can also be proved that no molecule is stable relative to its fragments in Thomas-Fermi theory [19].

Thomas-Fermi theory can be improved by adding a term for the exchange

energy, which was derived for the uniform electron gas by Dirac [20]

$$E_{\mathrm{X}}[\rho] = -\frac{3}{4}\left(\frac{3}{\pi}\right)^{1/3}\int \rho(\mathbf{r})^{4/3}\mathrm{d}\mathbf{r} \tag{1.36}$$

This additional term gives the Thomas-Fermi-Dirac (TFD) model. A similar term was derived by Slater in the context of wavefunction methods [21]. Slater modelled the complicated, non-local exchange contribution to Hartree-Fock theory using a similar form to Eq. 1.36, but with the addition of a semi-empirical parameter α that was generally set to give a more negative prefactor than Dirac's. This was known as the X_α or Hartree-Fock-Slater method.

Although the TFD model is an improvement over the original TF theory, it is still not useful for chemical systems due to the large error in the kinetic energy (it is difficult to deduce how the kinetic energy can be found from knowledge only of the electron density at a point). It is however possible to improve upon this model without discarding the exact result from the UEG. The Thomas-Fermi kinetic energy expression can be thought of as the first term in a Taylor expansion. A second term can then be derived which involves the gradient of the density. As the gradient is zero for the UEG, the result will still be exact in this limit. The gradient-corrected term is known as the Weizsacker correction [22], and is of the form

$$T^{\mathrm{W}}[\rho] = \frac{1}{8}\int \frac{|\nabla\rho(\mathbf{r})|^2}{\rho(\mathbf{r})}\mathrm{d}\mathbf{r} \tag{1.37}$$

Incorporating this term gives the Thomas-Fermi-Dirac-Weizsacker (TFDW) functional. Although this is an improvement, it still gives relatively poor results, and higher order corrections do not offer much further improvement [23].

1.3.2 The Hohenberg-Kohn theorems

Density functional theory was put on a firm theoretical foundation by the theorems of Hohenberg and Kohn in 1964 [24]. The first Hohenberg-Kohn

theorem relates to the nuclear-electron interaction potential

$$v_{\text{ext}}(\mathbf{r}_i) = -\sum_{A}^{M} \frac{Z_A}{r_{iA}} \tag{1.38}$$

which is also known as the external potential. The theorem proves that the external potential is uniquely determined, up to a constant, by $\rho(\mathbf{r})$.

The proof considers two external potentials, v_{ext} and v'_{ext}, which share the same ground state density. These correspond to different Hamiltonians $\hat{H}$ and $\hat{H}'$, ground state wavefunctions Ψ and Ψ', and ground state energies E_0 and E'_0. If Ψ' is used as a trial wavefunction for $\hat{H}$, then by the variational principle

$$\begin{aligned} E_0 < \langle \Psi' | \hat{H} | \Psi' \rangle &= \langle \Psi' | \hat{H}' | \Psi' \rangle + \langle \Psi' | \hat{H} - \hat{H}' | \Psi' \rangle \\ &= E'_0 + \int \rho(\mathbf{r})[v_{\text{ext}}(\mathbf{r}) - v'_{\text{ext}}(\mathbf{r})]\mathrm{d}\mathbf{r} \end{aligned} \tag{1.39}$$

We can also use Ψ as a trial wavefunction for $\hat{H}'$, giving

$$E'_0 < E_0 - \int \rho(\mathbf{r})[v_{\text{ext}}(\mathbf{r}) - v'_{\text{ext}}(\mathbf{r})]\mathrm{d}\mathbf{r} \tag{1.40}$$

By adding the inequalities we get the contradiction that $E_0 + E'_0 < E'_0 + E_0$, proving the theorem. The density therefore completely determines the Hamiltonian of Eq. 1.4 and hence the ground state wavefunction, and so the electronic energy can be written in terms of functionals of the density

$$E[\rho] = T[\rho] + V_{\text{Ne}}[\rho] + V_{\text{ee}}[\rho] \tag{1.41}$$

The second Hohenberg-Kohn theorem provides a DFT version of the variational principle

$$E[\tilde{\rho}] \geq E_0 \quad \text{for any} \quad \tilde{\rho} \tag{1.42}$$

The energy obtained from the functional of $\rho(\mathbf{r})$ will be equal to the exact ground state energy if the trial density $\tilde{\rho}(\mathbf{r})$ is equal to the true ground state density.

1.3.3 Kohn-Sham DFT

The Hohenberg-Kohn theorems prove that it is possible to write the electronic energy as a functional of the density, but it does not give any indication what the mathematical form of the functional is. The major problem of the Thomas-Fermi theory was its poor approximation to the kinetic energy, and it was this problem that was addressed by Kohn and Sham in 1965 [25].

The Kohn-Sham approach is based on the concept of a fictional non-interacting system of electrons, for which the exact kinetic energy is given by

$$T_{\mathrm{s}} = -\frac{1}{2}\sum_{i}^{N}\langle\chi_i|\nabla^2|\chi_i\rangle \tag{1.43}$$

and the electron density is

$$\rho_{\mathrm{s}}(\mathbf{r}) = \sum_{i}^{N}|\chi_i(\mathbf{r})|^2 \tag{1.44}$$

A non-interacting reference system is set up, with a Hamiltonian of the form

$$\hat{H}_{\mathrm{s}} = -\frac{1}{2}\sum_{i}^{N}\nabla_i^2 + \sum_{i}^{N}v_{\mathrm{s}}(\mathbf{r}) \tag{1.45}$$

which combines the kinetic energy operator with an effective potential v_{s}, which is chosen such that ρ_{s} is equal to the density ρ of the fully-interacting system. The exact wavefunction of the non-interacting system can be written as a Slater determinant consisting of Kohn-Sham orbitals. These orbitals are determined by a set of one-electron equations of a form similar to the Hartree-Fock equations

$$\left[-\frac{1}{2}\nabla^2 + v_{\mathrm{s}}(\mathbf{r})\right]\chi_i(\mathbf{r}) = \varepsilon_i\chi_i(\mathbf{r}) \tag{1.46}$$

In Kohn-Sham DFT, the kinetic energy of the non-interacting system, T_{s}, is used as an approximation to the kinetic energy of the real system, T. Although this way of calculating the kinetic energy is still not exact, it is much more accurate than the Thomas-Fermi approach. The electronic energy of Eq. 1.41 is rewritten as

$$E[\rho] = T_{\mathrm{s}}[\rho] + V_{\mathrm{Ne}}[\rho] + J[\rho] + E_{\mathrm{XC}}[\rho] \tag{1.47}$$

where the electron-electron interaction has been split into the known Coulomb part J and the unknown exchange-correlation energy E_{XC}, which includes the exchange and correlation energies familiar from Hartree-Fock theory as well as the small residual error in the kinetic energy

$$E_{\mathrm{XC}}[\rho] = (T[\rho] - T_{\mathrm{s}}[\rho]) + (V_{\mathrm{ee}}[\rho] - J[\rho]) \tag{1.48}$$

The form of the energy is therefore given by

$$\begin{aligned} E[\rho] &= -\frac{1}{2}\sum_{i}^{N}\langle\chi_i|\nabla^2|\chi_i\rangle + \int v_{\mathrm{ext}}(\mathbf{r}_1)\rho(\mathbf{r}_1)\mathrm{d}\mathbf{r}_1 \\ &\quad + \frac{1}{2}\iint \frac{\rho(\mathbf{r}_1)\rho(\mathbf{r}_2)}{r_{12}}\mathrm{d}\mathbf{r}_1\mathrm{d}\mathbf{r}_2 + E_{\mathrm{XC}}[\rho] \end{aligned} \tag{1.49}$$

where $\rho(\mathbf{r})$ is related to the Kohn-Sham orbitals by Eq. 1.44. In the notation of Eq. 1.14, this is

$$E^{\mathrm{KS}} = \sum_{i}^{N}(i|\hat{h}|i) + \frac{1}{2}\sum_{i}^{N}\sum_{j}^{N}(ii|jj) + E_{\mathrm{XC}}[\rho] \tag{1.50}$$

As in Hartree-Fock theory, this energy is minimised with respect to the orbitals according to the variational principle, giving the Kohn-Sham equations

$$\left(-\frac{1}{2}\nabla^2 + v_{\mathrm{ext}}(\mathbf{r}_1) + \int \frac{\rho(\mathbf{r}_2)}{r_{12}}\mathrm{d}\mathbf{r}_2 + v_{\mathrm{XC}}(\mathbf{r}_1)\right)\chi_i = \varepsilon_i\chi_i \tag{1.51}$$

with an effective potential given by

$$v_{\mathrm{eff}}(\mathbf{r}_1) = v_{\mathrm{ext}}(\mathbf{r}_1) + \int \frac{\rho(\mathbf{r}_2)}{r_{12}}\mathrm{d}\mathbf{r}_2 + v_{\mathrm{XC}}(\mathbf{r}_1) \tag{1.52}$$

The potential v_s of the non-interacting system is defined as the v_{eff} of the real system. The only unknown term is the exchange-correlation potential, v_{XC}, defined as the functional derivative of E_{XC} with respect to the density:

$$v_{\mathrm{XC}}(\mathbf{r}_1) = \frac{\delta E_{\mathrm{XC}}[\rho]}{\delta\rho(\mathbf{r}_1)} \tag{1.53}$$

The Kohn-Sham equations are exact in principle. However, the exact form of E_{XC} is not known and so in practice the theory is approximate.

Kohn-Sham DFT formally scales as N^4, although this can be reduced to N^2 and even to linear scaling by calculating the Coulomb term in a computationally efficient way.

1.3.4 Exchange-correlation functionals

In order to use the Kohn-Sham scheme for practical calculations, the exchange-correlation (XC) functional must be approximated. Generally, E_{XC} is split into exchange and correlation components which are approximated separately

$$E_{\mathrm{XC}} = E_{\mathrm{X}} + E_{\mathrm{C}} \tag{1.54}$$

The usual starting point for making these approximations is the uniform electron gas.

The local density approximation

The local density approximation (LDA) is based on the uniform electron gas model. The principle of the LDA is that the energy contribution of a point can be expressed as a local functional of the density (unlike, for example, the Coulomb energy, which depends on the density at every point in space). We have already seen its use in the TFD theory for the kinetic and exchange energies. The Kohn-Sham method uses a different approach for the kinetic energy, but it retains the Dirac expression for exchange. The LDA approximation to E_{XC} is defined as

$$E_{\mathrm{XC}}^{\mathrm{LDA}}[\rho] = \int \rho(\mathbf{r})\varepsilon_{\mathrm{XC}}(\rho(\mathbf{r}))\mathrm{d}\mathbf{r} \tag{1.55}$$

where $\varepsilon_{\mathrm{XC}}(\rho(\mathbf{r}))$ is the XC energy per electron, which is weighted with the probability density $\rho(\mathbf{r})$ of an electron being at the point in space concerned. $\varepsilon_{\mathrm{XC}}(\rho(\mathbf{r}))$ can be split into exchange (ε_{X}) and correlation (ε_{C}) components. The exchange part is given by the Dirac expression, i.e.

$$\varepsilon_{\mathrm{X}} = -\frac{3}{4}\left(\frac{3}{\pi}\right)^{1/3}\rho(\mathbf{r})^{1/3} \tag{1.56}$$

Correlation in the UEG cannot be expressed in such a simple analytic form. However, it was approximated to high accuracy by Ceperley and Alder [26] using quantum Monte-Carlo simulations. This was then converted into an analytic expression involving spin densities by Vosko, Wilk, and Nusair (VWN) [27]. Other representations of the correlation energy exist [28–31], but VWN is the most popular.

LDA exchange can also be expressed in terms of spin densities

$$\varepsilon_{\mathrm{X}} = -2^{1/3}\frac{3}{4}\left(\frac{3}{\pi}\right)^{1/3}\sum_{\sigma}\int \rho_{\sigma}(\mathbf{r})^{1/3}\mathrm{d}\mathbf{r} \tag{1.57}$$

where the sum is over the α and β spin densities. By the Hohenberg-Kohn theorem, it is not necessary to write the functional in terms of spin densities to get an exact answer, but in practice this approach offers more flexibility in the approximate form. When we refer to the LDA in this study, we combine the unrestricted LDA exchange form with VWN correlation.

Although LDA is a very drastic approximation for atoms and molecules, its performance in practice is surprisingly good [32]. In general, it gives reasonable vibrational frequencies and molecular structures (though bond lengths are consistently too long). However, LDA considerably overbinds molecules [33].

The generalised gradient approximation

Whilst the performance of LDA is better than expected, it is still not nearly of sufficient accuracy for chemical calculations. Fortunately, gradient corrections for LDA exchange can be derived in much the same way as the Weizsacker correction for the kinetic energy. The first such correction gives the Gradient Expansion Approximation (GEA) exchange functional [24, 34, 35]

$$E_{\mathrm{X}}^{\mathrm{GEA}} = E_{\mathrm{X}}^{\mathrm{LDA}} - \frac{7}{432\pi(6\pi^2)^{1/3}}\sum_{\sigma}\int \frac{|\nabla\rho_{\sigma}|^2}{\rho_{\sigma}^{4/3}}\mathrm{d}\mathbf{r} \tag{1.58}$$

Unfortunately, the GEA suffers from the severe problem that its potential diverges at long range. To counteract this the GEA can be multiplied by some

function of the reduced density gradient x_σ,

$$x_\sigma = \frac{|\nabla\rho_\sigma|}{\rho_\sigma^{4/3}} \tag{1.59}$$

The form of x_σ is such that a multiplication by any $f(x_\sigma)$ will still satisfy the exact exchange scaling condition

$$E_{\mathrm{X}}[\rho_\lambda] \;=\; \lambda E_{\mathrm{X}}[\rho] \tag{1.60}$$

where

$$\rho_\lambda(\mathbf{r}) \;=\; \lambda^3\rho(\lambda\mathbf{r}) \tag{1.61}$$

Functionals that modify the GEA in this way are known as generalised gradient approximations (GGAs). One of the most simple and popular GGA exchange forms was proposed by Becke in 1986 [33]

$$E_{\mathrm{X}}^{\mathrm{B86}} = E_{\mathrm{X}}^{\mathrm{LDA}} + \beta\sum_\sigma \int \frac{|\nabla\rho_\sigma|^2}{\rho_\sigma^{4/3}}\left(\frac{1}{1+\gamma x_\sigma^2}\right)\mathrm{d}\mathbf{r} \tag{1.62}$$

where the semi-empirical parameters are $\beta = -0.0036$ and $\gamma = 0.004$. At short range, $x_\sigma \to 0$, so the functional will behave like the GEA. At long range, when x_σ diverges, the functional collapses to LDA, so it does not suffer from the divergence problems of the GEA. However, behaving as the LDA at long-range is still not correct. Therefore Becke proposed another functional [36] that provided the correct asymptotic behaviour of the energy density

$$E_{\mathrm{X}}^{\mathrm{B88}} = E_{\mathrm{X}}^{\mathrm{LDA}} + \beta\sum_\sigma \int \rho_\sigma^{4/3}\frac{x_\sigma^2}{(1-6\beta x_\sigma \sinh^{-1} x_\sigma)}\mathrm{d}\mathbf{r} \tag{1.63}$$

where $\beta = -0.0042$ is determined by fitting to exact exchange energies. However, although it gives the correct asymptotic behaviour of the energy density, the XC potential from this functional is still not correct—it does not decay with the correct r^{-1} distance dependence.

Other GGA exchange functionals exist, usually with a more complex form for $f(x_\sigma)$ [37–50]. However, B86 and B88 are by far the most popular. B86

exchange is also the basis of Becke's 1997 [43] functional, which is a power-series expansion

$$E_{\mathrm{X}}^{\mathrm{B97}} = \sum_{\sigma} \int \varepsilon_{\mathrm{X}}^{\mathrm{LDA}} f(x_\sigma) \mathrm{d}\mathbf{r} \tag{1.64}$$

$$f(x_\sigma) = \sum_{i=0}^{m} c_{\sigma,i} \left(\frac{\gamma x_\sigma^2}{1+\gamma x_\sigma^2} \right)^i \tag{1.65}$$

where $\gamma = 0.004$. The B97 functional form is very flexible and its parameters can be fitted in a number of ways. It forms the basis of the B97-1 [47], B97-2 [51], HCTH [47] and 1/4 [50] functionals, and the OPTX [49] functional uses the $i = 2$ term in isolation (with a value of $\gamma = 0.006$).

An alternative approach is to devise a mathematical form that satisfies certain exact conditions [37, 40]. In these functionals there are no adjustable parameters. An example is the Perdew-Burke-Ernzerhof (PBE) functional [40], which uses the same exchange form as B86, but determines the parameters to conform with as many exact conditions as possible, rather than by a fit to exact data. Although this approach would seem to have a greater validity from a theoretical viewpoint, Becke has argued that both approaches to approximate DFT are equally valid [43] because we are trying to approximate an exact form which is known to exist from the Hohenberg-Kohn theorems. However, Perdew argues that such fitted functionals are unsatisfactory [52] because they may have no validity outside the systems they are fitted to. The functionals developed in this study all take the semi-empirical, adjustable approach.

The correlation functional can be gradient corrected in the same way as the exchange functional [53–57]. Popular correlation functionals include Perdew's P86 functional [53] and Perdew and Wang's PW91 functional [38]. Probably the best known is the LYP functional of Lee, Yang and Parr [55]. LYP goes beyond the uniform electron gas model because it is based on the analysis of Colle and Salvetti [58] of the correlation of the helium atom. Another popular gradient-corrected correlation functional is the PBE correlation functional [40], which is a non-empirical correlation functional used in the PBE GGA. Again, it is also possible to expand the correlation energy as a power series. An example is the B97 functional form, which is an expansion based on the PW91

correlation functional.

Any number of GGAs can be created by mixing and matching exchange and correlation functionals. Their names are usually taken from the constituent functionals, such as BLYP (B88 exchange and LYP correlation), OLYP (OPTX exchange and LYP correlation), BP86, and so on.

Meta-GGAs

Higher order gradient corrections to the exchange-correlation functional are possible. Again, they need to be carefully formulated to avoid divergence problems. The next derivative after the gradient is the Laplacian, $\nabla^2\rho$, and a number of functionals have been developed to incorporate this [59–61]. However, the Laplacian is a more numerically unstable quantity than the gradient and can pose problems from a computational viewpoint [62]. These functionals and others also often incorporate another new quantity, the non-interacting kinetic energy density

$$\tau_\sigma = \frac{1}{2}\sum_i^N |\nabla\psi_{i,\sigma}(\mathbf{r})|^2 \tag{1.66}$$

Functionals that incorporate either of the above quantities are collectively termed meta-GGAs. Non-empirical examples include PKZB [52] and TPSS [63], whereas VSXC [64] is a semi-empirical meta-GGA. Results obtained have been encouraging, although it is not clear whether they offer any significant improvement.

Hybrid functionals

A different approach to improving the GGA is to combine exact (i.e. Hartree-Fock) exchange with density functional correlation. This is known as Hartree-Fock-Kohn-Sham (HFKS) theory [25]. Although this seems like a natural approach to take, it does not work with standard DFT correlation functionals [65] because they only take into account dynamical correlation. Left-right correlation is handled by the local exchange functional, but Hartree-Fock exchange does not take into account this type of correlation and so new correlation functionals would have to be developed for a successful HFKS theory.

A more fruitful approach is to combine a fraction of exact Hartree-Fock exchange with a GGA functional, giving a so-called hybrid functional

$$E_{\mathrm{XC}}^{\mathrm{GGA}} = E_{\mathrm{X}}^{\mathrm{GGA}} + E_{\mathrm{C}}^{\mathrm{GGA}} + \alpha E_{\mathrm{X}}^{\mathrm{HF}} \tag{1.67}$$

The first hybrid functional was the 'half and half' method developed by Becke [66], which mixed 50% B88 exchange with 50% exact exchange, a fraction derived from the adiabatic connection formula [67]. A large fraction of exact exchange is known to give good results for kinetics calculations [68], but for all-round performance a smaller fraction is preferable.

The most popular hybrid functional is the three-parameter B3LYP [69, 70], which combines variable LDA exchange and correlation parameters, B88 exchange, LYP correlation and 21% exact exchange

$$E_{\mathrm{XC}}^{\mathrm{B3LYP}} = (1-\alpha)E_{\mathrm{X}}^{\mathrm{LDA}} + \alpha E_{\mathrm{X}}^{\mathrm{HF}} + \beta E_{\mathrm{X}}^{\mathrm{B88}} + \delta E_{\mathrm{C}}^{\mathrm{LYP}} + (1-\delta)E_{\mathrm{C}}^{\mathrm{VWN}} \tag{1.68}$$

Other hybrid functionals include the B97 series of functionals, all of which combine the B97 expansion with a fraction (19%-21%) of exact exchange [43, 47, 51].

Hybrid functionals generally perform better than GGAs for most properties. However, whether the mixing is theoretically justified is not clear. The good performance may simply be due to a cancellation of errors, though Perdew *et al.* used a perturbation theory argument to justify the inclusion of 25% exact exchange in hybrid functionals [71]. This figure has been used in the non-empirical PBE0 hybrid functional (based on the PBE GGA) [72].

It is also possible to devise hybrid meta-GGA functionals. Examples include the TPSS hybrid [63] and several functionals devised for kinetics calculations [73–75]. DFT can even be mixed with higher-level wavefunction theory to give doubly-hybrid functionals [76] although this loses the computational cost advantage of DFT.

1.4 Solving the equations

This section deals with the computational aspects of solving the Hartree-Fock (HF) or Kohn-Sham (KS) equations. Despite their different theoretical foundations, the equations themselves and hence the details of implementation are very similar. This is especially true for programs originally written for Hartree-Fock theory that were modified for DFT calculations, such as two of the packages used in this thesis: CADPAC [77] and DALTON [78].

1.4.1 Closed shell calculations

The first question that arises when considering a computational implementation is the form of the spin orbitals. Spin orbitals can be either restricted or unrestricted. Restricted spin orbitals are constrained to have the same spatial orbital for both the α and β spin functions, whereas the spatial orbitals in unrestricted spin orbitals are free to vary. Restricted calculations are usually performed on closed shell systems (where the number of α and β electrons are equal), though restricted open shell calculations are also possible.

For both types of calculation, the HF/KS equations have to be integrated over the spin functions. For closed shell restricted calculations the equations remain of the form

$$\hat{F}\psi_i = \varepsilon_i \psi_i \tag{1.69}$$

with spatial orbitals replacing the spin orbitals and a factor of a half occurring in the exchange operator. The corresponding energies are

$$E^{\mathrm{HF}} = 2\sum_{i}^{N/2}(i|\hat{h}|i) + \sum_{i}^{N/2}\sum_{j}^{N/2}[2(ii|jj) - (ij|ji)] \tag{1.70}$$

$$E^{\mathrm{KS}} = 2\sum_{i}^{N/2}(i|\hat{h}|i) + \sum_{i}^{N/2}\sum_{j}^{N/2}2(ii|jj) + E_{\mathrm{XC}}[\rho] \tag{1.71}$$

1.4.2 Introducing a basis

The form of the spatial orbitals now has to be defined. The orbitals are expanded in a set of basis functions $\{\phi_v\}$

$$\psi_i = \sum_v^K c_{vi}\phi_v \tag{1.72}$$

A natural choice of molecular basis is a linear combination of atomic orbitals (LCAO), but in practice any set of basis functions can be used. The form of the spatial orbitals is then substituted into the HF/KS equations

$$\hat{F}(\mathbf{r}_1)\sum_v^K c_{vi}\phi_v(\mathbf{r}_1) = \varepsilon_i \sum_v^K c_{vi}\phi_v(\mathbf{r}_1) \tag{1.73}$$

The equations are then multiplied on the left by another basis function $\phi_\mu^*(\mathbf{r}_1)$ and integrated to give K equations, forming a matrix equation running from $i = 1$ to K

$$\sum_v^K c_{vi}\int \phi_\mu^*(\mathbf{r}_1)\hat{F}(\mathbf{r}_1)\phi_v(\mathbf{r}_1)\mathrm{d}\mathbf{r}_1 = \varepsilon_i \sum_v^K c_{vi}\int \phi_\mu^*(\mathbf{r}_1)\phi_v(\mathbf{r}_1)\mathrm{d}\mathbf{r}_1 \tag{1.74}$$

In the context of Hartree-Fock theory these are known as the Roothaan-Hall equations [79, 80], and they apply equally to Kohn-Sham theory. The matrix $\mathbf{F}$ (the Fock matrix in HF theory, or the Kohn-Sham matrix in KS theory), has elements defined as

$$F_{\mu v} = \int \phi_\mu^*(\mathbf{r}_1)\hat{F}(\mathbf{r}_1)\phi_v(\mathbf{r}_1)\mathrm{d}\mathbf{r}_1 \tag{1.75}$$

and the overlap matrix $\mathbf{S}$ is

$$S_{\mu v} = \int \phi_\mu^*(\mathbf{r}_1)\phi_v(\mathbf{r}_1)\mathrm{d}\mathbf{r}_1 \tag{1.76}$$

Another matrix $\mathbf{C}$ defines the basis expansion coefficients C_{vi}, and $\boldsymbol{\varepsilon}$ defines a diagonal matrix of the orbital energies. The matrix equation can then be written as

$$\mathbf{FC} = \mathbf{SC}\boldsymbol{\varepsilon} \tag{1.77}$$

where

$$F_{\mu v}^{\mathrm{HF}} = H_{\mu v}^{\mathrm{core}} + \sum_{\lambda}^{K}\sum_{\sigma}^{K} P_{\lambda\sigma}\left[(\mu v|\sigma\lambda) - \frac{1}{2}(\mu\lambda|\sigma v)\right] \tag{1.78}$$

$$F_{\mu v}^{\mathrm{KS}} = H_{\mu v}^{\mathrm{core}} + \sum_{\lambda}^{K}\sum_{\sigma}^{K} P_{\lambda\sigma}(\mu v|\sigma\lambda) + V_{\mu v}^{\mathrm{XC}} \tag{1.79}$$

where the one electron terms are grouped into the core-Hamiltonian matrix

$$H_{\mu v}^{\mathrm{core}} = \int \phi_{\mu}^{*}(\mathbf{r}_1)\left[-\frac{1}{2}\nabla^2 - \sum_{A}^{M}\frac{Z_A}{r_{1A}}\right]\phi_v(\mathbf{r}_1)\mathrm{d}\mathbf{r}_1 \tag{1.80}$$

and the two electron terms are

$$(\mu v|\lambda\sigma) = \iint \phi_{\mu}^{*}(\mathbf{r}_1)\phi_v(\mathbf{r}_1)\frac{1}{r_{12}}\phi_{\lambda}^{*}(\mathbf{r}_2)\phi_{\sigma}(\mathbf{r}_2)\mathrm{d}\mathbf{r}_1\mathrm{d}\mathbf{r}_2 \tag{1.81}$$

with the density matrix

$$P_{\mu v} = 2\sum_{i}^{N/2} c_{\mu i}c_{vi}^{*} \tag{1.82}$$

It is the two electron terms that are responsible for the N^4 scaling of Hartree-Fock and Kohn-Sham theory.

There is one extra term in the Kohn-Sham matrix that replaces the Hartree-Fock exchange term with an exchange-correlation integral

$$V_{\mu v}^{\mathrm{XC}} = \int \phi_{\mu}^{*}(\mathbf{r}_1)v_{\mathrm{XC}}(\mathbf{r}_1)\phi_v(\mathbf{r}_1)\mathrm{d}\mathbf{r}_1 \tag{1.83}$$

Unlike the other matrix elements which are evaluated analytically, the form of V_{XC} is far too complex for $V_{\mu v}^{\mathrm{XC}}$ to be evaluated in that way. It is therefore evaluated numerically on a grid [81, 82]. For a GGA functional, $V_{\mu v}^{\mathrm{XC}}$ can alternatively be reformulated as

$$V_{\mu v}^{\mathrm{XC}} = \int \phi_{\mu}^{*}(\mathbf{r}_1)\frac{\partial F_{\mathrm{XC}}}{\partial\rho}\phi_v(\mathbf{r}_1)\mathrm{d}\mathbf{r}_1 + \int \frac{\partial F_{\mathrm{XC}}}{\partial\nabla\rho}\cdot\nabla[\phi_{\mu}^{*}(\mathbf{r}_1)\phi_v(\mathbf{r}_1)]\mathrm{d}\mathbf{r}_1 \tag{1.84}$$

Eqs. 1.83 and 1.84 are formally equivalent in the limit of an infinite grid.

1.4.3 Open shell calculations

Open shell molecules can be calculated using either a restricted open shell method (not considered in this thesis) or by an unrestricted method, in which the α and β spatial orbitals are allowed to differ. This leads to a pair of equations

$$\hat{F}^{\alpha}\psi_i^{\alpha} = \varepsilon_i^{\alpha}\psi_i^{\alpha} \tag{1.85}$$

$$\hat{F}^{\beta}\psi_i^{\beta} = \varepsilon_i^{\beta}\psi_i^{\beta} \tag{1.86}$$

The Fock operators of Hartree-Fock theory are given by

$$\hat{F}^{\alpha} = \hat{h}(\mathbf{r}_1) + \sum_j^{N^{\alpha}} \left[J_j^{\alpha}(\mathbf{r}_1) - K_j^{\alpha}(\mathbf{r}_1)\right] + \sum_j^{N^{\beta}} J_j^{\beta}(\mathbf{r}_1) \tag{1.87}$$

$$\hat{F}^{\beta} = \hat{h}(\mathbf{r}_1) + \sum_j^{N^{\beta}} \left[J_j^{\beta}(\mathbf{r}_1) - K_j^{\beta}(\mathbf{r}_1)\right] + \sum_j^{N^{\alpha}} J_j^{\alpha}(\mathbf{r}_1) \tag{1.88}$$

The Kohn-Sham operators are of a similar form but with the exchange operator replaced with a spin-dependent exchange-correlation term. α terms appear in the $\hat{F}^{\beta}$ and vice versa, which means that the two HF/KS equations are coupled and must be solved together. Matrix equations are formed in the same way as for restricted systems, giving

$$\mathbf{F}^{\alpha}\mathbf{C}^{\alpha} = \mathbf{S}\mathbf{C}^{\alpha}\boldsymbol{\varepsilon}^{\alpha} \tag{1.89}$$

$$\mathbf{F}^{\alpha}\mathbf{C}^{\beta} = \mathbf{S}\mathbf{C}^{\beta}\boldsymbol{\varepsilon}^{\beta} \tag{1.90}$$

These are known as the Pople-Nesbet equations [83] in the context of Hartree-Fock theory.

Unrestricted Hartree-Fock theory has the drawback that the wavefunction is no longer an eigenfunction of the total spin-squared ($\hat{S}^2$) operator, a problem known as spin contamination. This is not a problem for unrestricted Kohn-Sham theory because the Kohn-Sham Slater determinant is not intended to be an approximation to the true wavefunction [84], and so it does not have to be an eigenfunction of the $\hat{S}^2$ operator.

1.4.4 The self-consistent field procedure

The matrix elements $F_{\mu v}$ involve Coulomb and exchange (HF) / exchange-correlation (KS) integrals that depend on the spatial orbitals that are the solutions to the equations. The equations must therefore be solved using a self-consistent field procedure, in which an initial guess is taken at the orbitals and the equations iterated to convergence. The description below assumes a restricted closed shell formalism, but the principle is the same for unrestricted calculations.

At the start of the calculation, the one-electron matrix elements $S_{\mu v}$ and $H_{\mu v}^{\text{core}}$ and the two-electron integrals $(\mu\lambda|\sigma v)$ are calculated. These do not vary during the course of the calculation, although the overlap matrix $\mathbf{S}$ must be diagonalised so that the matrix equations can be written in the standard eigenvector form.

The density matrix $P_{\mu v}$ contains the basis expansion coefficients which do vary, and so an initial guess of $P_{\mu v}$ must be made. The simplest initial guess is to set the density matrix equal to zero, so that

$$F_{\mu v} = H_{\mu v}^{\text{core}} \tag{1.91}$$

It is also possible to guess a form for $P_{\mu v}$ using a method such as extended Hückel theory, which will generally give an improved initial guess.

Once the matrix $\mathbf{F}$ is formed, it is diagonalised to obtain the solutions for the matrices $\mathbf{C}$ and $\boldsymbol{\epsilon}$. $\mathbf{C}$ is the matrix of expansion coefficients, whose columns define the spatial orbitals (eigenvectors). $\boldsymbol{\epsilon}$ is the matrix of orbital energies (eigenvalues).

A new density matrix is then formed from the matrix $\mathbf{C}$, and the process repeated until the solutions converge. Convergence is accelerated by algorithms such as the direct inversion of the iterative subspace (DIIS) [85] and the level-shifting method [86].

Once the SCF procedure has converged, the final energy and other properties can be calculated.

1.4.5 Basis sets

A good choice of basis set is vital for reliable calculations. In general, the accuracy of the orbital description will increase with the size of the basis set. An infinite basis set corresponds to the highest accuracy available within a theory and is known as the limit of that theory. In practice it is not possible to use an infinite basis set and the choice of the finite basis set is a compromise between computational cost and accuracy.

Most basis sets in use today were originally designed for wavefunction theory calculations, but they have proven to be equally useful for DFT (although there have also been attempts to develop basis sets optimised specifically for DFT [87]). The natural choice for basis functions are Slater-type orbitals (STOs) [88], which decay as $e^{-\zeta r}$, where r is the distance from the nucleus. STOs are a good approximation to the exact solutions to the Schrödinger equation for one-electron systems. They model the cusp at $r = 0$ and have the correct exponential decay. However, most modern basis sets use Gaussian-type orbitals (GTOs) [89], which decay as $e^{-\alpha r^2}$. GTOs do not model the cusp correctly and they decay too quickly with r. However, GTOs are much easier to integrate than STOs, which is an important consideration because of the large number of two-electron integrals that have to be calculated for any sizeable molecular system.

The form of the GTOs can be improved by using contracted Gaussian functions (CGFs). These consist of a fixed linear combination of 'primitive' Gaussians that can be chosen to more closely resemble STOs, without losing much of the computational advantage of GTOs.

Minimal basis sets, such as STO-3G, consist of one contracted basis function for each atomic orbital (in the case of STO-3G, the CGF consists of 3 primitive Gaussians). These basis sets give only qualitative results and increases in computer power have essentially rendered them obsolete for practical applications. Larger basis sets use two or more CGFs for each atomic orbital and are termed double-zeta (DZ), triple-zeta (TZ), and so on.

Some basis sets use more CGFs for the important valence orbitals. These are known as split-valence basis sets, and include most of the standard basis sets used in the GAUSSIAN [90] software package, such as 3-21G, 4-31G and

6-31G, all of which use double-zeta quality for the valence orbitals and one CGF for the inner orbitals. 6-311G is of triple-zeta quality for the valence orbitals.

Basis sets are often improved by adding polarisation functions, such as d-type orbitals to the first row atoms and p-type functions to hydrogen. This example, added to 6-31G, would be written as 6-31G(d,p) or 6-31G**. Polarisation functions are also sometimes denoted by a 'P', such as the TZ2P basis set [91]. TZ2P is of triple-zeta quality and contains two polarisation functions per atom. Polarisation functions allow the wavefunction to more accurately describe a distorted charge distribution caused by the molecular environment or by an external field.

Another improvement is achieved with diffuse functions, which are designed to decay slowly in order to more accurately model the wavefunction at large distances from the nuclei. This is particularly useful for anions with a weakly bound electron, atoms with lone-pairs, and excitation energy calculations. For basis sets in GAUSSIAN, diffuse orbitals are denoted by a '+'.

Quantum chemistry packages that were originally designed for wavefunction theory (such as GAUSSIAN, CADPAC and DALTON) have carried over the use of Gaussian basis functions for DFT. Other packages that have been built from scratch for DFT often use different approaches, such as using Slater-type orbitals [92,93] or numerical basis sets [94].

Selected basis sets used in this thesis are presented in Table 1.1, with an indication of their size given by the primitive and contracted basis functions used for the carbon atom.

1.4.6 Property calculations

Once the HF/KS equations have been solved and the electronic energy determined, it is possible to calculate a wide range of chemical properties. Most properties can be thought of as a response to a perturbation of some kind, such as a change in geometry, an external electric or magnetic field, a nuclear magnetic moment, or radiation.

Geometry optimisations involve a change in energy on moving a nucleus

Table 1.1: Selected basis sets used in this thesis, with the primitive and contracted basis functions used for the carbon atom.

Basis set	Primitive	Contracted
6-31G*	10s4p1d	3s2p1d
Sadlej	10s6p4p	4s3p1d
TZ2P	11s6p2d	5s4p2d
6-311+G(2d,p)	12s6p2d	5s4p2d
6-311+G(2df)	12s6p2d1f	5s4p2d1f
6-311+G(3df,2p)	12s6p3d1f	5s4p3d1f
Huzinaga III	11s7p2d	7s6p2d
Huzinaga IV	11s7p3d1f	8s7p3d1f

from $\mathbf{R}$ to $\mathbf{R}'$, in order to find an energy minimum (or a maximum in one coordinate in the case of transition state optimisations). This can be written as a Taylor expansion in terms of the energy.

$$E(\mathbf{R}') = E(\mathbf{R}) + \left.\frac{\partial E}{\partial \mathbf{R}}\right|_{\mathbf{R}} (\mathbf{R}' - \mathbf{R}) + \frac{1}{2} \left.\frac{\partial^2 E}{\partial \mathbf{R}^2}\right|_{\mathbf{R}} (\mathbf{R}' - \mathbf{R})^2 + \ldots \tag{1.92}$$

where the first derivative is the energy gradient and the second derivative is the force constant or Hessian. These derivatives are usually calculated analytically. It is possible to optimise a geometry using only the energy gradients, but it is more efficient if the Hessian can be calculated (as it allows better optimisation schemes, although often an approximate Hessian is used, such as in CADPAC). For transition state optimisations, knowledge of the Hessian is essential. The second derivative is also required to calculate harmonic vibrational frequencies.

The effect of a uniform electric field ($\mathbf{F}$) can also be written as a Taylor expansion

$$E(\mathbf{F}) = E(0) + \left.\frac{\partial E}{\partial \mathbf{F}}\right|_{0} \mathbf{F} + \frac{1}{2} \left.\frac{\partial^2 E}{\partial \mathbf{F}^2}\right|_{0} \mathbf{F}^2 + \ldots \tag{1.93}$$

The first derivative equals the negative of the permanent dipole moment $\boldsymbol{\mu}_0$, the second the negative of the polarisability $\boldsymbol{\alpha}$, and the third and higher correspond to hyperpolarisabilities. Additional terms involving the multipole moments arise when the field is non-uniform.

A magnetic field ($\mathbf{B}$) can be treated in the same way

$$E(\mathbf{B}) = E(0) + \left.\frac{\partial E}{\partial \mathbf{B}}\right|_0 \mathbf{B} + \frac{1}{2}\left.\frac{\partial^2 E}{\partial \mathbf{B}^2}\right| \mathbf{B}^2 + \ldots \tag{1.94}$$

In this case the first derivative is the negative of the permanent magnetic dipole moment $\mathbf{m}_0$ (only present in degenerate open-shell states). The second derivative is proportional to the magnetisability $\boldsymbol{\zeta}$.

Finally, nuclear magnetic moments ($\mathbf{I}$) give

$$E(\mathbf{I}_1, \mathbf{I}_2, \ldots) = E(0) + \sum_i \left.\frac{\partial E}{\partial \mathbf{I}_i}\right|_0 \mathbf{I}_i + \frac{1}{2}\sum_{ij} \left.\frac{\partial^2 E}{\partial \mathbf{I}_i \partial \mathbf{I}_j}\right|_0 \mathbf{I}_i \mathbf{I}_j \ldots \tag{1.95}$$

The first derivatives are the hyperfine coupling constants $\mathbf{g}$ and the second derivative with respect to two different nuclear spins is the NMR spin-spin coupling constant $\mathbf{J}$.

Derivatives with respect to a mixture of these perturbations can also be important chemical properties. For example, the shielding constant $\boldsymbol{\sigma}$ is defined as

$$\boldsymbol{\sigma} = \mathbf{1} + \frac{\partial^2 E}{\partial \mathbf{B} \partial \mathbf{I}} \tag{1.96}$$

The calculation of individual properties will be discussed in further detail as they are encountered in this work.

The ultimate test of all chemical property calculations is comparison with experiment. It is important when comparing with experimental data to consider the effect of the experimental conditions. Quantum chemistry calculations correspond to 0 K and it may be necessary to correct the theoretical values for vibrational and rotational effects to ensure a fair comparison. Gas-phase experimental data is always preferable, as this is the most similar environment to a single molecule calculation. The effect of solvents has to be considered for liquid-phase data, although explicit modelling of solvent molecules is often beyond the scope of quantum treatments. For solid state calculations, an entirely new set of techniques is required, as discussed in Chapter 5.

1.5 This thesis

The focus of this thesis is the development of new exchange-correlation functionals in density functional theory. The approach used throughout is pragmatic and semi-empirical, but is justified by the fact that any improvement could be of real, practical benefit to the extensive DFT user community. The functionals we develop will be assessed for their performance for a variety of chemical systems and properties, not just those in the fitting data. If a functional—albeit semi-empirical—can provide a good quality description of a wide range of chemical properties, then it must contain appropriate physics.

In Chapter 2 we examine the performance of conventional DFT functionals for NMR shielding constants and investigate the link between the quality of the exchange-correlation potential and shielding constant results. We then develop two GGA functionals, denoted KT1 and KT2, which are specifically designed to improve performance for shielding constants. In Chapter 3 the KT1 and KT2 functionals are assessed for other magnetic properties, including magnetisabilities, chemical shifts, and spin-spin coupling constants, and for a further set of shieldings. In Chapter 4 the KT3 GGA functional is developed following extensive investigations into the form of the exchange and correlation functionals and the choice of fitting data. An assessment of KT3 is presented in Chapter 5. We also apply KT3 to the challenging shielding constant calculations of *o*-dichlorobenzene and selenium-containing molecules. Lastly, we assess KT3 for solid state calculations. In Chapter 6 we attempt to develop another GGA, KT4, by including reaction barriers in the fitting data and using a more flexible functional form. We also develop a hybrid functional, B97-3, using the same methodology (but without the emphasis on maintaining performance for shielding constants). In Chapter 7 we present an extensive chemical assessment of the KT4 and B97-3 functionals, and then apply B97-3 to the problem of the oxirene-ketene potential energy surface and the calculation of spin-spin coupling constants. Conclusions are presented in Chapter 8.

Unless otherwise stated, all calculations were performed using the CADPAC program. Throughout this work the exchange-correlation functionals we de-

velop are assessed by the calculation of errors (calculated – reference) over the assessment sets listed in Appendix A. Mean errors are denoted d, mean absolute errors $|d|$, and mean absolute percentage errors $|d|\%$.

Chapter 2

The KT1 and KT2 functionals

In this chapter two new semi-empirical GGA exchange-correlation functionals are developed with the aim of improving the performance of DFT for shielding constant calculations.

2.1 Shielding constants in DFT

The calculation of magnetic properties is vital for the interpretation of experimental nuclear magnetic resonance (NMR) and electron spin resonance (ESR) data. Hartree-Fock calculations often exhibit unacceptably large errors due to neglect of correlation effects [95], so DFT would seem to be a natural choice of method.

One problem with using DFT is that if an external magnetic field is present, the Hohenberg-Kohn theorems of Section 1.3.2 no longer hold. The exchange-correlation functional no longer just depends on the electron density but also on the current density $j(\mathbf{r})$ induced by the magnetic field

$$j(\mathbf{r}) = -\frac{\mathrm{i}}{2}\sum_i [\psi_i^*(\mathbf{r})\nabla\psi_i(\mathbf{r}) - \nabla\psi_i^*(\mathbf{r})\psi_i(\mathbf{r})] \tag{2.1}$$

Attempts have been made to develop 'current density functionals' [96,97], but it has been observed [96] that the effect of the current dependence is relatively small, and so the vast majority of calculations simply ignore this dependence

by assuming

$$E_{\mathrm{XC}}[\rho(\mathbf{r}), j(\mathbf{r})] \approx E_{\mathrm{XC}}[\rho(\mathbf{r})] \tag{2.2}$$

A second problem that all quantum chemical calculations face relates to the choice of a gauge origin. The external magnetic field is a perturbation that leads to extra terms in the electronic Hamiltonian. In addition to the magnetic flux density $\mathbf{B}$, there are terms involving the vector potential $\mathbf{A}$, which is related to $\mathbf{B}$ by

$$\mathbf{A}_O(\mathbf{r}) = \frac{1}{2}\mathbf{B} \times (\mathbf{r} - \mathbf{O}) \tag{2.3}$$

where $\mathbf{O}$ is the gauge origin, which should be free to move without affecting the results of any calculation (that is, it should be gauge invariant). However, if a finite basis set is used, this will not be the case, and so results will depend on the choice of gauge origin. There are several approaches to combat this problem, such as gauge including atomic orbitals (GIAO) [98] and localised orbitals/localised origins (LORG) [99]. In this chapter we use the LORG formalism, which requires the use of an extensive basis set to minimise gauge problems.

The shielding constant is defined as in Eq. 1.96. It is a second derivative property, which requires knowledge of the first order response of the wavefunction to the magnetic field perturbation. The perturbed wavefunction is written in terms of the Kohn-Sham orbitals for a general perturbation λ as [100]

$$\psi_j = \psi_j^0 + \lambda \sum_b C_{bj}^{\alpha} \psi_b + \ldots \tag{2.4}$$

where j and b denote occupied and virtual orbitals and α is the component of the applied field. In the case of a magnetic perturbation $\lambda = \mathrm{i}B^{\alpha}$. The linear response C_{bj}^{α} is determined from a set of coupled perturbed equations

$$\sum_{bj} (H_2)_{ai,bj} C_{bj}^{\alpha} = -l_{bj}^{\alpha} \tag{2.5}$$

where l_{bj}^{α} is the integral matrix of the angular momentum operator $\hat{l}^{\alpha}$. $\mathbf{H}_2$ is

the magnetic Hessian matrix [101]

$$(H_2)_{ai,bj} = (\epsilon_a - \epsilon_i)\delta_{ai,bj} + \xi\left[(aj|bi) - (ab|ij)\right] \tag{2.6}$$

where ξ is the fraction of exact exchange in the functional. For hybrid functionals the coupled perturbed equations must be solved directly, but for GGA functionals (where $\xi = 0$) they reduce to

$$C^{\alpha}_{bj} = -\frac{l^{\alpha}_{bj}}{\epsilon_b - \epsilon_j} \tag{2.7}$$

The shielding tensor expression is given by

$$\begin{aligned} \sigma^{A}_{\alpha\beta} &= \sum_{j} (j|(\mathbf{r}\cdot\mathbf{r}_A\delta^{\alpha\beta} - r^{\alpha}r^{\beta}_A)r^{-3}_A|j) \\ &- \sum_{bj} C^{\alpha}_{bj}\left[(j|l^{\beta}_A r^{-3}_A|b) + (b|l^{\alpha}_A r^{-3}_A|j)\right] \end{aligned} \tag{2.8}$$

which is an orbital reformulation of the original Ramsey expression [102]. The first term is the diamagnetic contribution to the shielding constant and the second term is the paramagnetic contribution. For GGA functionals the uncoupled expression is

$$\begin{aligned} \sigma^{A}_{\alpha\beta} &= \sum_{j} (j|(\mathbf{r}\cdot\mathbf{r}_A\delta^{\alpha\beta} - r^{\alpha}r^{\beta}_A)r^{-3}_A|j) \\ &- \sum_{bj} \frac{(b|l^{\alpha}|j)(j|l^{\beta}_A r^{-3}_A|b) + (b|l^{\alpha}_A r^{-3}_A|j)(j|l^{\beta}|b)}{\epsilon_b - \epsilon_j} \end{aligned} \tag{2.9}$$

The performance of conventional DFT for shielding constants is disappointing. Following Ref. [103], we calculated isotropic and anisotropic shielding constants for a set of 21 molecules (listed as assessment sets A1 and A2 in Appendix A) with LDA, the GGA HCTH, and the hybrid functional PBE0. We have chosen to highlight PBE0 because it has been claimed to give good performance for shielding constants [104]. However, in this earlier study it was only tested on an unchallenging set of carbon and hydrogen nuclei.

Our isotropic set contains 32 challenging first- and second-row main-group nuclei and the anisotropic set contains a subset of 11 nuclei. For linear and

symmetric top molecules the isotropic shielding constants are given by [105]

$$\sigma_{\text{iso}} = \frac{1}{3}(\sigma_{||} + 2\sigma_{\perp}) \tag{2.10}$$

where $\sigma_{||}$ is the component along the principal molecular axis and $\sigma_{\perp}$ is the component perpendicular to it. The anisotropic shielding constants are

$$\Delta\sigma = \sigma_{||} - \sigma_{\perp} \tag{2.11}$$

For all other symmetries

$$\sigma_{\text{iso}} = \frac{1}{3}\text{tr}\sigma \tag{2.12}$$

$$\Delta\sigma = \sigma_{\alpha\alpha} - \frac{1}{2}(\sigma_{\beta\beta} + \sigma_{\gamma\gamma}) \tag{2.13}$$

where σ_{ii} are the principal tensor components with $\sigma_{\alpha\alpha}$ the largest component. The shielding constants were calculated at near-experimental geometries, using a modified version of the extensive Huzinaga IV basis set [106, 107] as defined in Ref. [105]. (The modification is the choice of 3d1f polarisation functions for the second row atoms P, S, and Cl instead of 4d2f, which affects the results for systems containing these atoms marginally.)

Mean and mean absolute errors relative to experiment are presented in Table 2.1. The experimental reference values were taken from Ref [103]. Isotropic errors are presented with and without the challenging ozone nuclei, which contribute a significant portion of the error.

Remarkably, the least accurate functional in this assessment is PBE0. Other hybrid functionals give a similar performance [103]. LDA is an improvement, with the GGA HCTH functional giving the lowest errors of the group. This is a reversal of the usual finding that hybrid functionals are superior to GGAs. (This result applies only to main group nuclei. For transition metal absolute shielding constants, GGA functionals perform poorly whereas hybrid functionals perform comparatively well [108].) However, even the HCTH functional has unacceptably large errors.

The failure of DFT for main group shielding constants is well known, and

Table 2.1: Shielding constant error assessments for the LDA, HCTH, and PBE0 functionals and the MKS(BD) and MKS(PBE0) methods. All values are in ppm.

	LDA	HCTH	PBE0	MKS(BD)[a]	MKS(PBE0)
A1. Isotropic NMR shielding constants (ppm)					
d	−51.8	−32.4	−58.5	5.1	−2.7
$\|d\|$	52.2	32.4	58.8	16.7	15.4
Excluding O_3:					
d	−40.5	−25.2	−32.7	−1.9	−6.0
$\|d\|$	41.0	25.2	33.0	10.1	9.8
A2. Anisotropic NMR shielding constants (ppm)					
d	46.1	27.0	40.7	−1.7	−2.3
$\|d\|$	54.3	28.4	43.9	8.8	11.3

[a] Ref. [103]

is attributed to an overestimated paramagnetic contribution to the shielding [109]. This is caused by underestimated occupied-virtual eigenvalue differences on the denominator of the paramagnetic term in Eq. 2.9. A number of attempts have been made to improve the performance. Casida and co-workers have obtained notable improvements by explicitly correcting the eigenvalue differences based on arguments from sum-over-states density functional perturbation theory [109,110]. Patchkovskii *et al.* [111] have observed that a self-interaction corrected functional in the optimised effective potential approach leads to similar improvements. Wilson *et al.* [105] have demonstrated that the addition of an empirical amount of exact exchange in the Kohn-Sham equations for the orbitals used in the uncoupled GGA expression (Eq. 2.9) gives shieldings approaching coupled cluster accuracy. Model exchange-correlation potentials can also give improved shielding constants [112]. However, these methods all lie outside the standard Kohn-Sham formalism. It would be preferable to be able to calculate accurate shielding constants with a conventional functional. As GGAs appear to perform better than hybrid functionals, we chose to concentrate on functionals of the GGA form. Our starting point was another attempt to improve shielding constant performance known as the Multiplicative Kohn-Sham (MKS) method.

2.2 The MKS method

The MKS method [103] involves the calculation of shielding constants from a set of orbitals and eigenvalues determined from a reference electron density rather than from a conventional functional. It involves three stages. Firstly, a theoretical method and basis set are chosen to calculate a reference density matrix for a system. Either wavefunction or DFT methods can be used for this step. In the MKS nomenclature this method is given in parentheses. For example, MKS(BD) uses densities from the Brueckner Doubles wavefunction method, whereas MKS(PBE0) uses densities from the PBE0 density functional.

The second step is based on the Zhao-Morrison-Parr (ZMP) procedure [113]. The ZMP procedure is used, with the same basis set as in step 1, to determine the exchange correlation potential $v_{XC}(\mathbf{r})$ from the supplied density matrix [114]. The orbitals are constrained so that they give the reference density

$$\rho_0(\mathbf{r}) = 2\sum_i |\psi_i(\mathbf{r})|^2 \tag{2.14}$$

The electron-nuclear energy, Coulomb energy, and exchange-correlation energy are explicit functionals of the density (Eq. 1.47), and therefore the Kohn-Sham orbitals are obtained for that density by minimising the kinetic energy

$$T_s[\rho_0] = \min_{\chi_i} -\frac{1}{2}\sum_i^N \langle\chi_i|\nabla^2|\chi_i\rangle \tag{2.15}$$

This is the constrained search minimisation of Levy and Perdew [115]. Zhao, Morrison and Parr enforced the constraint on the density by ensuring that the self-repulsion was zero

$$\frac{1}{2}\iint \frac{[\rho(\mathbf{r}_1) - \rho_0(\mathbf{r}_1)][\rho(\mathbf{r}_2) - \rho_0(\mathbf{r}_2)]}{r_{12}} d\mathbf{r}_1 d\mathbf{r}_2 = 0 \tag{2.16}$$

Minimisation of Eq. 2.15 subject to the constraint of Eq. 2.16 gives a set of equations

$$\left[-\frac{1}{2}\nabla^2 + v_C^\lambda(\mathbf{r}_1)\right]\psi_i^\lambda(\mathbf{r}_1) = \epsilon_i^\lambda \psi_i^\lambda(\mathbf{r}_1) \tag{2.17}$$

where the effective constraint potential, $v_{\mathrm{C}}^{\lambda}(\mathbf{r}_1)$, is

$$v_{\mathrm{C}}^{\lambda}(\mathbf{r}_1) = \lambda \int \frac{[\rho^{\lambda}(\mathbf{r}_2) - \rho_0(\mathbf{r}_2)]}{r_{12}} \mathrm{d}\mathbf{r}_2 \tag{2.18}$$

and λ indicates a dependence on a Lagrange multiplier. To bring these equations into a conventional Kohn-Sham form, the Coulomb potential $v_{\mathrm{J}}^{\lambda}(\mathbf{r}_1)$ and the external potential $v_{\mathrm{ext}}(\mathbf{r}_1)$ are added. The Coulomb term is multiplied by the Fermi-Amaldi factor $(1 - \frac{1}{N})$ [116]. This is not theoretically required by the ZMP procedure, but it ensures that the exchange-correlation potential will exhibit the appropriate $-1/r$ asymptotic behaviour for any isolated system. The final ZMP equations are

$$\left[-\frac{1}{2}\nabla^2 + v_{\mathrm{ext}}(\mathbf{r}_1) + \left(1 - \frac{1}{N}\right) v_{\mathrm{J}}^{\lambda}(\mathbf{r}_1) + v_{\mathrm{C}}^{\lambda}(\mathbf{r}_1)\right] \psi_i^{\lambda}(\mathbf{r}_1) = \epsilon_i^{\lambda} \psi_i^{\lambda}(\mathbf{r}_1) \tag{2.19}$$

The exchange-correlation potential $v_{\mathrm{XC}}(\mathbf{r})$ is then identified as

$$v_{\mathrm{XC}}(\mathbf{r}) = -\frac{1}{N} v_{\mathrm{J}}^{\lambda}(\mathbf{r}) + v_{\mathrm{C}}^{\lambda}(\mathbf{r}) \tag{2.20}$$

If the exact density was supplied, the ZMP procedure would yield the exact, electron deficient limit of the exchange-correlation potential [44]. The potential exhibits a discontinuity at an integer number of electrons [117], and so the exact potential on the electron abundant side would be shifted from the ZMP potential.

These equations are solved iteratively, with the value of the Lagrange multiplier λ raised with each iteration. The formal value of λ should be infinity, but the final value is usually set to 900 when using a finite basis set [114]. When the exchange-correlation potential has converged, it is output on a standard numerical integration grid. This potential is in principle exact (within the limitations of a finite basis set and finite λ), should an exact electron density be input into the procedure. In practice the accuracy of the potential increases with the accuracy of the density supplied.

The third step is a Kohn-Sham shielding constant calculation using the uncoupled formalism of Eq. 2.9. The standard Kohn-Sham equations are solved, but rather than calculating $v_{\mathrm{XC}}(\mathbf{r})$ from a functional, the ZMP potential is

read from disk. Therefore only the Coulomb potential changes with each SCF iteration. As with conventional calculations, a large basis set (such as Huzinaga IV) has to be used in this step to minimise gauge problems. The basis set used in step 3 does not necessarily have to be the same as those used in steps 1 and 2, so a smaller, more computationally efficient basis set can be used for those steps.

Table 2.1 presents shielding constant errors for the MKS(BD) and MKS(PBE0) methods. The TZ2P basis set was used for steps 1 and 2, and the Huzinaga basis set for step 3. The MKS(BD) method is more than twice as accurate as HCTH. This reflects the high-quality BD electron density. MKS(PBE0) also gives excellent results, with errors comparable to MKS(BD). This indicates that the PBE0 electron density is equally good for calculating uncoupled shielding constant results. Other hybrid functional densities give similar results [103].

It is worth reiterating the difference between a conventional hybrid calculation (such as PBE0) and that of MKS(PBE0). In the former the shielding tensor is evaluated in the coupled manner from Eq. 2.8. The orbitals and eigenvalues are determined using a non-multiplicative exchange-correlation operator. In the latter method the shielding tensor is evaluated in an uncoupled manner from Eq. 2.9 and the orbitals and eigenvalues are from a multiplicative exchange-correlation potential. If the MKS method was used with a GGA, there would be little change in the results, as GGAs have no non-multiplicative part and are therefore already evaluated using the uncoupled methods. (Slight changes are observed due to the Fermi-Amaldi term and the finite value of λ [103].)

However, there are limitations with this method. Although MKS(PBE0) formally scales with system size as conventional DFT, in practice the computational cost is higher because of the additional cost of the ZMP stage. Convergence problems are also encountered in the ZMP procedure for larger systems and the method is not widely implemented in electronic structure codes.

Table 2.2: Isotropic shielding constants for three representative molecules. All values are in ppm.

Mol.	Nuc.	LDA	BLYP	HCTH	MKS(BD)	Eq. (2.26)[a]	*Ab initio*	Expt.
CO	C	−20.3	−14.8	−7.5	−1.5	2.8	5.6[b]	2.8 ± 0.9[b]
	O	−87.5	−77.3	−66.8	−45.0	−64.0	−52.9[b]	-36.7 ± 17.2[b]
N_2	N	−91.4	−84.6	−76.9	−67.4	−64.8	−58.1[b]	-59.6 ± 1.5[b]
PN	P	−73.7	−37.1	−7.6	41.7	18.2	86[c]	53[c]
	N	−414.9	−405.4	−378.5	−350.2	−371.9	−341[c]	−349[c]

[a] $\beta = -0.0045$, $\gamma = 0.1$
[b] Ref. [118], GIAO-CCSD(T), experimental values include rovibrational corrections
[c] Ref. [119]

2.3 Modelling the potential

The high quality MKS results demonstrate that a current-dependent functional is not necessary to obtain high quality shielding constants for these molecules. All that is required is accurate orbitals and eigenvalues obtained from an accurate exchange-correlation potential in Eq. 1.51. To investigate the influence of the potential further we considered three representative molecules from the shielding set: CO, N_2, and PN. Table 2.2 presents isotropic shielding constants for these molecules using the LDA, BLYP and HCTH functionals (with the Huzinaga IV basis set), and the MKS(BD) method. To ensure a fair comparison, we have recalculated the MKS(BD) shielding constants using the Huzinaga IV basis set for all three steps (with f functions removed for the ZMP step for technical reasons). The trends for the individual nuclei are the same as those for the overall errors. The shieldings of all the nuclei improve uniformly from LDA to BLYP to HCTH to MKS(BD). Table 2.3 presents anisotropic shielding constants for the same molecules. The same trends are observed.

The improvement in performance from LDA to BLYP to HCTH to MKS(BD) is a direct consequence of the differences in their exchange-correlation potentials. Figures 2.1, 2.2, and 2.3 plot the potentials for CO, N_2 and PN respectively, compared to ZMP potentials from BD densities. Conventional functionals average over the integer discontinuity in the potential, so to allow

Table 2.3: Anisotropic shielding constants for three representative molecules. All values are in ppm.

Mol.	Nuc.	LDA	BLYP	HCTH	MKS(BD)	Eq. (2.26)[a]	*Ab initio*	Expt.
CO	C	438.4	432.1	420.9	411.5	407.8	401.0[b]	406.1 ± 1.4[b]
	O	744.3	731.7	716.0	682.8	713.5	694.6[b]	676.1 ± 26[b]
N_2	N	644.7	636.8	625.1	610.4	608.9	596.5[b]	603 ± 28[b]
PN	P	1557.5	1505.6	1461.7	1386.0	1425.3	1334[c]	1376[c]
	N	1133.3	1121.5	1081.0	1038.2	1072.7	1023[c]	1048[c]

[a] $\beta = -0.0045$, $\gamma = 0.1$
[b] Ref. [118], GIAO-CCSD(T)
[c] Ref. [119]

comparison the ZMP potentials have been shifted up by half the discontinuity, approximated by [120]

$$\Delta = \varepsilon_{\mathrm{HOMO}} + I \tag{2.21}$$

where $\varepsilon_{\mathrm{HOMO}}$ is the highest occupied molecular orbital (HOMO) eigenvalue and I is the ionisation potential. We use experimental I values from Ref. [121].

For all three molecules, the agreement with the high quality ZMP potentials clearly improves from LDA to BLYP to HCTH. This is most evident in the intershell region, where the characteristic structure [122–124] is prominent in the ZMP potential. As noted previously [124], LDA completely fails to introduce the structure. The BLYP potential exhibits some structure due to the addition of density gradient information, although its magnitude is small and its position does not coincide with that of ZMP. The potential for BLYP diverges [125] to a negative value at the nuclei. The HCTH potentials provide a better description of the intershell structure, although they have an erratic shape. This is because ZMP potentials form part of the data that HCTH was fitted to, and the high number of parameters can be chosen to give a reasonable representation of the structure (although the form is not adequate to describe it smoothly). The vertical lines at the nuclei in the HCTH potential indicate a divergence to a positive value.

We therefore commenced our investigations by attempting to find a simple gradient correction to the LDA that would reproduce the intershell structure

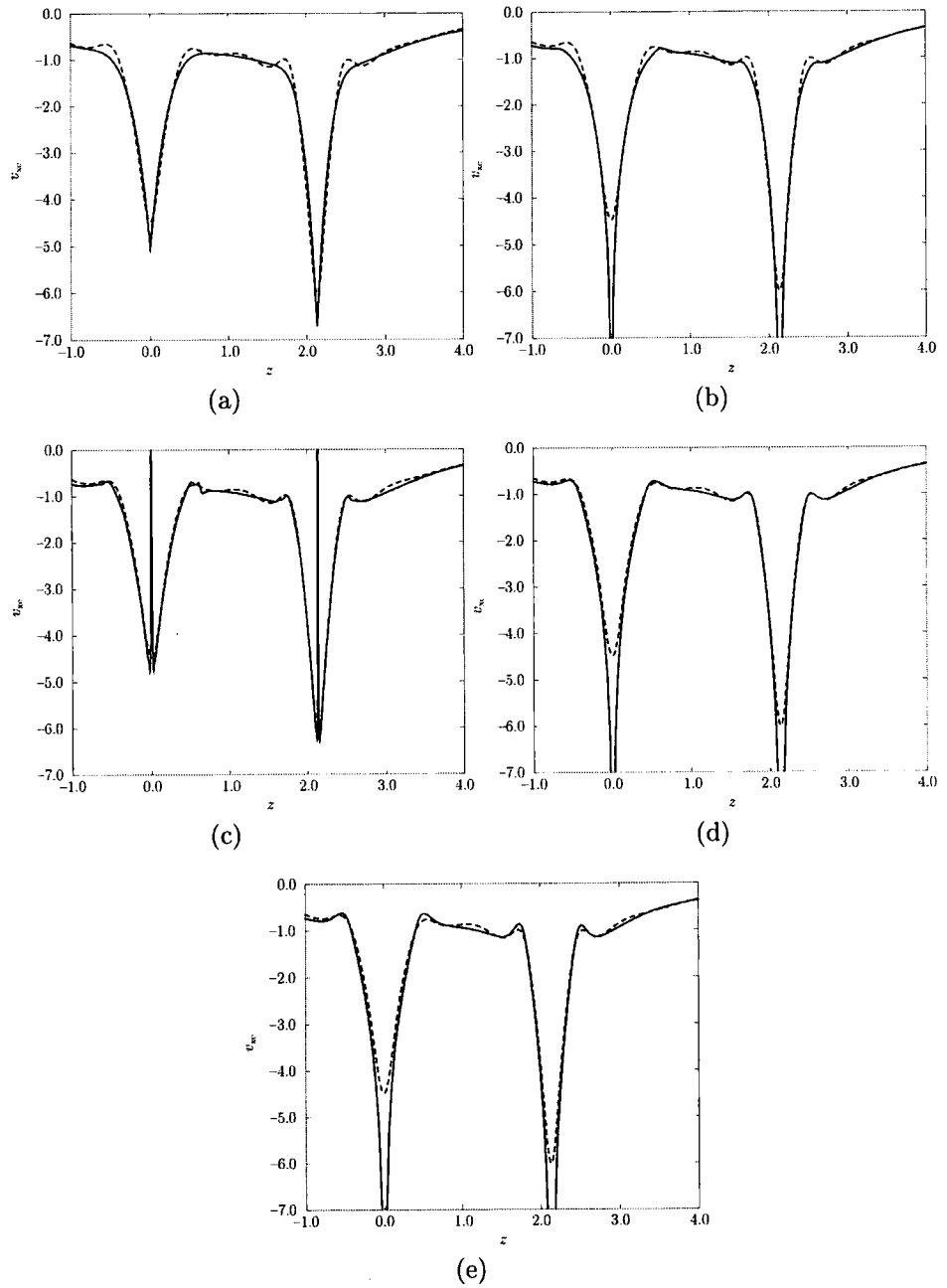

Figure 2.1: Exchange-correlation potentials for the CO molecule with (a) LDA, (b) BLYP, (c) HCTH, (d) Eqs. 2.26 and 2.31, and (e) KT1 (solid lines) plotted against a shifted ZMP potential using BD densities (dashed lines). All values are in au.

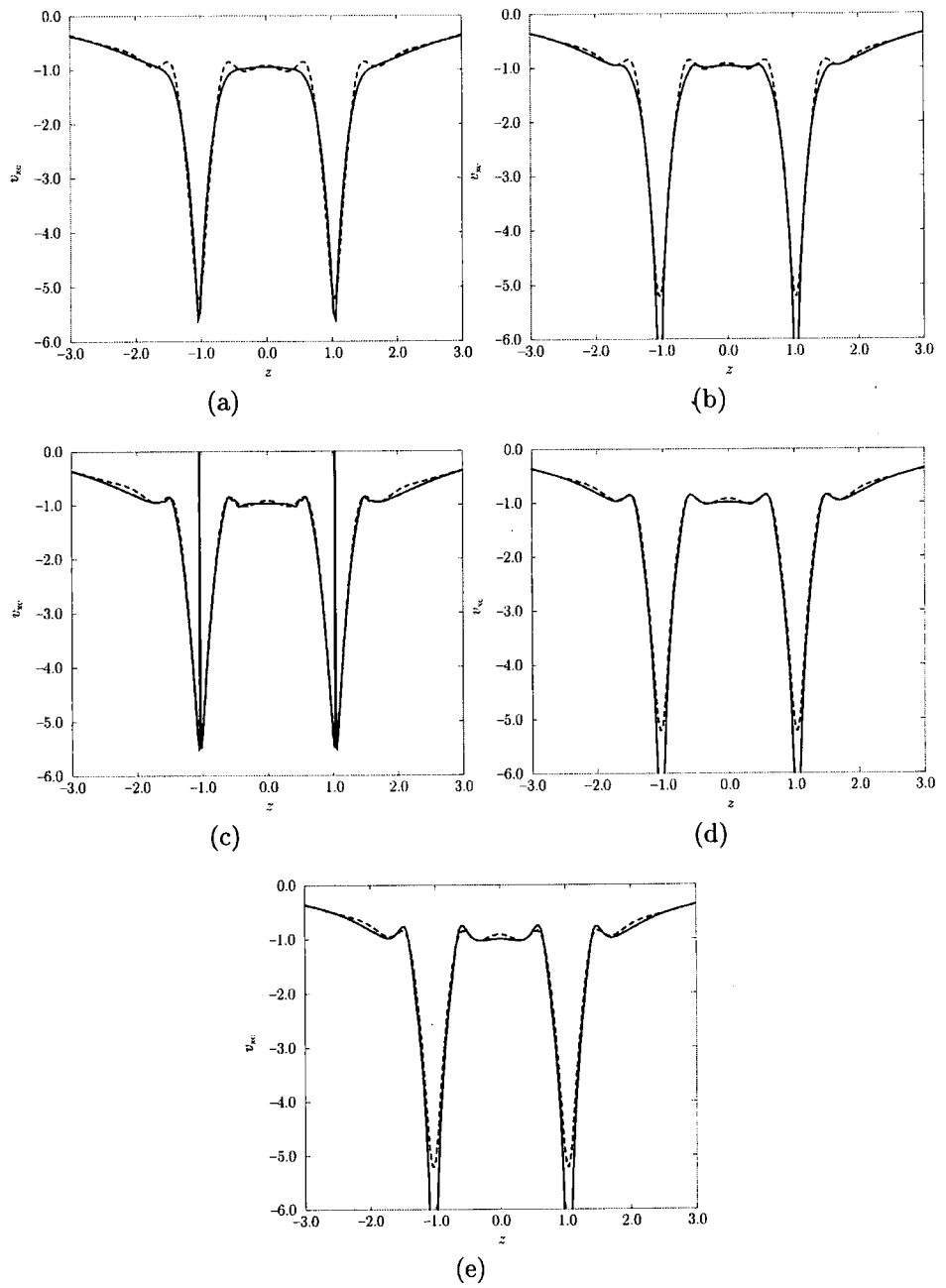

Figure 2.2: Exchange-correlation potentials for the N_2 molecule with (a) LDA, (b) BLYP, (c) HCTH, (d) Eqs. 2.26 and 2.31, and (e) KT1 (solid lines) plotted against a shifted ZMP potential using BD densities (dashed lines). All values are in au.

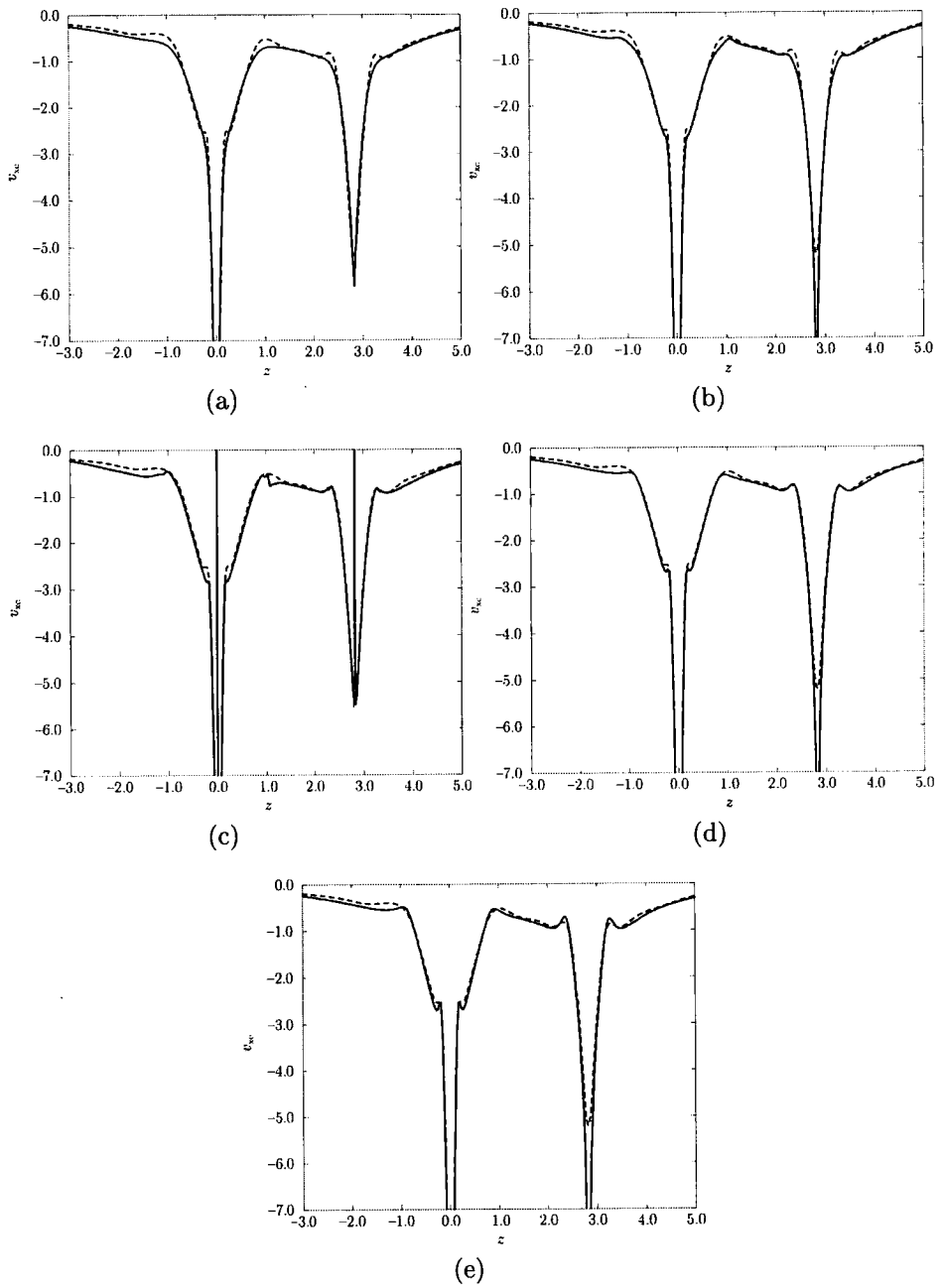

Figure 2.3: Exchange-correlation potentials for the PN molecule with (a) LDA, (b) BLYP, (c) HCTH, (d) Eqs. 2.26 and 2.31, and (e) KT1 (solid lines) plotted against a shifted ZMP potential using BD densities (dashed lines). All values are in au.

found in the ZMP potentials. The obvious choice would be to add conventional GGA corrections such as B86X or OPTX, which are functions of the reduced density gradient x_σ in Eq. 1.59. These contain semi-empirical parameters that were originally fitted to thermochemical data, but they could be adjusted to fit the ZMP potentials. However, extensive investigations demonstrated that it was not possible to recreate the intershell peak adequately even allowing these parameters to vary. This suggests that their mathematical form is deficient, and also explains the erratic shape of the HCTH potential (the HCTH expansion contains terms of the same form as B86X and OPTX but is more flexible).

It was therefore necessary to develop a new gradient correction that was capable of modelling the intershell peak. Our final form was based on an analysis of the form of the GGA exchange-correlation potential. For a functional with independent α and β spin parts this is given by [126]

$$v_{\mathrm{XC},\sigma} = v^{(1)}_{\mathrm{XC},\sigma} + v^{(2)}_{\mathrm{XC},\sigma} + v^{(3)}_{\mathrm{XC},\sigma} + v^{(4)}_{\mathrm{XC},\sigma} \tag{2.22}$$

where

$$\begin{aligned}
v^{(1)}_{\mathrm{XC},\sigma} &= \frac{\partial F_{\mathrm{XC}}}{\partial \rho_\sigma} \\
v^{(2)}_{\mathrm{XC},\sigma} &= -|\nabla\rho_\sigma| \frac{\partial^2 F_{\mathrm{XC}}}{\partial|\nabla\rho_\sigma|\partial\rho_\sigma} \\
v^{(3)}_{\mathrm{XC},\sigma} &= -\frac{1}{|\nabla\rho_\sigma|}\frac{\partial F_{\mathrm{XC}}}{\partial|\nabla\rho_\sigma|}\nabla^2\rho_\sigma \\
v^{(4)}_{\mathrm{XC},\sigma} &= -\frac{1}{|\nabla\rho_\sigma|^2}\left(\frac{\partial^2 F_{\mathrm{XC}}}{\partial|\nabla\rho_\sigma|^2} - \frac{1}{|\nabla\rho_\sigma|}\frac{\partial F_{\mathrm{XC}}}{\partial|\nabla\rho_\sigma|}\right)\sum_{\lambda\mu}^{xyz}\frac{\partial\rho_\sigma}{\partial\lambda}\frac{\partial^2\rho_\sigma}{\partial\lambda\partial\mu}\frac{\partial\rho_\sigma}{\partial\mu}
\end{aligned} \tag{2.23}$$

and F_{XC} is the exchange-correlation integrand defined by

$$E_{\mathrm{XC}} = \int F_{\mathrm{XC}}\mathrm{d}\mathbf{r} \tag{2.24}$$

By plotting the four components of $v_{\mathrm{XC},\sigma}$ individually, we found that it was the effect of the Hessian term $v^{(4)}_{\mathrm{XC},\sigma}$ that was responsible for the poor description of the intershell peaks in the case of BLYP (plots (b) of Figures 2.1–2.3), OLYP,

and similar functionals.

We therefore attempted to devise a functional for which $v^{(4)}_{\mathrm{XC},\sigma}$ was zero. The simplest way to achieve this is to set the term in parentheses equal to zero by ensuring that

$$\frac{\partial^2 F_{\mathrm{XC}}}{\partial|\nabla\rho_\sigma|^2} = \frac{1}{|\nabla\rho_\sigma|}\frac{\partial F_{\mathrm{XC}}}{\partial|\nabla\rho_\sigma|} \tag{2.25}$$

This can be trivially achieved with the form

$$E_{\mathrm{XC}}[\rho_\alpha,\rho_\beta] = E^{\mathrm{LDA}}_{\mathrm{XC}}[\rho_\alpha,\rho_\beta] + \beta\sum_\sigma \int \frac{|\nabla\rho_\sigma(\mathbf{r})|^2}{\rho^{4/3}_\sigma(\mathbf{r})+\gamma}\mathrm{d}\mathbf{r} \tag{2.26}$$

which closely resembles the gradient expansion approximation of Eq. 1.58. The only difference is the constant γ on the denominator. This changes the exchange-correlation potential from

$$v_{\mathrm{XC},\sigma}(\mathbf{r}) = v^{\mathrm{LDA}}_{\mathrm{XC},\sigma}(\mathbf{r}) + \frac{4\beta|\nabla\rho_\sigma(\mathbf{r})|^2}{3\rho^{7/3}_\sigma(\mathbf{r})} - \frac{2\beta\nabla^2\rho_\sigma(\mathbf{r})}{\rho^{4/3}_\sigma(\mathbf{r})} \tag{2.27}$$

in the case of the GEA to

$$v_{\mathrm{XC},\sigma}(\mathbf{r}) = v^{\mathrm{LDA}}_{\mathrm{XC},\sigma}(\mathbf{r}) + \frac{4\beta|\nabla\rho_\sigma(\mathbf{r})|^2\rho^{1/3}_\sigma(\mathbf{r})}{3(\rho^{4/3}_\sigma(\mathbf{r})+\gamma)^2} - \frac{2\beta\nabla^2\rho_\sigma(\mathbf{r})}{\rho^{4/3}_\sigma(\mathbf{r})+\gamma} \tag{2.28}$$

for the functional defined in Eq. 2.26. The addition of the constant prevents the potential from diverging at long range (as $\rho \to 0$). The conventional way to prevent the divergence is with a function of x_σ, but this will introduce complex Hessian contributions to the potential that will degrade it in the intershell region.

Eq. 2.26 is not a conventional exchange functional because it does not obey the exchange scaling condition, Eq. 1.60. In the limit of an infinite density it will scale like exchange, but for finite densities it introduces some correlation. However, because the term has been designed to replace conventional exchange functionals, we will refer to it as KT exchange or KTX (following the naming convention of Ref. [127]).

The KT exchange term was implemented as a set of Fortran subroutines

in CADPAC. The KTX equations were written in open shell form so that both restricted and unrestricted calculations could be carried out. One subroutine calculates the KTX contribution to F_{XC} and its analytic derivatives with respect to the α and β densities and density gradients that are necessary for the evaluation of the exchange-correlation contribution to the Fock matrix (Eq. 1.84). F_{XC} and its derivatives were checked for consistency using the Hellmann-Feynman theorem [128]. For a molecule in an electric field of strength F applied in the z-direction,

$$\frac{dE}{dF} = \left\langle \Psi \left| \frac{\partial \hat{H}}{\partial F} \right| \Psi \right\rangle = - \langle \Psi | \hat{\mu}_z | \Psi \rangle = -\mu_z \tag{2.29}$$

where μ_z is the dipole moment along the z axis. This is true for both an exact wavefunction and for any variational method, and so must hold in DFT. Therefore μ_z can be calculated numerically by finite difference

$$\mu_z = \frac{E(F + \delta F) - E(F - \delta F)}{2\delta F} \tag{2.30}$$

The energy was calculated in an external electric field of ± 0.0001 au and put into Eq. 2.30 to calculate μ_z. The values obtained for closed shell and open shell molecules were checked so that they agreed with a standard dipole moment calculation, proving that the Hellmann-Feynman theorem was holding and therefore that the orbitals were variationally optimised.

A second subroutine calculates the KTX contribution to the exchange-correlation potential explicitly from Eq. 2.22. This provides an alternative but formally equivalent route to solving the Kohn-Sham equations (where the Fock matrix contribution is calculated according to Eq. 1.83). The two subroutines were checked for consistency by ensuring that they converged to the same answers for both open-shell and closed-shell molecules as the size of the integration grid increased.

There are two adjustable parameters in the KT exchange term, which we varied to give the best reproduction of the intershell structure in the ZMP potentials. The β coefficient is approximately linearly related to the size of the intershell peak and the γ value prevents divergence but also effects the

shape of the potential nearer the nucleus. Optimal values were found to be

$$\beta = -0.0045 \qquad \gamma = 0.1 \tag{2.31}$$

The CO, N_2 and PN potentials for the functional defined by Eqs. 2.26 and 2.31 are shown in plots (d) of Figures 2.1–2.3. The description of the intershell structure is clearly in better agreement with the ZMP potentials than those of LDA, BLYP and HCTH. The intershell peaks are much more pronounced than for BLYP and they exhibit none of the erratic behaviour of the HCTH potential. This improvement is reflected in the shielding constants for the three molecules, which are presented in Tables 2.2 and 2.3. In all cases they are closer to experiment than the other conventional functionals.

The new functional was assessed by calculating the full A1 and A2 sets of shielding constants. Overall the results were an improvement over those of conventional functionals, but it was not competitive with MKS(BD) or MKS(PBE0). Compared to the experiment data the isotropic shielding constants remained too low and the anisotropic shielding constants too high.

We found that the calculated shielding constants, like the size of the intershell peak, had a roughly linear relationship with the β parameter in the KT exchange term. By increasing the magnitude of β, the shielding constants could be uniformly improved. The parameter values that best reproduced the experimental shielding constants were

$$\beta = -0.006 \qquad \gamma = 0.1 \tag{2.32}$$

The functional defined by Eqs. 2.26 and 2.32 will hereafter be denoted KT1. Table 2.4 presents a full breakdown of the isotropic shielding constants of set A1 for KT1, compared to LDA and HCTH. KT1 is a significant improvement over these conventional functionals, with the mean absolute error reduced to 13.0 ppm for all molecules or 10.0 ppm excluding O_3. This is comparable to the MKS methods and competitive with the best *ab initio* wavefunction methods. KT1 also has the advantage of being a computationally much simpler method than either MKS or the wavefunction methods. Table 2.5 presents the same breakdown for anisotropic shielding constants. Again, KT1 is the best

performing conventional functional with a mean absolute error of 11.5 ppm, comparable to the MKS methods and in this case superior to the best *ab initio* calculations.

The KT1 exchange-correlation potentials are shown in plots (e) of Figures 2.1–2.3. For all three molecules they slightly overestimate the size of the intershell peaks compared to the ZMP potentials. KT1 is therefore specifically fitted to shielding constants and not exchange-correlation potentials.

Table 2.4: A1 isotropic shielding constants for the LDA, HCTH, KT1, and KT2 functionals. All values are in ppm.

Mol.	Nuc.	LDA	HCTH	KT1	KT2	*Ab initio*	Expt.
HF	F	416.2	411.5	412.0	412.4	418.6[a]	419.7 ± 6[a]
H_2O	O	334.8	327.6	330.7	329.6	337.9[a]	357.6 ± 17.2[a]
CH_4	C	193.1	189.3	196.4	195.2	198.9[a]	198.4 ± 0.9[a]
CO	C	−20.3	−7.5	10.4	7.4	5.6[a]	2.8 ± 0.9[a]
	O	−87.5	−66.8	−56.1	−57.1	−52.9[a]	−36.7 ± 17.2[a]
N_2	N	−91.4	−76.9	−55.8	−59.7	−58.1[a]	−59.6 ± 1.5[a]
F_2	F	−284.2	−269.9	−193.6	−211.0	−186.5[a]	−192.8[a]
O′OO′	O′	−1532.6	−1438.2	−1246.3	−1278.7	−1208.2[a]	−1290[a]
	O	−921.8	−859.4	−796.9	−809.1	−754.6[a]	−724[a]
PN	P	−73.7	−7.6	48.2	48.5	86[b]	53[b]
	N	−414.9	−378.5	−357.3	−360.2	−341[b]	−349[b]
H_2S	S	733.9	720.1	746.9	741.0	754.6[c]	752 ± 12[c]
NH_3	N	266.3	259.8	265.9	264.5	270.7[a]	273.3 ± 0.1[a]
HCN	C	65.3	75.7	87.2	86.0	86.3[a]	82.1[a]
	N	−56.7	−33.4	−18.6	−19.4	−13.6[a]	−20.4[a]
C_2H_2	C	100.8	112.2	120.5	120.4	121.8[d]	117.2[e]
C_2H_4	C	40.9	53.4	64.3	63.2	71.2[f]	64.5[f]
H_2CO	C	−40.0	−17.7	−3.0	−4.7	4.7[a]	−4.4 ± 3[a]
	O	−493.5	−406.7	−383.8	−379.6	−383.1[a]	−375 ± 100[a]
N′NO	N′	87.7	94.9	106.8	102.1	100.5[g]	99.5[g]
	N	−2.3	8.5	14.2	12.2	5.3[g]	11.3[g]
	O	179.0	174.8	184.1	177.5	198.8[g]	200.5[g]
CO_2	C	50.0	57.5	65.0	63.7	63.5[f]	58.8[f]
	O	209.7	215.3	224.5	221.6	236.4[h]	243.4 ± 17[h]
OF_2	O	−667.5	−610.9	−516.7	−534.0	−465.5[h]	−473.1[h]
H_2CNN'	C	164.5	161.8	170.1	167.4	171.9[a]	164.5[a]
	N	−61.5	−51.0	−37.5	−41.7	−31.6[a]	−43.4[a]
	N′	−166.4	−155.6	−128.3	−138.4	−142.4[a]	−149.0[a]
HCl	Cl	959.5	949.4	964.9	962.1	962.3[i]	952[i]
SO_2	S	−242.9	−183.9	−127.8	−134.7	−134.2[c]	−126 ± 12[c]
	O	−282.0	−260.6	−243.7	−250.7	−170.4[c]	−205 ± 17[c]
PH_3	P	583.1	576.6	605.4	601.0	594[b]	599.9[i]
d		−51.8	−32.4	−4.7	−9.5	4.5	
$\|d\|$		52.2	32.4	13.0	13.2	11.2	
Excluding O_3:							
d		−40.5	−25.2	−4.0	−7.7	3.1	
$\|d\|$		41.0	25.2	10.0	10.9	8.2	

[a] Ref. [118], GIAO-CCSD(T), experimental values include rovibrational corrections (except HCN).
[b] Ref. [119].
[c] Ref. [129], IGLO-CASSCF.
[d] Ref. [130], GIAO-CCSD.
[e] Ref. [107].
[f] Ref. [131], GIAO-MP2.
[g] Ref. [132], GIAO-CCSD.
[h] Ref. [133], GIAO-CCSD.
[i] Ref. [134], GIAO-MP3.

Table 2.5: A2 anisotropic shielding constants for the LDA, HCTH, KT1, and KT2 functionals. All values are in ppm.

Mol.	Nuc.	LDA	HCTH	KT1	KT2	*Ab initio*	Expt.
HF	F	95.4	105.3	108.0	109.8	94.3[a]	93.8[a]
NH_3	N	−50.3	−47.9	−46.8	−46.3	−43.8[a]	−40.3[b]
CO	C	438.4	420.9	397.7	403.2	401.0[a]	406.1 ± 1.4[a]
	O	744.3	716.0	703.1	706.6	694.6[a]	676.1 ± 26[a]
N_2	N	644.7	625.1	596.7	604.0	596.5[a]	603 ± 28[a]
F_2	F	1155.8	1137.2	1026.5	1054.9	1011.7[a]	1050 ± 50[a]
H_2CO	C	194.5	167.1	152.3	154.7	158.3[a]	158.8[a]
PN	P	1557.5	1461.7	1382.2	1384.7	1334[c]	1376[c]
	N	1133.3	1081.0	1052.0	1057.9	1023[c]	1048[c]
HCl	Cl	281.1	300.1	279.8	287.7	279.8[b]	298[b]
PH_3	P	−82.3	−64.5	−69.9	−67.1	−64.5[d]	−64.5[b]
d		46.1	27.0	−2.1	4.1	−10.9	
$\|d\|$		54.3	28.4	11.5	8.8	14.4	

[a] Ref. [118], GIAO-CCSD(T).
[b] Ref. [134], GIAO-MP3.
[c] Ref. [119].
[d] Ref. [135], GIAO-MP2.

2.4 Thermochemical and structural assessment of KT1

KT1 was fitted to experimental shielding constant data, whereas most semi-empirical functionals are fitted to thermochemical data. We have seen that the latter perform badly for shielding constants, and in the same way KT1 might fail for thermochemical and other properties. It is essential to assess semi-empirical functionals for a range of properties using non-fitted data to establish how generally applicable they are.

Following Ref. [50], we assessed KT1 for three thermochemical properties: atomisation energies (set A3 in Appendix A), ionisation potentials (A4), and total atomic and ionic energies (A5). We also assessed KT1 for molecular bond length optimisations of the set A6, again following Ref. [50]. All calculations were performed using the TZ2P basis set. Mean and mean absolute errors are presented in Table 2.6.

An atomisation energy is defined as the energy required to break a molecule into its component atoms

$$E_{\mathrm{AE}} = \sum_A E_A - E_M \tag{2.33}$$

where E_A are the atomic energies and E_M is the molecular energy. An atomisation energy can be specified either as an electronic atomisation energy (written as D_e), which is the difference between the atomic energies and the electronic molecular energy, or as D_0, which is the difference between the atomic energies and the molecule in the ground vibrational state. These two definitions differ by the value of the molecule's zero point energy (ZPE). The experimental data we compare to in set A3 (from Ref. [46]) has been corrected for ZPEs, so we compare electronic atomisation energies D_e. The A3 atomisation energy set is similar to the G2-1 atomisation energy set of Pople *et al.* [136], but with NO, H_2S, and Si_2H_6 removed for incidental reasons [46]. A number of charged species have also been added, bring the total number of systems to 61.

KT1 atomisation energies for the A3 set are significantly improved compared to LDA, which suggests that addition of the KT exchange term is ben-

Table 2.6: Error assessments for thermochemistry and molecular bond lengths for the LDA, HCTH, KT1, and KT2 functionals. Units are given in parentheses.

	LDA	HCTH	KT1	KT2
A3. Atomisation energies (kcal mol^{-1})				
d	35.3	0.9	12.5	−0.1
$\|d\|$	35.3	3.2	13.2	6.4
A4. Ionisation potentials (kcal mol^{-1})				
d	3.1	0.1	1.2	−0.2
$\|d\|$	3.1	1.6	1.3	3.9
A5. Total atomic and ionic energies (kcal mol^{-1})				
d	241.5	−0.9	−333.5	−461.4
$\|d\|$	241.5	4.2	334.7	461.8
A6. G2 subset bond lengths (Å)				
d	0.014	0.012	0.014	−0.001
$\|d\|$	0.022	0.013	0.019	0.010
A7. Diatomic bond lengths (Å)				
d	−0.012	0.036	0.008	−0.010
$\|d\|$	0.017	0.037	0.026	0.020

eficial. However, it cannot compete with the HCTH GGA, which offers one of the best GGA performances for thermochemistry (which might be expected as it has been fitted to the A3 thermochemical data, unlike LDA or KT1).

Ionisation potentials are defined as the energy difference between a molecule or atom and the corresponding ion with one electron removed

$$E_{\mathrm{IP}} = E_{M+} - E_M \tag{2.34}$$

Ionisation potentials again involve ZPE corrections, although their effect is much smaller because the ZPE of the molecule will be close to the ZPE of the molecular ion. The set A4 consists of seven second-row atoms with reference experimental values taken from Ref. [46]. KT1 performs very well for this set, surpassing both LDA and HCTH (despite HCTH having been fit to this set).

The atomic and ionic energy set A5 consists of 18 first-row atoms and ions from H to Ne. The reference values are exact energies taken from Refs. [137, 138]. LDA gives a very high error over the set, which HCTH reduces considerably (again, HCTH was fitted to these energies). The performance of KT1 is very poor, with a large error of the opposite sign to LDA.

The final assessments are of bond length optimisations. The A6 set is a subset of the molecules from Pople's G2-1 set for which accurate geometries are known [46]. The KT exchange term again appears to be beneficial, with KT1 performing better than LDA. However, HCTH performs better still, as it was fitted to energy gradients. We also considered the performance of KT1 for the A7 set of 45 diatomic bond length optimisations [139]. This is a more balanced test of geometry performance than the A6 set, as it contains atoms drawn evenly from the first three rows of the s and p blocks of the periodic table. It is also complementary as the A6 set contains many hydrogen atoms, whereas the A7 set has none. The TZ2P basis set is not available for all of the atoms considered, so instead we used the similar-sized 6-311+G(2df) basis. KT1 improves greatly upon HCTH for the diatomics, but both functionals are inferior to LDA! This is generally true of most GGA functionals (see Ref. [139] for other results). The success of LDA is presumably down to the relatively heavy atoms included in the A7 set, and the lack of hydrogen atoms (LDA

performance is poor for light atoms, which are the most unlike the uniform electron gas model).

2.5 The fit code

To improve the performance of the KT1 functional for properties other than shielding constants, it was necessary to introduce more flexibility into the functional form. KT1 behaves like the LDA in the uniform electron gas limit (when $|\nabla\rho_\sigma| \to 0$), and hence satisfies this exact condition. However, it is commonly found that a functional's performance for real chemical systems can be improved by relaxing this condition [43,47,49]. This results in a functional of the form

$$\begin{aligned} E_{\mathrm{XC}}[\rho_\alpha,\rho_\beta] &= \alpha E_{\mathrm{X}}^{\mathrm{LDA}}[\rho_\alpha,\rho_\beta] + \beta \sum_\sigma \int \frac{|\nabla\rho_\sigma(\mathbf{r})|^2}{\rho_\sigma^{4/3}(\mathbf{r})+\gamma}\mathrm{d}\mathbf{r} \\ &+ \delta E_{\mathrm{C}}^{\mathrm{VWN}}[\rho_\alpha,\rho_\beta] \end{aligned} \tag{2.35}$$

The fitting procedure we used to optimise the parameters is a modified version of that used to develop the TH [44–46], HCTH [47], B97-1 [47], B97-2 [51], and 1/4 [50] functionals. These functionals were fitted against the thermochemical data and/or ZMP exchange-correlation potentials of the systems from sets A3, A4, and A5. (B97-1 was fitted only to thermochemical data, and 1/4 was fitted only to exchange-correlation potentials.)

For this study, we choose to fit only to thermochemical data. This is because we already know that KT exchange can reproduce the exchange-correlation potential well, whereas we do not know the correct coefficients to give good thermochemical properties. As part of our investigations we did attempt to fit to exchange-correlation potentials as well, but the fitting procedure tended to give a value for the KT exchange coefficient β of almost zero! We believe this is because it does not sufficiently emphasise the error in the intershell peak compared to other areas of the potential (which the KT exchange term models less well). We also noted that in changing from the TZ2P basis set to the larger Huzinaga IV, the position of the intershell peak in the ZMP potential moves to line-up more closely with that of KT1 (the agreement

with TZ2P ZMP potentials is less good than with the Huzinaga IV potentials shown in Figures 2.1–2.3). This could be another reason why the KT exchange term is minimised.

The fitting code uses a linear least-squares fit, and so it cannot be used to fit to the non-linear parameter γ, which was kept fixed at the KT1 value of 0.1. We have found that the performance for shielding constants is relatively insensitive to the value of γ, and that this value is near-optimal.

The linear parameters were fitted by the minimisation

$$\frac{\partial\Omega}{\partial\alpha} = \frac{\partial\Omega}{\partial\beta} = \frac{\partial\Omega}{\partial\delta} = 0 \tag{2.36}$$

which may be generalised to any number of coefficients if required. The quantity Ω is a measure of the thermochemical accuracy of the functional

$$\Omega = \sum_{\mathrm{A3}}^{61}[E_{\mathrm{AE}}^{\mathrm{calc}} - E_{\mathrm{AE}}^{\mathrm{expt}}]^2 + \sum_{\mathrm{A4}}^{7}[E_{\mathrm{IP}}^{\mathrm{calc}} - E_{\mathrm{IP}}^{\mathrm{expt}}]^2 + \sum_{\mathrm{A5}}^{18}[E_{\mathrm{TE}}^{\mathrm{calc}} - E_{\mathrm{TE}}^{\mathrm{expt}}]^2 \tag{2.37}$$

where AE represents the atomisation energies of the A3 set of molecules, IP the ionisation potentials of the A4 atoms, and TE the total energies of the A5 atoms and cations.

The initial energies E^{calc} are determined within the fit code by an approximate calculation on the relatively small grids of the ZMP potentials (although the ZMP potentials are not fitted to directly, the corresponding densities and density gradients are used in this calculation), and the first least-squares iteration is performed compared to supplied reference numbers. This gives initial values for the parameters α, β, and δ. The true self-consistent energies using the functional with these parameters are then calculated using CADPAC. These results are put back into the fitting procedure, and the whole cycle is iterated until the coefficients have converged. Convergence is usually achieved in four or five iterations.

Table 2.7: Coefficients for functionals derived from the fitting procedure. T denotes fitting to total energies, A to atomisation energies, and I to ionisation potentials. F denotes that the coefficient β was fixed at -0.006. All functionals use $\gamma = 0.1$

	α LDAX	β KTX	δ VWN
T,A,I	1.00473E + 0	−3.28801E − 3	5.92452E − 1
A,I	1.06134E + 0	−5.42852E − 3	5.68370E − 1
A	1.05606E + 0	−5.41846E − 3	5.78928E − 1
T,A,I,F	9.01668E − 1	−6.00000E − 3	9.06839E − 1
A,I,F (KT2)	1.07173E + 0	−6.00000E − 3	5.76727E − 1
A,F	1.07024E + 0	−6.00000E − 3	5.79792E − 1

2.6 The KT2 functional

We experimented with several different types of fits to optimise the functional of Eq. 2.35. Table 2.7 presents the coefficients found using the fitting procedure. Table 2.8 presents the thermochemical and structural assessments of these functionals.

The first fit, to total energies, atomisation energies and ionisation potentials, was not a success. The value of β came out at roughly half that chosen for KT1. This resulted in poor shieldings, with a mean absolute error of 25.3 ppm for the A1 set, compared to an error of 13.0 ppm for KT1. We attribute this problem to including total energies in the fit. We have already seen that the performance of KT1 for total energies is very poor, so it appears that this functional form is unable to reproduce both accurate total energies and accurate shielding constants.

We therefore fitted the functional again, but removed total energies from the fit. This is an unusual method of fitting semi-empirical functionals (which are often developed by fitting only to total energies), but it proved useful in this case. The KT exchange β coefficient rose to almost the same value as in KT1, giving shieldings with an error of 15.0 ppm. The A3 atomisation energies were also much improved over KT1, with an error of 6.3 kcal mol^{-1} compared to 13.2 kcal mol^{-1} for KT1. However, ionisation potentials worsened

Table 2.8: Error assessments for thermochemistry, molecular bond lengths, and isotropic shielding constants. T denotes fitting to total energies, A to atomisation energies, and I to ionisation potentials. F denotes that the coefficient β was fixed at -0.006. Units are given in parentheses.

	KT1	T,A,I	A,I	A	T,A,I,F	A,I,F (KT2)	A,F
A1. Isotropic NMR shielding constants (ppm)							
d	−4.7	−23.8	−12.9	−12.5	5.2	−9.6	−9.4
$\|d\|$	13.0	25.3	15.0	14.8	17.0	13.2	13.2
Excluding O_3:							
d	−4.0	−19.0	−10.4	−10.0	3.7	−7.2	−7.6
$\|d\|$	10.0	20.6	12.7	12.6	12.9	10.9	10.9
A3. Atomisation energies (ppm)							
d	12.5	3.7	0.6	0.6	−3.5	−0.1	−0.2
$\|d\|$	13.2	6.6	6.3	6.2	7.9	6.4	6.4
A4. Ionisation potentials (kcal mol^{-1})							
d	1.2	−7.4	−1.6	−2.0	−13.3	−0.2	−0.3
$\|d\|$	1.3	7.6	3.8	3.8	13.3	3.9	3.8
A5. Total atomic and ionic energies (kcal mol^{-1})							
d	−333.5	5.9	−372.3	−356.2	−7.6	−461.4	−457.4
$\|d\|$	334.7	12.6	372.1	357.1	35.9	461.8	457.9
A6. G2 subset bond lengths (Å)							
d	0.014	0.018	0.002	0.003	0.052	−0.001	−0.001
$\|d\|$	0.019	0.021	0.010	0.011	0.052	0.010	0.010

slightly, from 1.6 kcal mol^{-1} to 3.9 kcal mol^{-1}. We also fitted another functional to only atomisation energies, with very little change observed in either coefficients or properties. While the 'A,I' functional improved performance for thermochemistry, the original KT1 functional gave better shieldings. This is directly related to the value of the KT exchange β coefficient. We therefore fixed the value of β to the KT1 value of -0.006 ppm, in the knowledge that this gives highly accurate shieldings. We fitted the remaining parameters to all three sets of energy data, which gave very different coefficients but equally poor results to the non-fixed version.

Removing total energies from the fit again gave much improved results. Atomisation energies improved to the level of the 'A,I' functional (expected because the coefficients are similar), and ionisation potentials similarly improved. Shielding errors were reduced to 13.2 ppm, on a par with KT1.

The A6 set of bond lengths were also improved compared to KT1, with the error reducing to 0.010 Å (surpassing HCTH). Removing ionisation potentials from the fit had a negligible effect on the coefficients and results; as before. The best performing functional is therefore 'A,I,F', which following Ref. [127] we denote KT2. A summary of the performance of KT2 in comparison to LDA, HCTH, and KT1 is presented in Table 2.6. KT2 also performs well for the A7 set of diatomic bond lengths, with an error of 0.020 Å. This error is still not as low as that of LDA, and it is also not competitive with the best GGA, 1/4, which gives an error of 0.010 Å. However, 1/4 gives poor performance for non-structural properties [50] and so cannot be considered a general purpose functional.

The full breakdown of isotropic shielding constants for KT2 is presented in Table 2.4. We also assessed KT2 for the A2 set of anisotropic shielding constants. For this set KT2 gave better performance than KT1, with $d = 4.1$ ppm and $|d| = 8.8$ ppm. A full breakdown is presented in Table 2.5.

In conclusion, we are confident that KT2 gives comparable performance to KT1 for shielding constants, whilst improving thermochemical and structural performance. For thermochemical properties it is still not competitive with the best GGAs, but its performance is promising. For atomic and ionic energies its performance remains very poor, but we consider this to be relatively unimpor-

tant as practical chemical observations involve energy differences, where these errors cancel.

2.7 Rationalising the improvement in shielding constants

The impressive performance of KT1 and KT2 for shielding constants can be ascribed to the quality of their exchange-correlation potentials, and it is natural to assume that the description of the intershell peak in the valence region is particularly important. However, it is possible to get good quality shieldings without such a peak. For example, the MKS(B97-1) method [103] gives excellent shieldings (with $|d| = 16.5$ ppm over the A1 set), but does not have a noticeable peak in its potential. A more general explanation for the performance is required.

2.7.1 Split potentials

We first tested which regions of space were responsible for the improvement in shielding constants, looking at the N_2 and CO molecules. The potential was calculated on a numerical integration grid, so it was possible to apply the KT exchange correction only to certain parts of the grid, leaving other parts as the LDA. We placed spheres of radius R around each nucleus, and defined the potential as equal to KT1 inside the sphere, and LDA outside. If $R = 0$, the potential is LDA everywhere, whereas if $R = \infty$, the potential is KT1 everywhere. For intermediate values of R, the potential is split into two.

Figure 2.4 shows the effect of varying R on the shielding constant of N_2. Between $R = 0$ au and $R \approx 0.4$ au, the isotropic shielding constant varies by approximately 5 ppm. This demonstrates that the KT correction to the core is not very important for the shielding constant. Between $R \approx 0.4$ au and $R \approx 1.0$ au the change in shielding constant is much larger, nearer 40 ppm. This indicates that the valence region is very important for shielding constant results. For values of R above ≈ 1.0 au, the shielding constant variation is small, which shows that the shielding constant is insensitive to the asymptotic

region of the potential. This is consistent with Ref. [100], which showed that adding a correction to the potential in the asymptotic region did not affect the shielding constant results.

The CO molecule showed analogous results. Although we were dealing with two different nuclei at the same time, we did not have to vary the size of the spheres independently because the intershell structure occurs in roughly the same region of both nuclei. For molecules where this is not the case, such as PN, a more sophisticated analysis would be necessary.

Two further conclusions can be drawn from these results. Firstly, in both N_2 and CO, the variation in shielding constant in the core is roughly equivalent to the difference in shielding constant on increasing β from -0.0045 (the value that agrees most precisely with the ZMP potentials) to -0.006 (the value that gives the best shielding constants). This supports the argument that the increase in the β value in the KT exchange term is necessary to compensate for an inappropriate correction to the core that it gives. If KT exchange could be modified in some way to give a better description of the core, it would no longer be necessary to have such a high β value.

Secondly, closer inspection of the region between $R \approx 0.4$ au and $R \approx 1.0$ au in N_2 shows that the bulk of the shielding constant change actually occurs between $R \approx 0.4$ au and $R \approx 0.6$ au, and above that value the change is much less pronounced. This first region corresponds to the rise of the potential towards the intershell peak. The second region corresponds to a lowering of the potential to produce the characteristic turning shape. This suggests that it is the initial rise in the potential which is more important than the full turn. This indicates why potentials such as MKS(B97-1), which contain the rise but not the turn, also give good shielding constants.

Results for anisotropic shielding constants for N_2 and CO are presented in Figure 2.5. The results are analogous to the isotropic case.

2.7.2 HOMO-LUMO gaps

It has previously been observed that there is a correlation between GGA DFT shielding constants for main-group nuclei and occupied-virtual eigenvalue dif-

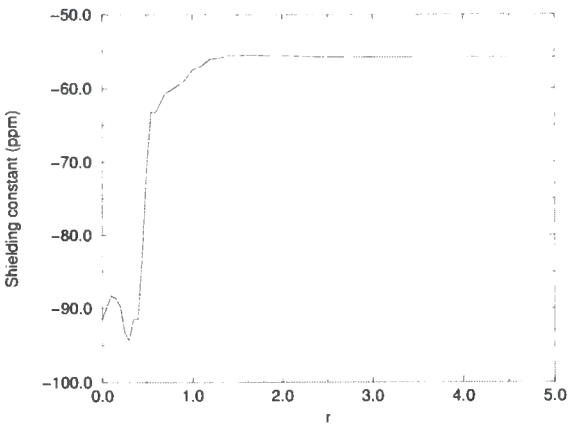

(a)

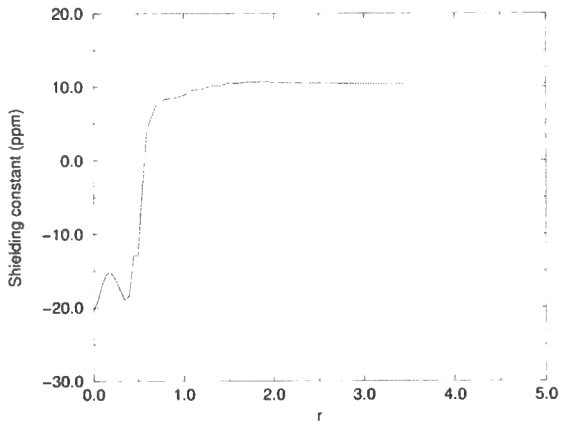

(b)

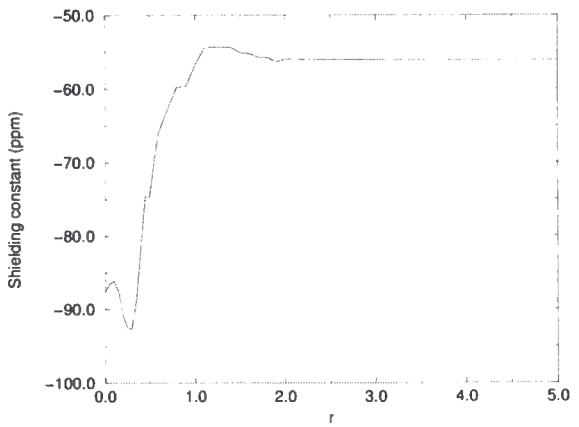

(c)

Figure 2.4: Spatial analysis (in au) of the isotropic shielding constant (ppm) for (a) N_2, (b) C nucleus of CO and (c) O nucleus of CO.

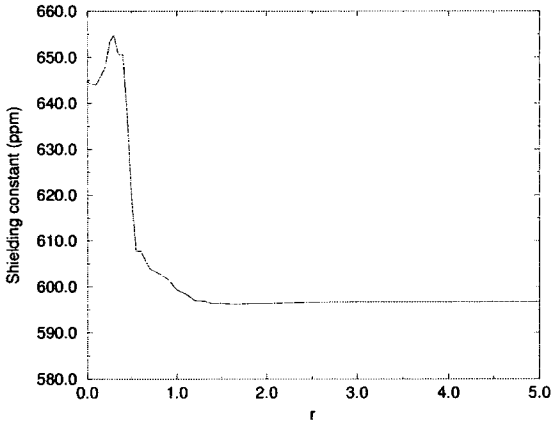

(a)

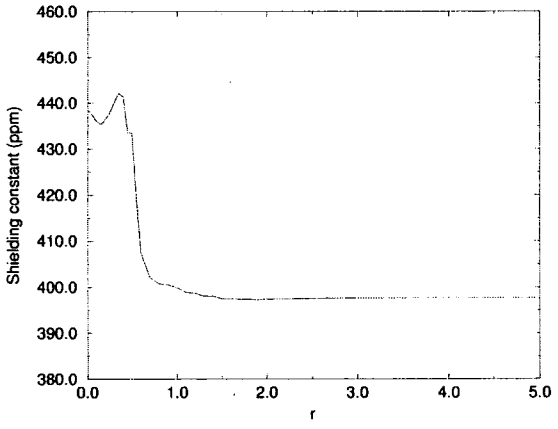

(b)

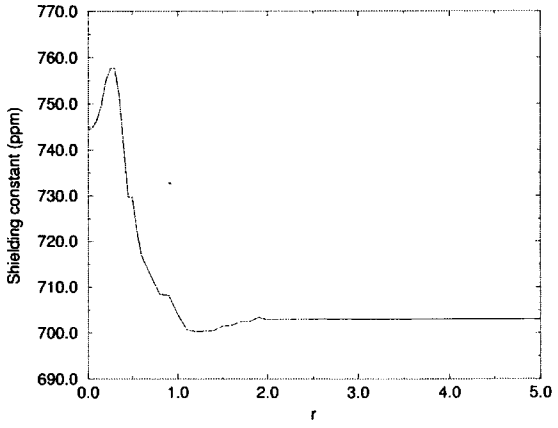

(c)

Figure 2.5: Spatial analysis (in au) of the anisotropic shielding constant (ppm) for (a) N_2, (b) C nucleus of CO and (c) O nucleus of CO.

ferences [109,110,112,140]. As discussed in Section 2.1, GGA shielding constant errors are caused by an overestimated paramagnetic contribution to the shielding, which is in turn caused by underestimated eigenvalue differences.

In Refs. [109,110] it was shown that shielding constants could be improved by adding an *ad hoc* correction to the denominator of the paramagnetic (second) term of Eq. 2.9. In Ref. [140], a similar improvement was found simply by increasing the lowest unoccupied Kohn-Sham eigenvalue (the LUMO), thus increasing the gap between it and the highest unoccupied (HOMO) eigenvalue. This works because the HOMO-LUMO gap often gives a particularly important paramagnetic contribution (it has the smallest occupied-virtual eigenvalue difference, which appears on the denominator of the expression). It should be noted, however, that neither of these approaches bring the shielding constants up to the standard of the best MKS methods or KT1/2.

We therefore considered the HOMO-LUMO eigenvalue differences corresponding to the KT1 and KT2 shielding calculations. The values for a subset of the A1 molecules in which the improvement in shielding constants is particularly significant are presented in Table 2.9, together with near-exact MKS(BD) gaps. When compared with LDA and HCTH, there is a clear increase in HOMO-LUMO gaps, as expected, and the KT1 and KT2 gaps are much closer to the MKS(BD) values. Moreover, for those molecules whose shielding constants were not improved by KT1 (such as H_2O and NH_3), the gaps remained small in comparison to those of MKS(BD). This confirms the view that there is an explicit link between the HOMO-LUMO gaps and the shielding constant results.

Table 2.9: Kohn-Sham HOMO-LUMO eigenvalue differences. All values are in atomic units.

Mol.	LDA	HCTH	KT1	KT2	MKS(BD)[a]
CO	0.253	0.263	0.269	0.272	0.27
N_2	0.302	0.309	0.316	0.319	0.32
F_2	0.126	0.136	0.154	0.155	0.16
PN	0.160	0.166	0.169	0.171	0.17
H_2CO	0.126	0.137	0.141	0.143	0.15
OF_2	0.122	0.132	0.144	0.145	0.16
SO_2	0.134	0.136	0.139	0.140	0.15

[a] Ref. [101].

Chapter 3

Assessment of KT1 and KT2

In this chapter we assess the KT1 and KT2 functionals for the computation of magnetisabilities, chemical shifts, and indirect nuclear spin-spin coupling constants, to establish whether their good performance for shielding constants is maintained for these other magnetic response properties. We also assess their performance for shielding constants of larger molecules than previously considered, using the GIAO formalism.

3.1 Magnetisabilities

The magnetisability of a molecule is defined as the second derivative of the electronic energy with respect to the magnetic field

$$\zeta = -\frac{\partial^2 E}{\partial \mathbf{B}^2} \tag{3.1}$$

For a GGA functional, the magnetisability tensor is expressed in terms of the Kohn-Sham orbitals and eigenvalues [141]

$$\zeta_{\alpha\beta} = -\frac{1}{4}\sum_j \left(j|(r^2\delta^{\alpha\beta} - r^\alpha r^\beta)|j\right) + \sum_{bj} \frac{(j|l^\alpha|b)(b|l^\beta|j)}{\varepsilon_b - \varepsilon_j} \tag{3.2}$$

with quantities as defined in the shielding constant tensor expression of Eq. 2.9. Like that expression, the tensor components are separated into diamagnetic and paramagnetic terms, with occupied-virtual eigenvalue differences in the

denominator of the latter. It is therefore anticipated that the KT exchange term will have a significant effect on the paramagnetic term.

Isotropic and anisotropic magnetisabilities are defined following Ref. [141]. For linear and symmetric top molecules, the isotropic magnetisability is given by

$$\zeta_{\rm iso} = \frac{1}{3}(\zeta_{||} + 2\zeta_{\perp}) \tag{3.3}$$

where $\zeta_{||}$ is the component along the major molecular axis and $\zeta_{\perp}$ is the component perpendicular to it. The anisotropic magnetisability is

$$\Delta\zeta = \zeta_{\perp} - \zeta_{||} \tag{3.4}$$

For all other symmetries, the isotropic magnetisability is

$$\zeta_{\rm iso} = \frac{1}{3}{\rm tr}\zeta \tag{3.5}$$

and the anisotropic magnetisabilities are

$$\begin{aligned} \Delta\zeta_1 &= 2\zeta_{xx} - \zeta_{yy} - \zeta_{zz} \\ \Delta\zeta_2 &= 2\zeta_{yy} - \zeta_{xx} - \zeta_{zz} \end{aligned} \tag{3.6}$$

where ζ_{ii} are the principal tensor components.

Relatively few DFT studies of magnetisabilities have been carried out [100, 141–143], and it is of interest to determine how well KT1 and KT2 perform. Following Ref. [141], we calculated isotropic magnetisabilities for the A8 set of 12 molecules (a subset of the A1 shielding constant set). Anisotropic magnetisabilities were calculated on the smaller A9 set of 10 molecules (with CH_4 and CO not included). The magnetisabilities were calculated at the same near-experimental geometries as for the shielding constant assessment, using the same modified Huzinaga IV basis set defined in Ref. [105], and a centre of mass gauge origin following Ref. [141].

Isotropic results are presented in Table 3.1 and anisotropic results in Table 3.2. It is difficult to find reliable experimental reference data for these properties, so errors are calculated relative to linearised coupled cluster doubles

Table 3.1: KT1 and KT2 isotropic magnetisabilities compared with HCTH and B97-2. All values are in 10^{-30} JT^{-2}.

Molecule	KT1	KT2	HCTH	B97-2	L-CCD[a]	MCSCF
HF	−179.1	−176.1	−176.4	−175.3	−176.0	−177.0[b]
H_2O	−238.1	−234.4	−233.9	−233.1	−234.7	−236.6[b]
CH_4	−321.2	−316.5	−314.5	−315.0	−317.1	−318.1[c]
CO	−215.0	−210.2	−203.5	−203.9	−212.4	−217.6[b]
N_2	−210.1	−205.4	−196.6	−197.9	−207.5	−211.4[e]
F_2	−176.5	−172.0	−165.9	−173.8	−174.0	−175.6[d]
O_3	128.7	135.3	180.5	237.5	–	97.8[b]
NH_3	−293.5	−289.3	−287.9	−287.7	−290.2	−293.1[b]
HCN	−276.0	−271.8	−262.9	−266.3	−274.5	−282.8[e]
C_2H_2	−379.7	−375.0	−365.3	−368.6	−373.5	−376.6[b]
H_2CO	−118.9	−120.1	−113.2	−118.7	−129.9	−133.4[b]
CO_2	−373.6	−369.0	−366.5	−370.0	–	−372.6[d]
$\|d\|$ (MCSCF)	5.7	7.7	15.9	18.7		
Excluding O_3:						
$\|d\|$ (L-CCD)	4.0	2.2	7.1	5.0		
$\|d\|$ (MCSCF)	3.4	5.0	9.9	7.7		

[a] Ref. [144], L-CCD.
[b] Ref. [145], GIAO-MCSCF.
[c] Ref. [146], GIAO-MCSCF.
[d] Ref. [147], GIAO-MCSCF.
[e] Ref. [148], GIAO-MCSCF.

Table 3.2: KT1 and KT2 anisotropic magnetisabilities compared with HCTH and B97-2. All values are in 10^{-30} JT^{-2}.

Molecule		KT1	KT2	HCTH	B97-2	L-CCD[a]	MCSCF
HF	$\Delta\zeta$	−8.8	−8.7	−8.9	−9.0	−8.5	−8.5[b]
H_2O	$\Delta\zeta_1$	−5.5	−5.3	−4.9	−4.4	–	−4.4[b]
	$\Delta\zeta_2$	7.5	7.8	7.3	7.8	6.9	7.3[b]
CO	$\Delta\zeta$	136.5	136.8	143.3	142.6	133.3	126.4[b]
N_2	$\Delta\zeta$	143.7	144.1	152.9	152.4	139.2	134.9[c]
F_2	$\Delta\zeta$	164.8	164.7	174.5	160.9	163.9	–
O_3	$\Delta\zeta_1$	1174.0	1179.8	1401.5	1588.3	–	1050.8[b]
	$\Delta\zeta_2$	2.6	5.6	−62.5	−55.2	–	12.8[b]
NH_3	$\Delta\zeta$	−17.7	−17.3	−17.3	−16.9	−17.2	−17.0[b]
HCN	$\Delta\zeta$	113.1	112.2	118.8	115.8	104.5	90.7[c]
C_2H_2	$\Delta\zeta$	44.4	43.3	48.4	46.5	38.6	33.7[b]
H_2CO	$\Delta\zeta_1$	418.1	411.6	442.8	441.7	431.8	408.9[b]
	$\Delta\zeta_2$	−75.8	−65.2	−64.9	−52.2	–	−47.4[b]
$\|d\|$ (MCSCF)		18.8	17.4	46.3	59.7		
Excluding O_3:							
$\|d\|$ (L-CCD)		4.2	4.8	7.8	6.3		
$\|d\|$ (MCSCF)		9.2	7.3	13.0	11.0		

[a] Ref. [144], L-CCD.
[b] Ref. [145], GIAO-MCSCF.
[c] Ref. [148], GIAO-MCSCF.

(L-CCD) and MCSCF results from Refs. [144–148].

Both KT1 and KT2 perform very well for magnetisabilities. For isotropic magnetisabilities, KT1 performs better than KT2 compared with MCSCF but KT2 performs better compared to L-CCD. The situation is reversed for anisotropic magnetisabilities. Both functionals outperform HCTH and B97-2 by a significant margin. B97-2 is the worst functional compared with MCSCF, but this error is dominated by ozone. When ozone is removed, B97-2 gives lower errors than HCTH. The KT1 and KT2 results are comparable with the more computationally demanding MKS(BD) and MKS(B97-1) methods [141].

Wilson *et al.* recently assessed the performance of KT1 and KT2 for the determination of rotational g tensors, which are closely related to magnetisabilities [149]. These two functionals were found to have the widest applicability and reliability of all the functionals considered in the study.

3.2 Chemical shifts

NMR properties are generally measured relative to a reference molecule, and so differences in shielding constants are measured rather than absolute shielding constants. These differences are termed chemical shifts (δ), and are defined for a given nucleus with an absolute shielding σ as

$$\delta = \sigma_{\text{ref}} - \sigma \tag{3.7}$$

where σ_{ref} is the absolute shielding constant of that nucleus in a reference molecule.

DFT is a long-established method for chemical shift calculations [150], and calculations have been performed on systems as diverse as transition metal complexes [151–153], fullerenes [154,155], lanthanides [156], and biological systems [157–161]. From Eq. 3.7, it might be expected that DFT calculations of chemical shifts would be subject to a cancellation of errors between the two absolute shieldings. However, the performance of LDA and GGA functionals for challenging nuclei (such as nitrogen, oxygen, and fluorine) remains poor and the inferior performance of hybrid functionals for shielding constants is

also observed for chemical shifts [111,112].

It is not obvious that the KT1 and KT2 functionals will give as good results for chemical shifts as they did for shielding constants — the improvement over other GGAs for shielding constants could just be a uniform rise, which would be cancelled out when shielding constant differences are considered. It is therefore important to assess them for a set of chemical shifts [162].

The A10 chemical shifts dataset is a subset of the systems in Ref. [111], in which the isotropic chemical shifts of 44 molecules containing H, C, N, O and F nuclei were studied. This has previously been used to assess the performance of the self-interaction corrected Vosko-Wilk-Nusair (SIC-VWN) method of Patchkovskii *et al.* [111] and the statistical average of orbital potentials (SAOP) method of Poater *et al.* [112]. SIC-VWN consists of the local density approximation modified with the self-interaction correction of Perdew and Zunger [30], calculated within the optimised effective potential formalism. SAOP is a model exchange-correlation potential.

For technical reasons, we considered only 36 of these molecules. It was therefore necessary to recalculate the results of the previous studies for this subset, in order to allow comparison. Following Ref. [112], we calculated the errors for each method by optimising the value of a notional reference shielding σ_{ref} such that the mean error for the calculated chemical shifts is zero. This process was carried out separately for each nucleus. All calculations were performed at the TZP-quality BP86 geometries from the supplementary information of Ref. [111], using the LORG formalism.

We used a standard CADPAC Van Duijneveldt contraction basis set, with 8s6p3d basis functions for C, N, O and F, and 6s3p for H, which is slightly smaller than that used for the SAOP assessment, but larger than that used for the SIC-VWN assessment. To quantify the agreement with the results in Refs. [111,112], we recalculated their LDA errors for the subset of 36 molecules. This involved using their quoted LDA chemical shifts and reference shieldings to determine the corresponding absolute shieldings using Eq. 3.7. A new set of reference shieldings and chemical shifts was then calculated for the subset by the method of minimising the mean error outlined above. The new errors are compared with our own LDA errors in Table 3.3.

Table 3.3: LDA reference shieldings σ_{ref} and mean absolute errors in isotropic chemical shifts for the A10 set. Values for Poater *et al.* [111] and Patchkovskii *et al.* [112] have been re-calculated from the data in the original references. All values are in ppm.

		C	H	N	O	F
This work						
	σ_{ref}	175.1	30.57	−112.9	173.3	302.6
	Mean abs. error	9.2	0.41	57.3	138.5	31.1
Poater *et al.* [112]						
	σ_{ref}	173.8	30.43	−114.3	176.6	306.2
	Mean abs. error	9.4	0.41	56.1	133.1	30.1
Patchkovskii *et al.* [111]						
	σ_{ref}	179.3	30.45	−106.6	192.6	314.7
	Mean abs. error	7.8	0.41	53.5	124.6	24.7

Our values are in good agreement with the large basis set calculations of Poater *et al.*, but not with the smaller basis set results of Patchkovskii *et al.* (in general their errors are smaller). This indicates that we can make a direct comparison of our methods with the SAOP results but not with those of SIC-VWN. Table 3.4 presents isotropic chemical shifts from the HCTH GGA functional, the B97-2 hybrid functional, the SAOP model potential (recalculated using the data in Ref. [112]), the MKS(B97-2) method, and the KT2 functional, all determined at BP86 geometries. These are compared with experimental values from Ref. [111].

Table 3.5 presents the corresponding reference shieldings σ_{ref} and mean absolute errors for each method. The HCTH results represent the best that can be obtained from previous GGA functionals, but as for shielding constants they are disappointing. In particular the errors from the N and O nuclei are very large. The hybrid functional B97-2 gives worse results overall, with O errors getting markedly larger. The H errors are similar in magnitude to a typical rovibrational correction, and the experimental values have not been corrected for these effects. A detailed assessment of these results would therefore require further analysis.

Results improve greatly when using SAOP, with the performance for O in particular improving notably. MKS(B97-2) improves even further, especially for O and F. KT2 is intermediate between these two methods. However, both

MKS(B97-2) and SAOP are non-standard methods. MKS(B97-2) in particular is computationally demanding, and neither method can be used to optimise geometries because they are not associated with well-defined functionals and therefore will not be invariant to translations. Optimisations in internal coordinates would suppress this problem, but the optimised geometry would then depend on the choice of internal coordinates [163].

The KT2 results, therefore, are encouraging. They offer a significant improvement over HCTH, the other GGA tested, and are surpassed only by MKS(B97-2). KT2 is also a much simpler method than MKS(B97-2) and less computationally costly.

Because KT2 is a well-defined functional, we were also able to test the geometry dependence of its chemical shifts. The structures of the 36 molecules were optimised using the same 8s6p3d/6s3p basis used for the chemical shifts, and the reference shielding and errors were re-calculated. Results are shown in Tables 3.4 and 3.5. Chemical shifts are clearly sensitive to the geometry, with N and O errors decreasing, although F errors get slightly larger. However, the lack of rovibrational corrections in the experimental chemical shift have to be taken into account. For the most part these corrections are small, because the correction for the absolute shielding is cancelled in part by the reference shielding, but for the F_2 molecule in particular the net shift correction is large, at approximately 35 ppm [164]. By including this result alone, the KT2 errors at the BP86 geometries and the KT2 geometries become almost identical, at 16.2 ppm. To keep consistency with the earlier studies we did not attempt to find rovibrational corrections for every experimental number. Although these corrections should be negligible for most molecules under consideration, these results should be considered a qualitative guide to functional performance rather than a precise assessment.

For comparison we also present the errors for the KT2 functional performed at geometries optimised using the 1/4 functional, which is known to have an excellent performance for structures in general [50,139]. The results show little change, and in fact overall they degrade slightly. Therefore we consider KT2 geometries to be of acceptable quality for achieving optimal chemical shift results for main-group systems.

Table 3.4: Isotropic chemical shifts. SAOP values have been re-calculated from the data in Ref. [112]. Unless otherwise stated, calculations are performed at TZP BP86 geometries. All values are in ppm.

Molecule	Nucleus	HCTH	B97-2	SAOP	MKS (B97-2)	KT2	KT2[a]	Expt[b]
CO	C	195.6	202.0	192.0	192.6	188.8	188.6	194.2
	O	296.0	272.0	313.4	345.4	330.8	354.3	386.3
CO_2	C	127.7	131.7	128.6	129.6	130.1	131.0	136.4
	O	11.4	−20.3	44.8	73.4	50.2	74.5	100.6
F_2	F	629.3	618.2	638.6	585.8	573.6	536.1	596.0
OF_2	O	967.9	869.1	952.6	905.6	910.5	853.3	817.1
	F	457.8	446.4	455.1	424.0	446.3	420.4	426.0
HOF	O	399.4	365.5	443.5	431.6	400.0	389.2	
	H	12.6	12.6	13.4	12.1	11.8	11.4	12.1
	F	206.9	187.8	191.4	203.2	197.8	186.8	194.0
NF_3	N	108.8	99.3	110.4	106.5	112.0	103.3	
	F	357.0	353.1	343.3	338.1	364.1	358.4	312.8
H_2O	O	−96.8	−130.8	−71.6	−27.4	−55.4	−35.7	0.0
	H	0.2	0.4	0.8	0.4	0.2	0.0	0.55
H_2O_2	O	154.3	109.7	177.4	204.7	181.2	184.6	210.6
	H	7.1	6.9	7.5	6.9	6.8	6.5	
HCN	C	108.1	111.5	111.1	108.5	106.2	108.1	113.0
	N	−60.0	−54.5	−54.5	−53.1	−54.9	−44.8	−41.3
	H	2.6	2.6	2.2	2.7	3.0	2.9	2.83
N_2	N	−12.5	−4.4	−8.4	−8.4	−10.8	−3.1	0.0
N_2O	N(terminal)	−180.4	−171.9	−168.1	−167.5	−168.0	−162.5	−161.1
	N(middle)	−98.3	−87.2	−86.3	−81.6	−82.7	−74.8	−72.9
	O	61.5	32.2	100.8	117.3	104.4	123.1	141.5
N_2O_3	N(NO)	654.6	544.9	541.5	520.3	535.6	466.0	366.0
	$N(NO_2)$	89.1	115.0	112.1	108.8	103.3	100.5	138.0
	O(NO)	1217.7	1089.5	1068.1	1069.0	1088.2	1036.0	891.0
	$O(NO_2)$	347.3	344.0	398.8	407.8	388.4	395.6	461.0
O_3	O(terminal)	1803.5	2047.1	1755.2	1566.8	1664.6	1587.0	1634.0
	O(middle)	1137.3	1387.9	1193.3	1122.1	1126.3	1116.2	1068.0
HF	F	−89.5	−74.3	−74.0	−64.3	−79.5	−66.2	−46.9
	H	1.7	2.1	3.3	2.1	1.5	1.4	2.10
NH_3	N	−350.0	−352.6	−349.0	−332.5	−335.9	−330.5	−326.2
	H	−0.4	−0.3	−0.5	−0.3	−0.4	−0.5	−0.09
CH_4	C	−3.5	−4.7	−5.7	−1.4	−1.1	−2.1	0.0
	H	−0.1	−0.1	−0.4	−0.1	−0.1	−0.1	0.00
C_2H_6	C	13.6	10.8	11.8	14.8	15.9	14.6	14.2
	H	0.7	0.6	0.4	0.7	0.8	0.8	0.74

continued on next page...

Table 3.4: *continued*

Molecule	Nucleus	HCTH	B97-2	SAOP	MKS (B97-2)	KT2	KT2[a]	Expt[b]
C_2H_4	C	131.3	131.9	133.2	130.5	129.8	130.2	130.5
	H	5.5	5.4	5.2	5.4	5.4	5.6	5.18
CH_2CCH_2	C(middle)	225.0	228.3	227.5	222.7	222.0	223.4	224.3
	C(terminal)	77.8	77.9	77.7	77.7	77.7	77.6	79.7
	H	4.7	4.6	4.2	4.6	4.7	4.8	
C_2H_2	C	71.2	72.8	74.6	72.7	71.5	73.4	77.9
	H	1.2	1.2	0.7	1.3	1.5	1.4	1.33
H_2CO	O	640.7	628.0	616.0	650.7	657.1	681.9	590.0
	C	204.2	204.3	205.6	201.8	199.5	200.1	195.2
	H	10.2	9.9	9.8	9.7	10.0	10.2	9.5
CH_3CHO	C(C(O)H)	207.9	209.1	210.8	207.4	203.7	204.1	201.7
	$C(CH_3)$	37.2	34.7	36.3	38.8	39.8	39.2	38.0
	O	568.7	555.2	548.9	586.4	591.4	613.7	628.0
	H(C(O)H)	10.2	9.9	9.9	9.8	10.1	10.4	
	$H(CH_3)$	1.8	1.8	1.6	2.0	1.8	2.1	1.79
CH_2CO	C(CO)	200.0	203.8	200.4	198.1	198.6	198.3	201.0
	$C(CH_2)$	1.9	1.8	2.3	3.7	3.3	2.2	9.5
	O	240.3	217.2	255.0	287.0	277.0	299.3	
	H	2.2	2.3	1.7	2.2	2.3	2.3	
CH_2CHCHO	O	572.2	550.0	542.2	580.9	588.7	611.5	615.1
	C(C(O)H)	201.3	203.0	202.7	198.4	197.7	198.5	201.2
	C(CH)	148.8	149.1	150.1	147.8	148.2	148.5	145.8
	$C(CH_2)$	146.9	147.3	149.7	145.6	144.0	145.6	144.6
	H(C(O)H)	9.9	9.7	9.5	9.5	9.8	10.1	
	H(CH)	6.3	6.4	6.2	6.3	6.4	6.6	
	$H(CH_2$,cis)	6.5	6.5	5.9	6.1	6.5	6.8	
	$H(CH_2$,trans)	6.2	6.2	6.3	6.4	6.1	6.3	
$(CH_2)_2O$	C	49.0	45.5	49.9	51.1	50.4	49.6	47.6
	O	−101.6	−144.9	−83.8	−34.9	−66.7	−44.2	−13.0
	H	2.4	2.3	2.1	2.4	2.4	2.4	
C_3O_2	C(middle)	−14.0	−16.7	−13.4	−14.8	−13.0	−12.6	−7.6
	C(terminal)	119.7	125.2	121.1	122.1	120.9	122.2	136.7
	O	89.2	58.3	121.5	148.0	125.0	150.8	
CH_3NH_2	C	37.3	34.0	36.6	38.4	40.1	39.1	36.8
	N	−325.6	−332.3	−326.6	−311.0	−312.2	−307.4	−311.7
	$H(CH_3)$	2.2	2.1	2.0	2.1	2.3	2.3	
	$H(NH_2)$	0.0	0.0	−0.2	0.1	0.1	0.0	0.27
CH_2NN	C	25.4	25.6	28.2	26.8	28.3	26.7	30.1
	N(middle)	−38.5	−40.8	−23.3	−27.7	−28.8	−21.7	−16.2
	N(terminal)	75.8	102.1	79.5	72.2	76.6	78.1	90.4
	H	3.1	3.2	2.7	3.1	3.3	3.4	

continued on next page...

Table 3.4: *continued*

Molecule	Nucleus	HCTH	B97-2	SAOP	MKS (B97-2)	KT2	KT2[a]	Expt[b]
CH_3CN	$C(CH_3)$	5.1	2.9	3.5	6.5	8.0	7.4	7.4
	C(CN)	119.1	121.5	121.8	118.8	117.1	118.9	121.3
	N	−69.2	−63.5	−64.1	−62.6	−61.5	−52.7	−52.8
	H	1.6	1.6	1.2	1.6	1.8	1.8	1.53
CH_3NC	$C(CH_3)$	30.6	28.6	29.8	32.1	33.9	33.4	33.8
	C(NC)	173.9	179.7	175.9	172.8	168.9	170.3	165.2
	N	−181.0	−180.2	−178.1	−169.8	−172.0	−162.2	−141.0
	H	2.9	2.8	2.5	2.9	3.0	3.1	
CH_3NO_2	C	68.1	66.9	68.7	68.5	70.7	68.9	68.4
	N	42.2	71.4	71.2	58.7	57.1	61.1	74.7
	O	589.1	580.5	613.5	601.4	609.5	617.4	639.0
	H	4.1	4.0	3.7	4.0	4.2	4.1	3.91
CH_3F	C	80.9	77.1	82.1	81.5	82.5	81.6	78.9
	F	−133.3	−127.4	−130.0	−111.0	−128.4	−114.0	−107.7
	H	4.1	4.0	4.1	4.1	4.2	4.4	4.00
CH_2F_2	C	124.8	119.5	123.6	124.2	126.5	125.4	117.6
	H	5.8	5.5	5.6	5.7	5.9	6.1	
	F	4.3	7.7	6.6	19.5	17.6	32.5	24.1
CHF_3	C	136.8	131.6	131.2	135.7	138.4	137.0	126.7
	H	6.7	6.4	6.4	6.5	6.8	7.0	
	F	71.0	76.3	73.3	84.9	87.1	100.9	89.1
CF_4	C	143.2	138.0	132.7	141.5	145.0	144.0	130.7
	F	88.1	96.6	89.5	103.6	102.3	115.1	104.2
COF_2	C	147.0	147.2	141.2	147.3	148.6	149.3	141.1
	O	202.4	180.4	216.5	255.0	237.6	258.2	
	F	141.5	148.7	139.4	149.3	152.3	163.2	141.5

[a] Evaluated at KT2 optimised geometries
[b] Ref. [111]

Table 3.5: Reference shieldings σ_{ref} and mean absolute errors in isotropic chemical shifts for the A10 set. SAOP values have been re-calculated from the data in Ref. [112]. Unless otherwise stated, calculations are performed at TZP BP86 geometries. All values are in ppm.

		^{13}C	^{1}H	^{15}N	^{17}O	^{19}F
HCTH						
	σ_{ref}	182.9	31.15	−95.6	216.1	309.7
	Mean abs. error	4.5	0.26	44.4	102.3	24.4
B97-2						
	σ_{ref}	184.0	31.16	−96.8	184.3	327.0
	Mean abs. error	4.7	0.17	29.3	136.2	18.1
SAOP						
	σ_{ref}	181.7	30.83	−94.2	249.4	337.2
	Mean abs. error	4.1	0.45	27.0	78.0	20.4
MKS(B97-2)						
	σ_{ref}	186.5	31.14	−76.1	290.4	340.4
	Mean abs. error	4.0	0.14	23.8	50.8	8.5
KT2						
	σ_{ref}	191.6	31.19	−76.5	260.4	321.0
	Mean abs. error	4.4	0.25	26.1	59.5	17.3
KT2[a]						
	σ_{ref}	194.0	31.69	−65.6	289.7	342.8
	Mean abs. error	4.0	0.35	16.1	42.8	19.7
KT2[b]						
	σ_{ref}	194.9	31.57	−65.2	303.7	349.9
	Mean abs. error	4.2	0.37	23.2	47.6	19.7

[a] Evaluated at KT2 optimised geometries
[b] Evaluated at 1/4 optimised geometries

3.3 Implementation in DALTON

The CADPAC program has some limitations with respect to magnetic properties. The GIAO formalism is not implemented, so calculations have to be performed using the LORG formalism with a large basis set. Also, CADPAC is not capable of calculating spin-spin coupling constant calculations. We therefore implemented the KT1 and KT2 functionals in the DALTON [78] program, which is not subject to these limitations.

The implementation of the KTX term required a similar set of Fortran subroutines to the CADPAC implementation, with the only difference being that the KTX equations were written in closed shell form as DALTON cannot do unrestricted calculations. To check the implementation, we confirmed that the converged energy of closed shell molecules from the two programs agreed to within the error introduced by the different numerical integration grids ($\approx 10^{-6}\ E_\mathrm{h}$). The Hellmann-Feynman test (Section 2.3) was performed to ensure a variational implementation.

3.3.1 GIAO shielding constants

Shielding constant calculations in DALTON are performed using the GIAO formalism [98] rather than LORG. To further validate our implementation and assess the effect of this change of gauge treatment, we recalculated the A1 set of isotropic shielding constants for KT1 and KT2 in DALTON. The same geometries as before were used, with the (unmodified) Huzinaga IV basis set. Another difference in DALTON is that by default spherical-harmonic basis functions are used (giving for example 5 d functions of the form xy, xz, yz, x^2-y^2, and $2z^2-x^2-y^2$), although it is also possible to use Cartesian basis functions (which would give 6 d functions of the form xy, xz, yx, x^2, y^2, and z^2). CADPAC can only use Cartesian basis functions, so for this check Cartesian functions were also used in DALTON.

Results are presented in Table 3.6. The LORG and GIAO results are in very good agreement, demonstrating a correct implementation. The effect of the gauge treatment is small for the Huzinaga IV basis set, as expected. (This is also a validation of our LORG results as GIAO results are more converged

Table 3.6: Comparison of LORG and GIAO isotropic shielding constants determined using the Huzinaga IV basis set. All values are in ppm.

		KT1		KT2	
Mol.	Nuc.	LORG	GIAO	LORG	GIAO
HF	F	412.0	410.9	412.4	411.4
H_2O	O	330.7	330.5	329.6	329.5
CH_4	C	196.4	196.3	195.2	195.1
CO	C	10.4	9.9	7.4	6.9
	O	−56.1	−55.9	−57.1	−56.9
N_2	N	−55.8	−56.0	−59.7	−59.9
F_2	F	−193.6	−193.0	−211.0	−210.4
O′OO′	O	−1246.3	−1246.0	−1278.7	−1278.4
	O′	−796.9	−796.6	−809.1	−808.9
PN	P	46.6	46.9	47.1	47.3
	N	−358.8	−358.3	−361.5	−361.0
H_2S	S	741.5	742.4	735.7	736.3
NH_3	N	265.9	266.1	264.5	264.6
HCN	C	87.2	86.9	86.0	85.7
	N	−18.6	−18.8	−19.4	−19.6
C_2H_2	C	120.5	120.3	120.4	120.2
C_2H_4	C	64.3	64.1	63.2	63.0
H_2CO	C	−3.0	−3.3	−4.7	−4.9
	O	−383.8	−383.5	−379.6	−379.3
N′NO	N′	106.8	106.4	102.1	101.7
	N	14.2	13.5	12.2	11.4
	O	184.1	184.3	177.5	177.6
CO_2	C	65.0	64.0	63.7	62.8
	O	224.5	224.4	221.6	221.4
OF_2	O	−516.7	−516.4	−534.0	−533.7
H_2CNN'	C	170.1	169.9	167.4	167.2
	N	−37.5	−37.9	−41.7	−42.1
	N′	−128.3	−128.7	−138.4	−138.8
HCl	Cl	961.3	965.2	958.6	962.3
SO_2	S	−149.5	−148.5	−156.8	−155.9
	O	−244.6	−244.8	−251.8	−251.8
PH_3	P	600.5	601.6	596.0	596.9

for a given basis set). Note that the results for molecules with second-row atoms (P, S, and Cl) differ from those in Table 2.4 due to the use here of the unmodified basis set.

We next assessed the KT1 and KT2 functionals for GIAO isotropic shielding constants of the A11 set of 14 systems. This set was previously studied by Helgaker *et al.* [165]. It is a very challenging set of highly correlated molecules, including charged species and two systems (CO_2 and N_2O) at non-equilibrium cyclic geometries. Calculations were performed using the geometries of Ref. [165] and the Huzinaga III basis set [106, 107] with spherical-harmonic basis functions. In Ref. [165] it was shown that under the GIAO formalism the Huzinaga III basis set gave essentially the same shielding constant results as the more computationally demanding Huzinaga IV.

Table 3.7 presents the results for KT1 and KT2 in comparison with LDA, the BLYP GGA, the hybrid functional B3LYP and reference *ab initio* and experimental data. The errors show a similar trend to that of the A1 shielding constant set. The BLYP errors are improved compared to LDA, and the hybrid functional B3LYP performs less well than BLYP. All three functionals give errors that are significantly too deshielded. The results for KT1 and KT2 are significantly improved, with both mean absolute errors and mean absolute percentage errors reduced by more than a factor of two over BLYP. This suggests that KT1 and KT2 perform as well for charged species and non-equilibrium geometries as they do for the neutral systems at equilibrium geometries. However, their performance compared to experiment is still inferior to the best *ab initio* wavefunction methods. (Note that the *ab initio* value for $C_6H_5N_2^+$ is not included in any error analysis because it was calculated using uncorrelated Hartree-Fock theory.)

The reason for the good performance of KT1 and KT2 is the same as for the A1 set, namely the raising of the occupied-virtual eigenvalue differences. For the systems in the A11 set, we observe that the KT1 and KT2 HOMO-LUMO gaps are noticeably larger than those of LDA and BLYP, repeating the findings of Table 2.9. This makes the paramagnetic contribution to the shielding constant smaller. To check this we calculated the average diamagnetic and paramagnetic contributions to the shielding constant for the A11 systems,

Table 3.7: GIAO isotropic shielding constants determined using the Huzinaga III basis set. All values are in ppm.

Mol.	Nuc.	LDA	BLYP	B3LYP	KT1	KT2	*ab initio*	Expt.[g]
CH_2	H	−62.5	−24.5	−29.8	−19.8	−16.8	−7.8[a]	
	C	−2003.2	−1135.3	−1252.6	−915.7	−868.8	−718[a]	
CF_2	C	−151.4	−139.3	−145.8	−91.2	−94.5	−101[a]	
	F	−117.6	−92.0	−77.6	−64.7	−60.5	−34[a]	
CF_4	C	37.3	35.8	44.6	53.7	52.2	64.4[b]	64.5
	F	219.2	224.6	236.2	231.9	231.9		
NO_2^-	N	−427.4	−420.1	−473.4	−350.5	−360.8	−360[a]	−368
	O	−492.1	−474.0	−502.1	−396.6	−409.0	−382[a]	−342 ± 20
linear-CO_2	C	48.7	48.5	48.3	63.2	61.9	63.5[b]	58.8
	O	207.9	210.1	211.4	222.0	218.9	236.4[c]	243 ± 17
cyclic-CO_2	C	−93.1	−87.9	−93.3	−52.1	−55.6	−50.6[a]	
	O	−138.4	−130.2	−138.8	−77.3	−89.6	−52.1[a]	
linear-N_2O	N_{term}	87.5	87.3	81.1	105.6	100.8	100.5[c]	99.5
	N_{cent}	−3.0	−5.2	−11.9	12.5	10.4	5.3[c]	11.3
	O	179.1	173.4	172.7	183.0	176.3	198.8[c]	200.5
cyclic-N_2O	N	−171.3	−169.3	−171.0	−126.5	−132.3	−87.3[a]	
	O	44.8	37.1	53.4	82.0	68.4	87.4[a]	
cis-N_2F_2	N	−172.9	−175.5	−183.7	−137.1	−143.2	−100.9[d]	−119.8
	F	−6.2	−3.3	14.5	27.2	21.7	80.7[d]	52.8
trans-N_2F_2	N	−256.3	−255.8	−266.3	−208.4	−216.9	−165.5[d]	−181.7
	F	14.5	18.4	40.3	47.5	42.9	103.7[d]	95.1
C_6H_6	C	39.9	40.9	43.0	61.0	59.6	64.0[b]	57.2
$C_2H_3^+$	C_α	−165.7	−165.7	−183.1	−128.7	−132.5	−143.0[e]	
	C_β	107.2	105.8	108.6	121.2	120.0	129.2[e]	
$C_7H_9^+$	C_α	−64.8	−62.5	−68.6	−37.1	−39.4	−36.6[e]	
	C_β	120.8	120.4	124.7	136.0	134.7	145.6[e]	
	$C_{\beta'}$	149.7	148.6	155.4	162.1	160.9	175.2[e]	
	C_γ	125.4	125.3	132.5	139.9	138.5	152.1[e]	
	$C_{\gamma'}$	128.1	127.0	133.6	141.9	140.5	156.5[e]	
$C_6H_5N_2^+$	N_α	−8.0	−6.5	−0.8	17.0	14.5	41.8[f]	15.9
	N_β	−102.4	−97.2	−97.1	−64.2	−69.5	−62.4[f]	−73.5
$\|d\|$ (Expt.)		44.5	42.5	46.2	17.6	19.3	11.3	
$\|d\|$ (*ab initio*)		91.4	56.7	62.8	23.7	24.3		
$\|d\|$% (Expt.)		52.4	51.7	51.1	15.5	16.6	13.7	
$\|d\|$% (*ab initio*)		86.1	61.6	68.0	28.5	28.1		

[a] Ref. [166], IGLO-MCSCF.
[b] Ref. [167], GIAO-MBPT(2).
[c] Ref. [132], GIAO-CCSD.
[d] Ref. [168], GIAO-FV CASSCF.
[e] Ref. [169], GIAO-CCSD(T).
[f] Ref. [170], LORG-SCF (not included in any error analysis).
[g] See Ref [165].

Table 3.8: Average diamagnetic (σ_d) and paramagnetic (σ_p) contributions to the calculated shielding constants ($\sigma = \sigma_d + \sigma_p$) of the A11 set, in ppm.

	LDA	BLYP	B3LYP	KT1	KT2
σ_d	391.6	393.2	393.0	395.2	396.3
σ_p	−486.0	−455.9	−460.6	−423.1	−426.4

which are presented in Table 3.8. The diamagnetic contributions show little variation, whereas as expected the KT1 and KT2 paramagnetic contributions are significantly less negative than those of the other functionals.

The reduced paramagnetic contribution can also be seen in the individual shielding constant tensor components. In Table 3.9, we present the individual tensor components for the CH_2 and CF_2 carbenes and cyclic CO_2 and N_2O, which were originally studied by van Wüllen and Kutzelnigg [166]. Those authors observed a strong deshielding xx component in the C shielding tensor of the carbenes that can be attributed to the lone pair on the carbon atom (all the systems are in the xz plane). They calculated this contribution using an MCSCF approach. By comparison, the xx components of our BLYP results are too deshielded, which explains why the overall BLYP shielding constants for the carbene are too deshielded. In contrast, the KT1 and KT2 values are much less deshielded, and the overall shielding constants are raised accordingly. In the case of cyclic CO_2 and N_2O, there is again a general trend for the KT1 and KT2 components to be more shielded than BLYP and hence closer to the MCSCF values. For CO_2 the xx components dominate due to lone pairs on the carbon and oxygen atoms. The same is seen for the O atom of N_2O, but for the N atom the zz tensor component dominates, due to excitations from the lone pairs into the N-N π^* orbital.

3.3.2 Spin-spin coupling constants

Indirect spin-spin coupling constants are, along with chemical shifts, the most important property for the interpretation of experimental NMR data, as they describe the size of the characteristic splittings observed in NMR spectra. The

Table 3.9: Shielding constant principal tensor components. All values are in ppm.

	BLYP	KT1	KT2	MCSCF[a]
CH_2 (C)				
σ_{xx}	−3228	−2631	−2494	−2120
σ_{yy}	209	217	216	201
σ_{zz}	−387	−333	−328	−237
CF_2 (C)				
σ_{xx}	−431	−327	−334	−397
σ_{yy}	11	30	27	52
σ_{zz}	2	23	23	42
Cyclic CO_2 (C)				
σ_{xx}	−349.2	−280.3	−286.6	−295.4
σ_{yy}	74.2	89.3	85.1	98.3
σ_{zz}	11.4	34.8	34.7	45.2
Cyclic CO_2 (O)				
σ_{xx}	−379.6	−302.3	−307.5	−297.5
σ_{yy}	80.7	110.7	93.1	156.3
σ_{zz}	−91.5	−40.4	−54.4	−15.0
Cyclic N_2O (N)				
σ_{xx}	−72.0	−27.3	−29.2	25.7
σ_{yy}	43.3	66.4	60.3	86.2
σ_{zz}	−479.2	−418.7	−428.1	−374.0
Cyclic N_2O (O)				
σ_{xx}	−254.4	−183.3	−207.1	−177.8
σ_{yy}	501.2	495.4	486.5	517.9
σ_{zz}	−135.7	−66.2	−74.3	−77.8

[a] Ref. [166].

indirect spin-spin coupling constant is defined as [171]

$$\mathbf{J}_{KL} = h\frac{\gamma_K}{2\pi}\frac{\gamma_L}{2\pi}\mathbf{K}_{KL} \tag{3.8}$$

where γ_K is the nuclear magnetogyric ratio of nucleus K, which depends on its isotope. Therefore spin-spin coupling constants are dependent on the isotopes involved (unlike shielding constants). $\mathbf{K}_{KL}$ is the reduced indirect spin-spin coupling constant, defined as

$$\mathbf{K}_{KL} = \frac{\partial^2 E}{\partial \mathbf{M}_K \partial \mathbf{M}_L} \tag{3.9}$$

where the nuclear magnetic moments $\mathbf{M}_K$ are related to the nuclear spins $\mathbf{I}_K$ by

$$\mathbf{M}_K = \gamma_K \hbar \mathbf{I}_K \tag{3.10}$$

The expression for $\mathbf{K}_{KL}$ was given by Ramsey [172] as

$$\begin{aligned}\mathbf{K}_{KL} &= \langle 0|\mathbf{h}_{KL}^{\mathrm{DSO}}|0\rangle + 2\sum_{s>0}\frac{\langle 0|\mathbf{h}_K^{\mathrm{PSO}}|s\rangle\langle s|\mathbf{h}_L^{\mathrm{PSO}}|0\rangle^T}{E_0 - E_s} \\ &\quad +2\sum_t \frac{\langle 0|\mathbf{h}_K^{\mathrm{FC}} + \mathbf{h}_K^{\mathrm{SD}}|t\rangle\langle t|\mathbf{h}_L^{\mathrm{FC}} + \mathbf{h}_L^{\mathrm{SD}}|0\rangle^T}{E_0 - E_t}\end{aligned} \tag{3.11}$$

where the first summation is over all singlet excited states and the second summation is over all triplet excited states. The diamagnetic spin-orbit (DSO), paramagnetic spin-orbit (PSO), spin-dipole (SD), and Fermi-contact (FC) operators are given by

$$\mathbf{h}_{KL}^{\mathrm{DSO}} = \frac{\alpha^4}{2}\sum_i \frac{(\mathbf{r}_{iK}^T\mathbf{r}_{iL})\mathbf{1} - \mathbf{r}_{iK}\mathbf{r}_{iL}^T}{r_{iK}^3 r_{iL}^3} \tag{3.12}$$

$$\mathbf{h}_K^{\mathrm{PSO}} = \alpha^2\sum_i \frac{\mathbf{r}_{iK}\times\mathbf{p}_i}{r_{iK}^3} \tag{3.13}$$

$$\mathbf{h}_K^{\mathrm{FC}} = \frac{8\pi\alpha^2}{3}\sum_i \delta(\mathbf{r}_{iK})\mathbf{s}_i \tag{3.14}$$

$$\mathbf{h}_K^{\mathrm{SD}} = \alpha^2\sum_i \frac{3(\mathbf{s}_i^T\mathbf{r}_{iL})\mathbf{r}_{iK} - r_{iK}^2\mathbf{s}_i}{r_{iK}^5} \tag{3.15}$$

The DSO and PSO components are similar in form to the diamagnetic and paramagnetic contributions to the shielding constant, but the SD and FC components do not have counterparts. The FC component contains a Dirac delta function which restricts its evaluation to the core of each nucleus. We expected that the KT1 and KT2 functionals would have a similar effect on the DSO and PSO contributions as they did for the shielding constant calculations, but it is unclear what effect they would have on the other contributions, especially the FC term, as the form of the KTX term at the nucleus was not considered in its development.

The spin-spin coupling constant is calculated using response theory as for shielding constants, but the SD and FC components require the additional evaluation of the electric Hessian. The analytic expression for this contains second derivatives of F_{XC} with respect to the density and density gradient, so an extra subroutine was implemented in DALTON to calculate these derivatives for the KTX term. This was checked for consistency with the other subroutines with the Hellmann-Feynman theorem by calculating the polarisability of closed shell molecules first analytically and then by finite difference of the dipole moment in a positive and negative uniform electric field.

Assessments of spin-spin coupling performance are less common than for shielding constants due to the greater complexity of the calculations, but some examples do exist [111, 171, 173–178]. To assess the performance of KT1 and KT2 for spin-spin couplings, we performed calculations on the A12 set of 11 molecules taken from Refs. [176] and [177]. All four contributions to the coupling constant were calculated.

The nature of the Fermi-contact term requires special attention to the choice of the basis set. It is important to have sufficient flexibility in the basis functions at the core. We therefore use the augmented Huzinaga III basis set of Ref. [176] (Huzinaga III-su3), in which the s functions are uncontracted and three further tight s functions are added. Spherical-harmonic basis functions were used. Near-experimental geometries from Ref. [103] were used (except for C_6H_6, for which $r_{CC} = 1.392$ Å, $r_{CH} = 1.086$ Å, and C_2H_6, for which $r_{CC} = 1.526$ Å, $r_{CH} = 1.088$ Å, $\theta_{CCH} = 107.4°$, $\theta_{HCH} = 111.5°$). Results are presented in Table 3.10. Again, we compare with the LDA, BLYP, and B3LYP

Table 3.10: Indirect spin-spin coupling constants determined using the Huzinaga III-su3 basis set. All values are in Hz.

Mol.		LDA	BLYP	B3LYP	KT1	KT2	Expt.[a]
HF	$^1J_{HF}$	395.9	390.0	439.3	344.7	335.1	538.0
CO	$^1J_{CO}$	26.7	22.7	19.4	25.8	27.3	15.7
$^{14}N^{15}N$	$^1J_{NN}$	4.3	3.1	1.8	3.9	3.9	1.7
H_2O	$^1J_{OH}$	−65.7	−72.6	−76.9	−66.2	−68.1	−86.0
	$^2J_{HH}$	−3.3	−6.4	−8.1	−6.3	−10.4	−8.2
$HC^{15}N$	$^1J_{CN}$	−8.1	−12.6	−18.1	−5.1	−5.5	−20.5
	$^1J_{CH}$	223.9	284.3	284.4	250.8	279.5	262.2
	$^2J_{NH}$	−6.3	−5.9	−7.5	−4.0	−3.0	−8.2
$^{14}NH_3$	$^1J_{NH}$	37.0	44.9	45.4	40.8	43.5	44.1
	$^2J_{HH}$	−5.0	−9.1	−10.4	−8.2	−12.5	−10.3
CH_4	$^1J_{CH}$	100.2	133.3	132.2	117.1	128.4	120.0
	$^2J_{HH}$	−7.3	−12.5	−13.3	−10.6	−15.6	−12.1
C_2H_2	$^1J_{CC}$	176.8	201.0	204.9	175.4	180.9	184.8
	$^1J_{CH}$	215.8	277.0	274.2	251.6	280.9	243.0
	$^2J_{CH}$	48.9	57.2	55.9	58.2	58.7	53.1
	$^3J_{HH}$	6.5	10.3	11.0	10.8	14.9	9.7
C_2H_4	$^1J_{CC}$	51.4	69.5	73.1	53.0	56.3	66.7
	$^1J_{CH}$	128.0	166.7	166.1	148.6	164.6	151.2
	$^2J_{CH}$	1.4	0.1	−1.4	2.7	−0.2	−1.2
	$^2J_{HH}$	4.5	4.9	3.4	6.3	3.5	2.0
	$^3J_{cis}$	10.0	13.1	13.1	12.1	14.6	10.5
	$^3J_{trans}$	14.7	20.5	20.2	20.8	25.0	16.7
C_2H_6	$^1J_{CC}$	11.4	21.8	24.5	11.4	13.2	34.5
	$^1J_{CH}$	103.9	137.2	136.4	121.1	133.4	125.2
	$^2J_{CH}$	−2.3	−3.9	−4.6	−2.8	−4.8	−4.7
	$^2J_{HH}$	−5.0	−9.1	−10.0	−7.3	−11.8	
C_6H_6	$^1J_{CC}$	42.6	56.7	60.1	42.1	45.0	56.1
	$^2J_{CC}$	0.5	−0.3	−1.8	0.4	−1.2	−1.7
	$^3J_{CC}$	9.8	10.5	11.2	8.9	9.6	9.4
	$^1J_{CH}$	129.9	167.2	166.8	149.6	166.4	153.8
	$^2J_{CH}$	3.3	3.1	2.0	4.4	2.8	1.4
	$^3J_{CH}$	6.1	7.9	8.1	7.8	8.6	7.0
	$^4J_{CH}$	−0.3	−0.8	−1.3	−0.6	−1.1	−1.0
	$^3J_{HH}$	6.9	9.0	8.8	8.3	9.5	7.0
	$^4J_{HH}$	1.2	1.6	1.3	2.0	1.9	1.2
	$^5J_{HH}$	0.2	0.5	0.8	0.4	0.9	0.6
$\|d\|$ (all)		12.9	10.0	8.0	10.8	12.6	
$\|d\|$[b]		9.1	6.0	5.3	5.5	7.0	
$\|d\|$% (all)		45.7	29.5	15.2	49.4	35.8	

[a] All experimental values include vibrational corrections (calculated at the B3LYP level), except C_2H_6. See Refs. [176,177].

[b] Excluding $^1J_{HF}$ in HF

functionals, against vibrationally-corrected experimental reference data. Errors are presented with and without the challenging $^1J_{HF}$ coupling of the HF molecule.

The trend here is different from that observed for the shielding constants. The errors improve from LDA to BLYP to B3LYP (unlike for shielding constants, the hybrid functional performs better than the GGA). The KT1 and KT2 errors are overall slightly worse than BLYP. KT1 and KT2 therefore offer no improvement for spin-spin couplings. They are particularly poor for HF, and if it is removed from the error analysis then the KT1 mean absolute error is close to that of B3LYP, whereas KT2 remains slightly worse than BLYP. Both functions have large percentage errors, which indicates that the couplings with small values are significantly in error.

The reason for the relatively poor performance of KT1 and KT2 can be deduced from the values of the individual components of the couplings. Table 3.11 presents the DSO, PSO, SD, and FC contributions to the coupling constants $^1J_{HF}$ in HF, $^1J_{CO}$ in CO, $^1J_{CH}$ in $HC^{15}N$, and $^1J_{CC}$ in C_2H_2. KT1 and KT2 give poor results for the first two couplings but are relatively accurate for the second two. The change in the DSO and PSO contributions are analogous to the findings for shielding constants. In all cases the DSO contributions vary very little, whereas the PSO contributions from KT1 and KT2 are smaller than from the other functionals. This is expected due to the presence of the occupied-virtual eigenvalue differences in the PSO term. Patchkovskii *et al.* suggest that such a reduction is desirable [111]. However, the spin-spin coupling constant results are dominated by the variation in the Fermi-contact term. In the first two couplings, the change in the Fermi-contact term for KT1 and KT2 causes the total results to degrade. In the second two couplings, the opposite occurs.

These conclusions are consistent with the findings of Patchkovskii *et al.* [111]. They assessed their SIC-VWN procedure for spin-spin couplings and obtained results similar to those of KT1 and KT2. This is because SIC-VWN also increases occupied-virtual eigenvalue differences, giving good chemical shifts, but again this can have a detrimental effect on the Fermi-contact term. The errors inherent in DFT spin-spin coupling calculations are therefore fundamentally

Table 3.11: Diamagnetic spin-orbit (DSO), paramagnetic spin-orbit (PSO), spin-dipole (SD) and Fermi-contact (FC) contributions to selected indirect spin-spin coupling constants. All values are in Hz.

	LDA	BLYP	B3LYP	KT1	KT2	Expt.
HF, $^1J_{HF}$						
DSO	0.3	0.3	0.3	0.4	0.3	
PSO	199.7	203.4	201.3	198.4	198.0	
SD	5.3	3.4	1.3	4.0	1.5	
FC	190.6	182.9	236.4	141.9	135.3	
Total	395.9	390.0	439.3	344.7	335.1	538.0
CO, $^1J_{CO}$						
DSO	0.1	0.1	0.1	0.1	0.1	
PSO	15.1	14.5	14.3	13.7	14.0	
SD	−4.8	−5.7	−6.1	−5.2	−5.7	
FC	16.4	13.8	11.1	17.3	18.9	
Total	26.7	22.7	19.4	25.8	27.3	15.7
$HC^{15}N$, $^1J_{CH}$						
DSO	0.5	0.4	0.4	0.4	0.4	
PSO	−0.5	−0.4	−1.0	−0.4	−0.4	
SD	0.7	0.6	0.5	0.6	0.7	
FC	223.3	283.7	284.4	250.1	278.8	
Total	223.9	284.3	284.4	250.8	279.5	262.2
C_2H_2, $^1J_{CC}$						
DSO	0.0	0.0	0.0	0.0	0.0	
PSO	6.6	7.1	8.4	5.9	6.3	
SD	8.4	10.8	11.6	8.8	10.5	
FC	161.8	183.2	184.9	160.6	164.1	
Total	176.8	201.0	204.9	175.4	180.9	184.8

different in nature to those for shielding constants.

3.3.3 MKS spin-spin coupling constants

Finally, we consider spin-spin couplings calculated using the MKS method, in order to further explore the relationship between the DFT functional used and the individual coupling components. The ZMP program was modified to print out the potential on a numerical grid compatible with DALTON, and DALTON was modified to read in the potential from disk for use in a spin-spin coupling calculation. An additional complication for MKS shielding constants is the need to calculate the electric Hessian, which requires explicit derivatives of F_{XC}. This was not the case for shielding constants, because they only require the magnetic Hessian which can be expressed solely in terms of the Kohn-Sham eigenvalues. The F_{XC} derivatives cannot be extracted from the ZMP orbitals and eigenvalues and therefore they must be calculated using a specific functional.

We considered the same four coupling constants as in the previous section. Table 3.12 presents MKS(BD) and MKS(B3LYP) results using LDA, BLYP, KT1, and KT2 as F_{XC}. The TZ2P basis set was used to calculate the ZMP potential and Huzinaga III-su3 for the coupling calculations. We also recalculated the MKS(B3LYP) results using the Huzinaga III-su3 basis to calculate the ZMP potential. The change in the results was insignificant, which suggests that TZ2P is a satisfactory basis set for the ZMP calculations (no extra core functions are required).

There are no straightforward conclusions that can be drawn from the MKS spin-spin coupling constant results. For some couplings, use of the MKS method improves the result, and for others the results are degraded. There is no consistency across the functionals used in F_{XC}, and the MKS(BD) and MKS(B3LYP) do not always change the result in the same direction. However, the results indicate that supplying improved orbitals and eigenvalues does not give overall improved results. This is in agreement with our findings from the conventional KT2 results.

Table 3.12: MKS indirect spin-spin coupling constants using F_{XC} =LDA, BLYP, KT1, and KT2 for the evaluation of the electric Hessian.

	LDA	BLYP	KT1	KT2	Expt.
HF, $^1J_{HF}$					
Non-MKS	395.9	390.0	344.7	335.1	538
MKS(BD)[a]	349.6	360.0	365.6	368.7	
MKS(B3LYP)[b]	371.4	381.2	387.0	390.4	
MKS(B3LYP)[c]	373.1	383.0	388.9	392.5	
CO, $^1J_{CO}$					
Non-MKS	26.7	22.7	25.8	27.3	15.7
MKS(BD)[a]	25.2	22.1	23.9	23.9	
MKS(B3LYP)[b]	25.4	22.0	24.0	23.8	
MKS(B3LYP)[c]	25.4	22.0	24.0	23.7	
$HC^{15}N$, $^1J_{CH}$					
Non-MKS	223.9	284.3	250.8	279.5	262.2
MKS(BD)[a]	211.2	247.9	234.8	254.7	
MKS(B3LYP)[b]	230.7	270.8	256.7	278.8	
MKS(B3LYP)[c]	233.0	273.4	259.2	281.6	
C_2H_2, $^1J_{CC}$					
Non-MKS	176.8	201.0	175.4	180.9	184.8
MKS(BD)[a]	163.2	177.6	173.9	178.1	
MKS(B3LYP)[b]	174.4	189.6	185.4	190.1	
MKS(B3LYP)[c]	176.0	191.4	187.1	191.8	

[a] Using TZ2P to calculate the ZMP potential, and Huzinaga III-su3 for the spin-spin calculation.
[b] Using TZ2P to calculate the ZMP potential, and Huzinaga III-su3 for the spin-spin calculation.
[c] Using Huzinaga III-su3 to calculate the ZMP potential and for the spin-spin calculation.

Chapter 4

The KT3 functional

The KT2 functional is superior to all other conventional exchange-correlation functionals for shielding constants, chemical shifts, rotational g tensors [149], and magnetisabilities. Its performance for thermochemical and structural properties is also good, but is surpassed by other GGA functionals. For example, the 1/4 functional provides better geometries and HCTH gives better atomisation energies. In this chapter, we attempt to derive a new functional which retains the good quality magnetic response performance of KT2, while also improving performance for other properties.

4.1 Choice of correlation functional (1)

KT1 and KT2 were both developed as simple corrections to the LDA. It was therefore natural to use the VWN correlation functional, which is a parametrisation of the LDA correlation energy involving a functional only of the density. Improved correlation functionals can be developed by including derivatives of the density into their mathematical form, just as GGA exchange improves over LDA exchange. We therefore considered the effect of using the gradient-corrected correlation functionals LYP and PBE instead of VWN. The new functionals take the form

$$E_{\mathrm{XC}}[\rho_\alpha,\rho_\beta] = \alpha E_{\mathrm{X}}^{\mathrm{LDA}}[\rho_\alpha,\rho_\beta] + \beta\sum_\sigma \int \frac{|\nabla\rho_\sigma(\mathbf{r})|^2}{\rho_\sigma^{4/3}(\mathbf{r})+\gamma}\mathrm{d}\mathbf{r} + \delta E_{\mathrm{C}}[\rho_\alpha,\rho_\beta] \qquad (4.1)$$

Table 4.1: Coefficients for functionals considering the replacement of VWN correlation with PBE or LYP. All functionals use $\gamma = 0.1$

	α LDAX	β KTX	δ C
PBE(1)	1.00000E + 0	−5.50000E − 3	1.00000E + 0
PBE(2)	1.07198E + 0	−6.00000E − 3	6.00000E − 1
LYP(1)	1.00000E + 0	−6.00000E − 3	1.00000E + 0
LYP(2)	1.09781E + 0	−6.74060E − 3	5.75228E − 1

where the correlation functional E_C may be LYP or PBE. Our first task was to construct the LYP/PBE equivalents of KT1 ($\alpha = \delta = 1$). The value of $\gamma = 0.1$ was retained to reproduce the intershell structure of the exchange-correlation potential and prevent divergence at long range. Therefore the only variable coefficient was β, which as for KT1 was fitted to the A1 isotropic shielding constant set.

Table 4.1 presents the coefficients for these functionals. The KT1-type functionals are denoted LYP(1) and PBE(1) respectively. Table 4.2 summarises their performance for some of the molecular assessments considered in Chapter 2. Overall their performance is slightly worse than KT1, and they are also marginally worse for the A1 shielding constants. The LYP and PBE functionals have a small but non-negligible effect on the shieldings, and they appear to match experiment less well as a result. This is because LYP and PBE introduce some unphysical distortions into the potential, particularly in the intershell region, which affects the shielding results. VWN does not introduce distortions of this kind as it a functional only of the density.

KT2-type functionals were also calculated, with the values of α and δ free to vary. The LYP(2) variant did not have a fixed value of β, because the fitted value of β was sufficiently high to give good quality shieldings. The value of β did have to be fixed in PBE(2).

As Table 4.2 shows, the LYP(2) and PBE(2) variants are again similar to KT2, but again their performance is not quite as good, in particular for the A3 atomisation energies. This is disappointing because LYP and PBE

Table 4.2: Error assessments for thermochemistry, molecular bond lengths, and isotropic shielding constants for the PBE and LYP functionals combined with KTX. Units are given in parentheses.

	PBE(1)	PBE(2)	LYP(1)	LYP(2)	KT1	KT2
A1. Isotropic NMR shielding constants (ppm)						
d	−2.5	−3.7	−3.3	−5.6	−4.7	−9.5
$\|d\|$	16.1	13.8	14.7	13.1	13.0	13.2
Excluding O_3:						
d	−1.7	−2.8	−2.8	−4.5	−4.0	−7.7
$\|d\|$	13.8	11.3	11.6	10.4	10.0	10.9
A3. Atomisation energies (ppm)						
d	15.8	0.7	13.9	0.5	12.5	−0.1
$\|d\|$	16.8	8.6	14.4	7.5	13.2	6.4
A4. Ionisation potentials (kcal mol^{-1})						
d	−6.5	−4.5	−8.6	−2.8	1.2	−0.2
$\|d\|$	6.5	5.4	8.6	4.7	1.3	3.9
A5. Total atomic and ionic energies (kcal mol^{-1})						
d	−152.4	−416.9	−210.9	−544.3	−333.5	−461.4
$\|d\|$	158.9	418.0	217.0	545.2	334.7	461.8
A6. G2 subset bond lengths (Å)						
d	0.014	−0.001	0.015	−0.009	0.014	−0.001
$\|d\|$	0.019	0.009	0.022	0.013	0.019	0.010

are generally believed to be better correlation functionals than VWN. The relatively good results for VWN are possibly a consequence of allowing the correlation coefficient to vary, rather than as a direct result of the quality of VWN. Nevertheless, VWN clearly remains the best correlation functional to use with functionals of this form.

The results also raise the question of why all three correlation functionals are scaled to approximately 60% of their standard values. It suggests that rather than there being a problem with the correlation functional, there is instead something intrinsically wrong with the energy characteristics of the KT exchange functional.

4.2 Modifying the exchange functional (1)

For non-magnetic properties, KT exchange is not an optimal functional. When developing the KT exchange term, we concentrated on the description of the intershell peak in the exchange-correlation potential. This description is better than any other GGA functional. From the perspective of the potential it could be argued that the problems with other properties are due to flaws in a different region of the potential that is not so important for shielding constants. We now consider whether these flaws can be fixed.

4.2.1 Asymptotic correction

All conventional GGA functionals, including KT1 and KT2, have potentials that die off too quickly at long range. The exact exchange-correlation potential should die off as $-1/r$ (to within a constant), where r is the distance from the nucleus. The LDA instead dies off exponentially. As $r \to \infty$, $\rho(\mathbf{r}) \to e^{-\alpha r}$ (in the limit of a complete basis) and so the LDA potential behaves as

$$-\rho^{1/3}(\mathbf{r}) \to -e^{-(1/3)\alpha r} \tag{4.2}$$

The behaviour of the GEA potential is worse as it diverges as r goes to infinity. At long range, the properties of the GEA potential of Eq. 2.27 are

$$\begin{aligned} v_{\mathrm{XC},\sigma}(\mathbf{r}) &\rightarrow -e^{-(1/3)\alpha r} + \frac{4\beta\alpha^2 e^{-2\alpha r}}{3e^{-(7/3)\alpha r}} - \frac{2\beta\alpha^2 e^{-\alpha r}}{e^{-(4/3)\alpha r}} \\ &\rightarrow -e^{-(1/3)\alpha r} + \frac{4}{3}\beta\alpha^2 e^{(1/3)\alpha r} - 2\beta\alpha^2 e^{(1/3)\alpha r} \end{aligned} \tag{4.3}$$

Both GEA terms diverge, but the third term (involving the Laplacian of the density) has a higher coefficient and so the potential diverges upwards (as β is usually negative). The correlation potential goes to zero at long range so it does not affect the divergence.

GGA functionals usually solve this problem by altering the form of the GEA such that it behaves like the LDA at long range. They therefore also die off exponentially, instead of the correct $-1/r$. Properties that depend on the long-range behaviour of the potential are therefore affected. The description of virtual orbitals and eigenvalues deteriorates, which in turn leads to poor Rydberg excitation energies and polarisabilities, among other properties. The extent to which it affects other properties, such as energies and structures, is less clear. Recently, Coulomb-attenuated hybrid functionals have been developed that vary the amount of exact exchange with distance to give improved performance for long-range properties [179, 180]. However, this can lead to a deterioration in properties at short-range [181].

We considered whether altering the KT functionals to give a better representation of the asymptotic potential, within the GGA formalism, might lead to improved property calculations. This was based on two beliefs: firstly, that the 1/4 functional gives good structures because its fit emphasised regions of the potential far from the nucleus; and secondly, any improvement to the potential should in some way improve the results gained from a functional.

One method of asymptotically correcting the potential is simply to alter its value at every point at long range to give the correct $-1/r$ behaviour [120]. However, this means the potential is no longer the derivative of a well-defined functional, and the calculations are therefore no longer within the GGA formalism. Instead, we attempted to modify the KT exchange functional form such that the corresponding potential behaves more like $-1/r$. This is a dif-

ficult task because the values of the density and its derivatives at long range are so low that any mathematical form that doesn't tend to zero or diverge is hard to find, and in any case will tend to magnify numerical instabilities.

Our first crude attempt to alter KT exchange involved adding on another term of the form

$$E_{\mathrm{XC}}[\rho_\alpha, \rho_\beta] = E_{\mathrm{XC}}^{\mathrm{KT1}}[\rho_\alpha, \rho_\beta] - 0.12 \sum_\sigma \int \rho_\sigma^{1.015}(\mathbf{r}) \tag{4.4}$$

which gave a corresponding potential

$$v_{\mathrm{XC},\sigma}[\rho_\alpha, \rho_\beta] = v_{\mathrm{XC},\sigma}^{\mathrm{KT1}} - 0.1218 \rho_\sigma^{0.015}(\mathbf{r}) \tag{4.5}$$

The low power of ρ meant that it still had an effect on the potential even at long range where the density is very low. The coefficients were determined by a fit to the ZMP potentials of CO, N_2, and PN, using the Excel fitting routine Solver. Solver is a general iterative non-linear fitting procedure, although the details of the fitting algorithm are proprietary. We denote the resulting functional AC(1). The assessment for this functional is presented in Table 4.3. It gives shielding constants of a similar standard to KT1 (as expected because the asymptotic region does not contribute much to shieldings), and the performance for the A6 bond length optimisations is slightly improved, but its atomisation energies are inferior to KT1. Its *ad hoc* nature was also unsatisfactory. We therefore concluded that it was not an improvement over KT1.

We next investigated a more sophisticated approach involving a direct modification to the KT term itself. From the discussion of the GEA divergence above, it is clear that a modification to the power of ρ will remove the divergence. Instead of the GEA form we used a functional of the form

$$E_{\mathrm{XC}}[\rho_\alpha, \rho_\beta] = E_{\mathrm{XC}}^{\mathrm{LDA}}[\rho_\alpha, \rho_\beta] + \beta \sum_\sigma \int \frac{|\nabla \rho_\sigma(\mathbf{r})|^2}{\rho_\sigma(\mathbf{r})} \mathrm{d}\mathbf{r} \tag{4.6}$$

Table 4.3: Error assessments for thermochemistry, molecular bond lengths, and isotropic shielding constants for the CC and AC functionals. Units are given in parentheses.

	AC(1)	AC(2)	CC(1)	CCAC(1)	CCAC(2)
A1. Isotropic NMR shielding constants (ppm)					
d	−5.8	−14.7	−10.9	−9.0	−13.8
$\|d\|$	12.9	17.3	14.0	12.9	14.7
Excluding O_3:					
d	−5.0	−12.4	−8.7	−7.4	−11.0
$\|d\|$	10.0	15.1	11.3	10.0	11.9
A3. Atomisation energies (kcal mol^{-1})					
d	15.0	−3.6	14.2	7.3	−0.4
$\|d\|$	15.4	8.3	14.7	10.2	6.5
A4. Ionisation potentials (kcal mol^{-1})					
d	80.0	−1.1	1.7	0.9	1.5
$\|d\|$	80.0	1.5	1.7	1.4	3.5
A5. Total atomic and ionic energies (kcal mol^{-1})					
d	−740.2	−372.4	−153.5	−216.1	−346.8
$\|d\|$	740.2	372.4	154.7	216.8	346.8
A6. G2 subset bond lengths (Å)					
d	0.009	0.024	0.013	0.016	0.001
$\|d\|$	0.016	0.024	0.018	0.018	0.010

The corresponding potential was

$$v_{\mathrm{XC},\sigma}(\mathbf{r}) = v^{\mathrm{LDA}}_{\mathrm{XC},\sigma}(\mathbf{r}) + \frac{\beta|\nabla\rho_\sigma(\mathbf{r})|^2}{\rho^2_\sigma(\mathbf{r})} - \frac{2\beta\nabla^2\rho_\sigma(\mathbf{r})}{\rho_\sigma(\mathbf{r})} \tag{4.7}$$

so at long range

$$v_{\mathrm{XC},\sigma}(\mathbf{r}) \rightarrow -e^{-(1/3)\alpha r} + \frac{\beta\alpha^2 e^{-2\alpha r}}{e^{-2\alpha r}} - \frac{2\beta\alpha^2 e^{-\alpha r}}{e^{-\alpha r}} \tag{4.8}$$

$$\rightarrow -e^{-(1/3)\alpha r} - \beta\alpha^2 \tag{4.9}$$

Therefore as r gets larger the potential will go to a positive constant (as β will be negative). The exact exchange-correlation potential also goes to a positive constant [117], so this functional has useful properties. However, its potential will not necessarily go like $-1/r$ as it approaches this constant. This can be shown by considering the case of the hydrogen atom, for which the density is a simple exponential for all values of r. Therefore the contribution of the new term to the potential will be constant, even though the exact hydrogen potential should go like $-1/r$. For heavier atoms, the density is more complex, and plots of the exchange-correlation potentials indicate a behaviour similar to $-1/r$.

This functional form is in fact the well-known Weizsacker correction to the kinetic energy functional from Section 1.3.1. There are problems involved with using this functional as an approximation to exchange. Firstly, it is dimensionally incorrect (it has the kinetic energy dimensions of $\rho^{5/3}$ rather than the exchange dimensions of $\rho^{4/3}$). As a consequence of this, it does not scale like exchange (Eq. 1.60), although of course neither does KT exchange. Also, the potential at short range is highly inaccurate (it gets increasingly too deep compared to the correct potential as it approaches the nucleus). The GEA is much more accurate at short range, indicating that the GEA has the correct power of ρ.

We therefore attempted to develop a functional which acts like the GEA at short range but like the Weizsacker functional at long range. This was

accomplished by multiplying the GEA form by a term

$$\frac{\rho^{1/3}}{\rho^{1/3}+1} \tag{4.10}$$

As $\rho^{1/3} \to 0$, $1 \gg \rho^{1/3}$, so this term will behave like $\rho^{1/3}$. However, as $\rho^{1/3} \to \infty$, $\rho^{1/3} \gg 1$, so the term will have no effect. Hence the functional will act like the GEA at short range and the Weizsacker functional at long range. The complete functional form simplified to

$$E_{\mathrm{XC}}[\rho_\alpha, \rho_\beta] = E_{\mathrm{XC}}^{\mathrm{LDA}}[\rho_\alpha, \rho_\beta] + \beta \sum_\sigma \int \frac{|\nabla \rho_\sigma(\mathbf{r})|^2}{\rho_\sigma^{4/3}(\mathbf{r}) + \gamma \rho_\sigma(\mathbf{r})} \mathrm{d}\mathbf{r} \tag{4.11}$$

The only difference between this form and KT1 is the multiplication of γ by $\rho_\sigma(\mathbf{r})$. We denote this functional AC(2). Its coefficients are

$$\beta = -0.009 \qquad \gamma = 1 \tag{4.12}$$

An assessment for AC(2) is presented in Table 4.3. Its performance for atomisation energies is improved compared to KT1, but both shielding constants and bond length optimisations have deteriorated. Considering the disadvantages of using this functional outlined above, it does not appear that it offers much advantage over KT1.

We also considered a combination of the KT exchange term and the AC(2) term to give more flexibility for the form of the potential in the core and valence regions. This did not offer significant improvement either.

4.2.2 Core correction

The KT exchange potential also requires improvement at short range, in the region we loosely define as the core. By the core we mean the potential from the nucleus to the edge of the intershell/valence region, rather than the potential at the point $r = 0$, which does not have any effect on molecular property calculations (except the Fermi-Contact term in spin-spin coupling calculations) and has been proven to diverge in GGAs [125].

Compared to the near-exact ZMP potential, the KT exchange potential is

too deep in the core (its slope is too high). One method for correcting this is to decrease the value of β. However, this will decrease the size of the intershell peak in the valence region and hence lead to inferior performance for shielding constants. Therefore we needed to decrease β in the core whilst keeping it high in the valence region. One way of achieving this is to replace β with a term such as

$$\beta - \beta' \frac{\rho^{4/3}}{\rho^{4/3} + \gamma'} \tag{4.13}$$

At low $\rho^{4/3}$ (i.e. in the intershell and tail regions of v_{XC}), this will behave like β. At high $\rho^{4/3}$ (in the core), it will behave like $\beta - \beta'$. This is the behaviour required. The resulting functional has the form

$$E_{\mathrm{XC}}[\rho_\alpha, \rho_\beta] = E_{\mathrm{XC}}^{\mathrm{KT1}}[\rho_\alpha, \rho_\beta] + \beta' \sum_\sigma \int \frac{|\nabla \rho_\sigma(\mathbf{r})|^2 \rho_\sigma^{4/3}(\mathbf{r})}{(\rho_\sigma^{4/3}(\mathbf{r}) + \gamma)(\rho_\sigma^{4/3}(\mathbf{r}) + \gamma')} \mathrm{d}\mathbf{r} \tag{4.14}$$

The new term is called the core correction (CC) term. We expected that this term would lead to an improvement in performance for bond lengths optimisations, based on the observation that the greatest difference between the 1/4 potential and the KT potential is in the core. We developed a KT1-style functional CC(1), for which the parameters are

$$\beta = -0.006 \qquad \beta' = 0.0075 \qquad \gamma = 0.1 \qquad \gamma' = 50 \tag{4.15}$$

Results are presented in Table 4.3. While there is a small improvement for bond lengths, the new term makes little difference to the results overall.

Finally, we considered a functional consisting of KT exchange combined with both the core correction term and the asymptotic correction term. We denote this CCAC. The full functional is of the following form

$$\begin{aligned} E_{\mathrm{XC}}[\rho_\alpha, \rho_\beta] &= \alpha E_{\mathrm{X}}^{\mathrm{LDA}}[\rho_\alpha, \rho_\beta] + \beta E_{\mathrm{X}}^{\mathrm{KT1}}[\rho_\alpha, \rho_\beta] + \delta E_{\mathrm{C}}^{\mathrm{VWN}}[\rho_\alpha, \rho_\beta] && (4.16) \\ &+ \beta' \sum_\sigma \int \frac{|\nabla \rho_\sigma(\mathbf{r})|^2 \rho_\sigma^{4/3}(\mathbf{r})}{(\rho_\sigma^{4/3}(\mathbf{r}) + \gamma)(\rho_\sigma^{4/3}(\mathbf{r}) + \gamma')} \mathrm{d}\mathbf{r} && (4.17) \\ &+ \beta'' \sum_\sigma \int \frac{|\nabla \rho_\sigma(\mathbf{r})|^2}{\rho_\sigma^{4/3}(\mathbf{r}) + \gamma'' \rho_\sigma(\mathbf{r})} \mathrm{d}\mathbf{r} && (4.18) \end{aligned}$$

Clearly this functional is much more complex than the original KT functional, and so a significant improvement in results is required to justify this. We built CCAC functionals both with and without the uniform electron gas condition, which we denote CCAC(1) and CCAC(2) respectively. The CCAC(1) coefficients are

$$\beta = -0.005 \qquad \beta' = 0.008 \qquad \beta'' = 0.0025 \qquad \gamma = 0.1 \qquad \gamma' = 50 \qquad \gamma'' = 1 \tag{4.19}$$

whereas the CCAC(2) coefficients are as for CCAC(1), but with the LDA coefficients set to

$$\alpha = 1.0639 \qquad \delta = 0.7 \tag{4.20}$$

Table 4.3 presents an analysis of their performance. CCAC(1) is a moderate improvement over KT1 for the A6 bond lengths and A3 atomisation energies, whereas CCAC(2) gives very similar results to KT2. The results are therefore not impressive, and cannot be used to justify the increased complexity of the functional. We also developed a version of CCAC with PBE correlation instead of VWN, for which similar results were obtained.

4.3 KT exchange as a correction

Instead of modifying the KT exchange form itself, a different approach can be taken. The KT term can be thought of as a correction to the LDA functional. From this point of view, the next logical step is to add the KT term to other functionals.

4.3.1 The 1/4 functional

Our first attempt to use the KT exchange term as a correction involved the 1/4 functional [50]. This is known to give excellent performance for structures, but poor magnetic properties. We hoped that by combining the two functionals in some way we could get good results for both properties simultaneously.

As a preliminary investigation we simply added the two functionals together. This improved the performance of 1/4 for magnetic properties greatly,

but unfortunately its performance for bond length optimisations deteriorated to the level of KT2. Therefore no benefit was gained. We next used the same fitting code used in Chapter 2, but fitted to ZMP potentials rather than thermochemistry (i.e. the same way 1/4 was determined). The fit procedure was the same as that described in Ref. [50], except that the KT exchange potential was subtracted from the ZMP potential before fitting (this was to prevent the minimisation effect discussed in Section 2.5 that had prevented us fitting KT1 and KT2 to potentials before). We therefore had to choose a value of β; our optimal value was $\beta = -0.0045$. We also experimented with weighting the density in the fit code: a power of 1/4 was optimal for structures (as it was for the 1/4 functional). Unfortunately, although shieldings improved by as much as the simple addition had done (giving a mean absolute error over the A1 set of 14 ppm), bond lengths also deteriorated by the same level (to an error for the A6 set of 0.014 Å, worse than KT2). Therefore we concluded that the corrected 1/4 functionals do not offer any improvement over the original KT1/2 functionals.

4.3.2 B97 exchange

1/4 is a complex functional, with 15 parameters. There is no easy way to gain insight into how it works, and no way of knowing if the fit code is successfully optimising it to work with the KT exchange term. We already know that fitting to potentials is flawed in the sense that it minimises the KT exchange term (which reproduces the potential very well). Therefore it would seem better to use a simpler functional form, and fit to energies.

We chose to investigate individual components of the B97 exchange form (which forms the basis of the 1/4 functional, among others, as discussed in Chapter 1). In particular, we looked at the third term in the exchange expansion, which forms the basis of the OPTX functional [49]. Handy and Cohen determined that of all the terms in the expansion, this term was the most important for energies when considered separately. It performed best when combined with LYP correlation to give the OLYP functional. We therefore start by considering KT exchange as a correction to OLYP.

Table 4.4: Coefficients for B97-based functionals with and without KTX. All functionals use $\gamma = 0.1$. T denotes fitting to total energies, A to atomisation energies, and I to ionisation potentials. F denotes that the KTX coefficient was fixed.

	LDAX	B86X	OPTX	KTX	LYP
OPTX only					
Orig.	1.05151E+0		−1.43169E+0		1.00000E+0
T,A,I	1.05144E+0		−1.45638E+0		9.54779E−1
A,I	1.07467E+0		−1.52494E+0		9.41011E−1
OPTX+KTX					
T,A,I	1.05641E+0		−1.52994E+0	2.79177E−4	9.62706E−1
A,I	1.07517E+0		−1.49182E+0	−1.89978E−4	9.36072E−1
A,I,F	1.08598E+0		−7.42401E+0	−4.50000E−3	8.27819E−1
B86X only					
T,A,I	9.97814E−1	−9.00532E−1			9.36461E−1
A,I	1.03751E+0	−9.32680E−1			8.73382E−1
B86X+KTX					
T,A,I	9.99237E−1	−9.29289E−1		1.75884E−4	9.40590E−1
A,I	1.04831E+0	−7.56998E−1		−1.80127E−3	8.57656E−1
A,I,F	1.07327E+0	−3.51377E−1		−6.00000E−3	8.22323E−1
B86X+OPTX+KTX					
T,A,I	1.04660E+0	−1.63516E−1	−1.27384E+0	2.91889E−4	9.63202E−1
A,I	1.05573E+0	−5.38433E−1	−4.63565E−1	−1.19096E−3	8.87936E−1
A,I,F	1.04306E+0	−1.01645E+0	8.70123E−1	−4.50000E−3	7.89950E+0

Correcting OPTX

The OLYP functional is

$$\begin{aligned} E_{\mathrm{XC}}[\rho_\alpha, \rho_\beta] &= \alpha E_{\mathrm{X}}^{\mathrm{LDA}}[\rho_\alpha, \rho_\beta] + \beta \sum_\sigma \int \rho_\sigma^{4/3}(\mathbf{r}) \left(\frac{\gamma x_\sigma^2}{1 + \gamma x_\sigma^2} \right)^2 \mathrm{d}\mathbf{r} \\ &+ \delta E_{\mathrm{C}}^{\mathrm{LYP}}[\rho_\alpha, \rho_\beta] \end{aligned} \tag{4.21}$$

where the coefficients are given in Table 4.4. OPTX was fitted to Hartree-Fock exchange energies, but OLYP was built without optimising the LYP coefficient. In order to make a fair comparison with our functionals we needed

to allow LYP to vary and fit the whole functional to our thermochemistry data set. Following the procedure of Chapter 2, we fitted both with and without total energies. The coefficients are presented in Table 4.4 and assessments in Table 4.5. Like all conventional GGAs, OLYP is poor for the A1 isotropic shielding constants (about the same standard as HCTH). Its performance for atomisation energies is superior to KT2, with or without total energies in the fit. With them included, the A6 bond length errors are poor, but without, they are of similar quality to KT2 (the A7 bond length errors are poor in both cases).

Our aim in combining OLYP with KT exchange is to obtain a functional with KT-standard shieldings and OLYP-standard atomisation energies, without harming performance for structural properties. We therefore fitted a four parameter functional, varying the LDA exchange, KT exchange, OPTX exchange and LYP correlation parameters. We kept the γ values of KT and OPTX at their original values of 0.1 and 0.006 respectively (note that the OPTX value differs from the original B97 expansion value of 0.004). Again as in Chapter 2, we fitted three types of functionals: with total energies, without total energies, and without total energies but with a fixed KT exchange coefficient. All the functionals were fitted to both atomisation energies and ionisation potentials.

Given the poor performance of KT1 and KT2 for total energies, it is unsurprising that the KT exchange term is minimised in the total energy fit. The performance of this functional is therefore no different from that of OLYP. Given that OLYP performs much better for atomisation energies than the LYP(2) functional, it is again not surprising that the KT exchange term is still minimised when total energies are taken out. In order to get good shielding constants, therefore, the KT exchange coefficient must be fixed. We experimented with several values, and the optimal value was found to be -0.0045. This is lower than for KT2, which is expected because OLYP gives shieldings with a significantly less negative mean error than LDA, so less of a correction from the KT exchange term is required. The advantage of this functional, however, is not its shieldings (which are of a similar quality to KT2), but its thermochemical and structural performance. Although at 5 kcal mol^{-1} the

Table 4.5: Error assessments for thermochemistry, molecular bond lengths, and isotropic shielding constants for the OLYP functional (O) with and without KTX (K). T denotes fitting to total energies, A to atomisation energies, and I to ionisation potentials. F denotes that the KTX coefficient was fixed. Units are given in parentheses.

	O Orig.	O T,A,I	O A,I	O,K T,A,I	O,K A,I	O,K A,I,F (OKTLYP)
A1. Isotropic NMR shielding constants (ppm)						
d	−30.7	−30.1	−31.3	−31.6	−30.4	−10.4
$\|d\|$	30.7	30.1	31.3	31.6	30.4	13.3
Excluding O_3:						
d	−23.9	−23.4	−24.4	−24.5	−23.7	−8.2
$\|d\|$	23.9	23.4	24.4	24.5	23.7	11.4
A3. Atomisation energies (kcal mol^{-1})						
d	3.5	0.6	0.5	0.6	0.5	0.2
$\|d\|$	4.5	3.1	3.1	3.2	3.0	5.0
A4. Ionisation potentials (kcal mol^{-1})						
d	−1.9	−2.6	0.2	−1.8	0.1	−0.7
$\|d\|$	2.6	3.2	1.5	2.5	1.6	2.5
A5. Total atomic and ionic energies (kcal mol^{-1})						
d	−1.8	−0.5	−81.0	−0.7	−95.4	−424.5
$\|d\|$	2.9	2.1	81.0	2.4	95.4	424.7
A6. G2 subset bond lengths (Å)						
d	0.015	0.017	0.010	0.016	0.010	0.000
$\|d\|$	0.015	0.017	0.011	0.016	0.011	0.008
A7. Diatomic bond lengths (Å)						
d	0.040	0.038	0.037	0.038	0.036	0.004
$\|d\|$	0.041	0.039	0.038	0.039	0.036	0.012

mean absolute error over the A3 set is higher than OLYP, it is still a significant improvement over KT2. The bond length performance is greatly improved over both KT2 and OLYP. It is of comparable quality to the 1/4 functional, which represents the best that DFT can currently achieve. For reference we denote this functional form OKTLYP.

Correcting B86X

Although the OKTLYP functional is a genuine improvement over KT2, there is still room for improvement in its performance for atomisation energies. Our target was to approach the quality of the OLYP functional (i.e. 3 kcal mol^{-1} for the A3 set) or surpass it without a deterioration in OKTLYP's performance for shieldings and structures.

The next step is to consider other terms in the B97 exchange expansion. Although Handy and Cohen [49] have observed that the OPTX term provides the best quality thermochemistry when considered on its own, that does not mean that it is the best term to use with KT exchange. We therefore considered the addition of KT exchange to the previous term in the B97 expansion, which is equivalent to Becke's 1986 exchange term (B86X)

$$\beta \sum_{\sigma} \int \rho_{\sigma}^{4/3}(\mathbf{r}) \left(\frac{\gamma x_{\sigma}^2}{1 + \gamma x_{\sigma}^2} \right) \mathrm{d}\mathbf{r} \tag{4.22}$$

As for OPTX, we started by fitting LDAX+B86X+LYP. Again, we fitted with and without total energies. Coefficients are presented in Table 4.4 and results in Table 4.6. Bond lengths and atomisation energies improved on removing total energies from the fit, but performance for shielding constants became slightly worse. Overall B86LYP does not perform as well as OLYP, justifying Handy and Cohen's claim that OPTX is a better exchange functional than B86X.

Next, we developed a functional analogous to OKTLYP, containing LDAX, B86X, KTX and LYP. As expected, the KTX term was minimised when its coefficient was not fixed, although when total energies were taken out of the fit it rose to a non-negligible value. When its coefficient was fixed at the value -0.0045 (as for OKTLYP), its performance for atomisation energies was better

Table 4.6: Error assessments for thermochemistry, molecular bond lengths, and isotropic shielding constants for the B86LYP functional (B) with and without KTX (K). T denotes fitting to total energies, A to atomisation energies, and I to ionisation potentials. F denotes that the KTX coefficient was fixed. Units are given in parentheses.

	B T,A,I	B A,I	B,K T,A,I	B,K A,I	B,K A,I,F
A1. Isotropic NMR shielding constants (ppm)					
d	−43.3	−47.2	−44.7	−35.2	−7.6
$\|d\|$	43.3	47.2	44.7	35.2	13.5
Excluding O_3:					
d	−34.8	−37.9	−35.9	−28.4	−6.5
$\|d\|$	34.8	37.9	35.9	28.4	10.8
A3. Atomisation energies (kcal mol^{-1})					
d	0.9	1.0	0.9	0.8	0.2
$\|d\|$	4.0	3.7	4.1	2.6	5.7
A4. Ionisation potentials (kcal mol^{-1})					
d	−1.7	2.8	−1.1	2.1	0.5
$\|d\|$	4.1	2.9	3.9	2.2	2.0
A5. Total atomic and ionic energies (kcal mol^{-1})					
d	0.4	−129.4	0.3	−260.3	−570.4
$\|d\|$	2.9	129.4	3.1	260.3	570.6
A6. G2 subset bond lengths (Å)					
d	0.021	0.010	0.021	0.005	−0.003
$\|d\|$	0.022	0.011	0.022	0.013	0.015
A7. Diatomic bond lengths (Å)					
d	0.042	0.027	0.042	0.016	−0.007
$\|d\|$	0.042	0.028	0.042	0.021	0.025

than OKTLYP, but bond lengths were worse and shieldings were not optimal (as might be expected, because B86LYP gives worse shieldings than OLYP and so requires a larger KT correction). To obtain optimal shieldings, we had to set the KTX coefficient to -0.006. The A3 atomisation energies for this functional were inferior to OKTLYP.

B86X and OPTX

The next step was to develop a five parameter functional, containing both B86X and OPTX. With the extra flexibility in the functional form, atomisation energies could improve further without the quality of shielding constants deteriorating. As before, we fitted three functionals. Fitting with total energies minimised KT exchange, and poor shieldings were still produced without them. Unfortunately, fixing the KTX coefficient did not produce the gains we expected. As can be seen in Table 4.4, the OPTX coefficient became highly positive, whilst the B86X term became large and negative. The resultant cancellation gave excellent atomisation energies, but its performance for shielding constants and bond lengths deteriorated dramatically. Errors are presented in Table 4.7. This problem will always occur given a sufficiently flexible functional form, because we were only fitting to energies.

We have also considered functionals incorporating the third and fourth power of the B97 expansion (as used in the HCTH functionals and 1/4, but not in the B97 functionals themselves). Using them on their own offered no advantage over OKTLYP, and attempting to combine them with the other terms led to the same problem we encountered with the combination of B86X and OPTX. In Chapter 6, we discuss a method of fitting explicitly to the shielding constants, which avoids this problem. In this chapter we pursue an alternative approach to go beyond OKTLYP, by readdressing the problem of the form of the KT exchange term.

4.4 Modifying the exchange functional (2)

One problem we have not addressed is the intrinsic performance of KT2 for thermochemistry. The gains OKTLYP has made have been primarily due to

Table 4.7: Error assessments for thermochemistry, molecular bond lengths, and isotropic shielding constants for the B86LYP functional (B) with OPTX (O) and KTX (K). T denotes fitting to total energies, A to atomisation energies, and I to ionisation potentials. F denotes that the KTX coefficient was fixed. Units are given in parentheses.

	B,O,K T,A,I	B,O,K A,I	B,O,K A,I,F
A1. Isotropic NMR shielding constants (ppm)			
d	−33.9	−34.4	−23.9
$\|d\|$	33.9	34.4	26.9
Excluding O_3:			
d	−26.6	−27.5	−19.4
$\|d\|$	26.6	27.5	22.6
A3. Atomisation energies (kcal mol^{-1})			
d	0.6	0.7	0.7
$\|d\|$	3.2	2.6	3.4
A4. Ionisation potentials (kcal mol^{-1})			
d	−1.6	1.6	2.6
$\|d\|$	2.6	1.7	2.6
A5. Total atomic and ionic energies (kcal mol^{-1})			
d	−0.6	−203.1	−480.8
$\|d\|$	2.4	203.1	480.8
A6. G2 subset bond lengths (Å)			
d	0.017	0.007	−0.001
$\|d\|$	0.017	0.010	0.020
A7. Diatomic bond lengths (Å)			
d	0.045	0.023	−0.005
$\|d\|$	0.045	0.023	0.039

the fact that a lower coefficient of KT exchange could be used. However, there is no systematic way of achieving an improvement in the KT form itself. In this section we outline some of the modifications that we have considered.

4.4.1 Functions of ρ_σ

The KT exchange form can be re-written in the form

$$\beta \sum_\sigma \int \frac{|\nabla \rho_\sigma(\mathbf{r})|^2}{\rho_\sigma^{4/3}(\mathbf{r})} \left(\frac{\rho_\sigma^{4/3}(\mathbf{r})}{\rho_\sigma^{4/3}(\mathbf{r}) + \gamma} \right) \mathrm{d}\mathbf{r} \tag{4.23}$$

that is, as the GEA multiplied by some $f(\rho_\sigma)$. This is the essential difference between KT exchange and standard GGA exchange; for the latter, the GEA is multiplied by some $f(x_\sigma)$, where x_σ is

$$x_\sigma(\mathbf{r}) = \frac{|\nabla \rho_\sigma(\mathbf{r})|}{\rho_\sigma^{4/3}(\mathbf{r})} \tag{4.24}$$

We spent some time searching for a form $f(x_\sigma)$ which gave good shielding constants, because this form satisfies certain universal properties which $f(\rho_\sigma)$ does not, such as the exchange scaling condition (Eq. 1.60). We were unable to find such a form, because x_σ fluctuates markedly in the intershell region and tends to distort the description of the intershell peak (this is also the reason why standard GGAs give poor shielding constants). The form of the potential is also more complex and difficult to interpret.

We therefore concentrated on investigating new forms of $f(\rho_\sigma)$ to see if they would improve atomisation energies. We experimented with an exponential form

$$f(\rho_\sigma) = e^{-\gamma/\rho_\sigma(\mathbf{r})} \tag{4.25}$$

This cuts off the potential at low ρ_σ but will tend towards the GEA at high ρ_σ. This function gave essentially identical results to KT exchange, so there is no reason to favour it.

Another function we investigated was

$$f(\rho_\sigma) = \frac{\rho_\sigma^{4/3}(\mathbf{r})}{\rho_\sigma^{4/3}(\mathbf{r}) + \frac{\gamma}{\rho_\sigma^{4/3}(\mathbf{r})}} \tag{4.26}$$

This modifies the behaviour in the region where the GEA is cut off. With an appropriate value of $\gamma = 0.002$, the intershell region is no longer affected by the cut off function (the magnitude of the peak is diminished slightly in KT exchange). Hence a lower value of $\beta = -0.0045$ could be used to get the same shielding results. However, the A3 atomisation energy errors remained at the level of KT2. Therefore this form has nothing to recommend it either.

4.4.2 KT expansion

A more complex modification is to write an expansion of the KT exchange term in the same way as B86X was expanded to give B97. This leads to terms of the form

$$\beta\gamma^n \sum_\sigma \int \frac{|\nabla\rho_\sigma(\mathbf{r})|^{2n}}{\rho_\sigma(\mathbf{r})^{(8n/3-4/3)} + \gamma^n} \mathrm{d}\mathbf{r} \tag{4.27}$$

where KT exchange is returned when $n = 1$ (save for the extra γ coefficient).

Although the atomisation energy errors could be improved using these terms, the shieldings deteriorated significantly. This is because it suffers from the same flexibility problems seen above when we added both B86X and OPTX to KTX. It is clear that highly flexible forms do not work with our current fitting procedure. We also attempted to use the second term in the expansion on its own (analogous to OPTX), but this caused performance for both shielding constants and atomisation energies to deteriorate compared to KT2.

4.4.3 α-β terms

The GEA is sometimes written in the form

$$\sum_{\sigma,\sigma'} \beta_{\sigma,\sigma'} \int \frac{\nabla\rho_\sigma(\mathbf{r})}{\rho_\sigma^{2/3}(\mathbf{r})} \frac{\nabla\rho_{\sigma'}(\mathbf{r})}{\rho_{\sigma'}^{2/3}(\mathbf{r})} \mathrm{d}\mathbf{r} \tag{4.28}$$

When written out in full, this implies an extra term involving an interaction between the α and β spins. Because it involves an interaction between different spins, this is a correlation term. An analogous KT-type term is

$$\sum_{\sigma,\sigma'} \beta_{\sigma,\sigma'} \int \frac{\nabla\rho_\sigma(\mathbf{r})\nabla\rho_{\sigma'}(\mathbf{r})}{[\rho_\sigma^{2/3}(\mathbf{r})\rho_{\sigma'}^{2/3}(\mathbf{r})] + \gamma} \mathrm{d}\mathbf{r} \tag{4.29}$$

In the restricted case, this will collapse to the ordinary KT exchange term. However, it will have an effect on open shell calculations (in particular, the fragments used to calculate atomisation energies). We therefore considered the addition of this extra term to the KT functional. However, although the fitted term had a large coefficient (about a third of the standard KT exchange term), it had no significant effect on the A3 atomisation energy errors.

4.5 Choice of correlation functional (2)

In parallel with our investigations of the exchange functional, we also considered more complex correlation functional forms to bring the atomisation energy errors down. Our first attempt involved combining both VWN and LYP correlation (as in the B3LYP functional). Unfortunately, the same flexibility problem emerged as before, with large opposite coefficients being given by the fitting code. This led to some improvement in atomisation energies but at the cost of other properties. A similar problem was encountered when we used the HCTH correlation functional, which consists of an eight term gradient-corrected expansion. This highly parameterised form brought the atomisation energy errors down to almost 2 kcal mol^{-1}, but the unphysical nature of the functional was evident in its very poor performance for shieldings and bond length optimisations. Once again we found that the number of parameters has to be kept to a minimum in our normal fitting procedure.

4.6 Non-fitted thermochemistry

The OKTLYP form is the best we have considered so far. Its performance for the A3 atomisation energy set and the A4 ionisation potential set is much

improved over KT2, although the poor performance for the A5 total atomic and ionic energies remains. The high quality performance for shielding constants is retained and bond length optimisations are much improved.

It is important to assess semi-empirical functionals for data outside the fitting set, and so we conducted more thermochemistry assessments on OKTLYP to confirm that its good performance is not confined to the A3 and A4 sets. Following Ref. [182], we considered the full G2 set of atomisation energies developed by Pople and co-workers [136, 183]. We used the standard 6-311+G(3df,2p) basis set and MP2/6-31(d) geometries [184] for all calculations. These were both available only in a format suitable for the GAUSSIAN program. We converted them using scripts written in the Perl programming language, which was chosen for its powerful text-processing capabilities. All experimental reference data from Ref. [182] had been corrected for zero-point energies. Errors are presented in Table 4.8.

The full G2 atomisation energy set is divided into two parts: G2-1 (A13 in this thesis) and G2-2 (A14). The G2-1 set is very similar to the A3 atomisation energy set (as discussed in Section 2.4) although different basis sets and geometries were used. The OKTLYP mean absolute errors are therefore similar (4.5 kcal mol^{-1} for A13 compared to 5.0 kcal mol^{-1} for A3). The G2-2 set, like G2-1, contains predominantly organic molecules, but the average number of atoms is larger than in G2-1. We would therefore expect the G2-2 errors to be larger, and that is the case. The G2-2 error is 6.8 kcal mol^{-1}, giving an overall error of 5.9 kcal mol^{-1}.

For comparison, the OLYP error over the full G2 set is 4.6 kcal mol^{-1} and the HCTH error is 5.5 kcal mol^{-1}. OKTLYP is therefore competitive with the performance of the best GGAs, but there is still room for improvement. We therefore investigated whether further improvements could be achieved by fitting to the full G2 set.

4.7 Rewriting the fit code

The original fit code of Chapter 2 was designed for use with the sets A3–A5 as the fitting data. For each system in the set there is a corresponding

Table 4.8: Error assessments for G2 thermochemistry, molecular bond lengths, and isotropic shielding constants for the OKTLYP-type functionals. Units are given in parentheses.

	Orig.	G2 fit 1[a]	G2 fit 2[b]	G2 fit 3[c] (KT3)
A13/14. G2 atomisation energies (kcal mol^{-1})				
G2-1:				
d	−0.6	−1.0	−1.0	−1.2
$\|d\|$	4.5	4.6	4.2	4.3
G2-2:				
d	4.3	0.4	0.4	0.4
$\|d\|$	6.8	5.4	4.9	5.0
Full G2:				
d	2.5	−0.1	−0.1	−0.2
$\|d\|$	5.9	5.1	4.7	4.7
A1. Isotropic NMR shielding constants (ppm)				
d	−10.4	−8.4	−11.3	−11.9
$\|d\|$	13.3	12.9	14.0	14.4
Excluding O_3:				
d	−8.2	−6.7	−8.9	−9.4
$\|d\|$	11.4	10.9	11.8	12.1
A6. G2 subset bond lengths (Å)				
d	0.000	0.004	0.003	0.000
$\|d\|$	0.008	0.009	0.008	0.008
A7. Diatomic bond lengths (Å)				
d	0.004	0.010	0.011	0.009
$\|d\|$	0.012	0.015	0.015	0.014

[a] KTX coefficient fixed at -0.0045
[b] KTX coefficient fixed at -0.004
[c] KTX coefficient fixed at -0.004, LDAX coefficient fixed at 1.092

grid of density and gradient points obtained from coupled cluster densities for fitting to the ZMP potential. It is not straightforward to add extra sets to the fitting procedure because the program assumes that a set of these points will be available for every new system added. As we do not fit to ZMP potentials, this assumption is not necessary. It proved easier to write the fit code again from scratch than to try to rework the original one.

The new fit code is written in Fortran and is also based on a linear least-squares fit, although the way the fitting procedure is initialised is slightly different. In the new procedure an initial guess for the functional parameters is required from which a set of property errors is calculated. These are then used as the basis of the next iteration. The exchange-correlation energy for a system is written as

$$E_{\mathrm{XC}} = \sum_{i}^{N} a_i f_i \tag{4.30}$$

where a_i is the coefficient of component i and f_i is the unit contribution to the exchange-correlation energy of component i. N is the total number of components ($N = 4$ in the case of OKTLYP). Our aim is to find the optimal change in the values of the coefficients δa_i, giving a new functional with components $a_i + \delta a_i$. Assuming that the energy is linear (i.e. ignoring changes in the density as the coefficients change), the error in a property for a molecule M is

$$\Delta^M = -\sum_{i}^{N} \delta a_i g_i^M \tag{4.31}$$

where Δ^M is the error in the property (calculated − experiment). If the property fitted to is an atomisation energy,

$$g_i^M = \sum_{A} f_i^A - f_i^M \tag{4.32}$$

where A are the constituent atoms. We then define a merit function

$$\Omega = \sum_{M} \left[\Delta^M + \sum_{i}^{N} \delta a_i g_i^M \right]^2 \tag{4.33}$$

We need to find the minimum of Ω, that is

$$\frac{\partial\Omega}{\partial(\delta a_j)} = 0 \qquad \text{for } j = 1 \ldots N \tag{4.34}$$

By differentiation

$$2\sum_M \left[\Delta^M - \sum_i^N \delta a_i g_i^M\right] g_j^M = 0 \tag{4.35}$$

so

$$\sum_M \Delta^M g_j^M = \sum_M \sum_i^N g_j^M g_i^M \delta a_i \tag{4.36}$$

or

$$h_j = \sum_i^N G_{ji}\delta a_i \tag{4.37}$$

This matrix equation is then solved using the LU decomposition routine also used in the old fit code [185] to find the change in components δa_i. For convenience we sometimes used Solver (the Microsoft Excel fit code) to solve the final equation instead, but we have confirmed that this gives identical results. The new functional is then used to calculate a new set of errors and the process is iterated until the coefficients have converged.

The new fit code requires the f_i contributions and atomisation energy errors for each system as input. We therefore modified CADPAC to print out the f_i contributions and used a Perl script to collate the information and calculate the g_i values. A second script was used to calculate and collate the property errors at each iteration.

4.8 Fitting to the G2 set

Using the new fit code, we fitted the OKTLYP form to the full G2 atomisation energy set. For simplicity, we did not include ionisation potentials in the fitting data, as we had observed previously that this made little difference to the outcome of the fit. We kept the KTX coefficient fixed at -0.0045 as before to ensure high quality shielding constants. The final parameters of this functional (G2 fit 1) are quite similar to those of the original OKTLYP, as shown in Table 4.9. Errors for the new functional are presented in Table 4.8. The

Table 4.9: Coefficients of OKTLYP-type functionals.

	LDAX	OPTX	KTX	LYP
Orig.	1.08598E + 0	−7.42401E − 1	−4.5E − 3	8.27819E − 1
G2 fit 1[a]	1.07658E + 0	−8.18190E − 1	−4.5E − 3	8.79537E − 1
G2 fit 2[b]	1.08256E + 0	−9.08093E − 1	−4.0E − 3	8.80366E − 1
G2 fit 3[c] (KT3)	1.09200E + 0	−9.25452E − 1	−4.0E − 3	8.64409E − 1

[a] KTX coefficient fixed at -0.0045
[b] KTX coefficient fixed at -0.004
[c] KTX coefficient fixed at -0.004, LDAX coefficient fixed at 1.092

mean absolute error for the full G2 set is lowered to 5.1 kcal mol^{-1}, surpassing HCTH (but still not quite at the same level as OLYP). This reduction is expected as the new functional includes the full G2 set in its fitting data. This is consistent with the finding that the new functional gives a marginally higher error than before for the G2-1 set (approximately equivalent to the old fitting data set A3). The performance for shielding constants also improves, but the bond length optimisation sets deteriorate slightly, with the bonds on average getting too long. This is due to the smaller value of the LDA exchange coefficient, which will make the density more diffuse and hence lead to longer bond lengths.

The improvement in shielding constants suggested that we might be able to decrease the KTX coefficient a little. Our next functional (G2 fit 2) reduced the KTX coefficient to −0.004. The change in the fitting coefficients was again small. The atomisation energy error was reduced further to 4.7 kcal mol^{-1}, essentially the same as OLYP. The A6 set of bond lengths also improved marginally, although the A7 diatomics set did not. Shielding constants deteriorated slightly as expected, but we felt this was an acceptable trade-off for the improvement in atomisation energies.

Finally, we observed that the bond lengths could be shortened by fixing the LDA exchange coefficient at a higher value. The optimal value was 1.092. This left only two fitted parameters, OPTX and LYP. The resulting functional (G2 fit 3) gave the same atomisation energy errors as before. The bond lengths

also shortened, although only the A7 diatomic set gave a reduction in the mean absolute errors. Again, shielding constants deteriorated slightly, but we decided this was acceptable. We denote this functional KT3 [186].

Chapter 5

Assessment of KT3

In this chapter we present a full assessment of the KT3 functional for the chemical properties considered in its development and for a number of new properties. The performance of KT3 is compared to a range of GGA and hybrid functionals. We then consider applications which require both the high quality structural predictions and shielding constant performance that KT3 provides.

5.1 Fitting data assessments

Table 5.1 presents a summary of the performance of KT3 for the sets considered in its development. The G2 atomisation energies set was the only one explicitly fitted to, but the LDA exchange and KT exchange parameters were fitted in the sense that they were chosen to ensure improved geometries and shielding constants respectively. Errors are compared to the KT1, KT2, PBE, HCTH, and OLYP GGAs, and the B3LYP, PBE0, and B97-2 hybrid functionals.

For the A1 set of isotropic shielding constants, the slight degradation from KT1 to KT2 to KT3 is apparent. However, the KT3 error of 14.4 ppm is still at least a factor of two improved over PBE, HCTH, and OLYP. OLYP is the best competing GGA with an error of 30.7 ppm. The hybrid functionals all perform worse than any GGA as previously observed.

The atomisation energies of the G2 set show a significant improvement from KT1 to KT2 to KT3. This is mainly due to the extra flexibility introduced

Table 5.1: Fitting data error assessments for the KT3 functional. Units are given in parentheses.

	KT1	KT2	KT3	PBE	HCTH	OLYP	B3LYP	PBE0	B97-2
A1. Isotropic NMR shielding constants (ppm)									
d	−4.7	−9.5	−11.9	−40.3	−32.4	−30.7	−60.7	−58.5	−50.4
$\|d\|$	13.0	13.2	14.4	40.3	32.4	30.7	60.7	58.8	50.4
A13/14. G2 atomisation energies (kcal mol^{-1})									
G2-1:									
d	12.9	−0.8	−1.2	6.3	−0.4	2.1	−0.8	−2.0	−0.7
$\|d\|$	13.4	6.2	4.3	7.9	3.3	3.2	2.7	3.2	2.2
G2-2:									
d	36.6	10.4	0.4	21.2	−2.1	1.7	−4.8	3.8	0.8
$\|d\|$	37.1	12.0	5.0	21.5	6.8	5.4	5.1	5.6	3.6
Full G2:									
d	27.8	6.2	−0.2	15.6	−1.4	1.8	−3.3	1.7	0.2
$\|d\|$	28.3	9.9	4.7	16.5	5.5	4.6	4.2	4.7	3.1
A6. G2 subset bond lengths (Å)									
d	0.014	−0.001	0.000	0.015	0.012	0.015	0.004	0.000	0.002
$\|d\|$	0.019	0.010	0.008	0.015	0.013	0.015	0.008	0.007	0.008
A7. Diatomic bond lengths (Å)									
d	0.008	−0.010	0.009	0.024	0.036	0.040	0.015	0.007	0.017
$\|d\|$	0.026	0.020	0.014	0.024	0.037	0.040	0.018	0.014	0.022

with each iteration of the KT functionals. KT3 is the only one of the three to be fitted to the full G2 set, but this only reduced the error from 5.9 kcal mol^{-1} (of the original OKTLYP, fitted to the A3 set) to 4.7 kcal mol^{-1}. The rest of the improvement over KT2 is due to the addition of the OPTX exchange term and the replacement of VWN with LYP. Compared to the other GGAs, KT3 is superior to PBE and HCTH, and gives essentially the same quality as OLYP (4.6 kcal mol^{-1}). OLYP represents arguably the best atomisation energy performance that GGAs are capable of, so this result is very encouraging. However, the best hybrid functionals perform better than the GGAs, with B97-2 giving the lowest error (3.1 kcal mol^{-1}).

KT3 gives very good performance for the A6 (0.008 Å) and A7 (0.014 Å) bond lengths, significantly improving over KT1 and KT2. It is also substantially more accurate than the other GGAs considered in this assessment, the best being PBE with mean absolute errors of 0.015 Å and 0.024 Å. The only superior GGA is the 1/4 functional considered earlier in this thesis. KT3 provides errors comparable to the hybrid functionals, which is a considerable achievement for a GGA. The best hybrid is PBE0, with errors of 0.007 Å and 0.014 Å, only marginally better than KT3.

5.2 Non-fitting data assessments

In Table 5.2, we present a new series of assessments to explore the performance of KT3 outside the set of fitting data. The first new properties that we consider are thermochemical. These are the ionisation potentials, electron affinities and proton affinities of the G2-1 set [136]. In previous chapters we have also considered ionisation potentials (the A4 set), but that set was very small and considered only atomic ionisation potentials. The G2-1 set considers a mixture of atoms and molecules and provides a more accurate measurement of quality. All three sets were calculated at the same 6-311+G(3df,2p) basis set as for the G2 atomisation energies, using the same quality MP2/6-31G(d) geometries from Ref. [184]. Adiabatic values are calculated rather than vertical values (that is, the geometries of the neutral and ionic systems were optimised separately). ZPE-corrected experimental reference values were taken

Table 5.2: Non-fitted data error assessments for the KT3 functional. Units are given in parentheses.

	KT1	KT2	KT3	PBE	HCTH	OLYP	B3LYP	PBE0	B97-2
A15. G2-1 ionisation potentials (eV)									
d	−0.06	−0.11	−0.03	0.01	−0.02	−0.12	0.01	0.02	−0.02
$\|d\|$	0.14	0.23	0.16	0.16	0.15	0.18	0.16	0.17	0.12
A16. G2-1 electron affinities (eV)									
d	0.11	−0.05	−0.07	0.08	−0.02	−0.11	−0.01	−0.05	−0.09
$\|d\|$	0.15	0.17	0.14	0.10	0.10	0.14	0.09	0.13	0.11
A17. G2-1 proton affinities (kcal mol^{-1})									
d	−4.1	−2.2	1.6	−1.6	2.5	1.0	−1.4	−0.4	1.8
$\|d\|$	4.9	3.5	2.3	2.6	2.5	2.0	2.2	2.4	1.8
A18. Hydrogen bond dimer distances (Å)									
d	−0.18	−0.21	−0.03	−0.03	0.26	0.26	0.01	−0.02	0.06
$\|d\|$	0.18	0.21	0.05	0.04	0.26	0.26	0.04	0.04	0.06
A19. Other bond lengths (Å)									
d	0.009	−0.008	−0.003	0.010	0.005	0.009	−0.002	−0.021	−0.016
$\|d\|$	0.022	0.018	0.012	0.015	0.017	0.015	0.014	0.023	0.017
A20. Bond angles (degrees)									
d	−0.8	−0.7	−0.5	0.0	0.1	−0.1	0.1	0.0	0.0
$\|d\|$	1.1	0.9	1.0	0.8	0.9	1.0	0.3	0.5	0.4
A21. Diatomic harmonic vibrational wavenumbers (cm^{-1})									
d	−13	4	−3	−16	−18	−21	3	20	12
$\|d\|$	21	15	15	21	26	27	20	26	26
A22. Isotropic electronic polarisabilities (au)									
d	1.16	0.68	0.32	0.76	0.41	0.57	0.36	0.03	−0.04
$\|d\|$	1.16	0.68	0.36	0.76	0.45	0.57	0.44	0.24	0.22
A23. Classical chemical reaction barriers (kcal mol^{-1})									
No.	6	9	12	10	15	14	15	16	16
d	−15.3	−11.4	−8.0	−7.8	−3.3	−5.6	−5.1	−4.4	−1.8
$\|d\|$	15.3	11.4	8.0	7.8	3.8	5.6	5.1	4.4	2.4

from Ref. [182] (strictly speaking, we are therefore evaluating the electronic contribution to the ionisation potential, electron affinity and proton affinity). Note that two of the systems of the G2-1 ionisation potential set, H_2S (^2A) and N_2 ($^2\Pi$), were excluded from our analysis because of convergence problems with the GGAs (the same problems were observed in Ref. [182]).

For ionisation potentials, KT3 has an error of 0.16 eV, which improves on KT2 but is still slightly inferior to the remarkably good performance of KT1 (0.14 eV). The KT3 error is typical of the GGAs considered, with PBE, HCTH, and OLYP all giving similar results. The hybrid functionals also do not improve over KT3, with the exception of B97-2 (0.12 eV).

An electron affinity is defined as the energy of a system M minus the energy of the same system with an additional electron.

$$E_{\mathrm{EA}} = E_M - E_{M^-} \tag{5.1}$$

The A16 electron affinity set consists of 25 small atoms and molecules. There is slightly more variation in performance for the set than there was for ionisation potentials. In this case KT3 is superior to KT1 and KT2, with an error of 0.14 eV. This is comparable with the other GGAs, but both PBE and HCTH give better results (0.10 eV). The best performing functional is the hybrid B3LYP, with an error of 0.09 eV.

A proton affinity is the energy of a system minus the energy of the same system with an additional proton.

$$E_{\mathrm{PA}} = E_M - E_{MH^+} \tag{5.2}$$

The A17 proton affinity set consists of 7 small molecules. It is important not to overinterpret the results for this set due to its size, but it still gives a good indication of relative performance. Again KT3 improves on KT1 and KT2, with an error of 2.3 kcal mol^{-1}. This also beats PBE and HCTH but OLYP improves further with an error of 2.0 kcal mol^{-1}. This is comparable with the hybrid functional results, with the best overall error given by B97-2 with 1.8 kcal mol^{-1}.

Overall the KT3 functional is competitive with the best GGA functionals

for all the thermochemical properties we have assessed. We have also calculated the errors for the KT3 functional over the A5 total atomic and ionic energy set considered in previous chapters. As expected, KT3 is very poor, with an error of 425.4 kcal mol^{-1}. This reflects the substantial amount of KT exchange present in KT3. As these errors cancel when energy differences are considered, we do not consider this to be a hinderance to practical use of this functional.

The second set of new properties we considered involved geometry optimisations. The KT3 functional was assessed for hydrogen bond dimer distances, another set of challenging bond lengths, and a set of bond angles.

The A18 hydrogen bond set consists of 5 systems, $(HF)_2$, $(HCl)_2$, $(H_2O)_2$, (CO)(HF), and (OC)(HF), each consisting of two molecules linked with a hydrogen bond. These are a subset of the systems considered in Ref. [187]. The calculations were performed using the TZ2P basis set, and the errors calculated for the F···F, Cl···Cl, O···O, O···F and C···F intermolecular distances against *ab initio* wavefunction results [187, 188]. Again, the quantitative results should not be overanalysed due to the small size of the set. KT3 gives a mean absolute error of 0.05 Å, a marked improvement over KT1 and KT2, which uniformly underestimate the distances. The KT3 error is comparable with PBE, with HCTH and OLYP uniformly overestimating the results. For this set KT3 is also competitive with the hybrid functionals, which give similar errors.

The A19 bond length set consists of the challenging molecules FOOF, FNO_2, O_3, and FO_2 (calculated with TZ2P) and two transition metal complexes, $Cr(CO)_6$ and $Ni(CO)_4$ (using the Wachters basis set [189] for the transition metal atoms and TZ2P for the others). In total it consists of 11 bond lengths. These systems were previously studied in Ref. [51], from where the reference experimental values were taken. KT3 gives a mean absolute error of 0.012 Å, which is the best out of all the functionals considered.

The A20 bond angles set consists of the polyatomic molecules from sets A6 and A19, giving a total of 13 bond angles. The errors are calculated relative to *ab initio* values for the A6 systems [47] and experimental values for the A19 systems [51]. Overall, the KT3 performance ($|d| = 1.0°$) is similar to the other KT functionals and all the other GGAs. The hybrid functionals perform

significantly better, with the lowest error given by B3LYP (0.3°).

Overall, the bond length optimisations are clearly a strength of the KT3 functional. For the A6, A7, A18, and A19 sets, KT3 gives results that are significantly improved over the other GGAs, and are competitive with the hybrid functionals. For bond angles the performance is not quite as good, but KT3 is still competitive with the other GGAs.

The next set is closely related theoretically to the geometry assessments. Harmonic vibrational wavenumbers are calculated as the square roots of the eigenvalues of the force constant matrix

$$f_{ij} = \frac{\partial^2 E}{\partial q_i \partial q_j} \tag{5.3}$$

where q_i are mass-weighted cartesian displacements. This gives a set of $3N$ normal mode vibrational frequencies, of which the six that correspond to translational and rotational degrees of freedom will be equal to zero (five in the case of linear molecules). Vibrational wavenumbers $\overline{\nu}$ are related to the vibrational frequencies by

$$\overline{\nu} = \nu / c \tag{5.4}$$

where ν is the vibrational frequency.

The A21 set consists of the same 45 diatomics considered in the A7 bond length optimisations. The wavenumber analysis is calculated at the A7 optimised geometries and compared to experimental reference values from Ref. [139]. KT3 gives an error of 15 cm^{-1}, which is equal to the already impressive error given by KT2. This is superior to all the other GGA and hybrids considered here. The nearest competing functional is B3LYP with an error of 20 cm^{-1}. This result is expected because wavenumber performance is usually closely correlated with performance for geometry optimisations. The 1/4 functional is better still [139], in line with its excellent performance for geometries, but we emphasise that 1/4 performs very poorly for other properties.

We also assessed the KT3 functional for the set of 14 static isotropic polarisabilities previously considered in Ref. [51]. The polarisability is a second derivative property (Eq. 1.93), and therefore requires the first order response of the wavefunction to the electric field perturbation. The polarisability is

given by [190]

$$\alpha_{\alpha\beta} = -4 \sum_{ai} C_{ai}^{\beta} P_{ia}^{\alpha} \tag{5.5}$$

where the dipole integral is

$$P_{ia}^{\alpha} = (\psi_i | r_\alpha | \psi_a) \tag{5.6}$$

The linear response C_{ai}^{β} is determined from a set of coupled perturbed equations

$$\sum_{bj} (H_1)_{ai,bj} C_{bj}^{\alpha} = -P_{ai}^{\alpha} \tag{5.7}$$

where $\mathbf{H_1}$ is the electric Hessian [120]. Unlike the magnetic Hessian, this does not reduce to a trivial form for GGAs, and the coupled perturbed equations have to be solved for all functionals. The isotropic polarisability is defined as

$$\alpha_{\text{iso}} = \frac{1}{3} \text{tr} \alpha \tag{5.8}$$

The polarisability calculations were performed using the Sadlej basis set [191] and the errors calculated relative to BD(T) values. This avoids problems with reference experimental values that have not been vibrationally corrected [192]. KT3 gives an error over the A22 set of 0.36 au, which is a substantial improvement over KT1 and KT2. KT3 is also substantially better than the other GGAs, with the best performance given by HCTH (0.45 au). It also beats B3LYP, but the other hybrid functionals are significantly improved over KT3, with B97-2 giving an error of 0.22 au.

Finally, we consider classical chemical reaction barrier heights, which are a very challenging property for DFT methods. They are defined as the energy of the transition state TS of a reaction minus the sum of the energies of the reactants R.

$$E_{\text{BH}} = E_{\text{TS}} - \sum_{R} E_R \tag{5.9}$$

This set was previously studied in Ref. [51]. We used a TZ2P basis set for the calculations. The transition states were found by a saddle point geometry optimisation and checked by confirming firstly that an imaginary vibrational

frequency was present (which indicates an energy maximum), and secondly that the energy of the transition state was higher than that of the reactants. For some reactions with some functionals we could not locate the transition state, and so we report the number of barriers calculated for each functional in Table 5.2. The errors were calculated over the successful barriers relative to the *ab initio* values quoted in Ref. [51].

The A23 is the only set we considered where KT3 was not competitive with the best GGA results. KT3 located 12 transition states and gave an error of 8.0 kcal/mol, which is significantly better than KT1 and KT2, and is comparable to PBE. However, the performance of OLYP and HCTH is better still, with HCTH locating 15 of the transition states and giving a remarkably low error of 3.8 kcal mol^{-1}. Of the hybrids only B97-2 beats this figure, with all the transition states located and an error of 2.4 kcal/mol.

The full set of assessments consists of 3,987 individual calculations. A full breakdown of the results is available in Ref. [193] (the supplementary information for Ref. [186]).

5.2.1 Magnetic properties

Finally, we compare the performance of KT3 to the earlier KT functionals for the magnetic property assessments of Chapters 2 and 3. Errors are presented in Table 5.3. Given the small degradation in the isotropic shielding constants, we expected that the performance of KT3 would be slightly worse for all the magnetic property sets (with the possible exception of spin-spin coupling constants). For the A2 anisotropic shielding constant set however, KT3's performance of 9.4 ppm is superior to KT1 (with KT2 having the smallest error of 8.8 ppm). This contrasts with the isotropic A1 set, where the performance is KT1 > KT2 > KT3. KT1 gives the best performance for isotropic magnetisabilities (5.7×10^{-30} JT^{-2} compared to MCSCF) whereas some degradation is observed for KT3. A similar result is found for anisotropic magnetisabilities, although in this case it is KT2 that gives the best performance ($|d| = 17.4\times 10^{-30}$ JT^{-2} compared to 22.9×10^{-30} JT^{-2} for KT3). The pattern is mixed for chemical shifts, with the ^{15}N and ^{17}O results worsened but ^{13}C and ^{19}F

Table 5.3: Non-fitted magnetic property assessments for the KT3 functional. Magnetisability errors are presented relative to MCSCF (including O_3). Units are given in parentheses.

	KT1	KT2	KT3
A2. Anisotropic NMR shielding constants (ppm)			
d	−2.1	4.1	6.7
$\|d\|$	11.5	8.8	9.4
A8. Isotropic magnetisabilities (10^{-30} JT^{-2})			
d	3.7	7.7	11.0
$\|d\|$	5.7	7.7	11.0
A9. Anisotropic magnetisabilities (10^{-30} JT^{-2})			
d	12.0	13.0	16.3
$\|d\|$	18.8	17.4	22.9
A10. Isotropic NMR chemical shifts (ppm)			
$\|d\|(^{13}C)$	4.5	4.4	4.4
$\|d\|(^{1}H)$	0.32	0.25	0.20
$\|d\|(^{15}N)$	25.7	26.1	29.1
$\|d\|(^{17}O)$	56.0	59.5	64.1
$\|d\|(^{19}F)$	16.7	17.3	16.8
A11. GIAO shielding constants (ppm)			
d	−20.4	−22.8	−21.5
$\|d\|$	23.7	24.3	23.1
A12. Indirect spin-spin coupling constants (Hz)			
d	−5.3	−2.2	0.2
$\|d\|$	10.8	12.6	13.9

remaining steady and ^{1}H actually improving.

The DALTON calculations also give interesting results. KT3 gives the best errors (23.1 ppm) for the A11 GIAO shielding constant sets, although the improvement is not significant. For spin-spin coupling constants, KT3 gives an error of 13.9 Hz, which is even worse than KT2. Again the error is dominated by the Fermi-contact term, which suggests that the source of this increased error is not the reduced amount of KT exchange, but actually some worsening of the description of the core.

Overall, however, the degradation for magnetic properties is small, and we believe it is well worth the trade-off for the substantial improvement in performance for the other chemical properties we have assessed. KT3 is overall the best performing GGA out of all those considered (KT1, KT2, KT3, PBE, HCTH, and OLYP), and for bond length optimisations and harmonic vibrational wavenumbers it is as accurate as the best hybrid functionals. The only assessments for which KT3 performs poorly are the A5 total energy set and the A23 classical reaction barriers. Unlike total energies, classical reaction barriers are a very important property for practical purposes, and in Chapter 6 we focus on building functionals with improved performance for reaction barriers. In the remainder of this chapter, we consider further applications of KT3.

5.3 *o*-dichlorobenzene

In a recent investigation of theoretically calculated ^{13}C NMR spectra of organic molecules [194], Bagno and co-workers highlighted the poor performance of conventional DFT functionals such as BLYP and B3LYP for the chemical shifts of halogen-bonded carbon nuclei. Table 5.4 illustrates this with the B3LYP, BLYP, and Hartree-Fock results for *o*-dichlorobenzene, calculated by Maslen [195] using the 6-311+G(2d,p) basis set at B3LYP/6-31G* geometries. By symmetry, there are three non-equivalent carbon sites: *ortho* (bonded to a chlorine atom), *meta* (adjacent to *ortho*), and *para* (furthest from the chlorine atoms). The experimental chemical shifts for *o*-dichlorobenzene span a range of 3.5 ppm, in the order *ortho* > *meta* > *para* (note this is the reverse of the corresponding shielding constant order). The B3LYP chemical shifts give

Table 5.4: Calculated HF, BLYP, and B3LYP shielding constants and B3LYP chemical shifts for *o*-dichlorobenzene from Ref. [195]. All values are in ppm.

Carbon nucleus	HF shielding	BLYP shielding	B3LYP shielding	B3LYP shift[a]	Expt. shift[b]
ortho	47.1	32.4	34.6	147.8	132.3
meta	54.8	44.7	45.8	136.6	131.0
para	58.7	49.6	50.5	132.0	128.8
Range	11.6	17.2	15.9	15.8	3.5

[a] Calculated using a TMS reference value of 182.47 ppm (B3LYP/6-311+G(2d,p)).
[b] Ref. [194].

the correct order, but a much higher range of 15.8 ppm. These shifts were calculated using a B3LYP reference shielding, but we can directly calculate the range from the original shielding constants (to within a rounding error) and so a reference shielding is not required. Both BLYP and Hartree-Fock also get the correct ordering. The BLYP range is higher still than B3LYP at 17.2 ppm, whereas Hartree-Fock gives a better result of 11.6 ppm. It therefore appears that the addition of correlation with DFT worsens the results. We examined whether any improvement could be gained by using KT3. This is an interesting test for the KT functionals as we have not previously studied any halogen-bonded carbon shielding constants (the only halogen-containing molecule we have studied is HCl in the A1 and A2 sets).

Table 5.5 presents the results. We first considered KT3 shielding constants calculated using the same 6-311+G(2d,p) basis set and B3LYP/6-31G* geometries. We also recalculated B3LYP to check that they agreed with Maslen's results and calculated KT2 results to compare to KT3. Shielding constants were calculated under the GIAO formalism using the DALTON program with spherical-harmonic basis functions.

Our B3LYP results agreed very well, with the same calculated range of 15.9 ppm. The KT3 shielding constants were significantly more shielded than B3LYP, as also observed in all our previous assessments. All three carbon atoms were raised by approximately 20 ppm. KT2 results were essentially identical to KT3. However, as the increase was uniform over all the atoms, the calculated range remained very similar to B3LYP (15.4 ppm in the case of

Table 5.5: Calculated B3LYP, KT2 and KT3 shielding constants for *o*-dichlorobenzene at various geometries and basis sets. All values are in ppm.

Carbon nucleus	B3LYP shielding	KT2 shielding	KT3 shielding	Expt.
6-311+G(2d,p) at B3LYP/6-31G* geometries				
ortho	34.8	53.8	54.1	
meta	46.0	64.4	64.8	
para	50.7	69.4	69.5	
Range	15.9	15.6	15.4	3.5
Huzinaga IV at B3LYP/6-31G* geometries				
ortho	27.2	44.6	44.4	
meta	39.1	55.8	55.6	
para	44.0	61.0	60.6	
Range	16.8	16.4	16.2	3.5
6-311+G(2d,p) at KT3/6-31G* geometries				
ortho	36.3	55.3	55.6	
meta	46.7	65.0	65.3	
para	51.8	70.3	70.4	
Range	15.5	15.0	14.8	3.5
6-311+G(2d,p) at B3LYP/6-311+G(2d,p) geometries				
ortho	36.2	55.0	55.3	
meta	47.3	65.5	65.9	
para	51.8	70.3	70.4	
Range	15.6	15.3	15.1	3.5

KT3). Therefore the KT functionals appear to offer no improvement.

We next examined whether the results had any dependence on the basis set or geometry used. The 6-311+G(2d,p) basis set used by Maslen is relatively small for shielding constant calculations even under the GIAO formalism, and we would expect the calculated shielding constants to be more shielded than they would be at the basis set limit (as the smaller basis set pulls the electron density in towards the nucleus, giving greater shielding). To eliminate basis set issues we recalculated all the numbers using the extensive Huzinaga IV basis. For all three functionals the shielding constants are lowered, but the shielding constant range increases to 16.8 ppm for BLYP and 16.2 ppm for KT3. Again, there is little improvement gained by moving from B3LYP to KT3.

To test the geometry dependence we also calculated results at KT3/6-31G* geometries using the original basis set for the shielding constant calculations. We found that the shielding constants rise slightly over the B3LYP geometry results, but there is a negligible change in the shielding constant ranges. Finally, we reoptimised the geometries at the B3LYP level using the larger 6-311+G(2d,p) basis set and recalculated the shielding constants. Again, the change in shielding constants was very small, and the change in the shielding constant range was insignificant.

In conclusion, we have eliminated the question of geometry and basis set dependence and we believe that the overestimated shielding constant range is a true failure of all the DFT functionals we considered. We did observe the usual increased shieldings from KT2 and KT3, but as this rise was uniform it did not affect the shielding constant range performance. Further investigation of this important issue is ongoing.

5.4 Selenium chemistry

Our previous shielding constant assessments have only considered first- and second-row nuclei. In this section we consider the performance of KT3 for the shielding constants of the third-row selenium nucleus, to give some indication of how KT3 performs for systems containing heavier atoms. We also take the opportunity to investigate the performance of KT3 for calculating the

Table 5.6: The basis sets used in the selenium assessments. For each set the contracted basis functions used for H, C–F, and Se are given.

Basis set	H	C,N,O,F	Se
Se1	3s2pd	5s4p2d1f	9s8p4d1f
Se2	3sp	6s3pd	8s10p5d1f
Se3	4s2pd	7s6p4d	8s10p5d1f

geometries of selenium-containing molecules.

A number of previous studies have investigated theoretical ^{77}Se shielding constants and chemical shifts [109, 196–205]. Bühl and co-workers have performed calculations at the GIAO-SCF, GIAO-MP2 [196] and GIAO-CCSD [197] levels of theory. Magyarfalvi and Pulay [198] have carried out similar investigations with GIAO-SCF and GIAO-MP2. Both concluded that correlated methods were necessary to give quantitative agreement with experiment for chemical shifts. Within DFT, Malkin *et al.* [109] (using their Loc. 1 approximation) and Schreckenbach *et al.* [199] showed that it was possible to obtain results for chemical shifts that are superior to GIAO-SCF. Wilson [200] showed that particularly accurate results were given by the empirical scheme of Wilson, Amos and Handy [105]. Magyarfalvi and Pulay [201] showed that applying a constant level shift to the virtual orbitals also improved the DFT results. These improvements indicate that selenium NMR results are influenced by eigenvalue differences in the same way as lighter main group elements, which suggests that improvements should also be seen with the KT3 functional.

We carried out a geometry optimisation assessment for the A24 set of 14 selenium-containing molecules from Ref. [196] followed by a shielding constant assessment for the A25 set of 7 molecules from Ref. [200]. The A25 set is a subset of A24. The shielding constant calculations were performed using the LORG formalism in CADPAC, which demanded careful attention to the choice of basis set. The basis sets we used are presented in Table 5.6.

We used the Se1 basis set for the geometry optimisations. Se1 is the same as that used for our A7 diatomic bond length assessment [139], and so we were confident that this would be suitable for geometry optimisations. However, the A7 set contained no hydrogens and so the hydrogen basis was undefined. 2pd

polarisation functions were added to hydrogen to give a good balance. The resulting basis set was 6-311+G(2df,2pd). Bond length results are presented in Table 5.7 and bond angles in Table 5.8, where KT3 is compared with the HCTH and OLYP GGAs and the B3LYP and B97-2 hybrid functionals. Of the GGAs, KT3 gives the best bond lengths, with a mean absolute error of 0.010 Å. KT3 is only beaten by the B97-2 hybrid functional (0.007 Å). The same trends are seen with the mean absolute percentage errors. For bond angles, KT3 beats all the other functionals, with an error of 0.6°. Overall, B97-2 gives marginally better geometries than KT3, with both being substantially better than the other functionals. This confirms our previous assertion of the quality of KT3 geometry predictions.

We next considered shielding constants. The choice of basis set is very important as we are working under the LORG formalism. We compared two basis sets, denoted Se2 and Se3. The Se2 basis set is taken from the work of Magyarfalvi and Pulay [201] (where it was used for calculating shielding constants). It is based on the pVTZ basis of Schäfer *et al.* [206], with the Se basis modified by the decontraction of the p functions and addition of diffuse functions as described in Ref. [198]. Se3 is similar to the basis set used in Ref. [200]. For the non-Se atoms the basis is Huzinaga III augmented with a single d function for hydrogen with exponent 1.3, and two diffuse d functions for C, O, and F, with exponents determined from the geometric progression. The Se3 basis for the selenium atom is the same used in Se2.

To compare the performance of Se2 and Se3, isotropic shielding constants for the A25 set were calculated with the KT3 functional at KT3 optimised geometries using both the LORG (in CADPAC) and GIAO (in DALTON) formalisms. Results are presented in Table 5.9. For a given basis set, GIAO should give results closer to the basis set limit than LORG. The results show that the shielding constants calculated with Se2 undergo a much larger change from LORG to GIAO than those calculated with Se3. Also, the Se2 GIAO results are much closer to the Se3 results with LORG and GIAO. This suggests that Se3 gives results closer to the basis set limit and therefore we used Se3 for the rest of our assessments.

Table 5.10 presents isotropic shielding constants for the A25 set and anisotropic

Table 5.7: Selected bond lengths for selenium-containing systems. All values are in Å.

Mol.	Param.	Expt.[a]	KT3	HCTH	OLYP	B3LYP	B97-2
$Se(CH_3)_2$	Se – C	1.945	1.946	1.957	1.959	1.963	1.945
SeH_2	Se – H	1.460	1.459	1.470	1.472	1.469	1.463
SeCO	Se = C	1.710	1.707	1.708	1.713	1.716	1.705
	C = O	1.154	1.161	1.161	1.165	1.152	1.150
H_2CSe	Se = C	1.756	1.749	1.751	1.755	1.752	1.742
CSe_2	Se = C	1.692	1.696	1.697	1.701	1.697	1.689
SeF_6	Se – F	1.685	1.704	1.714	1.720	1.706	1.692
CH_3SeH	Se – C	1.959	1.954	1.965	1.967	1.972	1.953
	Se – H	1.473	1.461	1.473	1.475	1.471	1.465
$(CH_3)_2CSe$	Se – C	1.768	1.773	1.779	1.782	1.778	1.767
	C – C	1.502	1.492	1.498	1.501	1.497	1.493
C_4H_4Se	Se – C	1.855	1.855	1.861	1.864	1.870	1.853
	C – C	1.370	1.363	1.365	1.368	1.359	1.358
	C – C	1.433	1.421	1.425	1.428	1.429	1.424
$SeOF_2$	Se – O	1.576	1.588	1.587	1.593	1.584	1.574
	Se – F	1.730	1.755	1.770	1.775	1.757	1.740
$(SiH_3)_2Se$	Se – Si	2.274	2.277	2.299	2.300	2.299	2.286
SeF_4	Se – F	1.771	1.787	1.804	1.809	1.795	1.780
	Se – F	1.682	1.710	1.718	1.724	1.709	1.695
trans-C_2H_5SeH	Se – H	1.440	1.461	1.473	1.475	1.471	1.465
	Se – C	1.962	1.970	1.984	1.986	1.988	1.968
	C – C	1.525	1.515	1.520	1.524	1.522	1.517
gauche-C_2H_5SeH	Se – H	1.467	1.462	1.473	1.475	1.472	1.466
	Se – C	1.957	1.964	1.978	1.980	1.983	1.964
	C – C	1.524	1.514	1.520	1.523	1.520	1.515
d			0.003	0.011	0.015	0.010	0.000
$\|d\|$			0.010	0.014	0.015	0.013	0.007
$\|d\|$%			0.6	0.8	0.9	0.8	0.5

[a] Experimental values, except MP2 values for $(CH_3)_2CSe$. See Ref. [196] and references therein.

Table 5.8: Selected bond angles for selenium-containing systems. All values are in degrees.

Mol.	Param.	Expt.[a]	KT3	HCTH	OLYP	B3LYP	B97-2
$Se(CH_3)_2$	C – Se – C	96.3	97.0	98.2	98.1	97.4	97.6
SeH_2	H – Se – H	90.9	90.7	90.8	90.8	91.3	91.3
H_2CSe	H – C – Se	121.3	121.8	121.9	121.9	121.8	121.8
CH_3SeH	C – Se – H	95.5	95.0	95.4	95.3	95.5	95.5
$(CH_3)_2CSe$	Se – C – C	122.6	122.3	122.1	122.1	122.3	122.3
C_4H_4Se	C – Se – C	87.8	87.5	87.5	87.5	87.1	87.5
$SeOF_2$	O – Se – F	104.8	104.8	105.0	105.0	104.7	104.7
$(SiH_3)_2Se$	Si – Se – Si	96.6	96.3	98.7	98.6	98.2	97.4
SeF_4	F – Se – F	169.2	169.9	172.1	171.9	169.9	169.6
	F – Se – F	100.6	100.4	100.1	100.1	100.3	100.4
trans-C_2H_5SeH	H – Se – C	93.5	95.2	95.2	95.1	95.5	95.6
	C – C – Se	108.7	109.5	110.3	110.5	109.7	109.7
gauche-C_2H_5SeH	H – Se – C	93.1	94.8	95.3	95.3	95.3	95.3
	C – C – Se	113.5	114.3	115.1	115.2	114.4	114.5
d			0.4	1.0	0.9	0.6	0.6
$\|d\|$			0.6	1.2	1.2	0.8	0.8
$\|d\|$%			0.6	1.1	1.1	0.8	0.8

[a] Experimental values, except MP2 values for $(CH_3)_2CSe$. See Ref. [196] and references therein.

Table 5.9: Isotropic NMR shielding constants for the KT3 functional calculated at KT3 geometries. All values are in ppm.

Mol.	Se2 LORG	Se2 GIAO	Se3 LORG	Se3 GIAO
$Se(CH_3)_2$	1669	1705	1706	1718
SeH_2	2101	2127	2112	2127
SeCO	2297	2302	2298	2303
H_2CSe	−1136	−1138	−1154	−1145
CSe_2	1548	1553	1549	1551
SeF_6	1101	1065	1092	1075
CH_3SeH	1863	1895	1887	1900

shielding constants for the A26 set (a subset of A25). The shieldings are calculated using self-consistently optimised geometries. Results are compared with CCSD [197] and experimental reference values. The experimental values were taken from Refs. [207–210]. The paramagnetic part was determined from the spin-rotation constant tensor of the relevant nucleus and the diamagnetic part estimated using the shielding constant of the free Se atom. Relativistic effects can be much reduced by using a non-relativistic value for the free atom (a residual error remains in the paramagnetic part). Therefore we do not need to consider applying any relativistic corrections to our calculated results. Of all the functionals, KT3 gives the best results, with a mean absolute error compared to experiment of 33 ppm and 156 ppm compared to CCSD. Only CCSD results were available for anisotropic shieldings, for which KT3 was again significantly better than the other functionals with an error of 260 ppm. The same trends are observed in the mean absolute percentage errors.

The B97-2 hybrid is the second best performing functional. It is substantially better than B3LYP and the other GGAs, with errors of 51 ppm and 208 ppm respectively. This reflects the high quality B97-2 geometries. The performance of KT3 is also partly due to its good geometries. To assess the functionals for their shielding constant performance alone, we recalculated all the shielding constants at the highest quality geometries (B97-2). Results are presented in Table 5.11. As expected, the discrepancy between KT3 and B97-2 and the other functionals narrows, although interestingly B97-2 remains substantially better than the HCTH and OLYP GGAs. Our previous observations that GGAs are uniformly superior to hybrids is only true for lighter main group elements. The KT3 functional again gives the best performance. The errors compared to CCSD improve slightly to 144 ppm for isotropic shieldings and 234 ppm for anisotropic shieldings, but they worsen for isotropic shielding compared to experiment to 36 ppm. The small differences suggest that KT3 geometries are equally acceptable for the calculation of selenium shielding constants. We are encouraged by the performance of KT3 for both geometries and shielding constants. Although the functional was developed with an emphasis on light, main-group atoms, it can clearly also be successful for heavier systems.

Table 5.10: Isotropic and anisotropic NMR shielding constants calculated at the respective optimised geometries of the functionals. All values are in ppm.

Mol.	Expt.	CCSD[a]	KT3	HCTH	OLYP	B3LYP	B97-2
			Isotropic Shieldings				
$Se(CH_3)_2$	1756 ± 64[b]	1878	1706	1623	1608	1632	1730
SeH_2	2101 ± 64[b]	2213	2112	2053	2057	2050	2094
SeCO	2348 ± 60[b]	2345	2298	2265	2261	2255	2297
H_2CSe	-1202 ± 200[c]	−741	−1154	−1462	−1477	−1612	−1389
CSe_2	1544 ± 80[d]	1596	1549	1498	1491	1464	1521
SeF_6	1138 ± 64[b]		1092	1009	1000	1023	1096
CH_3SeH	1911 ± 64[b]		1887	1816	1808	1822	1893
d (expt.)			−15	−113	−121	−137	−51
$\|d\|$ (expt.)			33	113	121	137	51
$\|d\|$% (expt.)			2	8	8	10	4
d (CCSD)			−156	−263	−270	−301	−208
$\|d\|$ (CCSD)			156	263	270	301	208
$\|d\|$% (CCSD)			15	26	26	30	21
			Anisotropic Shieldings				
$Se(CH_3)_2$		632	624	641	626	674	666
SeH_2		602	635	646	642	656	654
SeCO		993	1072	1116	1120	1127	1067
H_2CSe		−5147	−6248	−6859	−6862	−6984	−6596
CSe_2		2118	2197	2267	2276	2315	2231
d (CCSD)			−183	−277	−279	−282	−235
$\|d\|$ (CCSD)			260	407	409	453	345
$\|d\|$% (CCSD)			8	12	12	15	11

[a] Ref. [197]
[b] Ref. [207]
[c] Calculated using the spin-rotation constant, as in Ref. [209], but with a non-relativistic free atom shielding of 2998 ppm.
[d] Ref. [210]

Table 5.11: Isotropic and anisotropic NMR shielding constants calculated at B97-2 geometries. All values are in ppm.

Mol.	Expt.	CCSD[a]	KT3	HCTH	OLYP	B3LYP	B97-2
			Isotropic Shieldings				
$Se(CH_3)_2$	1756 ± 64[b]	1878	1699	1653	1644	1668	1730
SeH_2	2101 ± 64[b]	2213	2101	2069	2077	2065	2094
SeCO	2348 ± 60[b]	2345	2321	2288	2300	2280	2297
H_2CSe	-1202 ± 200[c]	−741	−1119	−1423	−1420	−1563	−1389
CSe_2	1544 ± 80[d]	1596	1572	1524	1530	1493	1521
SeF_6	1138 ± 64[b]		1114	1050	1052	1050	1096
CH_3SeH	1911 ± 64[b]		1878	1839	1835	1845	1893
d (expt.)			−4	−85	−82	−108	−51
$\|d\|$ (expt.)			36	85	82	108	51
$\|d\|$% (expt.)			2	6	6	8	4
d (CCSD)			−144	−236	−232	−270	−208
$\|d\|$ (CCSD)			144	236	232	270	208
$\|d\|$% (CCSD)			14	23	23	28	21
			Anisotropic Shieldings				
$Se(CH_3)_2$		632	617	650	632	670	666
SeH_2		602	632	646	642	657	654
SeCO		993	1039	1080	1062	1090	1067
H_2CSe		−5147	−6181	−6813	−6791	−6923	−6596
CSe_2		2118	2164	2227	2217	2271	2231
d (CCSD)			−186	−281	−287	−286	−235
$\|d\|$ (CCSD)			234	385	371	424	345
$\|d\|$% (CCSD)			7	11	10	13	11

[a] Ref. [197]
[b] Ref. [207]
[c] Calculated using the spin-rotation constant, as in Ref. [209], but with a non-relativistic free atom shielding of 2998 ppm.
[d] Ref. [210]

5.5 Solid state calculations

Semi-empirical functionals are rarely used in solid state calculations, because they often do not satisfy the uniform electron gas limit (which is argued to be more important for solids than for atoms and molecules [211]) and they are usually only fitted to chemically-relevant reference data. A previous study by Rushton *et al.* [212] considered the performance of the semi-empirical HCTH functional for a range of solid state properties. It was observed that HCTH gave a reasonable description for systems containing atoms present in its fitting data, but systems containing heavier atoms were much less well described.

To investigate the performance of KT3 for solid state properties we implemented it in the CASTEP program [213]. In CASTEP, the Kohn-Sham orbitals are represented as a linear combination of plane-waves. Unlike Gaussian functions, plane-waves are not localised and so they are well suited to treating periodic systems. The plane-wave formulation of the Kohn-Sham equations is computationally efficient and a very large basis set (approaching the basis set limit) can be used. However, plane-waves cannot efficiently describe core electrons (where the wavefunction oscillates) and so a pseudopotential approximation is used for the core region. By construction, the wavefunction of the pseudopotential does not oscillate and so can be described by a smaller number of plane-waves.

The closed-shell implementation of KT3 in CASTEP is similar to the implementation in CADPAC and DALTON, with a subroutine that calculates the energy contribution of the functional and its derivatives with respect to the density and density gradients. In the case of CASTEP, a further subroutine is required to calculate self-consistent pseudopotentials. Our implementation was checked using the Hellmann-Feynman theorem and by a comparison of isolated molecular geometry optimisation results with CADPAC. Following Ref. [212], all the assessments involved the A28 set of 10 Group IV and Group III-V semiconductors with diamond/zinc-blende structures. Errors were calculated relative to experimental reference values from Ref. [212].

An optimised lattice constant is the unit cell length at equilibrium and is the solid state equivalent of a geometry optimisation. Table 5.12 presents

Table 5.12: Optimised lattice constants. All values are in Å.

	Expt.[a]	LDA[a]	PW91[a]	HCTH[a]	OLYP	KT3
C	3.57	3.53	3.57	3.56	3.57	3.55
Si	5.43	5.38	5.46	5.50	5.46	5.39
Ge	5.66	5.54	5.71	5.80	5.77	5.69
SiC	4.35	4.30	4.36	4.37	4.35	4.32
AlN	4.37	4.31	4.39	4.43	4.36	4.32
AlP	5.45	5.41	5.49	5.54	5.51	5.43
AlAs	5.66	5.60	5.69	5.78	5.74	5.66
GaN	4.50	4.46	4.55	4.57	4.56	4.52
GaP	5.45	5.38	5.49	5.54	5.55	5.46
GaAs	5.65	5.57	5.70	5.81	5.80	5.70
d		−0.06	0.03	0.08	0.06	−0.00
$\|d\|$		0.06	0.03	0.08	0.06	0.03

[a] Ref. [212]

results for optimised lattice constants for KT3 and OLYP, compared to results from Ref. [212] for LDA, HCTH, and the non-empirical PW91 GGA, which is widely used for solid state calculations. In CASTEP, the LDA correlation energy is given by the Perdew-Zunger correlation functional [30]. LDA uniformly underestimates the lattice constants, whereas PW91, HCTH, and OLYP all overestimate them. Of these functionals, PW91 gives the lowest mean absolute error of 0.03 Å. KT3 gives the same mean absolute error as PW91. This is extremely encouraging as the systems in the A28 set are very different to those that KT3 was fitted to.

The second property considered was the bulk modulus, defined as

$$B = -\frac{1}{V}\frac{\mathrm{d}^2 E}{\mathrm{d}V^2} \tag{5.10}$$

where E is the electronic energy and V is the cell volume. The bulk modulus for each system was calculated numerically from several energy calculations at various cell volumes. Results are presented in Table 5.13. Remarkably, LDA gives the lowest mean absolute error of 5 GPa for this set. PW91, HCTH, and OLYP are all significantly less accurate, but KT3 gives an error much closer to LDA. It is encouraging that KT3 does not deteriorate for this set as much as the other GGAs, and it is particularly interesting that its performance is

Table 5.13: Bulk moduli. All values are in GPa.

	Expt.[a]	LDA[a]	PW91[a]	HCTH[a]	OLYP	KT3
C	442	457	425	428	429	443
Si	98.8	97	88	82	86	96
Ge	76.8	78	62	54	56	67
SiC		227	215	212	212	225
AlN	202	206	192	186	190	204
AlP		89	82	78	79	88
AlAs		75	71	60	64	72
GaN	190	199	173	161	153	171
GaP	88.7	89	77	69	68	80
GaAs	74.8	75	65	51	52	64
d		4	−13	−20	−20	−7
$\|d\|$		5	13	20	20	8

[a] Ref. [212]

superior to the non-empirical PW91.

Finally, we assessed KT3 for electronic band gaps at experimental lattice constants. The band gap is the difference between the highest valence band energy and the lowest conduction band energy. Conventional GGA functionals are known to perform relatively poorly for band gaps [214–216], with a significant part of the error ascribed to the integer discontinuity in the potential. The KT3 functional behaves like a normal GGA in this respect, but the increased HOMO-LUMO gaps it gives suggested that it might give a similar improvement for band gaps. Results are presented in Table 5.14. For this property LDA is the worst functional. Surprisingly, PW91 gives the highest error of all the GGAs of 0.97 eV. HCTH gives the lowest error of 0.76 eV. KT3 offers no real improvement over PW91, and gives a poor result for carbon (diamond).

In summary, KT3 gives results as good as or better than the other GGAs considered for lattice constant optimisations and bulk moduli and gives results comparable to PW91 for electronic band gaps. We therefore conclude that KT3 should not be ruled out for solid state calculations even though it does not satisfy the uniform electron gas condition and it was fitted only to chemically-relevant data. The results are particularly encouraging given the failure of the semi-empirical HCTH functional.

Table 5.14: Minimum electronic band gaps calculated at experimental lattice constants. All values are in eV.

	Expt.[a]	LDA[a]	PW91[a]	HCTH[a]	OLYP	KT3
C	5.48	4.12	4.20	4.22	4.10	3.89
Si	1.17	0.49	0.60	0.80	0.77	0.69
Ge	0.71	0.03	0.18	0.32	0.34	0.34
SiC	2.39	1.33	1.42	1.63	1.40	1.29
AlN		3.26	3.39	3.70	3.48	3.38
AlP	2.50	1.42	1.56	1.89	1.85	1.74
AlAs	2.32	1.32	1.39	1.66	1.73	1.60
GaN	3.45	1.74	1.73	1.99	1.67	1.33
GaP	2.35	1.40	1.55	1.80	1.86	1.74
GaAs	1.52	0.32	0.49	0.72	0.71	0.67
d		−1.08	−0.97	−0.76	−0.83	−0.96
$\|d\|$		1.08	0.97	0.76	0.83	0.96

[a] Ref. [212]

Chapter 6

The KT4 and B97-3 functionals

The KT3 functional gives excellent results for a wide variety of chemical properties while retaining the high quality shielding performance of KT1 and KT2. However, its performance for classical reaction barriers is not competitive with the best GGAs. In this chapter we attempt to develop a GGA that improves reaction barrier performance without a decline in performance for other properties. We then consider the development of hybrid functionals with the same methods.

6.1 The KT4 functional

6.1.1 The BH42/04 database

An obvious way to improve the performance of a semi-empirical functional for reaction barriers is to include the reaction barriers in the fitting data. Several hybrid functionals and hybrid meta-GGA functionals have been developed in this manner [68, 73–75, 217]. In every case it has been found that the fitting procedure results in a relatively high fraction of exact exchange. For example, the MPW1K hybrid functional of Truhlar and co-workers [68] features 43% exact exchange. This phenomenon was first observed for the original half-and-half hybrid functional [66], which gives relatively good reaction barriers despite being poor for other properties [218]. No pure GGA functionals have been designed in this way, and it is unclear how they will perform as they

Table 6.1: Basis set dependence of error assessments for BH42/04 classical chemical reaction barrier heights. All values are in kcal mol^{-1}.

	KT1	KT2	KT3	PBE	HCTH	OLYP	B3LYP	PBE0	B97-2
TZ2P									
d	−14.7	−12.7	−8.4	−9.7	−5.0	−6.4	−4.6	−4.7	−3.3
$\|d\|$	14.7	12.7	8.4	9.7	5.2	6.5	4.7	4.7	3.4
6-311+G(3df,2p)									
d	−14.6	−12.5	−8.1	−9.4	−4.7	−5.9	−4.4	−4.5	−3.1
$\|d\|$	14.6	12.5	8.1	9.4	4.8	6.0	4.5	4.5	3.3

contain no exact exchange.

To fit our functionals to reaction barriers requires a suitable fitting set. The A23 reaction barrier assessment set is not suited to fitting because its energies are calculated at optimised geometries. This means that the fit quality will not solely depend on the energy calculations as we would like. It also causes problems for the fitting procedure because transition states may not be located and the geometry dependence may cause convergence issues. We therefore require a barrier height assessment set that is calculated using a set of reference geometries.

The BH42/04 barrier height set of Zhao *et al.* [73] (also known as BH42/03) fulfills this criterion. It is the A29 set in this thesis. This set is the same as that in the earlier Database/3 of the same authors [219], but with one reaction removed because of an unreliable reference value. The BH42 set consists of 42 barrier heights from 21 predominantly hydrogen-transfer reactions (forward and reverse). The geometries were calculated at the QCISD level with the extensive MG3 basis set. They were taken from Ref. [220] and were converted into CADPAC format using Perl scripts.

We considered the same set of functionals as in Section 5.1 using both the TZ2P basis set (as used in the A23 barrier assessment) and the 6-311+G(3df,2p) basis set (used in the G2 thermochemistry calculations). Errors are presented in Table 6.1. The trends are similar to those of the A23 assessment. For the 6-311+G(3df,2p) basis set, KT1 gives the highest error of 14.6 kcal mol^{-1}, which is reduced significantly by KT2 and again by KT3, with an error of 8.1 kcal mol^{-1}. KT3 performs better than PBE (unlike for the A23 set) but

Table 6.2: Coefficients of functionals of the KT3 form (and B86X) fitted to barrier heights and other properties.

	LDAX	B86X	OPTX	KTX	LYP
FBH1	1.217782E + 0		−1.384829E + 0	−2.2780E − 3	3.51287E − 1
FBH2	1.111753E + 0		−1.798830E + 0	4.7300E − 4	9.69940E − 1
FBH3	1.152317E + 0		−1.151970E + 0	−4.0000E − 3	8.66580E − 1
FBH4	1.110964E + 0	3.20696E − 1	−1.924173E + 0	−2.0000E − 3	1.00000E + 0
FBH5	1.108981E + 0	5.61369E − 1	−2.166665E + 0	−2.0192E − 3	9.52262E − 1

as before is not competitive with OLYP or HCTH. HCTH gives the lowest GGA error of 4.8 kcal mol^{-1}. For the BH42 set all three hybrid functionals are superior to HCTH, with B97-2 giving the lowest error of 3.3 kcal mol^{-1}. Similar results are obtained with TZ2P, but the errors are slightly higher for all the functionals considered.

Using the extensive MG3S basis set, Zhao *et al.* obtained errors for B3LYP, PBE0 and B97-2 of 4.3, 4.3, and 3.1 kcal mol^{-1} respectively. Our 6-311+G(3df,2p) numbers give the best agreement with these values and so this basis set was selected for the fitting procedure.

6.1.2 Fitting to barriers

Fitting to the barrier heights of the BH42 set is similar to fitting to atomisation energies as both calculations involve energy differences. We followed the procedure of Section 4.7 with Eq. 4.32 redefined as

$$g_i^{\mathrm{BH}} = f_i^{\mathrm{TS}} - \sum_R f_i^R \tag{6.1}$$

where TS is the transition state and R are the reactants.

We commenced by fitting the KT3 form (LDAX, KTX, OPTX, and LYP) to the BH42 set. Our first functional (FBH1) was fitted only to barrier heights and all four KT3 parameters were allowed to vary. The resulting coefficients are given in Table 6.2. The KTX coefficient came out quite small (just over half

of the KT3 value), as did the LYP coefficient. The LDA exchange component increased dramatically, from the KT3 value of 1.092 to 1.218. This is analogous to the hybrid case where the fraction of exact exchange rises considerably. Results for the BH42 set are presented in Table 6.3. The mean absolute error is remarkably good, at 1.6 kcal mol^{-1}. This is significantly better than the KT3 error of 8.1 kcal mol^{-1} and is less than half the error of B97-2, the best performing functional we have considered. We then assessed FBH1 for the G2-1 atomisation energy set to give an indication of how well it performs for thermochemistry. The error was 21.9 kcal mol^{-1}, which is considerably less accurate than KT3 (4.3 kcal mol^{-1}). This highlights the danger of fitting a semi-empirical functional to a single chemical property (we first observed this for KT1, which is fitted only to shielding constants).

We therefore added the G2-1 atomisation energies to the fitting data. In order to minimise the computational cost of our initial investigations, we did not consider the G2-2 set at this time. The fitting program required no changes except the addition of an appropriate weighting factor to the g_i values to compensate for the different size of the barrier height and atomisation energy sets. The resulting functional, FBH2, had a smaller value for LDA exchange (1.112) and a much larger value for LYP. Both components were much closer to their KT3 values. The amount of OPTX exchange also increased. The KT exchange coefficient, however, became smaller in magnitude and positive.

FBH2 gives errors for BH42 of 3.1 kcal mol^{-1} (still surpassing B97-2) and a dramatically lower error of 3.1 kcal mol^{-1} for the G2-1 set. This is superior to KT3 and comparable to the best GGAs and hybrid functionals (see Table 5.1). It is not a satisfactory functional, however, because the small positive value for KT exchange gives poor shieldings. Errors for the A1 set are 31.3 ppm, which is comparable to OLYP (this is expected as the functional coefficients are similar to OLYP).

We therefore enforced good quality shieldings by fixing the KT coefficient at the KT3 value of -0.004. The FBH3 functional gives a shielding error of 17.5 ppm, which is not as good as KT3 but is greatly improved over FBH2 (and other GGAs). The reduction in flexibility of the functional leads to lower quality kinetics and thermochemistry, with an error of 5.7 kcal mol^{-1} for BH42

Table 6.3: Error assessments for functionals of the KT3 form (and B86X) fitted to barrier heights and other properties. Units are given in parentheses.

	FBH1	FBH2	FBH3	FBH4	FBH5
A29. BH42/04 classical chemical reaction barriers (kcal mol^{-1})					
d	0.0	−2.2	−5.7	−4.4	−4.9
$\|d\|$	1.6	3.1	5.7	4.5	5.0
A13/14. G2 atomisation energies (kcal mol^{-1})					
G2-1:					
d	−21.6	−1.0	−1.0	−0.3	−0.9
$\|d\|$	21.9	3.1	5.3	4.2	4.3
G2-2:					
d				−1.6	−0.8
$\|d\|$				5.2	5.1
Full G2:					
d				−1.1	−0.8
$\|d\|$				4.8	4.8
A1. Isotropic NMR shielding constants (ppm)					
d		−31.3	−14.2	−15.1	−12.1
$\|d\|$		31.3	17.5	17.4	15.9
Excluding O_3:					
d		−24.2	−11.1	11.5	−8.8
$\|d\|$		24.2	14.7	13.9	12.9
A6. G2 subset bond lengths (Å)					
d			−0.016	0.003	0.006
$\|d\|$			0.016	0.009	0.010
A7. Diatomic bond lengths (Å)					
d					0.029
$\|d\|$					0.034

and 5.3 kcal mol^{-1} for the G2-1 set. The barrier height performance is still better than KT3 but the G2-1 result is worse. Also, in order to improve the shielding quality to KT3 levels, the KT coefficient would have to become larger in magnitude, which would result in a further deterioration for BH42 and G2-1.

To summarise, it is possible to improve KT3's performance for barrier heights but only at the cost of atomisation energy quality. It is clear that we have reached the limits of accuracy for this functional form and further improvements require extra flexibility. We attempted to add several of the new forms discussed in Chapter 4, such as the KT expansion, VWN correlation, and the B86 exchange term. B86 exchange was the most successful.

By adding B86 exchange, we again ran into the problem of the B86X coefficient going negative and the OPTX coefficient going positive (see Section 4.3.2), leading to poor shieldings. To keep this problem under control, we considered the ratio of B86X:OPTX that gave the highest quality shieldings for various values of KTX. Using the non-linear fit code Solver, all the coefficients except KTX were then optimised while enforcing the ratio constraint on B86X:OPTX and forcing OPTX to be negative. We also decided to fit to the full G2 atomisation energy set (A13/14). The most satisfactory results were obtained using a B86X:OPTX of ratio 1:−6 with a KTX value of −0.002 and a fixed LYP value of 1. This functional, FBH4, gave promising barrier height results of 4.5 kcal mol^{-1} (better than all the other GGAs we consider) and full G2 atomisation energy errors of 4.8 kcal mol^{-1} (comparable with KT3). The shielding constant quality was maintained at the FBH3 level with an error of 17.4 ppm. We also calculated errors for the A6 set of bond lengths, for which FBH4 gave an error of 0.009 Å (compared to 0.008 Å for KT3).

Although the extra flexibility in the FBH4 functional led to better results in general, our approach to fitting to it was not very rigorous and the constraints we imposed would be likely to break down again if we attempted to add any more flexibility. The source of the problem is the need to force coefficients to values that are energetically unfavourable but are necessary to give good shielding constants. We therefore sought to find a method for explicitly fitting to shielding constants, thus removing the need for constraints.

6.1.3 Fitting to shieldings

Our method for fitting to shielding constants is conceptually simple and required no changes to our least squares algorithm. Our previous fits have all been to energetic quantities, for which the contributions of the individual functional components to the exchange-correlation energy can be formally separated. It is not possible to define a formal shielding constant contribution in the same way, so we have to find the equivalent quantity using a numerical method.

We assume that the dependence of the shielding constant σ on the component coefficients a_i can be written as

$$\sigma(a_i + \delta a_i) = \sigma(a_i) + \frac{\partial \sigma}{\partial a_i}\delta a_i \tag{6.2}$$

By ignoring higher derivatives, we assume linear behaviour and can use our least squares optimisation procedure. The shielding constant contribution from each component, f_i, is

$$f_i \equiv \frac{\partial \sigma}{\partial a_i} \tag{6.3}$$

In the case of shielding constants, g_i from Eq. 4.31 is equivalent to f_i. The fitting procedure then gives the change in components δa_i, and is then iterated to convergence. Therefore, in order to fit to shielding constants we simply have to calculate $\frac{\partial \sigma}{\partial a_i}$. This is found by one-point finite difference. A one-point method is used because a two-point method would have incurred too great a computational cost, and any inaccuracies introduced are not important in the context of the macro-iterative fitting procedure. The finite difference method uses a 5% change in the value of the parameter (this is preferable to a smaller value as it implicitly includes some of the non-linear behaviour ignored in Eq. 6.2, which helps to keep the earliest iterations numerically stable). Therefore

$$\frac{\partial \sigma}{\partial a_i} \approx \frac{\sigma(1.05a_i) - \sigma(a_i)}{0.05a_i} \tag{6.4}$$

We also had to multiply the shielding constant contributions by a very small weighting factor because of the different units used compared to the energetic

data.

The main disadvantage of this procedure is the significant increase in computational cost incurred by the finite difference method. Even with a one-point method, the entire A1 shielding constant set has to be calculated once for each component in the functional. We also found that the functionals became more difficult to converge, particularly when more components were added to the form. The functionals we present in this chapter are converged in the sense that the property assessments are converged to the accuracy given. It was not feasible to attempt to converge the individual coefficients, but we could also not reduce the number of significant figures in the coefficients as this would lead to a change in the property results and cause even more convergence problems. The problem of converging flexible functional forms to diverse fitting data has been observed previously for functionals such as HCTH [221].

The next functional, FBH5, took the same form as FBH4, but all the constraints were removed and the shielding constants were included in the fitting procedure. The coefficients of FBH5 are similar to FBH4 (which demonstrates that the constraints we placed on FBH4 were well chosen), and the assessment results are also similar. The accuracy of barrier heights is reduced slightly to 5.0 kcal mol^{-1}, while the full G2 set errors remain at 4.8 kcal mol^{-1}. The shielding constants benefit from the explicit fitting procedure, with the error over the A1 set reduced to 15.9 ppm (almost competitive with KT3). The G2 subset bond lengths are slightly reduced in accuracy. We also calculated errors for the A7 diatomic bond length set, which gave a disappointing result of 0.034 Å.

While the FBH5 results are overall quite impressive, the real advantage of explicitly fitting to shielding constants is the scope for increasing the flexibility of the functional form beyond that which we have previously considered. In the next section we demonstrate this by fitting to the 15-parameter HCTH functional form.

Table 6.4: Expansion parameters defining the HCTH functional [47].

$c_{X\sigma,0}$	1.09320E + 0
$c_{C\sigma\sigma,0}$	2.22601E − 1
$c_{C\alpha\beta,0}$	7.29974E − 1
$c_{X\sigma,1}$	−7.44056E − 1
$c_{C\sigma\sigma,1}$	−3.38622E − 2
$c_{C\alpha\beta,1}$	3.35287E + 0
$c_{X\sigma,2}$	5.59920E + 0
$c_{C\sigma\sigma,2}$	−1.25170E − 2
$c_{C\alpha\beta,2}$	−1.15430E + 1
$c_{X\sigma,3}$	−6.78549E + 0
$c_{C\sigma\sigma,3}$	−8.02496E − 1
$c_{C\alpha\beta,3}$	8.08564E + 0
$c_{X\sigma,4}$	4.49357E + 0
$c_{C\sigma\sigma,4}$	1.55396E + 0
$c_{C\alpha\beta,4}$	−4.47857E + 0

6.1.4 Fitting to the HCTH form

As discussed in Section 1.3.4, the HCTH functional [47] is based on the B97 functional expansion [43] (which also forms the basis for B97-2). B97 was originally designed as a hybrid functional, but it has proved to be equally applicable to the GGA form. For each expansion power i up to a limit of m (beginning at $i = 0$), there is one exchange coefficient ($c_{X\sigma,i}$), one same-spin correlation coefficient ($c_{C\sigma\sigma,i}$), and one opposite-spin correlation coefficient ($c_{C\alpha\beta,i}$). The original B97 functional was truncated at $m = 2$ (giving a total of 9 coefficients plus one exact exchange coefficient) because Becke observed that larger values of m led to an overfitted functional with unphysical coefficients. The B97-1 and B97-2 revisions retained this number of parameters. However, the fitting procedure for HCTH involved a large amount of extra fitting data (due to the inclusion of exchange-correlation potential data), and so a larger value of $m = 4$ was appropriate. The HCTH series of functionals therefore have 15 coefficients. For reference, the HCTH coefficients are given in Table 6.4. Our own original fitting data set (the BH42 barriers, full G2 atomisation energies, and A1 isotropic shielding constants) contained a total of 222 data points. This is substantially larger than the set used by Becke for the original B97 functional (116 data points). We were therefore able to fit to the HCTH form

($m = 4$) without overfitting.

The large number of components in HCTH increased the computational cost of the numerical fitting procedure further. To counteract this we automated the procedure by modifying CADPAC to change any given parameter by 5% if instructed to do so in the dataset. The calculations for each iteration could then be run as a single batch overnight.

We began by fitting to just the BH42 barriers and G2 atomisation energies. The coefficients of the resulting FBH6 functional are given in Table 6.5. Results are presented in Table 6.6. The LDA exchange coefficient ($c_{X\sigma,0}$) again rose significantly. As expected, FBH6 gives excellent results for the BH42 and G2 sets, but gives very poor shieldings, with an error over the A1 set of 36.1 ppm. The next functional, FBH7, reintroduced shielding constants into the fitting set. The coefficients of the functional changed substantially, with LDA exchange falling almost to the uniform electron gas value of unity. The reaction barrier and G2 atomisation energy errors worsened somewhat (to 2.6 kcal mol^{-1} and 3.7 kcal mol^{-1} respectively), but the shielding constants improved dramatically to 16.5 ppm. This is not quite of the same quality as KT3 but is competitive with FBH5. It is an interesting result because it is the first time good quality shielding constants have been achieved using the HCTH form, and the first time good quality shielding constants have been achieved with a GGA without the KT exchange term. FBH7 demonstrates that the HCTH form is sufficiently flexible to give good shielding constants. It is also surprising that high quality reaction barriers are achieved with such a low LDA exchange coefficient.

Unfortunately, FBH7 does not perform as well for other properties. Errors over the A6 bond lengths are acceptable but the A7 bond length error is poor at 0.030 Å (this is typical of a functional of the HCTH form). We also assessed FBH7 for the G2-1 ionisation potentials, electron affinities, and proton affinities. The results are extremely poor, with errors of 2.72 eV, 2.43 eV, and 13.0 kcal mol^{-1} respectively.

We took the pragmatic view of adding these properties to the fitting data. This did not cause any problems as they are simple energy differences that can be fitted in the same way as the reaction barriers and atomisation energies. In

Table 6.5: Expansion parameters defining the functionals of the HCTH form (and KTX) fitted to barrier heights and other properties.

	FBH6	FBH7	FBH8	FBH9
$c_{X\sigma,0}$	1.249754E + 0	1.016765E + 0	1.148202E + 0	1.137503E + 0
$c_{C\sigma\sigma,0}$	−1.691122E + 0	5.489207E + 0	−7.973017E − 1	−4.774522E − 1
$c_{C\alpha\beta,0}$	1.199467E + 0	9.659508E − 1	1.055780E + 0	7.399990E − 1
$c_{X\sigma,1}$	1.503437E + 0	−2.270551E + 0	−1.810442E + 0	−4.726323E − 1
$c_{C\sigma\sigma,1}$	−4.031978E + 0	2.263294E − 1	−5.923239E − 2	−9.278328E − 1
$c_{C\alpha\beta,1}$	−3.946719E + 0	2.201647E + 0	2.050114E + 0	3.421925E + 0
$c_{X\sigma,2}$	2.661678E + 0	1.446258E + 1	1.078928E + 1	8.246710E + 0
$c_{C\sigma\sigma,2}$	7.931091E + 0	2.173811E + 0	1.658771E + 0	2.717525E − 1
$c_{C\alpha\beta,2}$	−3.661360E + 0	−1.702580E + 1	−1.170078E + 1	−1.171057E + 1
$c_{X\sigma,3}$	8.738272E − 1	−1.615515E + 1	−9.387465E + 0	−7.171700E + 0
$c_{C\sigma\sigma,3}$	2.820932E + 0	2.221116E − 1	−1.563420E − 1	8.358988E + 0
$c_{C\alpha\beta,3}$	1.446167E + 1	1.115054E + 1	8.664478E + 0	2.987443E + 0
$c_{X\sigma,4}$	−7.591669E + 0	4.880042E + 0	−1.994121E + 1	−2.135559E + 0
$c_{C\sigma\sigma,4}$	−1.020223E + 1	−6.504032E − 1	1.351702E − 1	−8.873539E + 0
$c_{C\alpha\beta,4}$	−1.528694E + 0	4.328427E + 0	−3.189174E + 0	−4.578744E − 1
c_{KTX}				

	FBH10	FBH11	FBH12	FBH13 (KT4)
$c_{X\sigma,0}$	1.228727E + 0	1.171592E + 0	1.104216E + 0	1.209341E + 0
$c_{C\sigma\sigma,0}$	−3.003771E + 0	−7.186446E − 1	1.433555E + 0	−2.676674E + 0
$c_{C\alpha\beta,0}$	1.132752E + 0	8.635140E − 1	1.090405E + 0	1.114412E + 0
$c_{X\sigma,1}$	−2.902786E + 0	−2.286280E + 0	−8.725420E − 1	−2.407309E + 0
$c_{C\sigma\sigma,1}$	6.111999E + 0	−4.356303E − 2	−6.412536E + 0	7.038354E + 0
$c_{C\alpha\beta,1}$	3.413973E + 0	4.287278E + 0	2.192550E + 0	4.040817E + 0
$c_{X\sigma,2}$	1.239718E + 1	9.865171E + 0	3.415459E + 0	9.523125E + 0
$c_{C\sigma\sigma,2}$	−4.187639E + 0	−1.769516E + 0	6.456058E + 0	−9.093437E + 0
$c_{C\alpha\beta,2}$	−2.063354E + 1	−1.299663E + 1	−8.642138E + 0	−2.186552E + 1
$c_{X\sigma,3}$	−2.126939E + 1	−8.571224E + 0		−1.462289E + 1
$c_{C\sigma\sigma,3}$	−1.376225E + 1	2.171537E − 1		−7.153146E + 0
$c_{C\alpha\beta,3}$	1.972425E + 1	5.375507E + 0		1.339655E + 1
$c_{X\sigma,4}$	1.490510E + 1	1.438342E + 0		1.022631E + 1
$c_{C\sigma\sigma,4}$	1.865558E + 1	4.607201E + 0		1.551032E + 1
$c_{C\alpha\beta,4}$	−3.848758E + 0	−5.654672E + 0		5.573080E + 0
c_{KTX}	−4.970879E − 3	−8.041046E − 4	−2.958216E − 3	−4.882198E − 3

Table 6.6: Error assessments for functionals of the HCTH form (and KTX) fitted to barrier heights and other properties. Units are given in parentheses.

	FBH6	FBH7	FBH8	FBH9	FBH10	FBH11	FBH12	FBH13 (KT4)
A29. BH42/04 classical chemical reaction barriers (kcal mol^{-1})								
d	−0.3	−1.8	−4.4	−5.7	−4.5	−5.1	−5.6	−4.6
$\|d\|$	1.9	2.6	4.6	5.8	4.6	5.3	5.7	4.8
A13/14. G2 atomisation energies (kcal mol^{-1})								
G2-1:								
d	0.4	0.5	2.3	0.3	0.8	0.4	1.8	0.6
$\|d\|$	2.6	3.0	3.2	2.8	2.5	3.1	3.7	2.5
G2-2:								
d	0.2	−0.1	0.8	−0.1	−0.2	0.6	1.6	−0.3
$\|d\|$	2.7	4.1	4.9	3.7	3.5	5.0	4.9	3.4
Full G2:								
d	0.3	0.1	1.3	0.1	0.2	0.5	1.7	0.0
$\|d\|$	2.7	3.7	4.3	3.4	3.1	4.3	4.5	3.1
A1. Isotropic NMR shielding constants (ppm)								
d	−34.3	−3.7	−10.6	−17.1	−5.8	−14.6	−12.4	−8.7
$\|d\|$	36.1	16.5	16.0	18.2	15.3	18.2	16.7	15.1
Excluding O_3:								
d	−26.8	−2.3	−7.1	−12.9	−4.1	−10.6	−9.5	−6.5
$\|d\|$	28.8	16.0	13.0	14.1	14.2	14.3	14.1	13.3
A6. G2 subset bond lengths (Å)								
d	−0.028	0.005	0.016	0.007	−0.002	0.012	0.011	−0.001
$\|d\|$	0.031	0.010	0.017	0.010	0.008	0.012	0.012	0.008
A7. Diatomic bond lengths (Å)								
d	0.008	0.026	0.051	0.034	0.012	0.039	0.033	0.012
$\|d\|$	0.034	0.030	0.052	0.035	0.015	0.040	0.034	0.015
A15. G2-1 ionisation potentials (eV)								
d	0.19	2.72	0.03	0.07	−0.02	−0.03	−0.01	0.00
$\|d\|$	0.26	2.72	0.13	0.16	0.10	0.16	0.11	0.10
A16. G2-1 electron affinities (eV)								
d	−0.29	2.43	−0.01	−0.04	0.03	0.01	0.00	0.02
$\|d\|$	0.31	2.43	0.08	0.11	0.10	0.10	0.09	0.09
A17. G2-1 proton affinities (kcal mol^{-1})								
d	13.4	13.0	3.5	3.4	2.2	0.5	3.7	2.6
$\|d\|$	13.4	13.0	3.5	3.4	2.6	2.1	3.7	2.9

these cases g_i in Eq. 4.31 is redefined as

$$g_i^{\mathrm{IP}} = f_i^{M^+} - f_i^M \tag{6.5}$$

$$g_i^{\mathrm{EA}} = f_i^M - f_i^{M^-} \tag{6.6}$$

$$g_i^{\mathrm{PA}} = f_i^M - f_i^{MH^+} \tag{6.7}$$

The resulting FBH8 functional had another large change in the coefficients. The LDA exchange coefficient rose again, although not to the same level as FBH6. The reaction barriers lost 2 kcal mol^{-1} in accuracy, and the atomisation energy errors also deteriorated to 4.3 kcal mol^{-1}. The A1 shielding constants improved slightly to 16.0 ppm. The introduction of the other thermochemical properties into the fitting data leads to a great improvement in their errors, with A15, A16, and A17 giving 0.13 eV, 0.08 eV, and 3.5 kcal mol^{-1} respectively. The ionisation potential and electron affinity results are superior to KT3 (0.16 and 0.14 eV), but the proton affinities are not as good as KT3 (2.3 kcal mol^{-1}). The small A17 proton affinity set is dominated by the error of the C_2H_2 molecule, and we consider a change in error of 1 kcal mol^{-1} either way to not be significant. More problematic is the performance of FBH8 for bond length optimisations. The A6 error rose to 0.017 Å and the A7 error to 0.052 Å. These errors are worse than KT3 (0.008 Å and 0.014 Å), FBH5 (0.010 Å and 0.034 Å), and even the original HCTH functional (0.013 Å and 0.037 Å).

This problem was addressed by adding the bond length optimisations to the fitting data. As these are not energy differences, they had to be fitted numerically using the same procedure as for shielding constants. However, the combined number of systems in the A6 and A7 sets (91) is almost three times larger than in the A1 shielding constant set (32). The bond length optimisations in these sets also usually take longer to calculate than the shielding constants. It was therefore too computationally costly to attempt to fit to the full A6 and A7 sets. Instead we chose a representative sample of 26 diatomic systems (the A30 set). These were calculated using the TZ2P basis set or 6-311+G(2df) basis set as appropriate. The Group 1 diatomics from the A7 set were strongly represented as these contributed most to the errors of

HCTH-type functionals. In the fitting procedure g_i is equivalent to f_i, as for shielding constants. We found that the approximations in the least squares fitting procedure were not as accurate for geometries as for shielding constants and therefore each functional required more iterations for the property assessments to converge.

The FBH9 functional was fitted to reaction barriers, atomisation energies, shielding constants, ionisation potentials, electron affinities, proton affinities, and bond lengths. This leads to an improvement in performance for bond lengths compared to FBH8, but at the expense of the other fitted properties. The errors for the A6 and A7 bond lengths fell to 0.010 Å and 0.035 Å (comparable to FBH5). The barrier height errors were 5.8 kcal mol^{-1} (worse than FBH8) and the G2 errors were 3.4 kcal (better than FBH8). The shielding constant errors deteriorated slightly compared to FBH8 to 18.2 ppm, and ionisation potentials and electron affinities also got worse, whereas proton affinity errors stayed essentially constant. The coefficients of FBH9 are relatively similar to FBH8, which suggests that we have reached the limit of the HCTH form's flexibility.

In summary, the FBH9 functional is improved over KT3 for barrier heights and atomisation energies, but at the cost of other properties. Thus it does not satisfy our aim of retaining KT3's all-round performance. It appeared that we had reached the limit of the HCTH form's ability to get a wide range of properties correct simultaneously. Our next step was to increase flexibility by adding the KT exchange term.

The FBH10 functional was fitted to the same set of data as FBH9, but included KT exchange. The coefficients changed more than between FBH8 and FBH9, and the LDA exchange rose to a level similar to that of FBH6. The KT exchange coefficient was a little larger than in KT3, at approximately -0.005. The additional flexibility leads to an improvement in all the fitted properties. The reaction barrier set error falls to 4.6 kcal mol^{-1}, atomisation energies to 3.1 kcal mol^{-1}, and shielding constants to 15.3 ppm (almost KT3 standard), and the other properties also improve to roughly KT3 levels.

We also applied the FBH10 functional to the A5 total energy set, and found that it reproduced KT3's very poor performance with an error of 383.84 kcal

mol^{-1}. This is not surprising as KT exchange is present and there were no total energies in the dataset. We next investigated whether the HCTH+KTX form was sufficiently flexible to give good total energies as well as good performance for the other properties. The FBH11 functional contained the A5 set in its fitting data, which reduced the A5 error to 2.9 kcal mol^{-1}. Unfortunately, this resulted in a deterioration for all the other properties, and the KT exchange term coefficient was reduced to almost zero (as we have observed several times before when fitting to total energies).

We also considered whether all 15 of the HCTH parameters were necessary to achieve good results for all properties. The FBH12 functional was fitted to the same set of data as FBH10, but it contained only the first 9 parameters of the B97 expansion (the same number as in the B97 series of functionals) as well as KTX. Again, this resulted in significant deterioration in almost all the properties considered.

Finally, we assessed the FBH10 functional for the other sets we had considered when assessing KT3. Our full assessment of these properties (and others) is discussed in Chapter 7, but our conclusion was that the performance of FBH10 was satisfactory for all the properties except the A22 polarisability set. The KT3 error for this set is 0.36 au, but FBH10 gives an error of 0.55 au. Our last addition to the fitting data is the A22 set, which again had to be fitted numerically. In total our final fitting data set consisted of 348 data points. The resulting functional, FBH13, has similar coefficients to FBH10 and gives very similar results for the properties considered in Table 6.6. Its performance over the A22 set improved to 0.43 au, which is still not quite as good as KT3, but is now better than the non-KT GGAs. We denote this functional KT4.

6.2 Hybrid functionals

We now turn for the first time to the development of hybrid functionals. It is well-known that hybrid functionals give superior results to conventional GGAs for reaction barriers, and we therefore investigated whether we could develop a hybrid functional to give high quality reaction barriers following the same semi-empirical philosophy as for our GGA development. The aim now was to

Table 6.7: Expansion parameters defining the B97-2 functional [51]. ξ denotes the fraction of exact exchange.

$c_{X\sigma,0}$	8.27642E − 1
$c_{C\sigma\sigma,0}$	5.85808E − 1
$c_{C\alpha\beta,0}$	9.99849E − 1
$c_{X\sigma,1}$	4.78400E − 2
$c_{C\sigma\sigma,1}$	−6.91682E − 1
$c_{C\alpha\beta,1}$	1.40626E + 0
$c_{X\sigma,2}$	1.76125E + 0
$c_{C\sigma\sigma,2}$	3.94796E − 1
$c_{C\alpha\beta,2}$	−7.44060E + 0
$c_{X\sigma,3}$	
$c_{C\sigma\sigma,3}$	
$c_{C\alpha\beta,3}$	
$c_{X\sigma,4}$	
$c_{C\sigma\sigma,4}$	
$c_{C\alpha\beta,4}$	
ξ	2.10000E − 1

develop a functional that surpassed B97-2, the third revision of the B97 functional form. The first such functional, B97 [43], was developed by fitting to atomisation energies, ionisation potentials, and total energies. The B97 fitting data set of 116 points suffered from overfitting when more than 9 parameters were considered. The B97-1 functional was a self-consistent reparameterisation of B97, which retained the same number of parameters [47]. The B97-2 functional added data from ZMP exchange-correlation potentials to the fitting set (the same data that HCTH was fitted to) [51]. The aim of that work was to investigate whether this addition would improve performance compared to B97-1, and so the number of parameters remained at 9. For reference, the B97-2 coefficients are presented in Table 6.7. The additional size of the fitting set would have allowed more parameters to be used, and in this thesis we investigate whether a hybrid functional with 15 B97 expansion parameters (and KT exchange) gives a sufficient improvement in performance to justify the additional complexity.

Unlike B97-2 (but like the original B97 functional), we explicitly incorporated the fraction of exact exchange into our fitting procedure. For all properties the exact exchange contribution was calculated numerically.

Our first hybrid functional, FBH14, contained 15 B97 expansion terms, the KT exchange term, and a fraction of exact exchange. It was fitted to the full G2 atomisation energy set, the BH42 barriers, the G2-1 ionisation potentials, electron affinities, and proton affinities, and the A1 set of shielding constants. The resulting coefficients are presented in Table 6.8. Results are presented in Table 6.9. FBH14 is characterised by quite similar coefficients to our final KT4 GGA. The exact exchange coefficient is remarkably low (approximately 8%), which reflects the inclusion of shielding constants in the fitting procedure. The shielding constants have been calculated in the conventional coupled (non-Kohn Sham) manner, and it has been observed that shielding constants calculated in this way deteriorate as the amount of exact exchange increases [101]. Although the fraction of exact exchange is very low, there is still some deterioration in the shielding constants (the error over the A1 set is 17.7 ppm). This explains why the excellent BH42 barrier errors (3.1 kcal mol^{-1}) have been obtained from a high value of LDA exchange rather than a high fraction of exact exchange. In order to minimise the deterioration in the shielding constants, the fitting procedure has to keep the fraction of exact exchange low and so the LDA exchange value has to rise accordingly (as previously observed for the GGAs fitted to reaction barriers) in order to give high quality reaction barriers. With the exception of the reaction barriers, there is no real improvement in the chemical properties obtained by adding exact exchange, and so it is difficult to justify the additional complexity.

There is much discussion [103, 222] about how shielding constants should properly be calculated for hybrid functionals. If shielding constants are calculated in the conventional coupled manner, hybrid functionals such as PBE, B3LYP, and B97-2 give very poor results. But in an uncoupled (Kohn-Sham) formalism, such as the MKS method or the optimised effective potential, they give results competitive with the KT functionals. It is therefore not appropriate to try to fit hybrid functionals to coupled shielding constants. In this chapter we will continue to assess the functionals using the coupled formalism for consistency, but we discuss this question in more detail in Chapter 7.

The FBH15 functional is the same as FBH14 but with shielding constants removed from the fitting set. This resulted in a substantial change in coeffi-

Table 6.8: Expansion parameters defining the functionals of the HCTH form (and KTX) with a fraction ξ of exact exchange, fitted to reaction barriers and other properties.

	FBH14	FBH15	FBH16
$c_{X\sigma,0}$	1.184943E + 0	7.450703E − 1	7.488648E − 1
$c_{C\sigma\sigma,0}$	−3.569672E + 0	−6.577950E − 2	6.360573E − 1
$c_{C\alpha\beta,0}$	1.347736E + 0	1.220724E + 0	1.174137E + 0
$c_{X\sigma,1}$	−3.878492E + 0	−4.768328E − 1	−8.950794E − 1
$c_{C\sigma\sigma,1}$	6.877622E + 0	3.021952E + 0	−1.436848E + 0
$c_{C\alpha\beta,1}$	2.063401E + 0	−2.317052E + 0	−5.982782E − 1
$c_{X\sigma,2}$	1.565718E + 1	2.922525E + 0	4.909806E + 0
$c_{C\sigma\sigma,2}$	−9.060622E + 0	−2.883280E + 0	2.182693E + 0
$c_{C\alpha\beta,2}$	−1.815684E + 1	3.537381E + 0	−3.314793E + 0
$c_{X\sigma,3}$	−2.501428E + 1	−7.408743E + 0	−8.711994E + 0
$c_{C\sigma\sigma,3}$	−4.837158E + 0	−4.926586E + 0	−9.185343E − 1
$c_{C\alpha\beta,3}$	1.173940E + 1	6.103897E + 0	7.230777E + 0
$c_{X\sigma,4}$	1.557784E + 1	8.984854E + 0	7.888892E + 0
$c_{C\sigma\sigma,4}$	1.518807E + 1	6.851097E + 0	1.344506E + 0
$c_{C\alpha\beta,4}$	5.794021E + 0	−1.633065E + 1	−9.202861E + 0
c_{KTX}	−4.722414E − 3	−2.186151E − 4	
ξ	7.733800E − 2	2.729900E − 1	2.803440E − 1
	FBH17 (B97-3)	FBH18	
$c_{X\sigma,0}$	7.334648E − 1	7.191278E − 1	
$c_{C\sigma\sigma,0}$	5.623649E − 1	1.768011E − 1	
$c_{C\alpha\beta,0}$	1.133830E + 0	1.184808E + 0	
$c_{X\sigma,1}$	2.925270E − 1	7.737838E − 1	
$c_{C\sigma\sigma,1}$	−1.322980E + 0	2.983762E + 0	
$c_{C\alpha\beta,1}$	−2.811967E + 0	−3.007421E + 0	
$c_{X\sigma,2}$	3.338789E + 0	−5.950025E − 1	
$c_{C\sigma\sigma,2}$	6.359191E + 0	−3.461228E + 0	
$c_{C\alpha\beta,2}$	7.431302E + 0	8.131203E + 0	
$c_{X\sigma,3}$	−1.051158E + 1	−2.183118E − 1	
$c_{C\sigma\sigma,3}$	−7.464002E + 0	−2.258463E + 0	
$c_{C\alpha\beta,3}$	−1.969342E + 0	−8.048121E + 0	
$c_{X\sigma,4}$	1.060907E + 1	2.160877E + 0	
$c_{C\sigma\sigma,4}$	1.827082E + 0	2.851016E + 0	
$c_{C\alpha\beta,4}$	−1.174423E + 1	−3.839905E + 0	
c_{KTX}			
ξ	2.692880E − 1	2.710510E − 1	

Table 6.9: Error assessments for functionals of the HCTH form (and KTX) with a fraction ξ of exact exchange, fitted to barrier heights and other properties. Units are given in parentheses.

	FBH14	FBH15	FBH16	FBH17 (B97-3)	FBH18
A29. BH42/04 classical chemical reaction barriers (kcal mol^{-1})					
d	−2.9	−1.7	−2.1	−2.3	−2.3
$\|d\|$	3.1	1.9	2.2	2.4	2.4
A13/14. G2 atomisation energies (kcal mol^{-1})					
G2-1:					
d	0.5	0.1	0.2	−0.2	−0.4
$\|d\|$	2.8	1.9	1.9	1.9	1.9
G2-2:					
d	0.0	−0.2	0.2	−0.3	−0.5
$\|d\|$	3.2	2.8	3.0	2.5	2.5
Full G2:					
d	0.2	−0.1	0.2	−0.3	−0.4
$\|d\|$	3.1	2.5	2.6	2.3	2.3
A1. Isotropic NMR shielding constants (ppm)					
d	−5.7	−62.3	−57.7	−61.5	−64.1
$\|d\|$	17.7	62.6	58.0	61.5	64.1
Excluding O_3:					
d	−0.5	−33.8	−30.2	−34.2	−35.9
$\|d\|$	13.3	34.1	30.5	34.2	35.9
A6. G2 subset bond lengths (Å)					
d	−0.005	0.003	0.005	0.000	0.000
$\|d\|$	0.010	0.011	0.012	0.008	0.007
A7. Diatomic bond lengths (Å)					
d	0.009	0.016	0.019	0.011	0.013
$\|d\|$	0.018	0.024	0.026	0.016	0.018
A15. G2-1 ionisation potentials (eV)					
d	0.00	0.02	0.03	0.03	0.03
$\|d\|$	0.11	0.12	0.12	0.14	0.13
A16. G2-1 electron affinities (eV)					
d	0.01	−0.00	0.00	−0.03	−0.03
$\|d\|$	0.11	0.08	0.08	0.09	0.09
A17. G2-1 proton affinities (kcal mol^{-1})					
d	2.2	0.2	0.4	1.2	0.8
$\|d\|$	2.4	2.0	1.8	1.4	1.6

cients. The LDA exchange coefficient was reduced to a typical hybrid value of about 0.75, and the fraction of exact exchanges rose to around 27%. This is higher than B97-2 (21%) but not as high as the functionals designed specifically for kinetics calculations. The KT exchange term fell to almost zero, which is not surprising as it was only added to give good quality shielding constants. The conventional shielding constant performance of FBH15 rose to 62.6 ppm, a level typical of a hybrid functional (see Chapter 7 for further discussion). Atomisation energies and barrier heights improved, whereas bond lengths got slightly worse.

As KT exchange no longer appeared to be necessary for the properties that we fitted to, we removed it from the functional form (leaving effectively HCTH with exact exchange). The resulting functional, FBH16, suffered from slightly worse barriers (2.2 kcal mol^{-1}) and atomisation energies (2.6 kcal mol^{-1}), but shielding constants actually improved and the other properties remained comparable. This slight degradation in properties does not justify the addition of KTX.

FBH16 gives an error over the A5 total energy set of 141.7 kcal mol^{-1}. This is solely because total energies are not included in the fit. As KTX exchange is no longer in the functional form, there is no reason not to fit to total energies, and so they were added to the fit. The FBH16 is also poor for the A6 and A7 bond length optimisations, so the representative A30 set of bond lengths was also added to the fitting set. We found that the resulting functionals were not optimal for polarisabilities (with an error over the A22 set of 0.36 au, which is comparable to KT3 but not competitive with B97-2). Therefore the A22 set was also added to fit set. In summary, the final fitting set for the hybrid functional was the same as that of the KT4 GGA, but with shielding constants removed and total energies added. The final fitting set consisted of 316 data points.

The resulting FBH17 functional deteriorates slightly for barriers (2.4 kcal mol^{-1}) compared to FBH16, but improves for atomisation energies (2.3 kcal mol^{-1}). Coupled shielding constants get slightly worse, but the bond lengths improve significantly (as they have been fitted to), with an A6 error of 0.008Å and A7 error of 0.016Å. Overall the FBH17 functional does appear to be

superior to B97-2, in particular for barriers and atomisation energies, for which the B97-2 errors are 3.3 kcal mol^{-1} and 3.1 kcal mol^{-1} respectively.

Towards the end of our investigations we were given access to more powerful computing facilities. This meant we were able to investigate whether any further improvement in geometries could be obtained by fitting to the full A6 and A7 sets. The coefficients of the resulting FBH18 functional showed little change from FBH17, which suggests that our A30 subset was genuinely representative. The results showed a small improvement in the A6 set (with errors falling from 0.008Å to 0.007Å), but the error of the A7 set actually increased. There was little change in the other properties. Therefore FBH18 offers no improvement. For future reference we denote our final FBH17 functional as B97-3 (as it contains no KT exchange term) [223].

Chapter 7

Assessment of KT4 and B97-3

In this chapter we present an extensive chemical assessment of the KT4 and B97-3 functionals in comparison with the published GGAs and hybrids we have previously considered and the KT1, KT2, and KT3 GGAs. We then consider the performance of B97-3 for an enlarged spin-spin coupling constant assessment set.

7.1 Fitting data summary

We start by comparing the performance of KT4 and B97-3 with other functionals for the data used in the fitting procedure. KT4 and B97-3 are expected to perform well for these assessments. The fitting data set in total consists of 9 different properties, 348 data points, and 3,828 individual property calculations. Errors are presented in Table 7.1. As KT4 and B97-3 were designed specifically to give good reaction barriers, it is not surprising that they perform very well for the BH42/04 set. KT4 gives the joint lowest (with HCTH) mean absolute error out of the GGAs of 4.8 kcal mol^{-1}. This is a significant improvement over KT3 (8.1 kcal mol^{-1}). No GGA performs as well as the hybrid functionals. The best performing hybrid is B97-3 with an error of 2.4 kcal mol^{-1}, which is significantly better than the next best functional, B97-2 (3.3 kcal mol^{-1}).

The performance for the G2 atomisation energy set is equally good. KT4 gives the lowest error (3.1 kcal mol^{-1}) out of all the GGAs, with OLYP the

Table 7.1: KT4 and B97-3 fitting data error assessments. Units are given in parentheses.

	KT1	KT2	KT3	KT4	PBE	HCTH	OLYP	B3LYP	PBE0	B97-2	B97-3
A29. BH42/04 classical chemical reaction barriers (kcal mol^{-1})											
d	−14.6	−12.5	−8.1	−4.6	−9.4	−4.7	−5.9	−4.4	−4.5	−3.1	−2.3
$\|d\|$	14.6	12.5	8.1	4.8	9.4	4.8	6.0	4.5	4.5	3.3	2.4
A13/14. G2 atomisation energies (kcal mol^{-1})											
G2-1:											
d	12.9	−0.8	−1.2	0.6	6.3	−0.4	2.1	−0.8	−2.0	−0.7	−0.2
$\|d\|$	13.4	6.2	4.3	2.5	7.9	3.3	3.2	2.7	3.2	2.2	1.9
G2-2:											
d	36.6	10.4	0.4	−0.3	21.2	−2.1	1.7	−4.8	3.8	0.8	−0.3
$\|d\|$	37.1	12.0	5.0	3.4	21.5	6.8	5.4	5.1	5.6	3.6	2.5
Full G2:											
d	27.8	6.2	−0.2	0.0	15.6	−1.4	1.8	−3.3	1.7	0.2	−0.3
$\|d\|$	28.3	9.9	4.7	3.1	16.5	5.5	4.6	4.2	4.7	3.1	2.3
A15. G2-1 ionisation potentials (eV)											
d	−0.06	−0.11	−0.03	0.00	0.01	−0.02	−0.12	0.01	0.02	−0.02	0.03
$\|d\|$	0.14	0.23	0.16	0.10	0.16	0.15	0.18	0.16	0.17	0.12	0.14
A16. G2-1 electron affinities (eV)											
d	0.11	−0.05	−0.07	0.02	0.08	−0.02	−0.11	−0.01	−0.05	−0.09	−0.03
$\|d\|$	0.15	0.17	0.14	0.09	0.10	0.10	0.14	0.09	0.13	0.11	0.09
A17. G2-1 proton affinities (kcal mol^{-1})											
d	−4.1	−2.2	1.6	2.6	−1.6	2.5	1.0	−1.4	−0.4	1.8	1.2
$\|d\|$	4.9	3.5	2.3	2.9	2.6	2.5	2.0	2.2	2.4	1.8	1.4
A30. Fitting set of diatomic bond lengths (Å)											
d	0.006	−0.011	0.003	0.004	0.019	0.029	0.032	0.006	0.005	0.012	0.003
$\|d\|$	0.024	0.018	0.011	0.013	0.019	0.029	0.032	0.013	0.013	0.019	0.013
A22. Isotropic electronic polarisabilities (au)											
d	1.16	0.68	0.32	0.40	0.76	0.41	0.57	0.36	0.03	−0.04	0.06
$\|d\|$	1.16	0.68	0.36	0.43	0.76	0.45	0.57	0.44	0.24	0.22	0.26
A1. Isotropic NMR shielding constants (ppm)											
d	−4.7	−9.5	−11.9	−8.7	−40.3	−32.4	−30.7	−60.7	−58.5	−50.4	−61.5
$\|d\|$	13.0	13.2	14.4	15.1	40.3	32.4	30.7	60.7	58.8	50.4	61.5
A5. Total atomic and ionic energies (kcal mol^{-1})											
d	−333.5	−461.4	−425.4	−392.0	31.0	−0.9	−1.8	3.8	25.6	−0.1	−0.7
$\|d\|$	−334.7	461.8	425.4	392.0	31.0	4.2	2.9	4.5	25.6	3.4	2.7

next best at 4.6 kcal mol^{-1}. The performance of KT4 is superior to the hybrids B3LYP and PBE0, and equal to B97-2. The B97-3 hybrid has the lowest error (2.3 kcal mol^{-1}).

For ionisation potentials (0.10 eV) and electron affinities (0.09 eV), KT4 is the best performing GGA, and also gives the smallest or joint-smallest errors out of all the functionals. For proton affinities KT4's performance (2.9 kcal mol^{-1}) is inferior to KT3 (2.3 kcal mol^{-1}), but we consider this to be acceptable (see Section 6.1.4). B97-3 is not the best hybrid functional for the G2-1 ionisation potentials (it is beaten by B97-2), but it does give the joint lowest error for electron affinities and the lowest error (1.4 kcal mol^{-1}) for proton affinities.

For the A30 fitting set of bond lengths, KT4's error of 0.013 Å is slightly worse than KT3 (0.011 Å), but this is still a much lower error than any of the other GGAs. In fact, KT3 gives the lowest error of any functional, with three hybrids (B3LYP, PBE0, and B97-3) all giving the same performance as KT4. B97-2 gives a significantly higher error (0.019 Å), which is mainly due to the challenging Group 1 diatomics.

Despite being explicitly fitted to polarisabilities, KT4 is still not as accurate as KT3 for the A22 set, with errors of 0.43 and 0.36 au, respectively. To some extent this reflects the choice of weighting parameters in the fit. A greater emphasis on polarisabilities would have achieved a lower error, but at the cost of the other properties. An error of 0.43 au was considered to be acceptable because it was still superior to every other GGA. All the hybrid functionals give better results with the exception of B3LYP.

KT4 is slightly worse than KT3 for isotropic shielding constants, which in turn is worse than KT2 and KT1. In each case a slight decrease in accuracy for the A1 set is observed in return for improvements in a wider range of properties. KT4's error of 15.1 ppm is still much smaller than those of the other GGAs considered. All the hybrid results (calculated using the conventional coupled equations) are very poor (the B97-3 functional was not explicitly fitted to the A1 set). Hybrid shielding constant results are discussed further below.

The KT4 fitting data set did not contain the A5 total energy set, and as for the other KT functionals its error is very high (392.0 kcal mol^{-1}). We

believe this is inevitable to achieve good results for other properties when KT exchange is included in the functional form. The B97-3 functional does not include KT exchange and so the A5 set was included in the fitting data. Its performance is the best of all the functionals, with an error of 2.7 kcal mol^{-1}.

Overall, the KT4 and B97-3 perform very well over the sets they are fitted to, as expected. Their performance for reaction barriers and atomisation energies is very pleasing, particularly the former as previous functionals have tended to be unable to get good performance for reaction barriers and other properties simultaneously. In general, the KT4 functional maintains the performance of KT3 for other properties, with only minor degradation for some properties. The B97-3 hybrid functional gives excellent performance for all fitted properties, either comparable to or in most cases surpassing the performance of B97-2, PBE0, and B3LYP.

7.2 Non-fitting data assessments

The performance of KT4 and B97-3 is promising for the fitted data set, but the real test of semi-empirical functionals is over non-fitted data. In this section we assess our new functionals for a total of 23 non-fitted assessments, including 11 chemical properties not considered in the fitting data. The non-fitted assessments together consist of 552 reference data points (6,072 individual property calculations). Errors are presented in Tables 7.2–7.7. A full breakdown of the fitted and non-fitted assessments for the hybrid functionals considered is available from Ref. [224] (the supplementary information to Ref. [223]).

7.2.1 Kinetics and thermochemistry

The first set of non-fitted assessments relate to kinetics (classical reaction barrier heights) and thermochemistry (enthalpies of formation, ionisation potentials, and electron affinities).

The NHTBH38/04 classical chemical reaction barrier height set (A31) was developed by Truhlar and co-workers [225] to be complementary to the BH42/04 set. The BH42 set predominantly consists of hydrogen transfer reac-

tions, whereas the NHTBH38 set consists of 38 non-hydrogen transfer (NHT) reactions. These are divided into three groups: 6 heavy-atom transfer reactions, 8 unimolecular nucleophilic substitution reactions, and 4 unimolecular and association reactions. As for the BH42 set, both forward and reverse barrier heights are calculated. The calculations were performed at the same QCISD/MG3 geometries [226] and errors were calculated relative to correlated *ab initio* reference values. We used the same 6-311+G(3df,2p) basis set that was used for the BH42 set and the G2 thermochemistry calculations. This gives results of a similar quality to the MG3S basis set used in Ref. [225]. Errors are presented in Table 7.2. The results show a similar trend to that observed for the BH42 set, but not identical. The KT4 functional gives an overall error of 5.3 kcal mol^{-1}, which improves upon the KT3 error of 8.0 kcal mol^{-1}. However, unlike for BH42, KT4 is surpassed by the HCTH functional. HCTH is remarkably accurate for barriers even though it was not explicitly fitted to them (the good quality might arise from the inclusion of exchange-correlation potentials in the fit). KT4, on the other hand, appears to deteriorate for reactions outside its fitting set. This is often observed in semi-empirical functionals, but it is particularly clear here because the reactions are of very different types in the non-fitted set compared to the fitting set. Compared to KT4, HCTH is particularly good for nucleophilic substitution reactions. The B97-3 hybrid is more successful, giving the lowest error of all the functionals (1.5 kcal mol^{-1}). B97-3 therefore appears to be better adapted to a wide range of reaction types than KT4.

We also calculated KT4 and B97-3 errors for the A23 barrier set. For this set the barrier heights were calculated at the stationary points of the respective methods rather than at a set of reference geometries, and therefore it tests the quality of transition state geometries as well as energetics performance. For this set KT4 is the best performing GGA, with an error of 3.7 kcal mol^{-1} (slightly better than the HCTH error of 3.8 kcal mol^{-1}). Again, B97-3 is the best functional overall with an error of just 1.8 kcal mol^{-1}. Both KT4 and B97-3 locate all 16 transition states.

The next three assessments consider further thermochemical data from the 'G' sets of Curtiss *et al.* [227, 228]. The first of these (A32) is the G3-3 en-

Table 7.2: KT4 and B97-3 non-fitted reaction barrier and thermochemistry error assessments. Units are given in parentheses.

	KT1	KT2	KT3	KT4	PBE	HCTH	OLYP	B3LYP	PBE0	B97-2	B97-3
A31. NHTBH38/04 classical chemical reaction barriers (kcal mol^{-1})											
Heavy-atom transfer reactions											
d	−20.8	−17.7	−13.0	−9.0	−14.9	−8.1	−11.2	−8.5	−6.6	−3.1	−2.5
$\|d\|$	20.8	17.7	13.0	9.0	14.9	8.1	11.2	8.5	6.6	3.3	2.5
Nucleophilic substitution reactions											
d	−12.7	−11.7	−7.0	−4.2	−6.9	−2.1	−2.6	−3.3	−1.7	−1.3	−0.1
$\|d\|$	12.7	11.7	7.0	4.2	6.9	2.1	2.6	3.3	1.9	1.4	0.8
Unimolecular and association reactions											
d	−5.7	−4.2	−2.5	−1.3	−3.1	−0.9	−2.2	−1.6	−0.7	0.5	0.5
$\|d\|$	6.2	4.6	3.5	2.5	3.4	2.1	2.8	2.0	2.3	1.9	1.4
Overall:											
d	−13.4	−11.6	−7.7	−5.0	−8.4	−3.7	−5.2	−4.5	−3.0	−1.4	−0.7
$\|d\|$	13.4	11.7	8.0	5.3	8.5	4.0	5.4	4.6	3.5	2.1	1.5
A23. Classical chemical reaction barriers (kcal mol^{-1})											
No.	6	9	12	16	10	15	14	15	16	16	16
d	−15.3	−11.4	−8.0	−3.7	−7.8	−3.3	−5.6	−5.1	−4.4	−1.8	−1.6
$\|d\|$	15.3	11.4	8.0	3.7	7.8	3.8	5.6	5.1	4.4	2.4	1.8
A32. G3-3 enthalpies of formation (kcal mol^{-1})											
d	−69.7	−23.5	−0.9	5.9	−32.6	12.8	5.6	12.2	−9.0	0.7	2.0
$\|d\|$	69.7	23.8	5.1	6.7	32.6	13.7	6.9	12.2	10.2	6.2	4.7
A33. G2-2 ionisation potentials (eV)											
d	−0.19	−0.20	−0.14	−0.12	−0.17	−0.17	−0.29	−0.12	−0.11	−0.16	−0.10
$\|d\|$	0.23	0.29	0.26	0.23	0.24	0.28	0.34	0.23	0.22	0.21	0.18
A34. G2-2 electron affinities (eV)											
d	0.08	−0.05	−0.06	0.00	0.03	−0.04	−0.14	0.02	−0.01	−0.05	0.01
$\|d\|$	0.15	0.15	0.14	0.10	0.12	0.10	0.14	0.15	0.18	0.15	0.17

thalpies of formation set of 75 molecules. This is the third set after G2-1 (A13) and G2-2 (A14). The G3-3 set again consists largely of organic molecules, but in general they are larger than those in the G2 set. Together the three sets are known as the full G3 set (223 molecules). Previously we have compared our calculated atomisation energy results with electronic atomisation energies from Ref. [182]. In that work the experimental enthalpies of formation were converted into reference atomisation energies. However, the G3-3 set was not considered in that reference, so for this set we compare directly with the original enthalpies of formation (that is, instead of subtracting the correction from the experimental enthalpies of formation and comparing atomisation energies, we add the same correction onto our calculated atomisation energies and compare enthalpies of formation).

For a molecule $A_xB_yC_z$, the enthalpy of formation $\Delta_f H^0$ at 0 K is [183]

$$\begin{aligned} \Delta_f H^0(A_xB_yC_z) &= x\Delta_f H^0(A, 0\text{ K}) \\ &+ y\Delta_f H^0(B, 0\text{ K}) \\ &+ z\Delta_f H^0(C, 0\text{ K}) \\ &- D_0 \end{aligned} \tag{7.1}$$

where D_0 is the ZPE-corrected atomisation energy. The error when comparing enthalpies of formation is therefore minus the error when comparing atomisation energies. Our atomisation energies were corrected using scaled HF/6-31G(d) zero-point energies with a scaling factor of 0.8929. The atomic enthalpies of formation were taken from Ref. [183]. A temperature correction then had to be applied to the theoretical enthalpy of formation of each system to compare with the experimental values measured at 298 K. To maintain consistency with the A13 and A14 sets, we performed the calculations at MP2/6-31G(d) geometries with the 6-311+G(3df,2p) basis set. The geometries, zero-point energies, and temperature corrections were taken from Ref. [229]. Experimental reference values were taken from Ref. [227].

The results for the KT functionals are very interesting. As expected, KT1 is poor and KT2 is improved, but not competitive with the best GGAs. The KT3 functional gives a remarkably low mean absolute error of 5.1 kcal mol^{-1}.

This is superior to all the other GGAs and all of the previously published hybrids. KT4 does not perform as well as KT3, giving an error of 6.7 kcal mol^{-1}. This is a disappointing result given their relative performance for the G2 sets, although KT4 still surpasses all the other GGAs. KT3 and KT4 were both fitted to the full G2 atomisation energy set, but KT3 appears to be more robust with respect to systems outside the set. In fact, this result should be interpreted as a reflection of the high quality of KT3 rather than a flaw in KT4, as KT3's errors degrade far less than any other functional from G2 to G3-3. We would normally expect some degradation as the G3-3 set involves larger systems which would naturally lead to larger errors, but this is not the case for KT3. Of the hybrids, B97-3 gives the lowest error of 4.7 kcal mol^{-1}, which is significantly better than the next best functional, B97-2, at 6.2 kcal mol^{-1}. Therefore B97-3 also seems to be more robust than KT4 for non-fitted thermochemistry. Although proportionally B97-3 degrades more from G2 to G3-3 than KT3, its error remains lower.

We next considered the G2-2 ionisation potentials (49 systems) and electron affinities (32 systems) [228]. Again, we used MP2/6-31G(d) geometries with the 6-311+G(3df,2p) basis set and added scaled (0.8929) Hartree-Fock zero-point energy corrections (from Ref. [229]) to our calculated values rather than compare against electronic (i.e. ZPE-corrected) ionisation potentials and electron affinities as we did for the G2-1 sets in the fitting data. For these properties the corrections are small as the ZPE of the system and its ion are usually close. Experimental reference values were taken from Ref. [188]. The ionisation potential of CN and the electron affinity of C_2 were removed from their respective sets as CN^+ and C_2 are open-shell singlets.

KT4's performance for these sets is markedly better than for the G3-3 enthalpies of formation. It gives the joint lowest mean absolute error (with KT1!) out of the GGAs for the G2-2 ionisation potentials (0.23 eV). This is competitive with the hybrid functionals, although the lowest error is given by B97-3 (0.18 eV). For the G2-2 IP set, B97-3 performs better than B97-2, even though the reverse was true for the G2-1 IP set in the fitting data. All the functionals uniformly underestimate the ionisation potentials. For the G2-2 electron affinities, KT4 gives the joint lowest GGA error (with HCTH) of

Table 7.3: KT4 and B97-3 error assessments for the full G3 set of enthalpies of formation and the full G2 sets of ionisation potentials and electron affinities. Units are given in parentheses.

	KT1	KT2	KT3	KT4	PBE	HCTH	OLYP	B3LYP	PBE0	B97-2	B97-3
A13/14/32. Full G3 enthalpies of formation (kcal mol^{-1})											
d	−41.9	−12.0	−0.2	2.0	−21.3	5.3	0.7	6.3	−4.1	0.1	0.8
$\|d\|$	42.2	14.5	4.9	4.3	21.9	8.3	5.4	6.9	6.6	4.1	3.1
A15/33. Full G2 ionisation potentials (eV)											
d	−0.13	−0.16	−0.09	−0.07	−0.10	−0.11	−0.22	−0.06	−0.05	−0.10	−0.04
$\|d\|$	0.19	0.27	0.22	0.18	0.21	0.22	0.27	0.20	0.20	0.17	0.16
A16/34. Full G2 electron affinities (eV)											
d	0.10	−0.05	−0.06	0.01	0.05	−0.03	−0.13	0.01	−0.02	−0.07	−0.01
$\|d\|$	0.15	0.16	0.14	0.10	0.11	0.10	0.14	0.13	0.16	0.14	0.13

0.10 eV. This is a better performance than all of the hybrid functionals, with B3LYP and B97-2 giving the lowest error of 0.15 eV (B97-3 gives an error of 0.17 eV). Again this is the reverse of the finding for G2-1 electron affinities, where B97-3 gave a lower error than B97-2.

Finally, we present the results for the full G3 (= G2-1 + G2-2 + G3-3) enthalpy of formation and G2 (= G2-1 + G2-2) ionisation potential and electron affinity sets in Table 7.3. These errors contain a mixture of fitted and non-fitted data. The enthalpy of formation errors of sets A13 and A14 were calculated by taking minus the atomisation energy errors. KT4 gives the lowest GGA mean absolute error of 4.3 kcal mol^{-1}, which is now superior to the KT3 error because of its performance in the fitted G2 set. The lowest error overall is given by the B97-3 hybrid (3.1 kcal mol^{-1}). For the full G2 ionisation potentials, KT4 gives the lowest GGA error (0.18 eV) and B97-3 gives the lowest overall error (0.16 eV). For the full G2 electron affinities, KT4 gives the joint lowest overall error (with HCTH) of 0.10 eV. B97-3 gives the joint-lowest hybrid error (with B3LYP) of 0.13 eV.

In summary, KT4 and B97-3 give the best overall performance for their respective classes of functionals for kinetics and thermochemistry, although the KT4 functional is surpassed by the remarkably good HCTH non-hydrogen

transfer barrier results and the KT3 enthalpies of formation for the G3-3 set.

7.2.2 Structural response properties

We next consider properties related to geometry perturbations, namely optimised bond lengths, bond angles, hydrogen bond dimer distances, and harmonic vibrational wavenumbers. Results are presented in Table 7.4.

The first bond length optimisation sets we consider are the A35 G2 subset bond lengths and A36 diatomic bond lengths. These are equivalent to the original A6 and A7 sets but with the molecules used in the A30 fitting set removed. KT4 gives the lowest GGA mean absolute error of 0.007 Å for the A35 set, and with KT3 gives the joint-lowest error for A36 of 0.015 Å. With errors of 0.006 Å and 0.016 Å respectively, B97-3 gives good performance over these sets. PBE0 gives the best performance for both sets (0.004 Å and 0.011 Å).

The next assessment (A37) is a set of bond lengths of 16 radical diatomic species following Ref. [51]. Calculations were performed using the TZ2P basis set and errors calculated relative to reference experimental values. For this set KT3 and B97-2 give the joint lowest error of 0.009 Å. KT4 is marginally less accurate (0.010 Å) and B97-3 is slightly less accurate again (0.011 Å).

We also calculated errors for the A18 hydrogen bond dimer distance set, the A19 bond length set, and the A20 bond angle set that were previously discussed in Section 5.2. For the A18 and A19 sets, KT4's performance is reasonable, with errors of 0.09 Å and 0.015 Å respectively, but this is not as good as the results that KT3 attains. B97-3 gives a low error for the A18 set of 0.06 Å but gives the joint highest error with PBE0 of 0.023 Å for the A19 set. This is an anomalous result because both B97-3 and PBE0 perform very well for all the other bond length sets. However, this is a small set of diverse and challenging molecules and it is quite likely to highlight quirks such as this. For the A20 bond angles set, KT4 gives the same error (1.0°) as KT3, which is typical of a GGA functional. B97-3 gives an error of 0.5°, which is typical of a hybrid.

We also consider geometry optimisations of the selenium-containing molecules

Table 7.4: KT4 and B97-3 non-fitted geometry perturbation assessments. Units are given in parentheses.

	KT1	KT2	KT3	KT4	PBE	HCTH	OLYP	B3LYP	PBE0	B97-2	B97-3
A35. Non-fitted G2 subset bond lengths (Å)											
d	0.017	0.002	0.001	−0.001	0.014	0.009	0.012	0.004	−0.001	−0.000	0.000
$\|d\|$	0.018	0.008	0.008	0.007	0.014	0.009	0.012	0.006	0.004	0.005	0.006
A36. Non-fitted diatomic bond lengths (Å)											
d	0.011	−0.007	0.009	0.014	0.024	0.034	0.037	0.018	0.007	0.016	0.014
$\|d\|$	0.025	0.018	0.015	0.015	0.024	0.034	0.037	0.019	0.011	0.019	0.016
A37. Radical bond lengths (Å)											
d	0.024	0.007	0.007	0.004	0.017	0.012	0.016	0.007	−0.002	0.001	0.001
$\|d\|$	0.024	0.010	0.009	0.010	0.017	0.012	0.016	0.012	0.010	0.009	0.011
A18. Hydrogen bond dimer distances (Å)											
d	−0.18	−0.21	−0.03	0.07	−0.03	0.26	0.26	0.01	−0.02	0.06	0.06
$\|d\|$	0.18	0.21	0.05	0.09	0.04	0.26	0.26	0.04	0.04	0.06	0.06
A19. Other bond lengths (Å)											
d	0.009	−0.008	−0.003	−0.002	0.010	0.005	0.009	−0.002	−0.021	−0.016	−0.014
$\|d\|$	0.022	0.018	0.012	0.015	0.015	0.017	0.015	0.014	0.023	0.017	0.023
A20. Bond angles (degrees)											
d	−0.8	−0.7	−0.5	−0.1	0.0	0.1	−0.1	0.1	0.0	0.0	−0.1
$\|d\|$	1.1	0.9	1.0	1.0	0.8	0.9	1.0	0.3	0.5	0.4	0.5
A24. Selenium bond lengths (Å)											
d	0.020	0.002	0.003	0.003	0.017	0.011	0.015	0.010	−0.002	0.000	0.003
$\|d\|$	0.020	0.009	0.010	0.009	0.019	0.014	0.015	0.013	0.007	0.007	0.008
A25. Selenium bond angles (degrees)											
d	−0.4	−0.4	0.4	0.9	0.3	1.0	0.9	0.6	0.3	0.6	0.6
$\|d\|$	0.9	0.9	0.6	1.0	0.8	1.2	1.2	0.8	0.7	0.8	0.8
A21. Diatomic harmonic vibrational wavenumbers (cm^{-1})											
d	−13	4	−3	−11	−16	−18	−21	3	20	12	16
$\|d\|$	21	15	15	22	21	26	27	20	26	26	26

(sets A24 and A25) considered in Section 5.4. For bond lengths, KT4 (0.009 Å) is marginally better than KT3 (0.010 Å), whereas B97-3 (0.008 Å) is marginally worse than B97-2 (0.007 Å). For bond angles, KT4 deteriorates by 0.4° compared to KT3, but this gives an error of 1.0° which is still competitive with the other GGAs. B97-3 gives the same error as B97-2 (0.8°).

Finally, we consider the A21 set of diatomic harmonic vibrational wavenumbers from Section 5.2. These are usually correlated with accuracy of geometry optimisations. Although KT4 is on average only slightly less accurate for geometries than KT3, it gives a significantly higher error for the A21 set (22 cm^{-1} compared to 15 cm^{-1} for KT3). However, this is still competitive with the other GGAs. The B97-3 error (26 cm^{-1}) is comparable to that of B97-2 and PBE0.

Overall, KT4 maintains the excellent performance that KT3 gave for geometry properties, and B97-3 does the same compared to B97-2. However, there is some significant deterioration for KT4's hydrogen bond dimer distances, A20 bond angles, and diatomic vibrational wavenumbers. B97-3 is significantly worse than B97-2 for the A19 set of bond lengths, but is significantly better for the A36 set.

7.2.3 Magnetic response properties

In this section we consider the non-fitted magnetic response properties previously considered in Chapters 2 and 3. Results are presented in Table 7.5. The mean absolute error for anisotropic NMR shielding constants increases from 9.3 ppm for KT3 to 11.1 ppm for KT4. A similar degradation is seen for isotropic and anisotropic magnetisabilities (where errors are presented relative to MCSCF values including O_3). The same pattern is seen for the A10 chemical shifts set; the KT4 functional does improve slightly over KT3 for hydrogen shifts, but this may simply be due to the lack of vibrational corrections in the reference data. For all other nuclei a degradation is observed for KT4. We also considered the A26 and A27 sets of shielding constants for selenium-containing molecules. Errors are presented for calculations at optimised geometries (comparable with Table 5.10). Isotropic errors are presented versus experiment

Table 7.5: KT4 and B97-3 non-fitted magnetic response property error assessments. Units are given in parentheses.

	KT1	KT2	KT3	KT4	PBE	HCTH	OLYP	B3LYP	PBE0	B97-2	B97-3
A2. Anisotropic NMR shielding constants (ppm)											
d	−2.1	4.1	6.7	3.5	35.7	27.0	24.6	44.5	40.7	34.6	42.8
$\|d\|$	11.5	8.8	9.3	11.1	39.0	28.4	26.2	45.9	43.9	36.1	44.1
A8. Isotropic magnetisabilities (10^{-30} JT^{-2})											
d	3.7	7.7	11.0	13.4	13.4	15.9	13.3	15.9	19.1	18.7	20.5
$\|d\|$	5.7	7.7	11.0	13.4	14.4	15.9	13.6	16.1	19.4	18.7	20.6
A9. Anisotropic magnetisabilities (10^{-30} JT^{-2})											
d	12.0	13.0	16.3	17.7	31.8	30.7	28.6	45.4	53.9	47.4	55.3
$\|d\|$	18.8	17.4	22.9	24.8	50.7	46.3	45.8	59.7	69.3	59.7	68.3
A10. Chemical Shifts (ppm)											
$\|d\|(^{13}\mathrm{C})$	4.5	4.4	4.4	4.6	6.5	4.5	4.6	6.5	6.1	4.7	6.0
$\|d\|(^{1}\mathrm{H})$	0.32	0.25	0.20	0.17	0.31	0.26	0.27	0.20	0.20	0.17	0.18
$\|d\|(^{15}\mathrm{N})$	25.7	26.1	29.1	30.9	48.9	44.4	43.5	33.5	30.1	29.3	30.0
$\|d\|(^{17}\mathrm{O})$	56.0	59.5	64.1	66.2	113.8	102.3	100.0	147.0	154.4	136.2	157.0
$\|d\|(^{19}\mathrm{F})$	16.7	17.3	16.8	16.9	25.1	24.4	22.5	22.1	19.1	18.1	18.7
A26. Selenium isotropic NMR shielding constants (ppm)											
d	−42	−8	−15	−11	−155	−113	−121	−137	−41	−51	−42
$\|d\|$	49	24	33	39	155	113	121	137	52	51	42
A27. Selenium anisotropic NMR shielding constants (ppm)											
d	−218	−217	−183	−181	−359	−277	−279	−282	−273	−235	−217
$\|d\|$	315	286	260	245	511	407	409	453	366	345	332

and anisotropic errors versus CCSD numbers. For the isotropic shielding constants, KT4 again gives a slightly higher error than KT3, but for anisotropic shielding constants KT4 improves upon KT3 (from 260 ppm to 245 ppm). As KT4 selenium geometries are of a similar quality to KT3, it is likely that this results is a reflection of the uncertainty in the reference values of the selenium molecules.

In general, there is a small but noticeable increase in errors from KT3 to KT4 for each set. This reflects the emphasis put on the shielding constants in the fit (for KT4) and the magnitude of the KT exchange coefficient chosen (for KT3). In effect, an increase in the errors for magnetic properties has been allowed to occur in order to decrease errors for other properties such as reaction barriers.

The errors for the hybrid functionals in Table 7.5 are calculated using the conventional coupled formalism and as expected are poor compared to GGA results. Overall B97-3 is actually the worst performing of all the hybrid functionals, with only the shielding constants for the selenium molecules improving compared to B97-2. This is consistent with the findings of Ref. [101], which indicates that the increased fraction of exact exchange in B97-3 will lead to a deterioration in shielding constant quality. However, the coupled formalism is not consistent with Kohn-Sham theory. It is more appropriate to calculate magnetic properties using an uncoupled formalism such as the MKS method of Section 2.2. MKS errors for the hybrid functionals are presented in Table 7.6. They are up to 9 times smaller than the errors calculated by the coupled approach! Results for all four hybrid functionals are similar, which suggests that they are all capable of supplying high quality densities for use in the ZMP procedure. For the A1 isotropic and A2 anisotropic shielding constants sets, the MKS(B97-3) results (15.8 ppm and 9.8 ppm) are competitive with KT4 (15.1 ppm and 11.1 ppm). For isotropic and anisotropic magnetisabilities, MKS(B97-3) surpasses KT4, with errors of 5.0 ppm and 7.7 ppm for the former compared to 13.4 ppm and 24.8 ppm for the latter. The MKS(B97-3) chemical shift errors are also smaller for every nucleus. In summary, the poor B97-3 results in Table 7.5 are not problematic. When the more appropriate MKS method is used, the B97-3 errors are lower than those of B97-2.

Table 7.6: Magnetic response property error assessments calculated using the MKS method. Units are given in parentheses.

	B3LYP	PBE0	B97-2	B97-3
A1. Isotropic NMR shielding constants (ppm)				
d	−15.4	−2.7	−5.5	−1.5
$\|d\|$	20.8	15.4	15.8	15.8
A2. Anisotropic NMR shielding constants (ppm)				
d	9.5	−2.3	0.4	−3.6
$\|d\|$	11.3	11.3	8.8	9.8
A8. Isotropic magnetisabilities (10^{-30} JT^{-2})				
d	3.3	3.4	6.0	3.6
$\|d\|$	3.6	4.3	6.0	5.0
A9. Anisotropic magnetisabilities (10^{-30} JT^{-2})				
d	9.5	8.8	10.8	7.1
$\|d\|$	14.2	11.8	13.2	7.7
A10. Chemical Shifts (ppm)				
$\|d\|(^{13}\mathrm{C})$	4.9	4.3	3.9	4.1
$\|d\|(^{1}\mathrm{H})$	0.14	0.14	0.12	0.11
$\|d\|(^{15}\mathrm{N})$	26.7	22.7	23.9	21.6
$\|d\|(^{17}\mathrm{O})$	58.2	50.6	51.0	47.7
$\|d\|(^{19}\mathrm{F})$	10.6	9.1	8.5	8.9

Table 7.7: KT4 and B97-3 other non-fitted error assessments. Units are given in parentheses.

	KT1	KT2	KT3	KT4	PBE	HCTH	OLYP	B3LYP	PBE0	B97-2	B97-3
A38. Excitation energies (eV)											
d	−1.25	−1.18	−1.23	−1.35	−1.30	−1.29	−1.44	−0.86	−0.66	−0.74	−0.62
$\|d\|$	1.25	1.19	1.23	1.37	1.30	1.30	1.44	0.86	0.66	0.74	0.62
A39. Dipole moments (au)											
d	−0.044	−0.040	−0.043	−0.025	−0.025	−0.020	−0.034	−0.009	−0.002	−0.004	0.003
$\|d\|$	0.054	0.045	0.047	0.035	0.042	0.035	0.046	0.018	0.017	0.015	0.012
A40. Quadrupole moments (au)											
d	0.00	0.01	−0.02	−0.01	−0.05	−0.06	−0.06	−0.08	−0.03	−0.04	−0.04
$\|d\|$	0.18	0.17	0.19	0.18	0.19	0.19	0.20	0.14	0.12	0.13	0.11
A41. Hyperpolarisabilities (au)											
d	8.8	7.4	7.7	6.8	8.0	8.8	10.0	4.0	3.5	3.8	3.6
$\|d\|$	13.9	11.2	9.3	11.8	14.7	13.2	13.7	7.3	4.8	5.2	4.9

7.2.4 Other properties

Finally, we consider electronic excitation energies, multipole moments, and higher order static electric response properties. Errors are presented in Table 7.7. Excitation energies are calculated using time-dependent density functional theory (TD-DFT). If an electric field of frequency ω is applied to a system, the frequency dependent polarisability is given by [230]

$$\alpha_{\lambda\mu}(-\omega;\omega) = -2\sum_{ai\sigma} Z^{\lambda}_{ai\sigma} P^{\mu}_{ai\sigma} \tag{7.2}$$

where $P^{\mu}_{ai\sigma}$ are the dipole integral matrix elements and the linear response matrix elements $Z^{\lambda}_{ai\sigma}$ are found by solving the coupled-perturbed Kohn-Sham equations involving both the electric and magnetic Hessian matrices. The vertical excitation energies are the values of ω for which Eq. 7.2 diverges. The A38 excitation energy set consists of 7 vertical singlet electronic excitation energies from each of the molecules CO and N_2. Following Ref. [231], calculations were performed at near-experimental geometries using the Sadlej basis

set augmented with additional diffuse functions as defined in Ref. [120]. Of the GGAs, the lowest mean absolute error is given by the KT2 functional (1.19 eV) with some deterioration in moving to KT3 and KT4. The hybrid functionals give superior results to the GGAs, with B97-3 giving the lowest error of 0.62 eV. For all the functionals the errors arise primarily from the Rydberg excitations.

The A39 set consists of 10 small molecules with electric dipole moments determined using the Sadlej basis set [191] at experimental geometries (following Ref. [232]). KT4 and HCTH give the joint lowest GGA errors of 0.035 au. Smaller errors are given by the hybrid functionals, with the lowest of 0.012 au given by B97-3.

Like the dipole moment, the electric quadrupole moment is calculated from a simple expectation value

$$\Theta_{\alpha\beta} = \langle\Psi|r_\alpha r_\beta|\Psi\rangle \tag{7.3}$$

The A40 set of 15 quadrupole moments were calculated with respect to the centre of mass, using the Sadlej basis set at experimental geometries (following Ref. [232]). There is little variation in the GGA errors, with KT2 giving the lowest error of 0.17 eV. Hybrids again give smaller errors, with B97-3 the lowest at 0.11 au.

The first electric dipole hyperpolarisability is the next derivative after the polarisability in Eq. 1.93. To calculate this analytically would require an implementation of the third derivative of F_{XC} with respect to the density and gradient of the density. Instead, we calculated the hyperpolarisability tensor components by a finite difference of static polarisabilities in an applied electric field of ± 0.001 au.

The A41 hyperpolarisability set consists of 8 molecules. Following Ref. [233], hyperpolarisabilities were determined at experimental geometries using a Sadlej basis set modified by adding extra basis functions at lone-pair positions. Our error analysis concerns the average static hyperpolarisability $\beta_{||}$, which is defined as [233]

$$\beta_{||} = \frac{3}{5}(\beta_{xxz} + \beta_{yyz} + \beta_{zzz}) \tag{7.4}$$

Table 7.6: Magnetic response property error assessments calculated using the MKS method. Units are given in parentheses.

	B3LYP	PBE0	B97-2	B97-3
A1. Isotropic NMR shielding constants (ppm)				
d	−15.4	−2.7	−5.5	−1.5
$\|d\|$	20.8	15.4	15.8	15.8
A2. Anisotropic NMR shielding constants (ppm)				
d	9.5	−2.3	0.4	−3.6
$\|d\|$	11.3	11.3	8.8	9.8
A8. Isotropic magnetisabilities (10^{-30} JT^{-2})				
d	3.3	3.4	6.0	3.6
$\|d\|$	3.6	4.3	6.0	5.0
A9. Anisotropic magnetisabilities (10^{-30} JT^{-2})				
d	9.5	8.8	10.8	7.1
$\|d\|$	14.2	11.8	13.2	7.7
A10. Chemical Shifts (ppm)				
$\|d\|(^{13}\mathrm{C})$	4.9	4.3	3.9	4.1
$\|d\|(^{1}\mathrm{H})$	0.14	0.14	0.12	0.11
$\|d\|(^{15}\mathrm{N})$	26.7	22.7	23.9	21.6
$\|d\|(^{17}\mathrm{O})$	58.2	50.6	51.0	47.7
$\|d\|(^{19}\mathrm{F})$	10.6	9.1	8.5	8.9

except for CH_3CN where

$$\beta_{||} = \beta_{xxz} + \beta_{yyz} + \beta_{zzz} \tag{7.5}$$

The errors are presented relative to reference *ab initio* values from Ref. [233]. KT3 gives the lowest GGA error of 9.3 au. KT4 gives a higher error of 11.8 au, but this remains superior to the non-KT GGAs. The hybrid functionals all give a better performance, with the lowest error of 4.8 au given by PBE0. B97-3 gives essentially the same error.

To summarise our full assessment, the KT4 GGA and the B97-3 hybrid functional give notable improvements for some properties and maintain the performance of KT3 and B97-2 respectively for most other properties. As expected, they perform particularly well for the fitting data assessments, with notable improvements for both functionals for the BH42 reaction barriers and G2 atomisation energies. KT4 gives significant improvements over KT3 for the A31 and A23 barrier sets, but its performance for the A31 set is disappointing compared to HCTH. B97-3 gives significant improvements over B97-2 for both sets. KT4 is also disappointing for the G3-3 enthalpies of formation, with an error somewhat higher than the (remarkably low) KT3 error. Again, B97-3 improves significantly over B97-2. For the other properties KT4 generally maintains the performance of KT3, although there is some deterioration for the A18 hydrogen bond dimer distances and A21 vibrational wavenumbers. B97-3 generally maintains or improves performance compared to B97-2. It is arguable whether KT4 is overall a truly improved functional compared to KT3. Among the GGAs, KT4 provides the lowest or joint lowest error for 13 out of the 34 assessments, compared to 9 for KT3. Among the hybrids, B97-3 provides the lowest error for 18 of the assessments, compared to 7, 8, and 7 for B3LYP, PBE0, and B97-2 respectively (using MKS values for magnetic properties). We believe that, overall, B97-3 represents a significant improvement over B97-2 and the other hybrid functionals and so should be recommended for chemical applications of the types considered in this chapter.

7.3 Oxirene-ketene interconversion

Given the excellent performance of B97-3 for reaction barriers, we next investigated whether it can provide an accurate description of the potential energy surface for the interconversion from oxirene to ketene, which is known to be a challenging problem for DFT. Scott *et al.* [234] demonstrated from CCSD(T) calculations that the interconversion path contains two transition states (**2** and **4**) between the minima of oxirene (**1**), formylmethylene (**3**), and ketene (**5**). Figure 1 presents a schematic representation of their potential energy surface (taken from Ref. [235]).

The oxirene-ketene potential energy surface was previously studied using DFT by Wilson and Tozer [235]. They observed that the B3LYP and B97-1 functionals failed to predict the transition state **2** and falsely predicted that oxirene was a transition state. The B97-2 functional, however, did predict the correct transition state. These results are consistent with our reaction barrier assessments, for which B97-2 gives superior results to B3LYP. For these barrier assessments B97-3 gives results of higher quality than both B3LYP and B97-2, and so we would expect it to give good results for the oxirene-ketene potential energy surface.

Following Ref. [235], we performed geometry optimisations for the systems **1-5** using the TZ2P basis set. For the transition states **2** and **4** saddle point optimisations were performed and the transition state confirmed by the presence of a single imaginary harmonic vibrational frequency. Relative energies of the structures for B3LYP, PBE0, B97-2, and B97-3 are presented in Table 7.8. Our findings confirm that B3LYP is unable to locate the transition state **2**. The other three hybrids did locate the transition state, with B97-3 giving the closest relative energy to the CCSD(T) results. For structures **3**–**5**, PBE0 gives the closest results to CCSD(T). All the functionals are able to locate transition state **4**. Overall, the performance of B97-3 is comparable to that of B97-2, although PBE0 gives the highest quality results.

We also carried out the same geometry optimisations using the GGA functionals considered in previous assessments. None of the GGAs were able to locate transition state **2**, including KT4. This is further confirmation that the

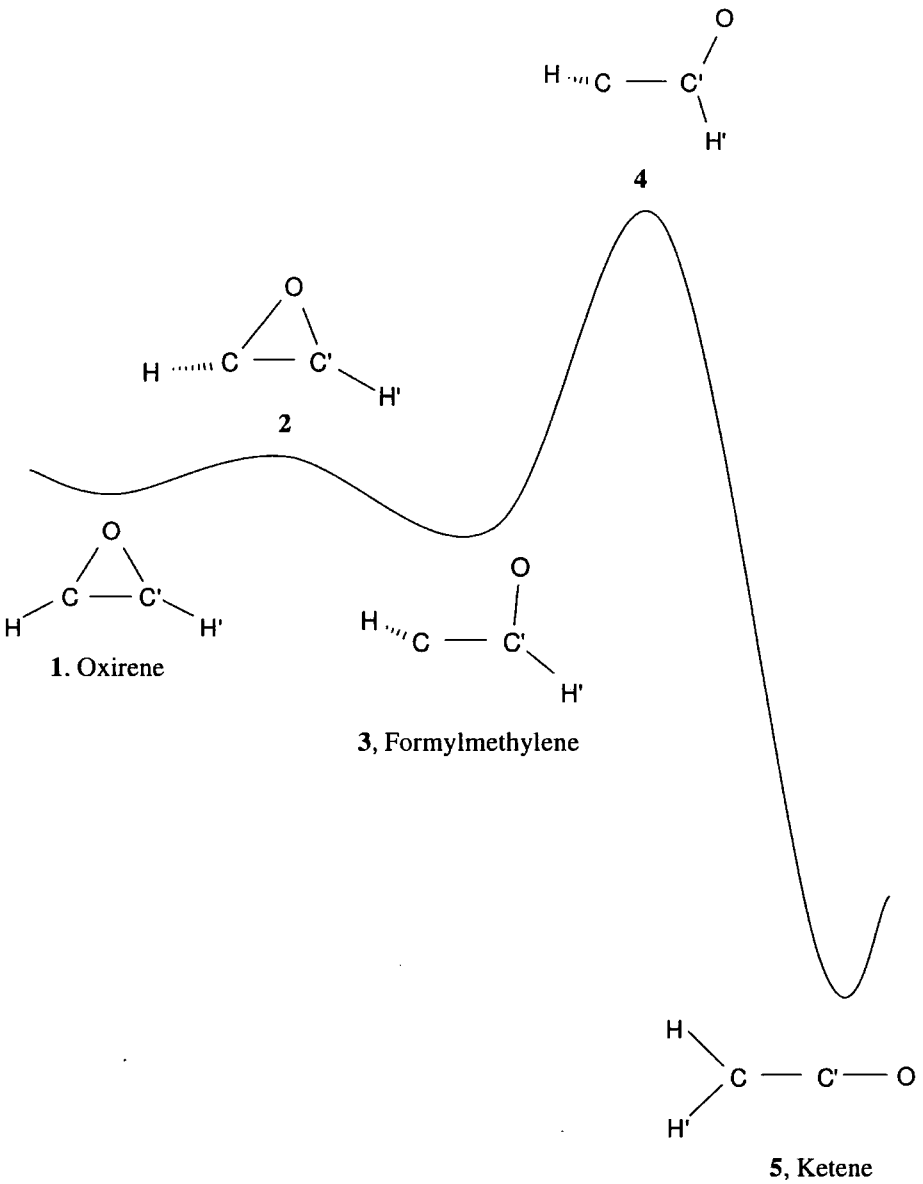

Figure 7.1: Schematic representation of the oxirene-ketene potential energy surface from CCSD(T) calculations [234].

Table 7.8: Relative energies for energy minima and transition states on the oxirene-ketene potential energy surface. All values are in kcal mol^{-1}.

	B3LYP	PBE0	B97-2	B97-3	CCSD(T)[a]
1. Oxirene	0.0	0.0	0.0	0.0	0.0
2.	–	+0.64	+0.31	+0.35	+0.44
3. Formylmethylene	−3.78	−0.74	−2.09	−1.94	−0.50
4.	+0.79	+4.92	+2.94	+2.17	+5.71
5. Ketene	−82.56	−81.20	−81.51	−82.38	−80.02

[a] Mean of CCSD(T)/cc-pVTZ(f) and CCSD(T)/cc-pVTZ(g) single-point energy calculations at CCSD(T)/6-311G(df,p) optimised geometries [234].

performance of KT4 for reaction barriers is not as reliable as that of B97-3.

7.4 Spin-spin coupling constants

Finally, we return to the problem of calculating accurate spin-spin coupling constants within DFT. In a recent study [236], Maximoff *et al.* demonstrated that it was possible to calculate $^1J_{CH}$ couplings accurately using the PBE GGA functional. Over a set of 96 couplings determined using an extensive selection of functionals, PBE gave the lowest mean absolute error of 3.49 Hz. It is surprising that it is possible to obtain such a low error with a GGA functional. This result is not due to the fact that PBE is a non-empirical functional, as the more sophisticated non-empirical TPSS meta-GGA gives a much higher error (24.98 Hz). It is also not a general result for GGAs. In particular the findings of Maximoff *et al.* confirmed our observations of KT2's relatively poor performance, with an error over their set of 20.48 Hz.

B97-2 was the best-performing hybrid functional, giving essentially the same error as PBE (3.51 Hz). It is therefore of interest to establish whether B97-3 maintains this high level of accuracy. We calculated $^1J_{CH}$ couplings for the A42 set of molecules. This is a subset of the molecules considered in Ref. [236] (six molecules were removed for technical reasons). The same aug-cc-pVTZ-J basis set [237] and the same geometries optimised at the PBE0/6-31+G(2df,p) level were used. Following Ref. [236], an *ad-hoc* correction of 5 Hz

was added to the calculated coupling constant to account for rovibrational effects. The calculations were performed using the DALTON program.

Table 7.9 presents results for the PBE, B3LYP, B97-2, and B97-3 functionals. The results for this subset follow the same trend as that observed in Ref. [236], and the overall errors agree to within 1 Hz. PBE gives the lowest mean absolute error of 4.30 Hz, closely followed by B97-2 with 4.37 Hz. There is a minor deterioration with B97-3 ($|d|$ = 4.61 Hz) compared to B97-2, but Maximoff *et al.* considered errors below a margin of ± 2 Hz to be equivalent because of uncertainties caused by solvent, geometry, rovibrational, and finite basis set size effects. B3LYP is significantly worse, with an error of 16.34 Hz.

The performance of PBE is remarkable but the A42 set considers only one type of coupling, which is expected to be relatively easy to calculate as it contains no highly electronegative atoms. To test the more general applicability of PBE, we assessed it for our previous A12 set, which contains more challenging couplings involving systems such as HF, CO, and N_2, and 2- to 5-bond couplings. Results are presented in Table 7.10. PBE continues to perform well for the $^1J_{CH}$ couplings in the set, but it is less accurate for the other types of coupling. PBE gives a mean absolute error of 8.0 Hz, the same error as B3LYP. B97-2 is substantially more accurate, and B97-3 is more accurate still, giving an error of 4.7 Hz. When the problematic HF coupling is removed, PBE surpasses B3LYP, but remains inferior to B97-2 and B97-3. The high performance of PBE therefore appears to be confined to $^1J_{CH}$ couplings, and for other types of coupling a hybrid functional such as B97-3 is preferable. Given the difficulty of computing spin-spin coupling constants, we are extremely encouraged by the success of B97-3.

Table 7.9: Indirect spin-spin coupling constants for the A42 set of $^1J_{CH}$ couplings marked in bold. All values are in Hz.

Mol.	Expt.[a]	PBE	B3LYP	B97-2	B97-3
HC≡CH	249.00	258.41	281.73	259.61	260.65
HC≡C(C_6H_5)	251.00	259.97	283.35	261.10	262.26
HC≡C(CH_2)$_2$OH	253.00	258.69	281.70	259.38	260.62
HC≡C(CH_2OH)	248.00	259.67	282.83	260.45	261.67
HC≡C(CH_3)	248.00	258.07	280.99	258.72	259.88
HC≡N	269.00	262.73	292.06	265.85	270.09
HC≡CF	275.50	290.86	314.59	290.01	290.94
HC≡CCl	270.00	276.10	299.19	276.30	276.98
HC≡C(CH_2Cl)	252.00	262.59	285.90	263.50	264.63
HC≡C(CH_2CN)	251.00	264.35	287.83	265.35	266.23
HC≡CCH=CH_2	251.70	260.29	283.87	261.57	262.60
HC≡C=C≡CH	259.00	266.75	290.97	268.57	269.33
HCH=CH_2	156.20	157.07	173.13	160.38	161.22
HCH=CH(CH_3)	153.10	154.29	170.28	157.62	158.52
H**C**H=CH(CH_3)	157.00	158.40	174.47	161.39	162.32
HCH=**C**H(CH_3)	152.00	151.06	166.11	154.02	155.01
H**C**H=CH−CH=CH_2	159.21	160.04	176.68	163.72	164.44
HCH=CH−CH=CH_2	154.91	155.68	171.93	159.40	160.02
HCH=C=CH_2	168.20	168.55	185.88	171.01	172.45
HCH=FCH	159.18	160.06	176.66	163.07	164.29
H**C**H=FCH	162.16	163.47	179.67	165.63	166.84
HCH=**FC**H	200.20	195.25	214.86	198.63	200.17
HC(O)C_6H_5	173.70	168.83	186.39	172.82	174.76
HCH=O	172.00	172.47	191.50	178.02	179.55
HC(O)CH_3	172.40	166.35	183.47	170.45	171.98
HC(O)NH_2	188.30	186.63	205.34	189.41	191.83
HC(O)N(CH_3)$_2$	191.20	188.11	206.60	190.53	193.03
HCOO(CH_3)	226.20	205.59	226.48	208.26	211.14
HC(O)F	267.00	252.45	276.43	253.92	257.36
trans-**HC**(CH_3)=NOH	163.00	148.06	165.04	152.53	153.77
cis-**HC**(CH_3)=NOH	177.00	184.54	201.27	186.04	187.27
HCH=CHCl	162.64	163.23	180.05	166.48	167.63
HCH=CHCl	160.89	161.73	177.81	164.39	165.39
HCH=**CH**Cl	194.86	194.20	212.88	196.65	198.68
HCH=CH(CN)	163.20	163.94	180.54	167.52	168.26

continued on next page

Table 7.9: *continued*

Mol.	Expt.[a]	PBE	B3LYP	B97-2	B97-3
HCH=CH(CN)	165.43	163.60	180.23	167.24	168.04
HCH=**C**H(CN)	176.74	170.62	187.73	173.11	174.89
HCH=CH(CHO)	156.60	161.82	178.85	165.84	166.76
HCH=CH(CHO)	162.30	160.69	176.98	164.18	164.82
HCH=**C**H(CHO)	162.30	157.82	174.12	160.67	162.08
HCH=**C**H(CCl_3)	169.00	170.15	186.81	172.12	173.86
HCH=CH(CCl_3)	162.00	162.01	178.05	164.92	165.88
trans-**H**C(CH_3)=CH(CH_3)	148.70	148.78	163.81	152.41	153.28
trans-**H**CCl=CHCl	199.10	197.57	217.22	200.57	202.73
cis-H(CN)C=CH(CN)	184.00	174.86	192.70	177.96	179.67
cis-**H**CCl=CHCl	197.30	196.66	215.56	198.90	200.99
HC$H_2$$CH_3$	124.90	124.99	138.03	127.02	128.65
HCH$(CN)_2$	145.20	138.13	152.74	139.20	142.27
HCH$(COOH)_2$	132.00	127.67	141.92	129.17	132.05
HCH(CN)CH_3	135.50	132.08	145.78	133.50	136.03
CH(CN)$(CH_3)_2$	135.50	131.54	144.93	132.90	135.57
HCH_2C(O)OCH_2CH_3	130.30	125.39	139.06	127.13	129.28
HCH_2C(O)C_6H_5	125.70	134.96	148.45	136.03	138.07
HCH_3	125.00	126.45	139.82	128.59	129.91
HCH_2CN	136.10	133.62	147.70	135.11	137.46
HCH_2COOH	130.00	125.70	139.32	127.31	129.50
HCH_2COH	127.00	128.79	142.29	130.45	132.34
HCH_2C≡CH	132.00	130.14	143.88	131.82	133.90
HCH(OH)HC$(CH_3)_2$	140.00	134.27	148.75	137.12	139.06
HC$H_2$$NO_2$	146.70	138.78	153.61	140.56	142.90
HCHF(CN)	166.00	155.52	171.72	157.92	160.54
HCH(OH)(CF_3)	147.50	140.80	156.25	143.47	145.85
HCH_2OCHO	147.00	144.23	159.87	147.17	149.36
(**H**CH_2)$_2$O	140.00	135.11	150.02	138.37	140.08
(**H**CH_2)$_2$NC(O)H	138.00	134.73	148.72	136.93	138.72
HCH(N$(CH_3)_2$)$_2$	136.60	138.21	152.49	140.42	142.49
HCF**H**C_6H_5	151.00	147.18	162.53	149.87	152.03
HCH$(NO_2)_2$	169.40	163.51	180.83	165.42	168.55
HCH_2OH	141.00	141.03	155.48	143.48	145.14
HC$H_2$$NH_2$	133.00	132.16	145.98	134.46	136.16
HCH_2OC_6H_5	143.00	138.98	154.13	141.98	143.96

continued on next page

Table 7.9: *continued*

Mol.	Expt.[a]	PBE	B3LYP	B97-2	B97-3
$HCHF_2$	184.50	177.48	195.26	181.02	183.01
HCF_3	239.10	234.17	253.53	235.01	236.59
$C_6H_5NH_2$ (o)	156.01	155.75	170.55	157.61	159.01
$C_6H_5NH_2$ (m)	156.90	158.03	173.15	160.20	161.65
$C_6H_5NH_2$ (p)	160.46	159.32	174.32	161.31	162.71
C_6H_5CHO (o)	160.95	158.10	173.01	160.02	161.41
C_6H_5CHO (m)	161.92	161.15	176.38	163.25	164.72
C_6H_5CHO (p)	160.43	159.20	174.37	161.51	162.90
C_6H_5OH (o)	158.35	153.62	168.65	155.73	157.22
C_6H_5OH (m)	158.99	158.15	173.17	160.29	161.72
C_6H_5OH (p)	160.84	161.63	176.74	163.45	164.89
$C_6H_3F_3$	168.28	167.29	183.66	169.10	171.06
C_6H_6	158.50	158.59	173.61	160.74	162.14
C_6H_5F (o)	155.00	161.95	177.59	163.95	165.58
C_6H_5F (m)	163.00	159.96	175.06	162.07	163.49
C_6H_5F (p)	161.00	161.26	176.44	163.21	164.66
$C_4H_4N_2$	206.00	203.61	221.07	204.57	206.33
d		−0.77	16.34	1.53	3.18
$\|d\|$		4.30	16.34	4.37	4.61

[a] Ref. [236]

Table 7.10: Indirect spin-spin coupling constants determined using the Huzinaga-III-su3 basis set. All values are in Hz.

Mol.		PBE	B3LYP	B97-2	B97-3	Expt.[a]
HF	$^1J_{HF}$	369.0	439.3	444.7	458.0	538.0
CO	$^1J_{CO}$	25.4	19.4	18.4	17.8	15.7
$^{14}N^{15}N$	$^1J_{NN}$	3.8	1.8	2.0	1.1	1.7
H_2O	$^1J_{OH}$	−67.1	−76.9	−74.5	−75.5	−86.0
	$^2J_{HH}$	−5.5	−8.1	−8.3	−7.4	−8.2
$HC^{15}N$	$^1J_{CN}$	−9.8	−18.1	−17.7	−20.9	−20.5
	$^1J_{CH}$	256.6	284.4	257.7	263.9	262.2
	$^2J_{NH}$	−5.5	−7.5	−6.2	−7.8	−8.2
$^{14}NH_3$	$^1J_{NH}$	40.8	45.4	42.3	43.5	44.1
	$^2J_{HH}$	−8.3	−10.4	−9.5	−9.4	−10.3
CH_4	$^1J_{CH}$	119.7	132.2	120.5	123.2	120.0
	$^2J_{HH}$	−12.0	−13.3	−11.4	−11.5	−12.1
C_2H_2	$^1J_{CC}$	189.7	204.9	201.9	199.6	184.8
	$^1J_{CH}$	252.2	274.2	251.5	254.7	243.0
	$^2J_{CH}$	54.0	55.9	50.6	54.3	53.1
	$^3J_{HH}$	10.3	11.0	10.3	10.0	9.7
C_2H_4	$^1J_{CC}$	63.4	73.1	71.8	70.6	66.7
	$^1J_{CH}$	151.1	166.1	152.8	155.3	151.2
	$^2J_{CH}$	−0.6	−1.4	−2.1	−1.0	−1.2
	$^2J_{HH}$	3.4	3.4	2.3	3.4	2.0
	$^3J_{cis}$	12.0	13.1	11.4	11.7	10.5
	$^3J_{trans}$	18.9	20.2	18.0	18.3	16.7
C_2H_6	$^1J_{CC}$	18.5	24.5	23.5	23.6	34.5
	$^1J_{CH}$	123.9	136.4	124.5	127.5	125.2
	$^2J_{CH}$	−4.1	−4.6	−4.4	−4.3	−4.7
	$^2J_{HH}$	−9.0	−10.0	−8.9	−8.7	
C_6H_6	$^1J_{CC}$	51.9	60.1	58.3	58.5	56.1
	$^2J_{CC}$	−0.7	−1.8	−2.7	−1.6	−1.7
	$^3J_{CC}$	10.5	11.2	11.6	10.5	9.4
	$^1J_{CH}$	152.6	166.8	153.3	156.4	153.8
	$^2J_{CH}$	2.4	2.0	1.2	2.0	1.4
	$^3J_{CH}$	7.4	8.1	7.7	7.6	7.0
	$^4J_{CH}$	−0.8	−1.3	−1.5	−1.2	−1.0
	$^3J_{HH}$	8.1	8.8	7.7	7.9	7.0
	$^4J_{HH}$	1.5	1.3	1.1	1.3	1.2
	$^5J_{HH}$	0.6	0.8	0.7	0.6	0.6
$\|d\|$ (all)		8.0	8.0	5.1	4.7	
$\|d\|$[b]		3.3	5.3	2.5	2.5	
$\|d\|$% (all)		23.7	15.2	14.3	11.3	

[a] All experimental values include vibrational corrections (calculated at the B3LYP level), except C_2H_6. See Refs. [176,177].
[b] Excluding $^1J_{HF}$ in HF

Chapter 8

Conclusions

With the development of accurate generalised gradient approximation (GGA) and hybrid functionals, Kohn-Sham density functional theory has rapidly become the most popular quantum mechanical method for chemical applications. However, the approximate functionals in the literature do not offer the same level of accuracy for all properties. The calculation of nuclear magnetic resonance (NMR) shielding constants is a notable failure for conventional DFT functionals. In this thesis, we demonstrated that it was possible to obtain highly accurate NMR shielding constants within the GGA formalism by the addition of a simple gradient-corrected term (KT exchange) to the local density approximation (LDA) functional. To the best of our knowledge this is the first time that shielding constants of this accuracy have been calculated using conventional DFT. These functionals, denoted KT1 and KT2, were also found to give excellent performance for magnetisabilities and chemical shifts. However, they offered no improvement over conventional GGAs for indirect spin-spin coupling constants, and they were not competitive with the best GGAs for non-magnetic properties such as atomisation energies, although KT2 gave good results for molecular bond length optimisations.

To improve upon KT2, a third functional was developed after extensive investigations into the form of the exchange and correlation components and the choice of fitting data. The new functional, KT3, featured an improved correlation functional and extra flexibility in the exchange representation form. The KT exchange term was retained to ensure high quality shielding constants.

KT3 also provides atomisation energies, ionisation potentials, electron affinities, proton affinities, bond angles, and electronic polarisabilities that are comparable to or surpass those of the best conventional GGAs. Its performance for equilibrium molecular bond lengths and diatomic harmonic vibrational wave numbers is as good as the best hybrid functionals. KT3 was also found to give excellent performance for geometry optimisations and shielding constant calculations of selenium-containing molecules, and is competitive with the non-empirical PW91 GGA for solid state optimised lattice constants, bulk moduli, and electronic band gaps.

KT3 is not competitive with the best GGAs for classical chemical reaction barriers, but performance could be improved by including barrier heights in the fitting data. However, it was observed that the KT3 form was not sufficiently flexible to obtain high quality reaction barriers whilst maintaining the good performance of KT3 for other properties. A more flexible functional form based on Becke's B97 exchange-correlation expansion was used, but with the addition of the KT exchange term to maintain shielding constant performance. The resulting functional, KT4, was fitted to a large and diverse set of fitting data in order to explore the limits of accuracy achievable within the GGA formalism. For assessments in the fitting data, KT4 performed extremely well, in particular for reaction barriers and atomisation energies. We also assessed KT4 for an extensive set of non-fitted data. In general, KT4 maintained the high accuracy of KT3, but its performance for non-fitted reaction barriers and thermochemistry fell short of our expectations.

We next attempted to develop a hybrid functional that was able to give high quality performance for reaction barriers and provide competitive results for other properties. This functional, B97-3, was also based on the B97 form, but KT exchange was removed because it did not prove possible to obtain high quality shielding constants using the conventional coupled formalism. B97-3 provided very high quality reaction barriers and atomisation energies for both the fitted and non-fitted data, and therefore appeared to be a more generally applicable functional than KT4. B97-3 also gave performance competitive with (and in many cases superior to) the best hybrid functionals for ionisation potentials, electron affinities, proton affinities, total energies, equi-

librium molecular bond lengths, diatomic harmonic vibrational wavenumbers, electronic excitation energies, dipole moments, quadrupole moments, polarisabilities and hyperpolarisabilities. Furthermore, when magnetic properties were calculated using the more appropriate uncoupled MKS formalism, the results were competitive with the KT GGAs. B97-3 also maintained the high quality performance of B97-2 for the oxirene-ketene potential energy surface and indirect spin-spin coupling constants.

In summary, the KT3 functional is recommended for the calculation of magnetic properties (with the exception of spin-spin coupling constants) and is an excellent general-purpose functional for situations where hybrids cannot be used. The B97-3 hybrid functional is recommended for general purpose calculations, but especially for reaction barriers and thermochemical properties. If the appropriate uncoupled method is available, B97-3 also provides high-quality magnetic properties. For systems such as those considered in this study, B97-3 is the most accurate hybrid functional available in the literature. Further investigation of B97-3 is essential.

Appendix A

Assessment systems

This appendix lists the systems and basis sets of the assessment sets used in this thesis. The value in parenthesis gives the number of quantities in each assessment.

A1. Isotropic NMR shielding constants [nuclei]

Huzinaga IV basis
HF [F], H_2O [O], CH_4 [C], CO [C,O], N_2 [N], F_2 [F], O_3 [O,O′], PN [P,N], H_2S [S], NH_3 [N], HCN [C,N], C_2H_2 [C], C_2H_4 [C], H_2CO [C,O], N_2O [N,N′,O], CO_2 [C,O], OF_2 [O], H_2CNN [C,N,N′], HCl [Cl], SO_2 [S,O], PH_3 [P]. {32}

A2. Anisotropic NMR shielding constants [nuclei]

Huzinaga IV basis
HF [F], NH_3 [N], CO [C,O], N_2 [N], F_2 [F], H_2CO [C], PN [P,N], HCl [Cl], PH_3 [P]. {11}

A3. Atomisation energies

TZ2P basis
H_2, LiH, BeH, CH, $CH_2(^1A)$, $CH_2(^3B)$, CH_3, CH_4, NH, NH_2, NH_3, OH, H_2O, HF, Li_2, LiF, C_2H_2, C_2H_4, C_2H_6, CN, HCN, CO, HCO, H_2CO, CH_3OH, N_2, N_2H_4, O_2, H_2O_2, F_2, CO_2, $SiH_2(^1A)$, $SiH_2(^3B)$, SiH_3, SiH_4, PH_2, PH_3, HCl,

Na_2, Si_2, P_2, S_2, Cl_2, NaCl, SiO, CS, SO, ClO, ClF, CH_3Cl, CH_3SH, HOCl, SO_2, HF^+, HCl^+, CO^+, N_2^+, O_2^+, P_2^+, S_2^+, Cl_2^+. {61}

A4. Ionisation potentials

TZ2P basis
Na, Mg, Al, Si, P, S, Cl. {7}

A5. Total atomic and ionic energies

TZ2P basis
H, He, Li, Be, B, C, N, O, F, Ne, Li^+, Be^+, B^+, C^+, N^+, O^+, F^+, Ne^+. {18}

A6. G2 subset bond lengths

TZ2P basis
H_2, LiH, BeH, CH, $CH_2(^1A)$, $CH_2(^3B)$, CH_3, CH_4, NH, NH_2, NH_3, OH, H_2O, HF, Li_2, LiF, C_2H_2, C_2H_4, CN, HCN, CO, HCO, H_2CO, N_2, O_2, H_2O_2, F_2, CO_2, HCl, Na_2, Si_2, P_2, S_2, Cl_2, NaCl, SiO, CS, SO, ClO, ClF. {46}

A7. Diatomic bond lengths

6-311+G(2df) basis
Li_2, LiNa, LiK, Na_2, NaK, K_2, N_2, NP, NAs, P_2, PAs, As_2, F_2, FCl, FBr, Cl_2, ClBr, Br_2, LiF, LiCl, LiBr, NaF, NaCl, NaBr, KF, KCl, KBr, BF, BCl, BBr, AlF, AlCl, AlBr, GaF, GaCl, GaBr, CO, CS, CSe, SiO, SiS, SiSe, GeO, GeS, GeSe. {45}

A8. Isotropic magnetisabilities

Huzinaga IV basis
HF, H_2O, CH_4, CO, N_2, F_2, O_3, NH_3, HCN, C_2H_2, H_2CO, CO_2. {12} (excluding O_3 and CO_2 for L-CCD errors)

A9. Anisotropic magnetisabilities

Huzinaga IV basis
HF, H_2O, CO, N_2, F_2, O_3, NH_3, HCN, C_2H_2, H_2CO. {13} (excluding H_2O $\Delta\zeta_1$, O_3, and H_2CO $\Delta\zeta_2$ for L-CCD errors, and F_2 for MCSCF errors)

A10. Isotropic NMR chemical shifts [nuclei]

8s6p3d/6s3p basis
CO [C,O], CO_2 [C,O], F_2 [F], OF_2 [O,F], HOF [H,F], NF_3 [F], H_2O [O,H], H_2O_2 [O], HCN [C,N,H], N_2 [N], N_2O [N(terminal),N(middle),O], N_2O_3 [N(NO),N(NO_2),O(NO),O(NO_2)], O_3 [O(terminal),O(middle)], HF [F,H], NH_3 [N,H], CH_4 [C,H], C_2H_6 [C,H], C_2H_4 [C,H], CH_2CCH_2 [C(middle),C(terminal)], C_2H_2 [C,H], H_2CO [O,C,H], CH_3CHO [C(C(O)H),C(CH_3),O,H(CH_3)], CH_2CO [C(CO),C(CH_2)], CH_2CHCHO [O,C(C(O)H),C(CH),C(CH_2)], $(CH_2)_2O$ [C,O], C_3O_2 [C(middle),C(terminal)], CH_3NH_2 [C,N,H(NH_2)], CH_2NN [C,N(middle),N(terminal)], CH_3CN [C(CH_3),C(NC),N,H], CH_3NC [C(CH_3),C(NC),N], CH_3NO_2 [C,N,O,H], CH_3F [C,F,H], CH_2F_2 [C,F], CHF_3 [C,F], CF_4 [C,F], COF_2 [C,F]. {85}

A11. GIAO isotropic shielding constants [nuclei]

Huzinaga III basis
CH_2 [H,C], CF_2 [C,F], CF_4 [C,F], NO_2^- [N,O], linear-CO_2 [C,O], cyclic-CO_2 [C,O], linear-N_2O [N_{term},N_{cent},O], cyclic-N_2O [N,O], *cis*-N_2F_2 [N,F], *trans*-N_2F_2 [N,F], C_6H_6 [C], $C_2H_3^+$ [C_α,C_β], $C_7H_9^+$ [C_α,C_β,$C_{\beta'}$,C_γ,$C_{\gamma'}$], $C_6H_5N_2^+$ [N_α,N_β]. {31}

A12. Indirect spin-spin coupling constants [coupling]

Huzinaga III-su3 basis
HF [$^1J_{HF}$], CO [$^1J_{CO}$], $^{14}N^{15}N$ [$^1J_{NN}$], H_2O [^1J_O, $^2J_{HH}$], $HC^{15}N$ [$^1J_{CN}$, $^1J_{CH}$, $^2J_{NH}$], $^{14}NH_3$ [$^1J_{NH}$, $^2J_{HH}$], CH_4 [$^1J_{CH}$, $^2J_{HH}$], C_2H_2 [$^1J_{CC}$, $^1J_{CH}$, $^2J_{CH}$, $^3J_{HH}$], C_2H_4 [$^1J_{CC}$, $^1J_{CH}$, $^2J_{CH}$, $^2J_{HH}$, $^3J_{cis}$, $^3J_{trans}$], C_2H_6 [$^1J_{CC}$, $^1J_{CH}$, $^2J_{CH}$], C_6H_6 [$^1J_{CC}$, $^2J_{CC}$, $^3J_{CC}$, $^1J_{CH}$, $^2J_{CH}$, $^3J_{CH}$, $^4J_{CH}$, $^3J_{HH}$, $^4J_{HH}$, $^5J_{HH}$]. {35}

A13. G2-1 atomisation energies

6-311+G(3df,2p) basis
LiH, BeH, CH, $CH_2(^3B)$, $CH_2(^1A)$, CH_3, CH_4, NH, NH_2, NH_3, OH, H_2O, HF, $SiH_2(^1A)$, $SiH_2(^3B)$, SiH_3, SiH_4, PH_2, PH_3, H_2S, HCl, Li_2, LiF, C_2H_2, C_2H_4, C_2H_6, CN, HCN, CO, HCO, H_2CO, CH_3OH, N_2, N_2H_4, NO, O_2, H_2O_2, F_2, CO_2, Na_2, Si_2, P_2, S_2, Cl_2, NaCl, SiO, CS, SO, ClO, ClF, Si_2H_6, CH_3Cl, CH_3SH, HOCl, SO_2. {55}

A14. G2-2 atomisation energies

6-311+G(3df,2p) basis
BF_3, BCl_3, AlF_3, $AlCl_3$, CF_4, CCl_4, OCS, CS_2, COF_2, SiF_4, $SiCl_4$, N_2O, ClNO, NF_3, PF_3, O_3, F_2O, ClF_3, C_2F_4, C_2Cl_4, CF_3CN, propyne, allene, cyclopropene, propene, cyclopropane, propane, butadiene, 2-butyne, methylene cyclopropane, bicyclobutane, cyclobutene, cyclobutane, isobutene, *trans* butane, isobutane, spiropentane, benzene, CH_2F_2, CHF_3, CH_2Cl_2, $CHCl_3$, methylamine, methyl cyanide, nitromethane, methyl nitrite, methyl silane, formic acid, methyl formate, acetamide, aziridine, cyanogen, dimethylamine, *trans* ethylamine, ketene, oxirane, acetaldehyde, glyoxal, ethanol, dimethylether, thiooxirane, dimethyl sulfoxide, ethanethiol, dimethyl sulfide, CH_2CHF, ethyl chloride, vinyl chloride, acrylonitrile, acetone, acetic acid, acetyl fluoride, acetyl chloride, propyl chloride, isopropanol, methyl ethyl ether, trimethylamine, furan, thiophene, pyrrole, pyridine, H_2, SH, CCH, C_2H_3, CH_3CO, H_2COH, CH_3O, CH_3CH_2O, CH_3S, C_2H_5, $(CH_3)_2CH$, $(CH_3)_3C$, NO_2. {93}

A15. G2-1 ionisation potentials

6-311+G(3df,2p) basis
Li, Be, B, C, N, O, F, Na, Mg, Al, Si, P, S, Cl, CH_4, NH_3, OH, H_2O, HF, SiH_4, PH, PH_2, PH_3, SH, $H_2S(^2B)$, HCl, C_2H_2, C_2H_4, CO, $N_2(^2\Sigma)$, O_2, P_2, S_2, Cl_2, ClF, CS. {36} (H_2S (^2A) and N_2 ($^2\Pi$) excluded due to convergence problems)

A16. G2-1 electron affinities

6-311+G(3df,2p) basis
C, O, F, Si, P, S, Cl, CH, CH_2, CH_3, NH, NH_2, OH, SiH, SiH_2, SiH_3, PH, PH_2, SH, O_2, NO, CN, PO, S_2, Cl_2. {25}

A17. G2-1 proton affinities

6-311+G(3df,2p) basis
NH_3, H_2O, C_2H_2, SiH_4, PH_3, H_2S, HCl. {7}

A18. Hydrogen bond dimer distances

TZ2P basis
$(HF)_2$, $(HCl)_2$, $(H_2O)_2$, (CO)(HF), (OC)(HF). {5}

A19. Other bond lengths

Wachters basis (transition metals)
TZ2P basis (other atoms)
FOOF, FNO_2, O_3, FO_2, $Cr(CO)_6$, $Ni(CO)_4$. {11}

A20. Bond angles

TZ2P basis
CH_2 (^{3}B), CH_2 (^{1}A), NH_2, NH_3, H_2O, C_2H_4, HCO, H_2CO, H_2O_2, FOOF, FNO_2, O_3, FO_2. {13}

A21. Diatomic harmonic vibrational wavenumbers

As A7.

A22. Isotropic electronic polarisabilities

Sadlej basis
HF, H_2O, N_2, CO, F_2, NH_3, CO_2, CH_4, C_2H_4, PH_3, H_2S, SO_2, HCl, Cl_2. {14}

A23. Classical chemical reaction barriers [transition state]

TZ2P basis
H + H_2 [H−H_2]; CH_4+CH_3 [H_3CH−CH_3]; H_2+CH_3 [HH−CH_3]; H_2+NH_2 [HH−NH_2]; H_2+OH [HH−OH]; CH_4+OH [H_3CH−OH]; H+N_2 [H−N_2]; N+O_2 [N−O_2]; O+HCl [O−HCl]; H+N_2O [H−N_2O]; H+N_2O [NNOH]; H+N_2O [H−ON_2]; H+NO [H−NO]; O+H_2 [O−H_2]; H+HF [H−FH]; H+HCl [H−ClH]. {16}

A24. Selenium bond lengths

6-311+G(2df,2pd) basis
$Se(CH_3)_2$, SeH_2, SeCO, H_2CSe, CSe_2, SeF_6, CH_3SeH, $(CH_3)_2CSe$, C_4H_4Se, $SeOF_2$, $(SiH_3)_2Se$, SeF_4, trans-C_2H_5SeH, gauche-C_2H_5SeH. {25}

A25. Selenium bond angles

6-311+G(2df,2pd) basis
$Se(CH_3)_2$, SeH_2, H_2CSe, CH_3SeH, $(CH_3)_2CSe$, C_4H_4Se, $SeOF_2$, $(SiH_3)_2Se$, SeF_4, trans-C_2H_5SeH, gauche-C_2H_5SeH. {14}

A26. Selenium isotropic NMR shielding constants

See text for discussion of basis sets
$Se(CH_3)_2$, SeH_2, SeCO, H_2CSe, CSe_2, SeF_6, CH_3SeH. {7}

A27. Selenium anisotropic NMR shielding constants

See text for discussion of basis sets
$Se(CH_3)_2$, SeH_2, SeCO, H_2CSe, CSe_2. {5}

A28. Solid state calculations

C, Si, Ge, SiC, AlN, AlP, AlAs, GaN, GaP, GaAs. {10}

A29. BH42/04 classical chemical reaction barriers

6-311+G(3df,2p) basis
H + HCl → H_2 + Cl, OH + H_2 → H + H_2, CH_3 + H_2 → H + CH_4, OH +

$CH_4 \rightarrow CH_3 + H_2O$, $H + H_2 \rightarrow H_2 + H$, $OH + NH_3 \rightarrow H_2O + NH_2$, $HCl + CH_3 \rightarrow Cl + CH_4$, $OH + C_2H_6 \rightarrow H_2O + C_2H_5$, $F + H_2 \rightarrow HF + H$, $O + CH_4 \rightarrow OH + CH_3$, $H + PH_3 \rightarrow PH_2 + H_2$, $H + ClH' \rightarrow HCl + H'$, $H + HO \rightarrow H_2 + O$, $H +$ *trans*-$N_2H_2 \rightarrow H_2 + N_2H$, $H + H_2S \rightarrow H_2 + HS$, $O + HCl \rightarrow OH + Cl$, $NH_2 + CH_3 \rightarrow CH_4 + NH$, $NH_2 + C_2H_5 \rightarrow C_2H_6 + NH$, $C_2H_6 + NH_2 \rightarrow NH_3 + C_2H_5$, $NH_2 + CH_4 \rightarrow CH_3 + NH_3$, *s-trans cis*-$C_5H_8 \rightarrow$ *s-trans cis*-C_5H_8. {42}

A30. Fitting set of diatomic bond lengths

TZ2P basis

H_2, BeH, CH, OH, P_2, O_2, LiH, NH, CN, CO, F_2, HCl, Li_2, Na_2.

6-311+G(2df) basis

LiK, NAs, Cl_2, NaBr, AlF, SiS, NaK, NP, FBr, KF, BCl, GeO. {26}

A31. NHTBH38/04 classical chemical reaction barriers

6-311+G(3df,2p) basis

Heavy-atom transfer reactions

$H + N_2O \rightarrow OH + N_2$, $H + FH \rightarrow HF + H$, $H + ClH \rightarrow HCl + H$, $H + FCH_3 \rightarrow HF + CH_3$, $H + F_2 \rightarrow HF + F$, $CH_3 + FCl \rightarrow CH_3F + Cl$.

Nucleophilic substitution reactions

$F^- + CH_3F \rightarrow FCH_3 + F^-$, $F^- \cdots CH_3F \rightarrow FCH_3 \cdots F^-$, $Cl^- + CH_3Cl \rightarrow ClCH_3 + Cl^-$, $Cl^- \cdots CH_3Cl \rightarrow ClCH_3 \cdots Cl^-$, $F^- + CH_3Cl \rightarrow FCH_3 + Cl^-$, $F^- \cdots CH_3Cl \rightarrow FCH_3 \cdots Cl^-$, $OH^- + CH_3F \rightarrow HOCH_3 + F^-$, $OH^- \cdots CH_3F \rightarrow HOCH_3 \cdots F^-$.

Unimolecular and association reactions

$H + N_2 \rightarrow HN_2$, $H + CO \rightarrow HCO$, $H + C_2H_4 \rightarrow CH_3CH_2$, $CH_3 + C_2H_4 \rightarrow CH_3CH_2CH_2$, $HCN \rightarrow HNC$. {38}

A32. G3-3 enthalpies of formation

6-311+G(3df,2p) basis

1,2-butadiene, isoprene, cyclopentane, *n*-pentane, neopentane, 1,3-cyclohexadiene, 1,4-cyclohexadiene, cyclohexane, *n*-hexane, 3-methyl pentane, toluene, *n*-heptane,

1,3,5,7-cyclooctatetraene, *n*-octane, napthalene, azulene, methyl acetate, *t*-butanol, aniline, phenol, divinyl ether, tetrahydrofuran, cyclopentanone, 1,4-benzoquinone, pyrimidine, dimethyl sulfone, chlorobenzene, succinonitrile, pyrazine, acetyl acetylene, crotonaledehyde, acetic anhydride, 2,5-dihydrothiophene, 2-methyl propanenitrile, methyl ethyl ketone, isobutyraldehyde, 1,4-dioxane, tetrahydrothiophene, *t*-butyl chloride, *n*-butyl chloride, pyrrolidine, 2-nitrobutane, diethyl ester, 1,1-dimethoxy ethane, *t*-butanethiole, diethyl disulfide, *t*-butylamine, tetramethyl silane, 2-methyl thiophene, *N*-methyl pyrrole, tetrahydropyran, diethyl ketone, isopropyl acetate, tetrahydrothiopyran, piperidine, *t*-butyl methyl ether, 1,3-difluorobenzene, 1,4-difluorobenzene, fluorobenzene, diisopropyl ether, PF_5, SF_6, P_4, SO_3, SCl_2, $POCl_3$, PCl_5, Cl_2O_2S, PCl_3, Cl_2S_2, $SiCl_2$, CF_3Cl, C_2F_6, CF_3, C_6H_5. {75}

A33. G2-2 ionisation potentials

6-311+G(3df,2p) basis
H, He, Ne, Ar, BF_3, BCl_3, B_2F_4, CO_2, CF_2, OCS, CS_2, CH_2, CH_3, C_2H_5, C_3H_4, $CH_2{=}C{=}CH_2$, $(CH_3)_2CH$, C_6H_6, $C_6H_5CH_3$, HCO, CH_2OH, CH_3O, CH_3OH, CH_3F, CH_2S, CH_2SH, CH_3SH, CH_3Cl, C_2H_5OH, CH_3CHO, CH_3OF, C_2H_4S, $(CN)_2$, C_4H_4O, C_4H_4NH, C_6H_5OH, $C_6H_5NH_2$, B_2H_4, NH, NH_2, N_2H_2, N_2H_3, HOF, SiH_2, SiH_3, Si_2H_2, Si_2H_4, Si_2H_5, Si_2H_6. {49} (CN excluded as CN^+ is an open-shell singlet.)

A34. G2-2 electron affinities

6-311+G(3df,2p) basis
Li, B, Na, Al, CCO, CF_2, NCO, NO_2, O_3, OF, SO_2, S_2O, CCH, $CH_2{=}CH$, $CH_2{=}C{=}C$, $CH_2C{=}CH$, $CH_2{=}CHCH_2$, HCO, CHF, CH_3O, CH_3S, CH_2S, CH_2CN, CH_2NC, HCCO, CH_2CHO, CH_3CO, CH_3CH_2O, CH_3CH_2S, LiH, HNO, HOO. {32} (C_2 excluded as it is an open-shell singlet.)

A35. Non-fitted G2 subset bond lengths

As A6 but with those molecules in A30 removed. {31}

A36. Non-fitted diatomic bond lengths

As A7 but with those molecules in A30 removed. {28}

A37. Radical bond lengths

TZ2P basis
BH^+, NH^+, OH^+, BeF, BN, BO, C_2^+, CF, NF, NO, OF, F_2^+, Al_2, SiCl, NS, PO. {16}

A38. Electronic excitation energies [transition]

Augmented Sadlej basis
CO
$F\,^1\Sigma^+$ [$\sigma \rightarrow 3d\,\sigma$], $E\,^1\Pi$ [$\sigma \rightarrow 3p\,\pi$], $C\,^1\Sigma^+$ [$\sigma \rightarrow 3p\,\sigma$], $B\,^1\Sigma^+$ [$\sigma \rightarrow 3s$], $D\,^1\Delta$ [$\pi \rightarrow \pi^*$], $I\,^1\Sigma^-$ [$\pi \rightarrow \pi^*$], $A\,^1\Pi$ [$\sigma \rightarrow \pi^*$].
N2
$^1\Pi_u$ [$\pi_u \rightarrow 3s\,\sigma_g$], $^1\Sigma_u^+$ [$\sigma \rightarrow 3p\,\sigma_u$], $^1\Pi_u$ [$\sigma \rightarrow 3p\,\pi_u$], $^1\Sigma_g^+$ [$\sigma \rightarrow 3s\,\sigma_g$], $^1\Delta_u$ [$\pi_u \rightarrow \pi_g$], $^1\Sigma_u^-$ [$\pi_u \rightarrow \pi_g$], $^1\Pi_g$ [$\sigma_g \rightarrow \pi_g$]. {14}

A39. Electric dipole moments

Sadlej basis
CO, H_2O, H_2S, HCl, HF, LiH, LiF, NH_3, PH_3, SO_2. {10}

A40. Electric quadrupole moments

Sadlej basis
C_2H_4 (*xx*, *zz*), CO, CO_2, CS_2, H_2, H_2O (*xx*, *zz*), HCl, HF, N_2, NH_3, PH_3, SO_2 (*xx*, *zz*). {15}

A41. Static electric hyperpolarisabilities

Augmented Sadlej basis
HF, H_2O, NH_3, CO, H_2S, H_2CO, CH_3F, CH_3CN. {8}

A42. $^1J_{CH}$ spin-spin coupling constants

aug-cc-pVTZ-J basis
HC≡CH, **HC**≡C(C_6H_5), **HC**≡C(CH_2)$_2$OH, **HC**≡C(CH_2OH), **HC**≡C(CH_3), **HC**≡N, **HC**≡CF, **HC**≡CCl, **HC**≡C(CH_2Cl), **HC**≡C(CH_2CN), **HC**≡CCH=CH_2, **HC**≡C=C≡CH, **HC**H=CH_2, **HC**H=CH(CH_3), H**CH**=CH(CH_3), HCH=**CH**(CH_3), H**CH**=CH−CH=CH_2, **HC**H=CH−CH=CH_2, **HC**H=C=CH_2, **HC**H=FCH, H**CH**=FCH, HCH=F**CH**, **HC**(O)C_6H_5, **HC**H=O, **HC**(O)CH_3, **HC**(O)NH_2, **HC**(O)N(CH_3)$_2$, **HC**OO(CH_3), **HC**(O)F, *trans*-**HC**(CH_3)=NOH, *cis*-**HC**(CH_3)=NOH, **HC**H=CHCl, H**CH**=CHCl, HCH=**CH**Cl, **HC**H=CH(CN), H**CH**=CH(CN), HCH=**CH**(CN), **HC**H=CH(CHO), H**CH**=CH(CHO), HCH=**CH**(CHO), HCH=**CH**(CCl_3), H**CH**=CH(CCl_3), *trans*-**HC**(CH_3)=CH(CH_3), *trans*-**HC**Cl=CHCl, *cis*-H(CN)C=CH(CN), *cis*-**HC**Cl=CHCl, **HC**H_2CH_3, **HC**H(CN)$_2$, **HC**H(COOH)$_2$, **HC**H(CN)CH_3, **CH**(CN)(CH_3)$_2$, **HC**H_2C(O)OCH_2CH_3, **HC**H_2C(O)C_6H_5, **HC**H_3, **HC**H_2CN, **HC**H_2COOH, **HC**H_2COH, **HC**H_2C≡CH, **HC**H(OH)HC(CH_3)$_2$, **HC**H_2NO_2, **HC**HF(CN), **HC**H(OH)(CF_3), **HC**H_2OCHO, (**HC**H_2)$_2$O, (**HC**H_2)$_2$NC(O)H, **HC**H(N(CH_3)$_2$)$_2$, **HC**FHC_6H_5, **HC**H(NO_2)$_2$, **HC**H_2OH, **HC**H_2NH_2, **HC**H_2OC_6H_5, **HC**HF_2, **HC**F_3, $C_6H_5NH_2$ (o), $C_6H_5NH_2$ (m), $C_6H_5NH_2$ (p), C_6H_5CHO (o), C_6H_5CHO (m), C_6H_5CHO (p), C_6H_5OH (o), C_6H_5OH (m), C_6H_5OH (p), $C_6H_3F_3$, C_6H_6, C_6H_5F (o), C_6H_5F (m), C_6H_5F (p), $C_4H_4N_2$. {88}

Appendix B

Publications

1. *The exchange-correlation potential in Kohn-Sham nuclear magnetic resonance shielding calculations*
   T.W. Keal and D.J. Tozer
   J. Chem. Phys., 2003, **119**, 3015.

2. *Improved NMR chemical shifts in density functional theory*
   M.J. Allen, T.W. Keal, and D.J. Tozer
   Chem. Phys. Lett., 2003, **380**, 70.

3. *GIAO shielding constants and indirect spin-spin coupling constants: performance of density functional methods*
   T.W. Keal, D.J. Tozer, and T. Helgaker
   Chem. Phys. Lett., 2004, **391**, 374.

4. *A semiempirical generalized gradient approximation exchange-correlation functional*
   T.W. Keal and D.J. Tozer
   J. Chem. Phys., 2004, **121**, 5654.

5. *Selenium chemistry with DFT: molecular structures and ^{77}Se NMR shielding constants*
   T.W. Keal and D.J. Tozer
   Mol. Phys., 2005, **103**, 1007.

6. *Semiempirical hybrid functional with improved performance in an extensive chemical assessment*
   T.W. Keal and D.J. Tozer
   J. Chem. Phys., 2005, **123**, 121103.

7. *Investigation of Coulomb attenuated exchange-correlation functionals*
   M.J.G. Peach, T.U. Helgaker, P. Salek, T.W. Keal, O. Lutnaes, D.J. Tozer, and N.C. Handy
   Phys. Chem. Chem. Phys., 2005, in press.

Appendix C

Conferences attended and talks given

9 July 2003
13th Annual Northern Universities Meeting on Chemical Physics
University of Durham
Poster presentation

7–12 September 2003
10th International Conference on the Applications of Density Functional Theory in Chemistry and Physics
Vrije Universiteit Brussel, Brussels, Belgium
Poster presentation

21–22 October 2003
CCWP course on the DALTON quantum chemistry package
King's College, London, UK

24–29 July 2004
Molecular Quantum Mechanics: The No Nonsense Path to Progress. An International Conference in Honour of Professor Nicholas C. Handy
University of Cambridge, UK
Poster presentation

24 September 2004
CCP1 special interest group meeting on DFT response properties
CCLRC Daresbury Laboratory, UK

13 April 2005
25th Anniversary Graduate Student Meeting of the Royal Society of Chemistry's Theoretical Chemistry Group
University of Nottingham, UK
Talk given on 'Semi-empirical fitting of exchange-correlation functionals'

11–15 September 2005
11th International Conference on the Applications of Density Functional Theory in Chemistry and Physics
Université de Genève, Geneva, Switzerland
Poster presentation

15 September 2005
Seminar
Universität Heidelberg, Heidelberg, Germany
Talk given on 'Development of new exchange-correlation functionals in DFT'

20 September 2005
Seminar
Max-Planck-Institut für Kohlenforschung, Mülheim an der Ruhr, Germany
Talk given on 'Development of semi-empirical exchange-correlation functionals'

Bibliography

[1] E. Schrödinger, *Phys. Rev.*, 1926, **28**, 1049.

[2] P.A.M. Dirac, *Proc. Roy. Soc.*, 1928, **A117**, 610; P.A.M. Dirac, *ibid.*, 1928, **A118**, 351.

[3] M. Born and J.R. Oppenheimer, *Ann. Physik*, 1927, **84**, 457.

[4] C.E. Eckart, *Phys. Rev.*, 1930, **36**, 878.

[5] W. Pauli, *Phys. Rev.*, 1940, **58**, 716.

[6] D.R. Hartree, *Proc. Cambridge Phil. Soc.*, 1928, **24**, 89.

[7] V. Fock, *Z. Physik*, 1930, **61**, 126.

[8] J.C. Slater, *Phys. Rev.*, 1930, **35**, 210.

[9] P.-O. Löwdin, *Adv. Chem. Phys.*, 1959, **2**, 207.

[10] J.A. Pople, M. Head-Gordon, and K. Raghavachari, *J. Chem. Phys.*, 1987, **87**, 5968.

[11] J. Čižek, *J. Chem. Phys.*, 1966, **45**, 4256; J. Čižek, *Adv. Chem. Phys.*, 1969, **14**, 35.

[12] K.A. Brueckner, *Phys. Rev.*, 1954, **96**, 508.

[13] B.O. Roos, *Int. J. Quantum Chem. Symp.*, 1980, **14**, 175; L.M. Cheung, K.R. Sundberg, and K. Ruedenberg, *Int. J. Quantum Chem.*, 1979, **16**, 1103.

[14] H.-J. Werner and E.-A. Reinsch, *J. Chem. Phys.*, 1982, **76**, 3144.

[15] C. Møller and M.S. Plesset, *Phys. Rev.*, 1934, **46**, 618.

[16] E. Bright-Wilson, as reported by R.G. Parr to N.C. Handy. See also E. Bright-Wilson, 'Structural Chemistry and Molecular Biology', ed. A. Rich and N. Davidson, Freeman, San Francisco, 1968, pp 753–760.

[17] L.H. Thomas, *Proc. Cambridge Phil. Soc.*, 1927, **23**, 542.

[18] E. Fermi, *Rend. Accad. Lincei*, 1927, **6**, 602.

[19] E. Teller, *Rev. Mod. Phys.*, 1962, **34**, 627.

[20] P.A.M. Dirac, *Proc. Cambridge Phil. Soc.*, 1930, **26**, 376.

[21] J.C. Slater, *Phys. Rev.*, 1951, **81**, 385.

[22] C.F. von Weizsacker, *Z. Physik*, 1935, **96**, 431.

[23] W. Stich, E.K.U. Gross, P. Malzacher, and R.M. Dreizler, *Z. Phys. A*, 1982, **309**, 5.

[24] P. Hohenberg and W. Kohn, *Phys. Rev.*, 1964, **136**, B864.

[25] W. Kohn and L.J. Sham, *Phys. Rev.*, 1965, **140**, A1133.

[26] D.M. Ceperley and B.J. Alder, *Phys. Rev. Lett.*, 1980, **45**, 566.

[27] S.J. Vosko, L. Wilk, and M. Nusair, *Can. J. Phys.*, 1980, **58**, 1200.

[28] O. Gunnarsson and B.I. Lundqvist, *Phys. Rev. B*, 1976, **13**, 4274.

[29] H. Stoll, C.M.E. Pavlidou, and H. Preuss, *Theoret. Chim. Acta*, 1978, **49**, 143; H. Stoll, E. Golka, and H. Preuss, *ibid.*, 1980, **55**, 29.

[30] J.P. Perdew and A. Zunger, *Phys. Rev. B*, 1981, **23**, 5048.

[31] G.S. Painter, *Phys. Rev. B*, 1981, **24**, 4264.

[32] B.G. Johnson, P.M.W. Gill, and J.A. Pople, *J. Chem. Phys.*, 1993, **98**, 5612.

[33] A.D. Becke, *J. Chem. Phys.*, 1986, **84**, 4524.

[34] E.K.U. Gross and R.M. Dreizler, *Z. Phys. A*, 1981, **302**, 103.

[35] F. Herman, J.P. Van Dyke, and I.B. Ortenburger, *Phys. Rev. Lett.*, 1969, **22**, 807.

[36] A.D. Becke, *Phys. Rev. A*, 1988, **38**, 3098.

[37] J.P. Perdew and Y. Wang, *Phys. Rev. B*, 1986, **33**, 8800.

[38] J.P. Perdew and Y. Wang, *Phys. Rev. B*, 1992, **45**, 13244; J.P. Perdew, J.A. Chevary, S.H. Vosko, K.A. Jackson, M.R. Pederson, D.J. Singh, and C. Fiolhais, *ibid.*, 1992, **46**, 6671.

[39] G.J. Laming, V. Termath, and N.C. Handy, *J. Chem. Phys.*, 1993, **99**, 8765.

[40] J.P. Perdew, K. Burke, and M. Ernzerhof, *Phys. Rev. Lett.*, 1996, **77**, 3865.

[41] P.M.W. Gill, *Mol. Phys.*, 1996, **89**, 433.

[42] M. Filatov and W. Thiel, *Mol. Phys.*, 1997, **91**, 847.

[43] A.D. Becke, *J. Chem. Phys.*, 1997, **107**, 8554.

[44] D.J. Tozer and N.C. Handy, *J. Chem. Phys.*, 1998, **108**, 2545.

[45] D.J. Tozer and N.C. Handy, *J. Phys. Chem. A*, 1998, **102**, 3162.

[46] N.C. Handy and D.J. Tozer, *Mol. Phys.*, 1998, **94**, 707.

[47] F.A. Hamprecht, A.J. Cohen, D.J. Tozer, and N.C. Handy, *J. Chem. Phys.*, 1998, **109**, 6264; A.D. Boese, N.L. Doltsinis, N.C. Handy, and M. Sprik, *ibid.*, 2000, **112**, 1670; A.D. Boese and N.C. Handy, *ibid.*, 2001, **114**, 5497.

[48] R.D. Adamson, P.M.W. Gill, and J.A. Pople, *Chem. Phys. Lett.*, 1998, **284**, 6.

[49] N.C. Handy and A.J. Cohen, *Mol. Phys.*, 2001, **99**, 403.

[50] G. Menconi, P.J. Wilson, and D.J. Tozer, *J. Chem. Phys.*, 2001, **114**, 3958.

[51] P.J. Wilson, T.J. Bradley, and D.J. Tozer, *J. Chem. Phys.*, 2001, **115**, 9233.

[52] J.P. Perdew, S. Kurth, A. Zupan, and P. Blaha, *Phys. Rev. Lett.*, 1999, **82**, 2544.

[53] J.P. Perdew, *Phys. Rev. B*, 1986, **33**, 8822.

[54] A.D. Becke, *J. Chem. Phys.*, 1988, **88**, 1053.

[55] C. Lee, W. Yang, and R.G. Parr, *Phys. Rev. B*, 1988, **37**, 785; B. Miehlich, A. Savin, H. Stoll, and H. Preuss, *Chem. Phys. Lett.*, 1989, **157**, 200.

[56] A.D. Becke, *J. Chem. Phys.*, 1995, **104**, 1040.

[57] A.J. Cohen and N.C. Handy, *Mol. Phys.*, 2001, **99**, 607.

[58] R. Colle and O. Salvetti, *Theor. Chim. Acta*, 1975, **37**, 329.

[59] E.I. Proynov, A. Vela, and D.R. Salahub, *Chem. Phys. Lett.*, 1994, **230**, 419.

[60] M. Filatov and W. Thiel, *Phys. Rev. A*, 1998, **57**, 189.

[61] H.L. Schmider and A.D. Becke, *J. Chem. Phys.*, 1998, **109**, 8188.

[62] R. Neumann and N.C. Handy, *Chem. Phys. Lett.*, 1997, **266**, 16.

[63] J. Tao, J.P. Perdew, V.N. Staroverov, and G.E. Scuseria, *Phys. Rev. Lett.*, 2003, **91**, 146401.

[64] T. Van Voorhis and G.E. Scuseria, *J. Chem. Phys.*, 1998, **109**, 400.

[65] E. Clementi and S.J. Chakravorty, *J. Chem. Phys.*, 1990, **93**, 2591.

[66] A.D. Becke, *J. Chem. Phys.*, 1993, **98**, 1372.

[67] J. Harris and R.O. Jones, *J. Phys. F*, 1974, **4**, 1170; O. Gunnarsson and B.I. Lundqvist, *Phys. Rev. B*, 1976, **13**, 4274; D.C. Langreth and J.P. Perdew, *ibid.*, 1977, **15**, 2884; J. Harris, *Phys. Rev. A*, 1984, **29**, 1648.

[68] B.J. Lynch, P.L. Fast, M. Harris, and D.G. Truhlar, *J. Phys. Chem. A*, 2000, **104**, 4811.

[69] A.D. Becke, *J. Chem. Phys.*, 1993, **98**, 5648.

[70] P.J. Stephens, F.J. Devlin, C.F. Chabalowski, and M.J. Frisch, *J. Phys. Chem.*, 1994, **98**, 11623.

[71] J.P. Perdew, M. Ernzerhof, and K. Burke, *J. Chem. Phys.*, 1996, **105**, 9982.

[72] M. Ernzerhof and G.E. Scuseria, *J. Chem. Phys.*, 1999, **110**, 5029; C. Adamo and V. Barone, *ibid.*, 1999, **110**, 6158.

[73] Y. Zhao, B.J. Lynch, and D.G. Truhlar, *J. Phys. Chem. A*, 2004, **108**, 2715.

[74] Y. Zhao and D.G. Truhlar, *J. Phys. Chem. A*, 2004, **108**, 6908.

[75] A.D. Boese and J.M.L. Martin, *J. Chem. Phys.*, 2004, **121**, 3405.

[76] Y. Zhao, B.J. Lynch, and D.G. Truhlar, *J. Phys. Chem. A*, 2004, **108**, 4786.

[77] R.D. Amos, I.L. Alberts, J.S. Andrews, A.J. Cohen, S.M. Colwell, N.C. Handy, D. Jayatilaka, P.J. Knowles, R. Kobayashi, G.J. Laming, A.M. Lee, P.E. Maslen, C.W. Murray, P. Palmieri, J.E. Rice, E.D. Simandiras, A.J. Stone, M.-D. Su, and D.J. Tozer, CADPAC6.5. The Cambridge Analytic Derivatives Package 1998.

[78] T. Helgaker, H.J.Aa. Jensen, P. Jørgensen, J. Olsen, K. Ruud, H. Ågren, A.A. Auer, K.L. Bak, V. Bakken, O. Christiansen, S. Coriani, P. Dahle, E.K. Dalskov, T. Enevoldsen, B. Fernandez, C. Hättig, K. Hald, A. Halkier, H. Heiberg, H. Hettema, D. Jonsson, S. Kirpekar, R. Kobayashi,

H. Koch, K.V. Mikkelsen, P. Norman, M.J. Packer, T.B. Pedersen, T.A. Ruden, A. Sanchez, T. Saue, S.P.A. Sauer, B. Schimmelpfenning, K.O. Sylvester-Hvid, P.R. Taylor, and O. Vahtras, Dalton release 1.2 (2001), an electronic structure program.

[79] C.C.J. Roothaan, *Rev. Mod. Phys.*, 1951, **23**, 69.

[80] G.G. Hall, *Proc. Roy. Soc.*, 1951, **A205**, 541.

[81] A.D. Becke, *J. Chem. Phys.*, 1988, **88**, 2547.

[82] C.W. Murray, N.C. Handy, and G.J. Laming, *Mol. Phys.*, 1993, **78**, 997.

[83] J.A. Pople and R.K. Nesbet, *J. Chem. Phys.*, 1954, **22**, 571.

[84] J.A. Pople, P.M.W. Gill, and N.C. Handy, *Int. J. Quantum Chem.*, 1995, **56**, 303.

[85] P. Pulay, *J. Comput. Chem.*, 1982, **3**, 556.

[86] M.F. Guest and V.R. Saunders, *Mol. Phys.*, 1974, **28**, 819.

[87] N. Godbout, D.R. Salahub, J. Andzelm, and E. Wimmer, *Can. J. Chem.*, 1992, **70**, 560.

[88] J.C. Slater, *Phys. Rev.*, 1930, **36**, 57.

[89] S.F. Boys, *Proc. Roy. Soc.*, 1958, **A200**, 542.

[90] M.J. Frisch, G.W. Trucks, H.B. Schlegel, G.E. Scuseria, M.A. Robb, J.R. Cheeseman, J.A. Montgomery, K.N. Kudin, J.C. Burant, J.M. Millam, S.S. Iyengar, J. Tomasi, V. Barone, B. Mennucci, M. Cossi, G. Scalmani, N. Rega, G.A. Petersson, H. Nakatsuji, M. Hada, M. Ehara, K. Toyota, R. Fukuda, J. Hasegawa, M. Ishida, T. Nakajima, Y. Honda, O. Kitao, H. Nakai, M. Klene, X. Li, J.E. Knox, H.P. Hratchian, J.B. Cross, C. Adamo, J. Jaramillo, R. Gomperts, R.E. Stratmann, O. Yazyev, A.J. Austin, R. Cammi, C. Pomelli, J.W. Ochterski, P.Y. Ayala, K. Morokuma, G.A. Voth, P. Salvador, J.J. Dannenberg, G. Zakrzewski, S. Dapprich, A.D. Daniels, M.C. Strain, O. Farkas, D.K. Malick, A.D. Rabuck, K.

Raghavachari, J.B. Foresman, J.V. Ortiz, Q. Cui, A.G. Baboul, S. Cliord, J. Cioslowski, B.B. Stefanov, G. Liu, A. Liashenko, P. Piskorz, I. Komaromi, R.L. Martin, D.J. Fox, T. Keith, M.A. Al-Laham, C.Y. Peng, A. Nanayakkara, M. Challacombe, P.M.W. Gill, B. Johnson, W. Chen, M.W. Wong, C. Gonzalez and J.A. Pople, Gaussian 03, Gaussian, Inc., Pittsburgh PA, 2003.

[91] T.H. Dunning, Jr., *J. Chem. Phys.*, 1971, **55**, 716; S. Huzinaga, *ibid.*, 1965, **42**, 1293.

[92] G. te Velde, F.M. Bickelhaupt, E.J. Baerends, C. Fonseca Guerra, S.J.A. van Gisbergen, J.G. Snijders, and T. Ziegler, *J. Comput. Chem.*, 2001, **22**, 931.

[93] A.J. Cohen and N.C. Handy, *J. Chem. Phys.*, 2002, **117**, 1470.

[94] B. Delley, *J. Chem. Phys.*, 1990, **92**, 508.

[95] J. Gauss and J.F. Stanton, *Adv. Chem. Phys.*, 2002, **123**, 355.

[96] A.M. Lee, N.C. Handy, and S.M. Colwell, *J. Chem. Phys.*, 1995, **103**, 10095.

[97] A.D. Becke, *Can. J. Chem.*, 1996, **74**, 995.

[98] R. Ditchfield, *J. Chem. Phys.*, 1972, **56**, 5688; K. Wolinski, J.F. Hinton, and P. Pulay, *J. Am. Chem. Soc.*, 1990, **12**, 8251.

[99] A.E. Hansen and T.D. Bouman, *J. Chem. Phys.*, 1985, **82**, 5035.

[100] P.J. Wilson, R.D. Amos, and N.C. Handy, *Mol. Phys.*, 1999, **97**, 757.

[101] P.J. Wilson and D.J. Tozer, *J. Chem. Phys.*, 2002, **116**, 10139.

[102] N.F. Ramsey, *Phys. Rev.*, 1950, **78**, 699.

[103] P.J. Wilson and D.J. Tozer, *Chem. Phys. Lett.*, 2001, **337**, 341.

[104] C. Adamo, M. Cossi, and V. Barone, *J. Mol. Struct. (Theochem)*, 1999, **493**, 145.

[105] P.J. Wilson, R.D. Amos, and N.C. Handy, *Chem. Phys. Lett.*, 1999, **312**, 475.

[106] S. Huzinaga, 'Approximate Atomic Functions', University of Alberta, Edmonton, 1971.

[107] W. Kutzelnigg, U. Fleischer, and M. Schindler, 'NMR-Basic Principles and Progress', ed. P. Diehl, E. Fluck, H. Günther, R. Kosfield, and J. Seelig, Springer, Heidelberg, 1990, vol. 23.

[108] P.J. Wilson, R.D. Amos, and N.C. Handy, *Phys. Chem. Chem. Phys.*, 2000, **2**, 187.

[109] V.G. Malkin, O.L. Malkina, M.E. Casida, and D.R. Salahub, *J. Am. Chem. Soc.*, 1994, **116**, 5898.

[110] E. Fadda, M.E. Casida, and D.R. Salahub, *Int. J. Quantum Chem.*, 2003, **91**, 67.

[111] S. Patchkovskii, J. Autschbach, and T. Ziegler, *J. Chem. Phys.*, 2001, **115**, 26.

[112] J. Poater, E. van Lenthe, and E.J. Baerends, *J. Chem. Phys.*, 2003, **118**, 8584.

[113] Q. Zhao, R.C. Morrison, and R.G. Parr, *Phys. Rev. A*, 1994, **50**, 2138.

[114] D.J. Tozer, V.E. Ingamells, and N.C. Handy, *J. Chem. Phys.*, 1996, **105**, 9200.

[115] M. Levy and J.P. Perdew, in 'Density Functional Methods in Physics', ed. R.M. Dreizler and J. da Providencia, Plenum, New York, 1985, pp 11–30.

[116] E. Fermi and E. Amaldi, *Mem. R. Acad. Italia*, 1934, **6**, 117.

[117] J.P. Perdew, R.G. Parr, M. Levy, and J.L. Balduz, Jr., *Phys. Rev. Lett.*, 1982, **49**, 1691.

[118] J. Gauss and J.F. Stanton, *J. Chem. Phys.*, 1996, **104**, 2574.

[119] T.D. Bouman and A.E. Hansen, *Chem. Phys. Lett.*, 1990, **175**, 292.

[120] D.J. Tozer and N.C. Handy, *J. Chem. Phys.*, 1998, **109**, 10180.

[121] Ionisation potentials: CO and N_2: A.W. Potts and T.A. Williams, *J. Electron Spectrosc. Relat. Phenom.*, 1974, **3**, 3; PN: D.K. Bulgin, J.M. Dyke, and A. Morris, *J. Chem. Soc., Faraday Trans. 2*, 1977, **73**, 983.

[122] C.O. Almbladh and A.C. Pedroza, *Phys. Rev. A*, 1984, **29**, 2322.

[123] F. Aryasetiawan and M.J. Stott, *Phys. Rev. B*, 1988, **38**, 2974.

[124] R. van Leeuwen and E.J. Baerends, *Phys. Rev. A*, 1994, **49**, 2421.

[125] C.J. Umrigar and X. Gonze, *Phys. Rev. A*, 1994, **50**, 3827.

[126] N.C. Handy, D.J. Tozer, G.J. Laming, C.W. Murray, and R.D. Amos, *Isr. J. Chem.*, 1993, **33**, 331.

[127] T.W. Keal and D.J. Tozer, *J. Chem. Phys.*, 2003, **119**, 3015.

[128] R.P. Feynman, *Phys. Rev.*, 1939, **56**, 340.

[129] K. Ruud, T. Helgaker, R. Kobayashi, P. Jørgensen, K.L. Bak, and H.J.A. Jensen, *J. Chem. Phys.*, 1994, **100**, 8178.

[130] J. Gauss and J.F. Stanton, *J. Chem. Phys.*, 1995, **103**, 3561.

[131] J.R. Cheeseman, G.W. Trucks, T.A. Keith, and M.J. Frisch, *J. Chem. Phys.*, 1996, **104**, 5497.

[132] J. Gauss and J.F. Stanton, *J. Chem. Phys.*, 1995, **102**, 251.

[133] J. Gauss, *Chem. Phys. Lett.*, 1992, **191**, 614.

[134] H. Fukui, T. Baba, J. Narumi, H. Inomata, K. Miura, and H. Matsuda, *J. Chem. Phys.*, 1996, **105**, 4692.

[135] K. Wolinski, C.L. Hsu, J.F. Hinton, and P. Pulay, *J. Chem. Phys.*, 1993, **99**, 7819.

[136] L.A. Curtiss, K. Raghavachari, G.W. Trucks, and J.A. Pople, *J. Chem. Phys.*, 1991, **94**, 7221.

[137] S.J. Chakravorty, S.R. Gwaltney, E.R. Davidson, F.A. Parpia, and C. Froese Fischer, *Phys. Rev. A*, 1993, **47**, 3649.

[138] W.-M. Hoe, A.J. Cohen, and N.C. Handy, *Chem. Phys. Lett.*, 2001, **341**, 319.

[139] G. Menconi and D.J. Tozer, *Chem. Phys. Lett.*, 2002, **360**, 38.

[140] M.J. Allen and D.J. Tozer, *Mol. Phys.*, 2002, **100**, 433.

[141] P.J. Wilson and D.J. Tozer, *J. Mol. Struct.*, 2002, **602-603**, 191.

[142] P.J. Wilson, R.D. Amos, and N.C. Handy, *J. Mol. Struct. (Theochem)*, 2000, **506**, 335.

[143] A. Rizzo, C. Cappelli, B. Jansik, D. Jonsson, P. Salek, S. Coriani, D.J.D Wilson, T. Helgaker, and H. Ågren, *J. Chem. Phys.*, 2005, **122**, 234314.

[144] S.M. Cybulski and D.M. Bishop, *J. Chem. Phys.*, 1997, **106**, 4082.

[145] K. Ruud, T. Helgaker, and P. Jørgensen, *J. Chem. Phys.*, 1997, **107**, 10599.

[146] K. Ruud, P.-O. Åstrand, and P.R. Taylor, *J. Chem. Phys.*, 2000, **112**, 2668.

[147] K. Ruud, P.R. Taylor, and M. Jaszunski, *J. Phys. Chem. A*, 2000, **104**, 168.

[148] A. Rizzo, T. Helgaker, K. Ruud, A. Barszczewicz, M. Jaszunski, and P. Jørgensen, *J. Chem. Phys.*, 1995, **102**, 8953.

[149] D.J.D. Wilson, C.E. Mohn, and T. Helgaker, *J. Chem. Theory Comput.*, 2005, **1**, 877.

[150] M. Bühl, M. Kaupp, O.L. Malkina, and V.G. Malkin, *J. Comput. Chem.*, 1999, **20**, 91.

[151] M. Kaupp, V.G. Malkin, O.L. Malkina, and D.R. Salahub, *Chem. Phys. Lett.*, 1995, **235**, 382.

[152] A.W. Ehlers, Y. Ruiz-Morales, E.J. Baerends, and T. Ziegler, *Inorg. Chem.*, 1997, **36**, 5031.

[153] D.L. Bryce and R.E. Wasylishen, *Phys. Chem. Chem. Phys.*, 2002, **4**, 3591.

[154] J. Nossal, R.K. Saini, A.K. Sadana, H.F. Bettinger, L.B. Alemany, G.E. Scuseria, W.E. Billups, M. Saunders, A. Khong, and R. Weisemann, *J. Am. Chem. Soc.*, 2001, **123**, 8482.

[155] G.Y. Sun and M. Kertesz, *J. Phys. Chem. A*, 2001, **105**, 5212.

[156] G. Schreckenbach, S.K. Wolff, and T. Ziegler, *J. Phys. Chem. A*, 2000, **104**, 8244.

[157] A. DerHovanessian, P.R. Rablen, and A. Jain, *J. Phys. Chem. A*, 2000, **104**, 6056.

[158] J. Czerneky, *J. Phys. Chem. A*, 2001, **105**, 1357.

[159] X.P. Xu and D.A. Case, *Biopolymers*, 2002, **65**, 408.

[160] V.I. Polshakov, R.R. Biekofsky, B. Birdsall, and J. Feeney, *J. Mol. Struct.*, 2002, **602**, 257.

[161] E. Oldfield, *Ann. Rev. Phys. Chem.*, 2002, **53**, 349.

[162] M.J. Allen, T.W. Keal, and D.J. Tozer, *Chem. Phys. Lett.*, 2003, **380**, 70.

[163] D.J. Tozer, *J. Chem. Phys.*, 2000, **112**, 3507.

[164] C.J. Jameson, A.K. Jameson, and P.M. Burrell, *J. Chem. Phys.*, 1980, **73**, 6013.

[165] T. Helgaker, P.J. Wilson, R.D. Amos, and N.C. Handy, *J. Chem. Phys.*, 2000, **113**, 2983.

[166] C. van Wüllen and W. Kutzelnigg, *J. Chem. Phys.*, 1996, **104**, 2330.

[167] J. Gauss, *J. Chem. Phys.*, 1993, **99**, 3629.

[168] M. Jaszuński, T. Helgaker, and K. Ruud, *Magn. Reson. Chem.*, 1996, **34**, 646.

[169] J. Gauss and J.F. Stanton, *J. Mol. Struct. (Theochem)*, 1997, **398-399**, 73.

[170] R. Challoner, R.K. Harris, and J.A. Tossell, *J. Magn. Reson.*, 1997, **126**, 1.

[171] T. Helgaker, M. Watson, and N.C. Handy, *J. Chem. Phys.*, 2000, **113**, 9402.

[172] N.F. Ramsey, *Phys. Rev.*, 1953, **91**, 303.

[173] V.G. Malkin, O.L. Malkina, and D.R. Salahub, *Chem. Phys. Lett.*, 1994, **221**, 91.

[174] R.M. Dickson and T. Ziegler, *J. Phys. Chem.*, 1996, **100**, 5286.

[175] V. Sychrovský, J. Gräfenstein, and D. Cremer, *J. Chem. Phys.*, 2000, **113**, 3530.

[176] T.A. Ruden, O.B. Lutnaes, T. Helgaker, and K. Ruud, *J. Chem. Phys.*, 2003, **118**, 9572.

[177] M. Pecul and T. Helgaker, *Int. J. Mol. Sci.*, 2003, **4**, 143.

[178] M. Pecul, J. Sadlej, and T. Helgaker, *Chem. Phys. Lett.*, 2003, **372**, 476.

[179] H. Iikura, T. Tsuneda, T. Yanai, and K. Hirao, *J. Chem. Phys.*, 2001, **115**, 3540.

[180] T. Yanai, D.P. Tew, and N.C. Handy, *Chem. Phys. Lett.*, 2004, **393**, 51.

[181] M.J.G. Peach, T.U. Helgaker, P. Salek, T.W. Keal, O. Lutnaes, D.J. Tozer, and N.C. Handy, *Phys. Chem. Chem. Phys.*, 2005, in press.

[182] C. Adamo, M. Ernzerhof, and G.E. Scuseria, *J. Chem. Phys.*, 2000, **112**, 2643.

[183] L.A. Curtiss, K. Raghavachari, P.C. Redfern, and J.A. Pople, *J. Chem. Phys.*, 1997, **106**, 1063.

[184] Retrieved October 2003 from the website of L.A. Curtiss: http://chemistry.anl.gov/compmat/comptherm.htm

[185] W.H. Press, S.A. Teukolsky, W.T. Vetterling, and B.P. Flannery, 'Numerical Recipes in Fortran 77', Cambridge University Press, Cambridge, 1992, p34.

[186] T.W. Keal and D.J. Tozer, *J. Chem. Phys.*, 2004, **121**, 5654.

[187] C. Tuma, A.D. Boese, and N.C. Handy, *Phys. Chem. Chem. Phys.*, 1999, **1**, 3939.

[188] V.N. Staroverov, G.E. Scuseria, J. Tao, and J.P. Perdew, *J. Chem. Phys.*, 2003, **119**, 12129.

[189] A.J.H. Wachters, *J. Chem. Phys.*, 1970, **52**, 1033.

[190] S.M. Colwell and N.C. Handy, *Chem. Phys. Lett.*, 1994, **217**, 271.

[191] A.J. Sadlej, *Collect. Czech. Chem. Commun.*, 1988, **53**, 1995; *Theor. Chim. Acta.*, 1991, **79**, 123.

[192] A.J. Russell and M.A. Spackman, *Mol. Phys.*, 1995, **84**, 1239; *ibid*, 1997, **90**, 251.

[193] EPAPS Document No. E-JCPSA6-121-307435. Available via a direct link from Ref. [186] online, or via the EPAPS homepage (http://www.aip.org/pubservs/epaps.html), or from ftp.aip.org in the directory /epaps/.

[194] A. Bagno, F. Rastrelli, and G. Saielli, *J. Phys. Chem. A*, 2003, **107**, 9964.

[195] P.E. Maslen, private communication.

[196] M. Bühl, W. Thiel, U. Fleischer, and W. Kutzelnigg, *J. Phys. Chem.*, 1995, **99**, 4000.

[197] M. Bühl, J. Gauss, and J.F. Stanton, *Chem. Phys. Lett.*, 1995, **241**, 248.

[198] G. Magyarfalvi and P. Pulay, *Chem. Phys. Lett.*, 1994, **225**, 280.

[199] G. Schreckenbach, Y. Ruiz-Morales, and T. Ziegler, *J. Chem. Phys.*, 1996, **104**, 8605.

[200] P.J. Wilson, *Mol. Phys.*, 2001, **99**, 363.

[201] G. Magyarfalvi and P. Pulay, *J. Chem. Phys.*, 2003, **119**, 1350.

[202] C.A. Bayse, *Inorg. Chem.*, 2004, **43**, 1208.

[203] J. Komulainen, R.S. Laitinen, and R.J. Suontamo, *Can. J. Chem.*, 2002, **80**, 1435.

[204] P.O. Astrand, K.V. Mikkelsen, P.Jørgensen, K. Ruud, and T. Helgaker, *J. Chem. Phys.*, 1998, **108**, 2528.

[205] J. Lounila, J. Vaara, Y. Hiltunen, A. Pulkkinen, J. Jokisaari, M. Ala-Korpela, and K. Ruud, *J. Chem. Phys.*, 1997, **107**, 1350.

[206] A. Schäfer, H. Horn, and R. Ahlrichs, *J. Chem. Phys.*, 1992, **97**, 2571.

[207] C.J. Jameson, 'Specialist Periodical Reports: Nuclear Magnetic Resonance', Royal Society of Chemistry, London, 1997, vol. 26.

[208] C.J. Jameson and A.K. Jameson, *Chem. Phys. Lett.*, 1987, **135**, 254.

[209] C.J. Jameson, 'Specialist Periodical Reports: Nuclear Magnetic Resonance', Royal Society of Chemistry, London, 1989, vol. 18.

[210] C.J. Jameson and A.C. De Dios, 'Specialist Periodical Reports: Nuclear Magnetic Resonance', Royal Society of Chemistry, London 1999, vol. 28.

[211] S. Kurth, J.P. Perdew, and P. Blaha, *Int. J. Quantum Chem.*, 1999, **75**, 889.

[212] P.P. Rushton, S.J. Clark, and D.J. Tozer, *Phys. Rev. B*, 2001, **63**, 115206.

[213] M.D. Segall, P.J.D. Lindan, M.J. Probert, C.J. Pickard, P.J. Hasnip, S.J. Clark, and M.C. Payne, *J. Phys.: Cond. Matt.*, 2002, **14**, 2717.

[214] D.R. Hamann, *Phys. Rev. Lett.*, 1979, **42**, 662.

[215] M.T. Yin and M.L. Cohen, *Phys. Rev. B*, 1982, **26**, 5668.

[216] G.B. Bachelet and N.E. Christensen, *Phys. Rev. B*, 1985, **31**, 879.

[217] J.K. Kang and C.B. Musgrave, *J. Chem. Phys.*, 2001, **115**, 11040.

[218] J.L. Durant, *Chem. Phys. Lett.*, 1996, **256**, 595.

[219] B.J. Lynch and D.G. Truhlar, *J. Phys. Chem. A*, 2003, **107**, 3898.

[220] Retrieved October 2004 from the website of D.G. Truhlar: http://comp.chem.umn.edu/database/

[221] D.J. Tozer, private communication.

[222] A.J. Cohen, Q. Wu, and W.T. Yang, *Chem. Phys. Lett.*, 2004, **399**, 84.

[223] T.W. Keal and D.J. Tozer, *J. Chem. Phys.*, 2005, **123**, 121103.

[224] EPAPS Document No. E-JCPSA6-123-301537. Available via a direct link from Ref. [223] online, or via the EPAPS homepage (http://www.aip.org/pubservs/epaps.html), or from ftp.aip.org in the directory /epaps/.

[225] Y. Zhao, N. González-García, and D.G. Truhlar, *J. Phys. Chem. A*, 2005, **109**, 2012.

[226] Retrieved March 2005 from the website of D.G. Truhlar: http://comp.chem.umn.edu/database/

[227] L.A. Curtiss, K. Raghavachari, P.C. Redfern, and J.A. Pople, *J. Chem. Phys.*, 2000, **112**, 7374.

[228] L.A. Curtiss, P.C. Redfern, K. Raghavachari, and J.A. Pople, *J. Chem. Phys.*, 1998, **109**, 42.

[229] Retrieved April 2005 from the website of L.A. Curtiss: http://chemistry.anl.gov/compmat/comptherm.htm

[230] S.M. Colwell, N.C. Handy, and A.M. Lee, *Phys. Rev. A*, 1996, **53**, 1316.

[231] M.J. Allen and D.J. Tozer, *Mol. Phys.*, 2003, **101**, 421.

[232] A.J. Cohen and Y. Tantirungrotechai, *Chem. Phys. Lett.*, 1999, **299**, 465.

[233] A.J. Cohen, N.C. Handy, and D. J. Tozer, *Chem. Phys. Lett.*, 1999, **303**, 391.

[234] A.P. Scott, R.H. Nobes, H.F. Schaefer III, and L. Radom, *J. Am. Chem. Soc.*, 1994, **116**, 10159.

[235] P.J. Wilson and D.J. Tozer, *Chem. Phys. Lett.*, 2002, **352**, 540.

[236] S.N. Maximoff, J.E. Paralta, V. Barone, and G.E. Scuseria, *J. Chem. Theory Comput.*, 2005, **1**, 541.

[237] P.F. Provasi, G.A. Aucar, and S.P.A. Sauer, *J. Chem. Phys.*, 2001, **115**, 1324.